ABERRANT METABOLIC AND SIGNALING PATHWAYS UNDERLIE IMPAIRED STEM CELL FUNCTION IN HUMAN OBESITY

ABERRANT METABOLIC AND SIGNALING PATHWAYS UNDERLIE IMPAIRED STEM CELL FUNCTION IN HUMAN OBESITY

BY

KANWALDEEP SINGH, M.Sc. (Honours)

A Thesis Submitted to the School of Graduate Studies in Partial Fulfillment of the

Requirements for the Degree Doctor of Philosophy

McMaster University

DESCRIPTIVE NOTE

Doctor of Philosophy (2019)

Biochemistry and Biomedical Sciences

McMaster University, Hamilton, Ontario, Canada

TITLE:	Aberrant metabolic and signaling pathways underlie impaired stem cell function in human obesity
AUTHOR:	Kanwaldeep Singh, M.Sc. (Honours)
SUPERVISOR:	Dr. Bradley Doble
NUMBER OF PAGES:	xx, 265

ABSTRACT

Obesity is a major health problem, and it is increasing at an alarming pace in developed and developing countries worldwide. Obesity increases the likelihood for many other diseases, such as type 2 diabetes, coronary heart disease, metabolic syndrome, hyperlipidemia, and some types of cancer. Chronic calorie-overload, genetic predisposition, and physical inactivity are the primary factors contributing to energy imbalance during obesity. In response to a positive energy balance, adipose tissues start expanding to store excessive nutrients in the form of lipids via two mechanisms: 1) by recruiting more adipocyte progenitors, resulting in increased adipocyte number – adipocyte hyperplasia; and 2) through an excessive accumulation of lipids in existing adipocytes – adipocyte hypertrophy. The former process is considered a metabolically healthy way to expand adipose tissue, while the latter is associated with the development of complications, such as insulin resistance. During conditions of chronic energy excess, as is found in obesity, adipose tissue loses its ability to recruit/activate progenitors, and adipose tissue expansion occurs primarily through adipocyte hypertrophy, ultimately resulting in inflamed and dysfunctional adipose tissue. Although studies have looked at hypertrophic and hyperplastic processes during adipocyte development, we still lack a meaningful understanding of the molecular mechanisms contributing to the reduced adipogenesis observed in obesity.

In this thesis, I created a metabolic map of healthy and obese human adipogenesis *in vitro* by using global transcriptomics, proteomics and functional cellular bioenergetics tools, providing a more systematic understanding of normal and obesity-influenced human adipogenesis. I isolated and characterized adipose tissue-resident stem cells (ADSCs) from different healthy, overweight, and obese individuals to create an *in vitro* model for studying obesity. I found that cells from

morbidly obese individuals inherently retained obesity-associated metabolic derangements, and hence, can serve as a cellular model that is very well-suited to study the factors contributing to the reduced adipogenesis that is observed in the context of obesity. By utilizing this model, I identified metabolic aberrations at molecular and functional levels in the two major cellular energy generating pathways, glycolysis and oxidative phosphorylation. I demonstrate that these pathways drive impaired stem cell function during adipogenesis in obese patient-derived ADSCs. Further, I was able to rescue impaired stem cell function and adipogenesis by stimulating metabolism and improving mitochondrial health in obese cells. In addition, through "omics" approaches, I identified a number of signaling pathways that are aberrantly regulated during obese versus healthy adipogenesis. One such pathway, which was prominently dysregulated in obese cells was the Wnt signaling pathway, wherein observed dynamic changes in Wnt antagonist expression, required for normal adipogenesis, did not occur in these cells. Functional studies revealed that aberrant Wnt signaling closely associated with defects in metabolism, which paralleled my earlier observations obtained through functional metabolic studies in obese cells, suggesting that cellular metabolism can be potentially targeted to improve stem cell function in obese cells. Building on that notion, I developed and validated a novel high-throughput functional drug-screening assay targeting obese adipogenesis, based on functional measurements of metabolic parameters such as mitochondrial activity and induction of the browning of white adipocytes.

Overall, this study presents novel insights into the mechanisms that modulate human adipogenic differentiation in obesity, by using disease relevant *in vitro* models that can serve as a platform for the discovery of novel therapeutics, offering the opportunity to identify novel

targetable pathways and biomarkers for the management of obesity and its associated metabolic complications.

ACKNOWLEDGEMENTS

First, I must thank Dr. Bradley Doble for being my mentor throughout this PhD and without whom I would not have made it to this point. Brad has both mentored me and allowed me the freedom to make my own decisions and follow up on my own ideas. I am grateful for your support and guidance during pivotal periods along the way. I must also thank Dr. Eva Szabo for her support and guidance throughout my graduate studies. I am also sincerely thankful to my committee members, Dr. Gregory Steinberg and Dr. Matthew Miller, for their ongoing support and providing helpful insights into my scientific endeavors over the last 6 years.

I must also thank all my past and present lab mates, who have become my second family and lifelong friends. I have been fortunate to spend the last 6 years surrounded by an awesome group of intelligent and hilarious people. I have been fortunate to have the opportunity to work at this institute. Thank you to all who helped me overcome technical issues, for sharing meaningful conversations about life stories, experimental procedures, and sharing hours of laughter. As part of the team I also had the opportunity to mentor graduate and undergraduate students, and a special thanks to them, especially Brandon and Derek, for helping out with the project.

Mere words would be less to express my gratitude, love and respect for my family, my parents, my brother, friends and above all 'The Almighty' who always stood by me at the difficult moments and boosted my morale. A very special thanks to my wife, Jasmeet. You were always there when I needed you the most. Thank you for refusing to believe I wasn't going to make it!!!

TABLE OF CONTENTS

LIST OF ABBREVIATIONS AND ACRONYMS

5-HT	5-hydroxytryptamine
ACC	Acetyl CoA carboxylase
ADSCs	Adipose-tissue derived stem cells
ALDOA	Aldolase, fructose-bisphosphate A
ANOVA	Analysis of variance
AP-1	Activating protein-1
APC	Adenomatous polyposis coli
APCs	Adipocyte precursor cells
aPKC	atypical forms of protein kinase C
Aregs	Adipogenesis-regulatory cells
ATF	Activating transcription factor
ATP	Adenosine triphosphate
BAT	Brown adipose tissue
bFGF	basic Fibroblast growth factor
BMI	Body Mass Index
BMP	Bone morphogenetic protein
BODIPY	Boron-dipyrromethene
C/EBPα	CAAT/enhancer-binding protein alpha
C/EBPβ	CAAT/enhancer-binding protein beta
C/EBPδ	CAAT/enhancer-binding protein delta
cAMP	Cyclic adenosine monophosphate
CB1	Type I cannabinoid
CD	Cluster of differentiation
cDNA	Complementary DNA
CFU-F	Fibroblast-Colony forming unit
CM	Conditioned medium
COXIV	Cytochrome c oxidase subunit 4I1
CREB	cAMP response element binding protein
CRP	C-reactive protein
Cyt c	Cytochrome c
DAPI	4′,6-diamidino-2-phenylindole
DKK	Dickkopf
DMEM	Dulbecco's modified eagle medium
DMSO	Dimethyl sulfoxide
DNA	Deoxyribonucleic acid
DPBS	Dulbecco's phosphate buffered saline
DRP1	Dynamin-related protein 1
Dvl	Dishevelled
EBs	Embryoid bodies
ECM	Extracellular matrix
EGF	Epidermal growth factor
ER	Endoplasmic reticulum
ERRα	Estrogen-related receptor α
ETC	Electron transport chain

FABP4	Fatty acid binding protein 4
FASN	Fatty acid synthase
FBS	Fetal bovine serum
FCCP	Carbonyl cyanide-p-trifluoromethoxyphenylhydrazone
FDA	Food and Drug Administration
FFAs	Free fatty acids
FIPs	Fibro-inflammatory progenitors
FOXO1	Forkhead box protein O1
FZD	Frizzled
GABPα	GA repeat-binding protein α
G-CSF	Granulocyte colony stimulating factor
GDFs	Growth differentiation factors
GDNF	Glial cell-derived neurotrophic factor
GLP-1	Glucagon-like peptide-1
GLUT4	Glucose transporter 4
glycoPER	Proton efflux rate specific to glycolysis
GM-CSF	Granulocyte/macrophage colony-stimulating factor
GO	Gene ontology
GRA	Glycolytic rate assay
GSK3β	Glycogen synthase kinase 3β
GWAS	Genome-wide association studies
HFD	High fat diet
HGF	Hepatocyte growth factor
HK2	Hexokinase 2
IBMX	1-methyl-3-isobutyl xanthine
IFN	Interferon
IGF	Insulin-like growth factor
IGF1R	Insulin-like growth factor 1 receptor
IL-6	Interleukin 6
IL-8	Interleukin 8
IMMT	Inner membrane mitochondrial protein
INSR	Insulin receptor
iPSCs	induced Pluripotent stem cells
IRS	Insulin receptor substrates
ISCT	International Society for Cellular Therapy
JAK	Janus Kinase
KEGG	Kyoto Encyclopedia of Genes and Genomes
KLF	Kruppel-like factor
KOSR	KnockOut Serum Replacement
LRPs	Low-density lipoprotein receptor-related proteins
MAPK	Mitogen-Activated Protein Kinase
MCP1	Monocyte chemoattractant protein 1
MEF-CM	Mouse embryonic fibroblasts-conditioned medium
MEFs	Mouse embryonic fibroblasts
MEM	Minimal essential medium
mESCs	Mouse embryonic stem cells
MSCs	Mesenchymal stem cells

MST	Mito stress test
mtDNA	Mitochondrial DNA
MTF1	Mitofusin 1
MTF2	Mitofusin 2
MT-ND1	Mitochondrially encoded NADH dehydrogenase 1
MT-ND3	Mitochondrially encoded NADH dehydrogenase 3
MT-ND5	Mitochondrially encoded NADH dehydrogenase 5
mTOR	Mammalian target of rapamycin
NAC	N-acetylcysteine
NADH	Nicotinamide adenine dinucleotide reduced
NCD	Non-communicable diseases
NEAA	Non-essential amino acids
NGF	Nerve growth factor
NPCs	Neural precursor cells
Nrf	Nuclear respiratory factor
OCR	Oxygen consumption rate
OPA1	Optic atrophy 1 (Mitochondrial dynamin Like 120kDa protein)
ORO	Oil Red O
OxPhos	Oxidative phosphorylation
PCA	Principal component analysis
PDHA	Pyruvate dehydrogenase
PDK1	Pyruvate dehydrogenase kinase isozyme 1
PFA	Paraformaldehyde
PFKFB3	6-phosphofructo-2-kinase/fructose-2,6-biphosphatase 3
PGC1α	Peroxisome proliferator-activated receptor gamma coactivator-1 alpha
PHB1	Prohibitin 1
PI3K	Phosphatidylinositol 3-kinase
PIP2	Phosphatidylinositol 3,4 bisphosphate
PIP3	Phosphatidylinositol 3,4,5 trisphosphate
PKA	Protein kinase A
PKB	Protein kinase B
PLIN1	Perilipin
PPARγ	Peroxisome proliferator-activated receptor γ
PTEN	Protein phosphatase and tensin homologue
ROS	Reactive oxygen species
RT-PCR	Reverse transcriptase-polymerase chain reaction
SAR	Structure–activity relationship
SAT	Subcutaneous adipose tissue
SDF-1	Stromal derived factor 1
SDHA	Succinate dehydrogenase complex flavoprotein subunit A
SDS-PAGE	Sodium dodecyl sulfate-polyacrylamide gel electrophoresis
SEM	Standard Error of the Mean
SFRPs	Secreted frizzled-related proteins
SGBS	Simpson-Golabi-Behmel syndrome
SHH	Sonic hedgehog
SIRT1	Sirtuin 1
SOD1	Superoxide dismutase 1

SREBP-1	Sterol response element–binding protein-1
STAT	Signal transducer and activator of transcription
SVF	Stromal vascular fraction
TAC	Transcriptome analysis console
TCA cycle	Tricarboxylic acid cycle
TCF/LEF	T-Cell Factor/Lymphoid Enhancer Factor
TFAM	Mitochondrial transcription factor A
TGFβ	Transforming growth factor β
TIMM23	Translocase of inner mitochondrial membrane 23
TLR4	Toll-like receptor 4
TMT-MS	Tandem mass tag-mass spectrometry
TNFα	Tumor necrosis factor α
TOMM20	Translocase of outer mitochondrial membrane 20
TZDs	Thiazolidinediones
UCP1	Uncoupling protein 1
VEGF	Vascular endothelial growth factor
WAT	White adipose tissue
WNT	Wingless-related MMTV Integration site
XF	Extracellular flux

LIST OF FIGURES AND TABLES

CHAPTER 1

CHAPTER 2

CHAPTER 3

CHAPTER 4

CHAPTER 5

APPENDICES

PREFACE

APPENDIX 1

APPENDIX 2

CHAPTER 1: INTRODUCTION

1.1 Overview

Obesity is a complex disorder with a strong correlation for developing chronic diseases such as type 2 diabetes, atherogenic dyslipidemia, cardiovascular disease, non-alcoholic fatty liver disease, and several types of cancer (Bhaskaran et al., 2014; Mitchell et al., 2011; Noureddin et al., 2015). Recent extensive collaborative consortia revealed that in 2015, at least 1.9 billion adults aged 18 and older were overweight and approximately 650 million of these were obese (Global burden of disease: Obesity collaboration 2017; NCD Risk Factor Collaboration, 2016). The prevalence of overweight or obese individuals has nearly doubled since 1980 and has been the fifth leading cause for global deaths (Hossain et al., 2007). According to the 2014 Canadian Community Health Survey, over 5.3 million adults are obese, and according to the 2015 Canadian Health Measures Survey, 28.1%, or more than one in four adults in Canada, have obesity requiring medical support to manage their disease (Canadian Obesity Network, 2017). The etiology of obesity is complex and is attributed to various aspects including, but not limited to, one's genetic makeup, fetal environment, metabolic factors, diet, and physical activity (Mitchell et al., 2011). Regardless of its multifaceted nature, obesity is uniformly measured by using the Body Mass Index (BMI - the weight in kilograms divided by the square of the height in meters), which is considered the most practical diagnostic tool available, although it is a crude index, not distinguishing between the specific distribution of fat and lean body mass (Heymsfield and Wadden, 2017). According to BMI, the general population is classified into five categories: underweight (BMI < 18.5 kg/m^2), normal weight (BMI 18.5-24.9 kg/m^2), overweight (BMI 25.0-29.9 kg/m^2), class I obesity (BMI 30.0-34.9 kg/m^2), class II obesity (BMI 35.0-39.9 kg/m^2) and class III obesity (also referred as

morbid obesity) (BMI > 40 kg/m^2) (Purnell, 2018). Obesity presents a crisis for the health care system, with extensive socioeconomic consequences that include a financial burden estimated at nearly $7.1 billion (Anis et al., 2011), which is projected to rise to $8.8 billion by 2021 (Canadian Obesity Network, 2017; Nadeau et al., 2013).

1.2 Adipose tissue

Adipose tissue is one of the largest organs in the body. White adipose tissue (WAT) represents around 10%-20% of total body-weight in lean adults but can reach over 50%, or even up to 70%, in severely obese persons (Hausman et al., 2001). WAT was thought to be a mere repository for excess energy in the form of triglycerides. However, in recent decades, adipose tissue has been shown to be an important endocrine organ functioning in the regulation of whole-body metabolism, energy intake, and fat storage. It is thus, also a major contributor to the metabolic consequences of obesity (Greenberg et al., 2006). Adipocyte lipid uptake, and storage as triglycerides, allows for expansion of adipose tissue and is an adaptive response to overnutrition, protecting other tissues from the deleterious effects of excess lipids. Beyond their role in nutrient handling and metabolism, adipocytes are highly active secretory cells producing hormones, adipokines, and chemokines that contribute to immunity, inflammation, vascular growth, and matrix remodeling (Sun et al., 2011). In response to energy needs, WAT expands by increasing cell size (hypertrophy) or cell number (hyperplasia) in the tissue (Ghaben and Scherer, 2019).

1.2.1 White adipose tissue distribution

WAT is divided into different depots, mainly subcutaneous (abdominal, femoral and gluteal) and visceral (omental, mesenteric, retroperitoneal, pericardial and gonadal) adipose tissues, as well as ectopic intrahepatic, intra-muscular, and intra-pancreatic fat, all of which have

different characteristics and contributions to whole-body metabolism (Bjorndal et al., 2011) (Fig. 1). Subcutaneous adipose tissue (SAT) is the largest body fat reserve and is, in total, over 4-5 times larger than visceral adipose tissue (Wajchenberg et al., 2000). SAT is divided between the upper body (abdominal) and lower body (femoral and gluteal) in a sex-specific manner (Ross et al., 1994), and both compartments contribute differently to the metabolic function of the body (Fruhbeck, 2008; Manolopoulos et al., 2010). SAT stores ~80-90% of total body fat, mainly in the abdominal, subscapular (on the upper back), gluteal and femoral areas. A smaller portion of body fat (10- 20%, depending on sex and individual-specific traits) resides viscerally in the abdominal cavity (Arner, 1997; Wronska and Kmiec, 2012).

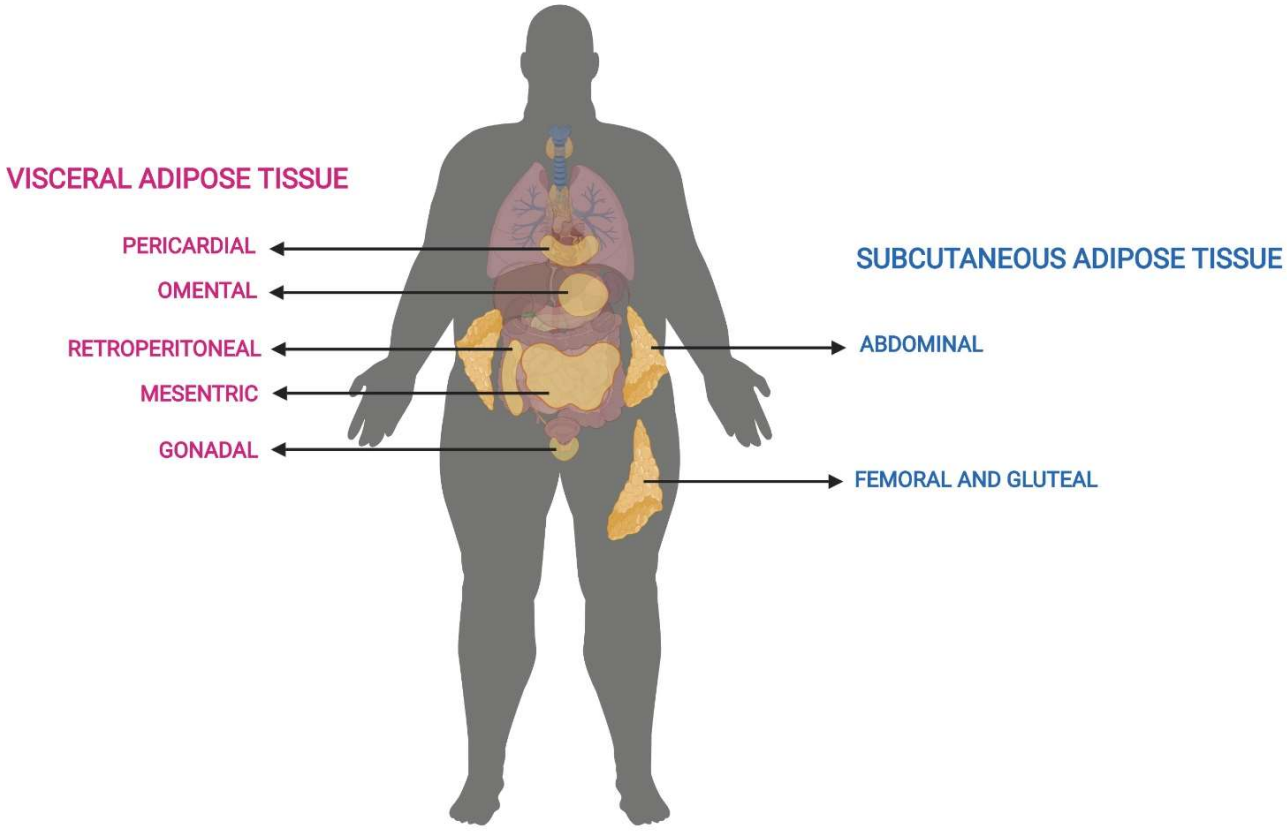

Fig. 1: Distribution of white fat in humans.

1.2.2 Cellular composition of white adipose tissue

Approximately 75% of adipose tissue weight consists of lipids. The remainder comprises adipose tissue matrix, which includes collagen, lymph and blood vessels, as well as endothelial cells, smooth muscle cells, pericytes, immune cells (macrophages, lymphocytes and other inflammatory cells), fibroblast-like preadipocytes, and adipose tissue derived stem cells (ADSCs), that collectively constitute the stromal vascular fraction (SVF) of adipose tissue (Bourin et al., 2013).

White adipocytes are unilocular and contain a large lipid droplet surrounded by a layer of cytoplasm. The remainder of an adipocyte is a small cytoplasm containing all cellular organelles, including mitochondria, and an adipocyte cell membrane encompassing the cytoplasm and lipid droplet. The nucleus is flattened and located on the periphery (Fig. 2A). The fat stored in WAT is composed primarily of triglycerides and cholesteryl esters (Hausman et al., 2001).

ADSCs are a stromal component of adipose tissues, characterized by plastic adherence when plated *in vitro*. They predominantly reside within vessel walls and perivascular niches where they provide signals for adipocyte and vascular development and participate in injury repair (Ma et al., 2014). ADSCs, together with the preadipocytes (that they give rise to), are responsible for the maintenance, renewal and expansion of white adipose tissue in normal and excess energy states (Cawthorn et al., 2012).

1.2.3 Other types of adipose tissue

WAT is the most prevalent and largest adipose tissue depot. However, other types of adipose tissue also exist. Brown adipose tissue (BAT) has different morphological and functional

features than WAT. Brown adipocytes are smaller in size, and unlike white adipocytes, only ~50% of the cell volume is occupied by lipids, which are divided into several small droplets inside the cell (Giordano et al., 2016) (Fig. 2A). Brown adipocytes in humans reside in small areas around the large blood vessels, especially in the supraclavicular region (Bartelt and Heeren, 2014). Brown adipocytes have very high mitochondrial content. They do not store energy but dissipate it by producing heat, and their activity is regulated by the sympathetic nervous system (Fig. 2C). Thermogenesis by brown adipocytes is dependent on the uncoupling of mitochondria, which is achieved by a unique, cold-inducible protein, the uncoupling protein 1 (UCP1). UCP1 belongs to a family of mitochondrial carriers. It disrupts formation of adenosine triphosphate (ATP), leading to a direct conversion of nutrient energy into heat (Morrison et al., 2014; Kajimura and Saito, 2013).

Newer findings have established a beige or brite (brown in white) adipocyte population that resides in white adipose depots. It shares several characteristics with classical brown adipocytes, including multilocular fat droplets, a high mitochondrial content, and expression of a brown-like gene program, e.g. UCP1 (Lo and Sun, 2013). Brite cells can be induced by cold and a broad spectrum of hormones and drugs that include peroxisome proliferator-activated receptor γ (PPARγ) agonists and β-adrenergic agonists (Fig. 2). Thus, beige cells in WAT is also defined as inducible BAT. Classical and inducible BAT are difficult to distinguish because of the similarities in their molecular and functional profiles (Pfeifer and Hoffmann, 2014).

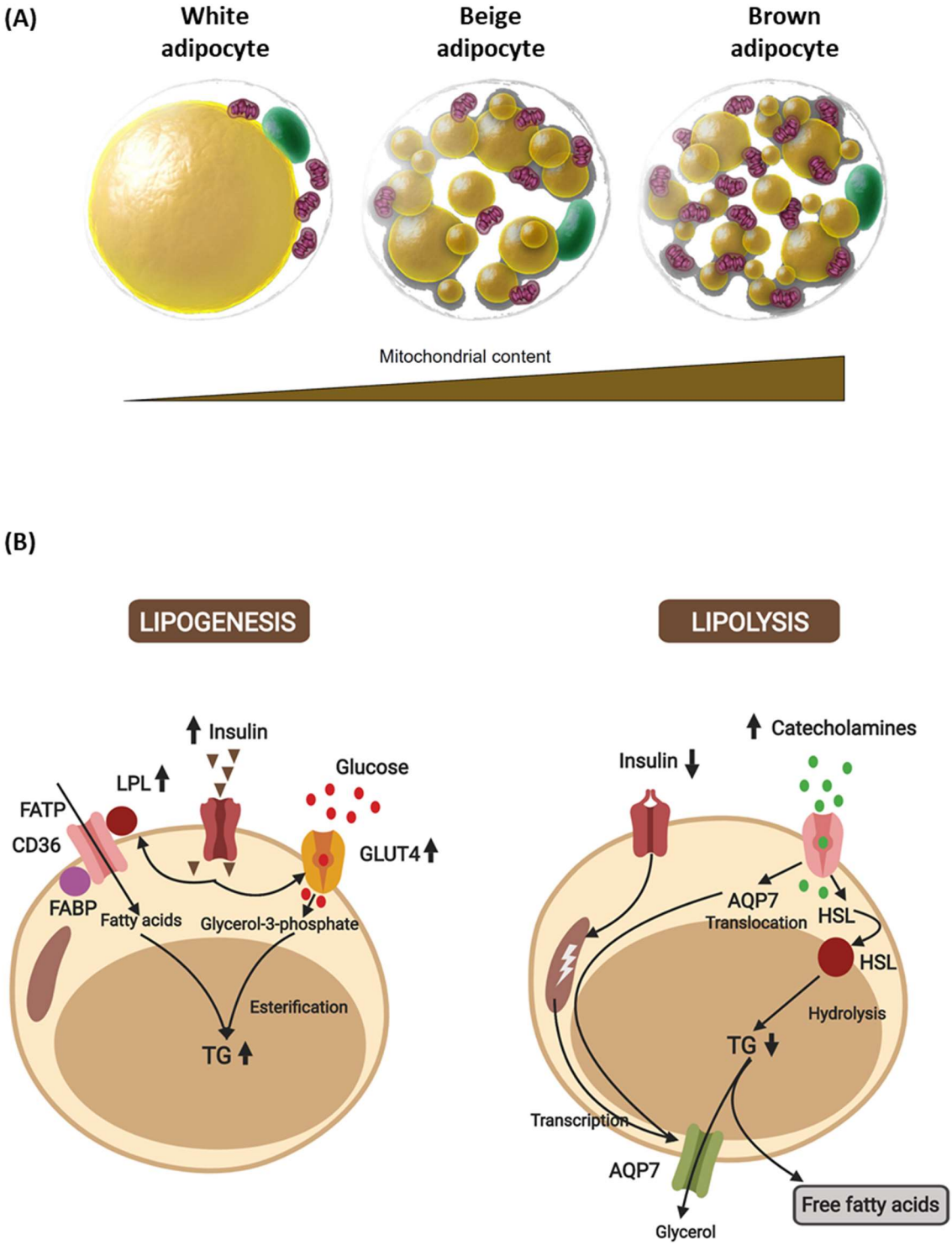
(A)
White adipocyte
Beige adipocyte
Brown adipocyte
Mitochondrial content
(B)
LIPOGENESIS
LIPOLYSIS
Insulin
LPL
Glucose
FATP
CD36
GLUT4
FABP
Fatty acids
Glycerol-3-phosphate
Esterification
TG
Catecholamines
Insulin
AQP7
Translocation
HSL
HSL
Hydrolysis
TG
Transcription
AQP7
Free fatty acids
Glycerol

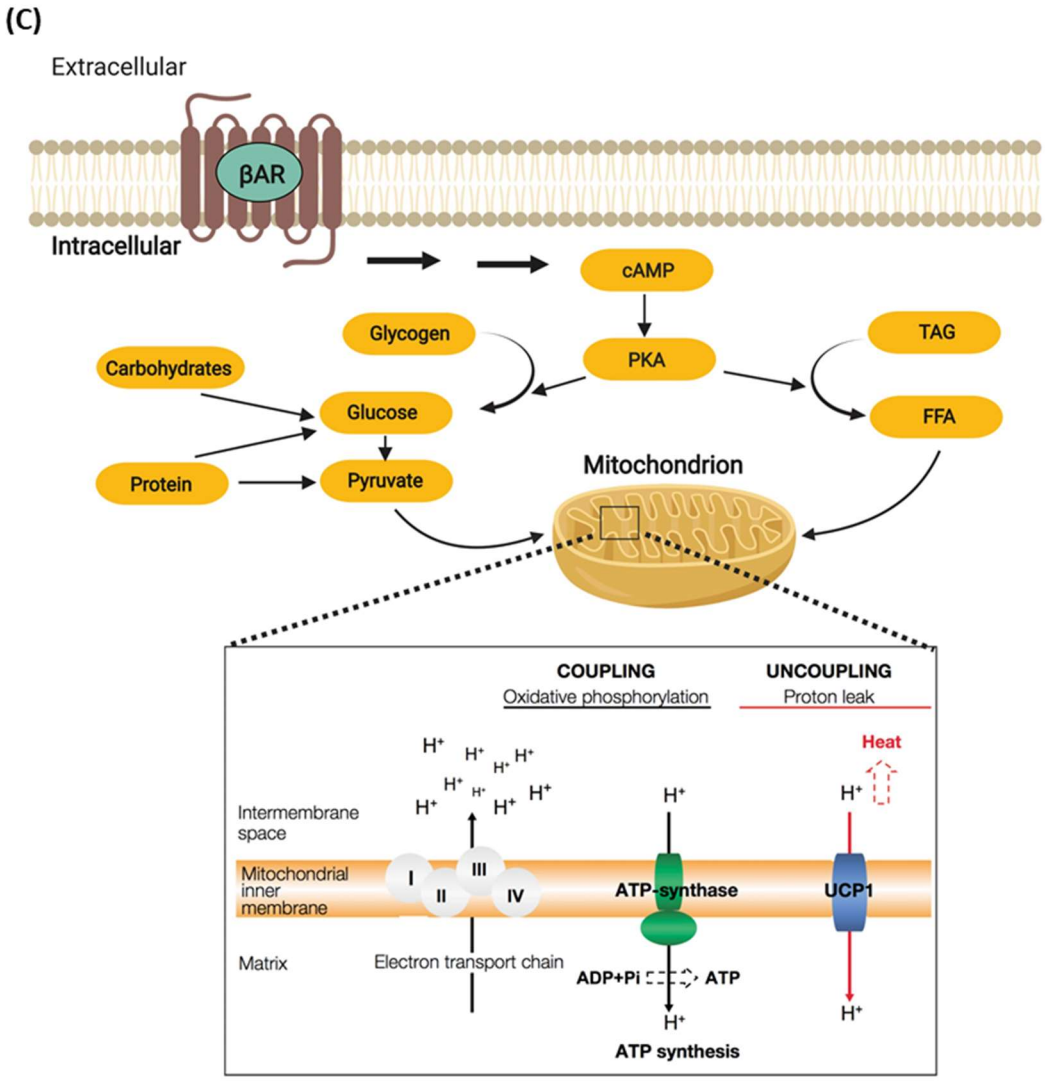

Fig. 2: Functions of white and brown/beige adipose tissue. (A) White, beige and brown adipocytes are morphologically and functionally very distinct and differ with respect to their mitochondrial content, and number and size of lipid droplet(s) in them. **(B)** The major physiological function of white adipose tissue is maintenance of metabolic homeostasis through storage (lipogenesis) and release (lipolysis) of free fatty acids in response to nutritional demands of the body. **(C)** Brown and beige adipocytes are thermogenic and dissipate energy in the form of heat upon induction with cold and/or β-adrenergic stimulation. (Fig. 2C adapted from Tseng et al., 2010).

1.3 Adipogenesis

Adipogenesis is the process by which stem cells, or precursors/preadipocytes derived from them, develop into mature adipocytes. Stem cells undergo sequential transitions categorized into two stages: (1) an initial "commitment phase" in which the stem cells get specified to the adipocyte lineage to become preadipocytes, followed by; (2) a "terminal differentiation" phase where the preadipocytes develop into mature fat-laden adipocytes (Henry et al., 2012).

Adipogenesis is an important mechanism for adipose tissue expansion in response to metabolic needs, given that mature adipocytes are fully differentiated cells incapable of mitotic division that can only provide expansion through an increase in size. Adipocyte turnover is sustained throughout life by a delicate balance between adipogenesis and apoptosis, which requires a constant source of adipocyte precursor cells. Adipocyte turnover studies using ^{14}C in WAT have shown that around 10% of the body's fat cells are regenerated each year, and the formation of adipocytes is a lifelong regulated process (Spalding et al., 2008). *In vitro* adipogenesis closely mimics the *in vivo* phenomenon, in terms of cell growth arrest and remodeling, with subsequent lipid accumulation (Cornelius et al. 1994; Stacey et al. 2009). Moreover, adipocytes derived *in vitro* possess the characteristics shown by adipocytes *in vivo*, including lipid storage, insulin sensitivity, and endocrine properties.

1.4 *In vitro* models for studying adipogenesis

1.4.1 Animal cellular models of adipogenesis

In vitro systems are invaluable for studying the molecular details of adipocyte differentiation. They provide a platform to investigate adipogenesis under tightly controlled and

reproducible conditions. Animal cell models have been commonly used to study adipocyte biology and adipogenesis, since they are easily attained, are cost effective, and are well characterized within the literature (Table 1). Preadipocyte cell lines are committed to the adipocyte lineage and can be induced to differentiate into mature adipocytes. 3T3-L1 and 3T3-F442A cells, isolated from Swiss 3T3 mouse embryos, are used most frequently for studying preadipocyte differentiation (Green and Meuth, 1974; Green and Kehinde, 1975). Since these are both clonal cell lines, the cell population responds to treatments and conditions homogeneously and provides a consistent source of preadipocytes due to its ability to tolerate a high number of passages. 3T3-F442A cells display more advanced commitment in the adipocyte lineage in comparison to the 3T3-L1 model, and they are capable of accumulating more fat (Green and Kehinde, 1976; Mandrup et al., 1997). Despite minimal differences between these two models, the 3T3-L1 cell line has been exhaustively used in adipogenesis research and is regarded as the "gold standard" of preadipocyte cell models.

In contrast to preadipocyte cell lines (3T3-L1 and 3T3-F442A), multipotent animal cell lines, such as C3H10T1/2 cells derived from C3H mouse embryos (Reznikoff et al., 1973), are developmentally more primitive and are capable of mimicking mesenchymal stem cells (MSCs) that can be induced to differentiate into the various lineages MSCs give rise to. This particular model has been extensively used to study the early adipogenic commitment process and has provided the research platform that identified the roles of bone morphogenetic proteins (BMPs) in early adipocyte commitment (Xue et al., 2014).

In addition, there are other less frequently used cell lines, each conferring its own unique advantages in studying adipocyte biology. Ob17 cells, were derived from adipocyte precursors in epididymal fat pads of genetically obese C57BL/6J *ob/ob* mice. Ob17 cells have a shorter doubling

time and higher adipogenic capacity than 3T3-L1 and 3T3-F422A cells (Negrel et al., 1978). Upon differentiation, they attain morphological and biochemical properties of mature rodent fat cells (Alihaud et al., 1983). OP9 cells are mouse bone marrow-derived stromal cells, which are advantageous for high throughput screening, as they are capable of rapidly accumulating fat droplets 72 hours post-induction (Wolins et al., 2006; Lane et al., 2014). Primary mouse embryonic fibroblasts (MEFs) obtained from multipotent cells of early mouse embryos have also been utilized to study adipogenesis, as they are easily maintained and undergo rapid proliferation and differentiation (Fei et al., 2011). However, owing to the cellular heterogeneity of this embryonic tissue, it is often difficult to attain homogeneity in the cell population (Garfield, 2010). Lastly, in addition to murine cells, porcine and feline preadipocytes have also been utilized, since they show greater similarity to human cells (Bohan et al., 2014; Riedel et al., 2016).

1.4.2 Human cellular models to study adipogenesis

While there are similarities between mouse and human adipocytes, there are also considerable differences regarding their adipokine levels, epigenome, and responsiveness to exogenous stimuli. Accordingly, the precise translation of observations gained from mouse adipocyte development to humans is yet to be resolved (Mikkelsen et al., 2010; Lindroos et al., 2013). Thus, human cell models are gaining traction in *in vitro* studies. Moreover, they are better applicable to physiologically relevant studies of obesity and its implications for metabolic disease and homeostasis disturbances (Ruiz-Ojeda et al., 2016). The cellular composition of human adipose tissue comprises adipocytes and the SVF that is composed of ADSCs, preadipocytes, endothelial cells and immunological cells. ADSCs can be efficiently isolated from adipose tissue, show self-renewal capacity, and maintain the ability to undergo differentiation into many

mesenchymal cell types including adipocytes, osteoblasts and myoblasts, *in vitro* (Bunnell et al., 2008; Rodriguez et al., 2005). The major advantages of using ADSCs as a cellular model are their multipotency, their high expansion capacity, their ability to be passaged a number of times, and their capacity to be cryopreserved for long periods of time (Lee and Fried, 2014). Moreover, once differentiated into mature adipocytes, these cells mimic characteristics of freshly isolated adipocytes, secrete adipokines, and respond to physiological concentrations of hormones (Storck et al., 2015).

ADSCs isolated *in vitro* are characterized according to the guidelines provided by the Mesenchymal and Tissue Stem Cell Committee of the International Society for Cellular Therapy (ISCT), which states that human MSCs, regardless of their source of origin, should match the following criteria: i) they have to be plastic-adherent in standard cell culture conditions; ii) ≥ 95% of cells must express CD105, CD90 and CD73 markers and must be negative (≤ 2% of positive cells) for CD45, CD34, CD14 or CD11b, CD79a or CD19 and class-II major histocompatibility complex molecules (MHC class II); iii) the cells must be able to differentiate into osteoblasts, adipocytes and chondroblasts under standard *in vitro* differentiation conditions (Dominici et al., 2006; Bourin et al., 2013).

Another cell line taken from SVF are primary preadipocyte cells, which are already committed to the adipocyte lineage. These primary adipocytes share many characteristics with ADSCs. However, one of the main differences is that preadipocytes already express PPARγ, which indicates that, unlike ADSCs, these cells are already specified towards the adipocyte lineage (Cawthorn et al., 2012). Preadipocytes also present an excellent model for studying adipogenesis;

however, they have limited renewal capacity, which restricts their use as a model system (Darimont and Mace, 2003).

Simpson-Golabi-Behmel syndrome (SGBS) cells represent another cellular model for studying human adipogenesis. These cells were derived from the SVF of SAT from an infant with Simpson-Golabi-Behmel syndrome (Wabitsch et al., 2001). SGBS preadipocytes are not transformed or immortalized. However, they can proliferate and maintain their differentiation capacity for up to 50 generations and upon differentiation, exhibit a gene expression profile comparable to that of mature human adipocytes (Fischer-Posovszky et al., 2008).

Table 1: Cell models used to study adipogenesis.

Cell model and source	Differentiation conditions	Characteristics
Animal cell models		
C3H10T1/2 From C3H mouse embryos (Reznikoff et al., 1973)	Demethylating agent 5-azacytidine and 10% FBS, insulin and DEX	• Multipotent cells that mimic MSCs and can differentiate into both white and brown adipocytes. • Another derivative, A33 preadipocytes have higher adipogenic capacity (Bowers and Lane, 2007).
3T3-L1 From Murine Swiss 3T3 cells in embryos (Green and Meuth, 1974; Green and Kehinde, 1975)	Insulin, DEX, IBMX, FBS	• Gold standard of preadipocyte cell lines • Tolerates a high number of passages, homogeneous response to treatments • Less costly to use than freshly isolated cells
3T3-F442A From Murine Swiss 3R3 cells (Green and Kehinde, 1976; Mandrup et al., 1997)	Insulin, DEX, IBMX, FBS	• Similar to 3T3-L1 cells, but is more advanced in adipocyte commitment
OP9 From mouse bone marrow-derived stromal cells (Wolins et al., 2006)	Insulin Oleate medium: MEM-α with 0.2% FBS, insulin, oleate bound to albumin, penicillin, and streptomycin.	• Fast adipogenic differentiation (72 hours) • Ability to passaged for long periods of time in culture • Suitable for high throughput screening (Lane et al., 2014)
Ob17 From adipose precursors in epididymal fat pads of genetically obese mice (Negrel et al., 1978)	Adipose conversion factor, insulin, triiodothyronine	• Have a shorter doubling time and higher adipogenic capacity than 3T3-L1 and 3T3-F422A cells • Exhibit morphological and biochemical properties of mature rodent fat cells (Alihaud et al., 1983)
Mouse Embryonic Fibroblasts (MEFs) From mouse embryonic fibroblasts (Garfield, 2010)	Insulin, IBMX, DEX, FBS, PPARγ agonist	• Proliferate rapidly and large numbers of cells can be produced from a single embryo (Garfield, 2010). • Capable of differentiating into adipocytes with variable efficiency (10-70%). • When immortalized, differentiate only when induced by a pro-adipogenic transcription factor (Rosen and MacDougald, 2006)
Porcine preadipocytes From SVF of pig adipose tissue (Bohan et al., 2014)	FBS, insulin, transferrin, hydrocortisone and rosiglitazone	• Phylogenetically closer to humans • Cells are more relevant to human physiology than murine cells. • More costly and difficult to isolate
Feline preadipocytes From adipose tissue of cats (Riedel et al., 2016)	Insulin, DEX, biotin, pantothenate, IBMX, and PPARγ agonist	• Show more similarity to human cells than murine cell lines

Cell model and source	Differentiation conditions	Characteristics
Human cell models		
Human ADSCs Isolated from SVF (Bunnell et al., 2008; Rodriguez et al., 2005)	IBMX, indomethacin, DEX, Insulin	• Exhibit donor and depot specific characteristics • Multipotent (gives rise to many lineages) • Can be passaged many times • Display phenotypic characteristics of freshly isolated adipocytes
Human Preadipocytes Isolated from SVF (Cawthorn et al., 2012; Church et al., 2015)	Insulin, IBMX, PPARγ agonist or indomethacin, DEX	• Already committed to adipogenic differentiation • Have limited renewal capacity • When immortalized, require the addition of PPARγ agonists
SGBS cells SVF of adipose tissue of an infant with SGBS (Wabitsch et al., 2001)	Insulin, triiodothyronine, cortisol, PPARγ agonist	• Can proliferate and maintain their differentiation capacity for up to 50 generations • High capacity for adipocyte differentiation

Abbreviations: DEX, Dexamethasone; IBMX, 1-methyl-3-isobutyl xanthine; MEM, Minimal essential medium

1.4.3 Depot-, gender- and age-specific diversity in ADSCs

ADSCs also reflect gender- (Aksu et al., 2008), age- (Alt et al., 2012; Choudhery et al., 2014; de Girolamo et al., 2009; van Harmelen et al., 2004) and depot-specific (Padoin et al., 2008; Wong et al., 2018; van Harmelen et al., 2004; Faustini et al., 2010; Jurgens et al., 2008; Di Taranto et al., 2015) characteristics, which are useful for assessing adipose tissue differences in proliferation and/or differentiation capacity across these categories. Abdominal subcutaneous adipose tissue-derived ADSCs from three males and three females showed that ADSCs from males had more osteogenic differentiation potential than cells collected from females (Aksu et al., 2008). The quantity and multilineage differentiation potential of ADSCs derived from abdominal subcutaneous adipose tissue (Alt et al., 2012; van Harmelen et al., 2004) and lipoaspirates (Choudhery et al., 2014; de Girolamo et al., 2009) of healthy donors was shown to decline with

age. Moreover, adipose tissue depot selection has also been shown to affect the yield (Padoin et al., 2008; Faustini et al., 2010; Jurgens et al., 2008), proliferation (van Harmelen et al., 2004) and differentiation potential (Di Taranto et al., 2015; Wong et al., 2018) of isolated ADSCs. These findings suggest that these ADSC characteristics are useful for studying depot-, gender- and age-specific differences in adipose tissue biology. Understanding these characteristics could assist in choosing the most promising adipose-depots and age groups for the isolation of ADSCs and could guide their use in regenerative medicine, which requires ADSCs with efficient differentiation and proliferation capacities. Importantly, the wide spectrum of differences observed in the proliferation and differentiation capacity of ADSCs within these categories strongly reflects the need to have age-, gender-, and depot-matched adipose tissue donors, to realize the full potential of these cells as an *in vitro* disease model, particularly for metabolic diseases such as obesity.

1.5 Transcriptional control of adipogenesis

Adipogenesis is regulated by a tightly orchestrated transcriptional cascade, where different transcription factors activate or repress the expression of each other in a sequential manner, ultimately imparting an adipocyte phenotype to the cell. The major players in the transcriptional cascade that regulates adipogenesis include CAAT/enhancer-binding protein (C/EBP) family members: C/EBPα, C/EBPβ, and C/EBPδ, and the nuclear receptor peroxisome proliferator-activated receptor γ (PPARγ), which have been shown to be important regulators of adipocyte differentiation both *in vitro* and *in vivo* (Christopher et al., 2011; Siersbaek et al., 2012) (Fig. 3).

1.5.1 Hierarchical expression of transcription factors during adipogenesis

The majority of our understanding regarding the transcriptional networks that control adipogenesis comes from *in vitro* adipogenesis studies conducted on 3T3-L1 or 3T3-F442A

murine preadipocyte cell lines that were originally generated almost forty years ago in the laboratory of Dr. Howard Green at Harvard University (Green, 1975; Green 1976).

Adipogenic differentiation is initiated from post-confluent growth-arrested MSCs or preadipocytes by stimulation with a pharmacological cocktail comprising the synthetic glucocorticoid, dexamethasone, the cyclic adenosine monophosphate (cAMP) elevating agent, 1-methyl-3-isobutyl xanthine (IBMX), and pharmacological doses of insulin, thereby resulting in activation of three signaling pathways: the IBMX-mediated protein kinase A (PKA) pathway, the glucocorticoid-mediated pathway and the insulin/insulin-like growth factor (IGF) tyrosine kinase pathway (Siersbaek and Mandrup, 2011; Tang and Lane, 2012). IBMX stimulates cAMP levels which further induces PKA-mediated phosphorylation of cAMP response element binding protein (CREB), resulting in increased expression of C/EBPβ. C/EBPβ, together with glucocorticoids, facilitates the induction of C/EBPδ (Cao et al., 1991; Zhang et al., 2004). The activation of these two transcription factors constitutes the first wave of transcriptional cascades that regulate adipogenesis.

In the second wave of transcriptional activation, C/EBPβ and C/EBPδ increase the expression of C/EBPα and PPARγ, which are considered to be the two most critical adipogenic transcription factors, by binding to their promoters. Once activated, C/EBPα and PPARγ regulate each other via positive feedback and function together as pleiotropic transcriptional activators of hundreds of genes that are responsible for establishing mature adipocytes (Lee, 2017). Genome-wide studies of mature 3T3-L1 adipocytes have shown PPARγ and C/EBPα binding motifs to be in close vicinity to each other and to be present together at ~ 60% of endogenous genes that are

induced during terminal differentiation, showing that they cooperatively orchestrate terminal differentiation of adipocytes (Lefterova et al., 2008).

1.5.2 Transcription factors as effectors of adipogenesis

The C/EBP and PPARγ transcription factors are among the most important transcription factors regulating the process of adipogenesis. Consequently, a number of *in vitro* and *in vivo* studies have been conducted using gain-of-function/loss-of-function of these factors, resulting in our better understanding of this process.

The C/EBP family consists of six isoforms of basic leucine zipper transcription factors: C/EBPα, β, δ, γ, ε, and ζ, out of which, C/EBPα, β, δ have been shown to promote adipogenesis *in vitro* and *in vivo* (Sarjeant and Stephens, 2012). Loss-of-function experiments have shown that attenuation of either C/EBPβ or -δ resulted in inhibition of adipogenesis in murine preadipocytes (Yeh et al., 1995). Preadipocytes from C/EBPβ$^{-/-}$ mice were found to have an aberrant adipogenic differentiation potential, which could be rescued upon forced expression of C/EBPβ (Tang et al., 2003). Mice lacking C/EBPβ and -δ were found to have defective adipogenic differentiation, further suggesting the importance of these early wave transcription factors during adipogenesis (Tanaka et al., 1997). Ectopic expression of the C/EBPα was reported to promote the adipogenic program in a variety of mouse fibroblastic cell types (Freytag et al., 1994). By using an adipocyte-specific knockout model, C/EBPα was shown to be essential for adipose tissue regeneration and adipogenesis (Wang et al., 2015).

PPARγ is a member of a superfamily of hormone nuclear receptors and exists as two isoforms, PPARγ1 and PPARγ2. PPARγ1 is expressed at low levels in multiple tissues, while PPARγ2 is selectively expressed in adipose tissue (Fajas et al., 1997) and is strongly upregulated

during adipogenesis (Tontonoz et al., 1994; Ren et al., 2002), suggesting a specific role for this isoform in adipocyte differentiation. PPARγ is shown be required and sufficient for adipogenic differentiation both *in vitro* and *in vivo* (Wu et al. 1998; Rosen et al., 1999), with adipose tissue-specific PPARγ knockout mice showing reduced adipose tissue weight along with adipocyte hypertrophy indicative of suppression of adipogenesis in the absence of PPARγ (He et al., 2003). Further, cross-talk between C/EBPα and PPARγ was reported to be critical for adipogenesis, with C/EBPα required for the maintenance of PPARγ expression in adipocytes (Wu et al., 1999). Given their significance, C/EBPα and PPARγ are considered to be master regulators of adipogenesis. As such, many pro- and anti-adipogenic factors modulate adipogenesis by altering the expression levels and/or activities of PPARγ and C/EBPα (Tang and Lane, 2012).

In addition to C/EBPs and PPARγ, there are several other transcription factors that are known to regulate the process of adipogenesis including the activating protein-1 (AP-1) family of transcription factors, members of the signal transducer and activator of transcription (STATs), members of the Kruppel-like factor (KLF) family of proteins, and sterol response element–binding protein-1 (SREBP-1) (White and Stephens, 2010).

AP-1 is a large group of transcription factors that includes v-Jun, c-Jun, JunB, JunD, v-Fos, c-Fos, FosB, Fra1, Fra2, and activating transcription factors (ATF2, ATF3/LRF1, and B-ATF). Upon activation, AP-1 proteins form homodimers or heterodimers and interact with DNA, thereby regulating genes involved in proliferation and differentiation of various cell types. In the context of adipogenesis, mRNA expression of c-Fos, c-Jun, Fos-B, and Fra1 was shown to be induced upon adipogenic stimulation in murine preadipocytes. AP-1 was shown to regulate expression of the adipocyte marker aP2 via interactions between c-Fos and the regulatory

sequences of the aP2 promoter (Distel et al., 1987). Additionally, mice with fat-specific disruptions in C/EBP and Jun transcriptional activity, display impaired adipose tissue development (Moitra et al., 1998).

The STAT family of mammalian transcription factors is comprised of seven proteins (STATs 1, 2, 3, 4, 5A, 5B, and 6), which are activated by Janus Kinase (JAK). The JAK-STAT pathway is present in almost all cell types and mediates the actions of numerous cytokines, growth factors, and peptide hormones. Several STATs, especially STAT5A and STAT5B, are known to enhance murine (Stephens et al., 1996) and human adipogenesis *in vitro* (Harp et al., 2001). Ectopic expression of STAT5A stimulated adipocyte differentiation along with activation of PPARγ in murine fibroblasts (Nanbu-Wakao et al. 2002; Floyd and Stephens, 2003). Moreover, growth hormones have also been shown to exert their pro-adipogenic effects through STAT5A/5B-PPARγ pathway (Kawai et al., 2007).

Among the KLF family of transcription factors, KLFs 4, 5, 6, and 15 have been shown to have a positive effect on adipogenesis during the first wave of transcriptional cascades, where KLF4 is induced within 30 minutes after exposure to an adipogenic cocktail. It subsequently binds to the C/EBPβ promoter and increases its expression (Birsoy et al., 2008). KLF5 expression has been shown to be induced during the early stages of adipocyte differentiation by C/EBPβ and C/EBPδ. KLF5 contributes to the induction of PPARγ, thereby increasing adipocyte differentiation both *in vitro* and *in vivo* (Oishi et al., 2005). By contrast, KLFs 2 and 7 are negative regulators of adipogenesis, as ectopic expression of KLF2 in 3T3-L1 preadipocytes (Banerjee et al., 2003) and KLF7 in human preadipocytes (Kawamura et al., 2006) has been shown to significantly inhibit adipocyte development and expression of PPARγ and C/EBPα.

SREBP-1 has three isoforms: SREBP-1a, SREBP-1c, and SREBP-2 (Hua et al., 1995). In response to insulin, expression of SREBP-1c, also known as adipocyte determination and differentiation-dependent factor 1 (ADD-1), is induced in 3T3-L1 cells, stimulating adipogenesis. SREBP-1c overexpression has also been shown to be accompanied by an increase in the expression of adipocyte-specific genes and lipid accumulation (Kim and Spiegelman, 1996).

1.6 Extracellular signaling pathway messengers as effectors of adipogenesis

Wnt/β-catenin, bone morphogenetic protein (BMP), and transforming growth factor β (TGFβ) signaling pathways are the three most significant extracellular signaling pathways regulating a multitude of cellular processes in a variety of cell types. Several members of these pathways have been reported to modulate adipogenic differentiation in both murine and human cellular and *in vivo* models, as described below.

1.6.1 Wnt signaling as effector of adipogenesis

The name Wnt is derived from a combination of two homologous genes; Wg (the *Drosophila* wingless gene) and Int [the murine homologue MMTV (mouse mammary tumour virus) integration site 1 gene]. Wnts comprise a large family of extracellular effectors secreted by many different cell types, which upon binding to corresponding Frizzled receptors (FZDs) and Low-density lipoprotein receptor-related proteins (LRPs), activate downstream signaling pathways (Sethi and Vidal-Puig, 2010). The hallmark of this signaling pathway is the regulation of the transcriptional activity of the cofactor β-catenin (CTNNB1), which is the core mediator of canonical Wnt/β-catenin signaling.

In the absence of Wnt proteins, cytoplasmic β-catenin is recruited to a degradation complex containing Glycogen synthase kinase-3 (GSK-3), Adenomatous polyposis coli (APC), and Axin. This primes β-catenin for ubiquitination and proteasomal degradation. Wnt ligand binding to its receptors activates signaling through Dishevelled (Dvl), leading to the inactivation of the degradation complex, thereby resulting in the accumulation of cytosolic β-catenin. β-catenin translocates to the nucleus and coactivates the TCF/LEF (T-cell factor/lymphoid enhancer-binding factor) family of transcription factors to activate Wnt/TCF target genes, which include *AXIN2*, *MYC*, and *CCND1* (Logan and Nusse, 2004; Buechling and Boutros, 2011). Wnt signaling is also regulated by extracellular antagonists including: (1) Secreted frizzled-related proteins (SFRPs), which inhibit Wnt signaling by directly binding and sequestering Wnts from their receptors; and (2) Dickkopf (DKK) family members, which inhibit canonical Wnt signaling by binding as high-affinity antagonists of LRP co-receptors (Jones and Jomary, 2002; Kawano and Kypta, 2003).

Several studies have shown that activation of the Wnt signaling pathway leads to inhibition of adipogenic differentiation in rodent MSCs and preadipocytes, while simultaneously directing their differentiation towards osteogenic or myogenic lineages. Specifically, treatment with Wnts Wnt3A, Wnt6, Wnt10A, or Wnt10B or ectopic expression of β-catenin have been shown to inhibit adipogenesis by preventing activation of C/EBPα and PPARγ (Shang et al., 2007a; Shang et al., 2007b; Bennett et al., 2002; Kang et al., 2007; Ross et al., 2000). On the other hand, expression of secreted extracellular Wnt antagonists: DKK1 and SFRP4 has been shown to spike during early stages of adipogenesis, thereby stimulating adipogenic differentiation in 3T3-L1 preadipocytes and human MSCs (Christodoulides et al., 2006; Visweswaran et al., 2015). Moreover, poor adipogenic differentiation potential of adipose progenitor cells in hypertrophic obesity has been

shown to be associated with maintained Wnt activation and lack of induction of *DKK1* (Gustafson and Smith, 2012). The role of Wnt signaling in adipogenesis has also been shown *in vivo*, where adipocyte-specific Wnt10B overexpression in transgenic mice results in higher bone mass and reduced fat mass, indicating that Wnt10B shifts mesenchymal cell fate towards the osteoblast lineage, suppressing adipogenic commitment (Longo et al., 2004).

In addition to β-catenin-dependent Wnt signaling, a few Wnts, primarily Wnt5A and Wnt11, are known to mediate Wnt signaling predominantly through a β-catenin–independent pathway, known as the non-canonical Wnt pathway. *In vitro*, inhibition of Wnt5A has been reported to reduce adipogenesis, suggesting a pro-adipogenic role for this Wnt (Nishizuka et al., 2008), whereas a more recent study has shown it to be anti-adipogenic in rodent MSCs (Tang et al., 2018). Wnt5A along with reduced expression of Wnt antagonist, SFRP5, was shown to contribute to insulin resistance and metabolic dysfunction in *in vivo* murine models of obesity (Ouchi et al., 2010). In addition, it is now clear that there is crosstalk between canonical and non-canonical Wnt signaling, where Wnt5B, another non-canonical Wnt ligand, has been shown to promote adipogenesis in 3T3-L1 cells by partially antagonizing the canonical Wnt/β-catenin pathway (Kanazawa et al., 2005).

1.6.2 TGFβ signaling as an effector of adipogenesis

The TGFβ superfamily consists of 33 members and includes TGFβ1-3, BMPs, growth differentiation factors (GDFs), activins, and nodal-related proteins. In the canonical signaling pathway, TGFβ members bind to their receptors, which ultimately phosphorylate and activate SMAD proteins and control gene transcription. TGFβ can also act through noncanonical signaling pathways that involve activation of several kinase cascades including the MAPK pathways (Herpin

et al., 2004). TGFβ has been shown to be expressed in murine preadipocytes, 3T3-F442A cells, and to inhibit adipogenesis through SMAD3-mediated signaling during the early stages of adipocyte differentiation (Choy et al., 2000). TGFβ has also been reported to inhibit adipocyte differentiation of human MSCs, while enhancing chondrocyte differentiation (Zhou et al., 2004).

Several BMPs, which are members of the TGFβ superfamily, have also been implicated in adipogenesis. BMP2 has been shown to induce PPARγ and to promote adipocyte differentiation in human ADSCs through the activation of Smad1 and p38 MAPK signaling pathways (Lee et al., 2014). Treatment with BMP4 has been shown to improve adipogenesis in human ADSCs, whereas addition of the BMP4 inhibitor, Noggin, reduces differentiation capacity, suggesting that endogenous BMP4 acts as a pro-adipogenic factor (Gustafson et al., 2015).

Activin A is a secreted homodimer of inhibin βA. Activin A binds to type I and type II Activin receptors, which act through the classical TGFβ signaling pathway, activating SMAD2/3. Activin A inhibits adipogenesis by affecting the transcriptional cascade upstream of PPARγ in 3T3-L1 preadipocytes (Hirai et al., 2005). Similarly, Activin A exerts anti-adipogenic effects during adipogenesis in human ADSCs, which is mediated through Smad2-dependent mechanisms that reduce C/EBPα and PPARγ expression (Zaragosi et al., 2010).

Among the GDF members of the TGFβ superfamily, GDF5 and GDF8 modulate adipogenesis in opposite ways. GDF5 is a pro-adipogenic factor, whose expression is increased during differentiation of 3T3-L1 preadipocytes. It has been shown to promote adipogenesis by enhancing cell entry into S phase and inducing the expression of genes related to adipocyte differentiation (Pei et al., 2014). On the contrary, GDF8, also known as myostatin, has been shown

to inhibit adipogenesis in human MSCs and preadipocytes through cross-talk between TGFβ/Smad and Wnt/β-catenin/TCF4 signaling, resulting in downregulation of PPARγ (Guo et al., 2008).

1.7 Regulation of adipogenesis by Insulin and IGF

Insulin is an anabolic peptide hormone secreted from pancreatic beta cells in response to increased plasma glucose. It promotes glucose uptake into peripheral tissues, such as skeletal muscle and adipocytes, for utilization or storage. Insulin-like growth factors (IGFs), IGF1 and IGFII, are produced in the liver and locally within tissues, including adipose tissues, and have been found to play an important role in adipose tissue development (Poulos et al., 2010). Insulin is a potent adipogenic hormone, which during adipogenesis *in vitro*, controls the activation and deactivation of transcription factors required for efficient adipocyte differentiation, at both early and late phases (Klemm et al., 2001; Zhang et al., 2009). Insulin and IGFs stimulate both the proliferation and differentiation of preadipocytes. Accordingly, insulin is an obligate hormone in adipogenic induction media for many cell types including human MSCs and 3T3-L1 preadipocytes (Hauner, 1990). 3T3-L1 preadipocytes predominantly express IGF1 receptor (IGF1R), and upon induction of adipogenesis, the insulin receptor (INSR) number increases several fold in response to insulin stimulation, with cells becoming more responsive to insulin at the level of metabolic regulation (Smith et al., 1988). Inactivation of INSR has been shown to reduce adipogenesis in 3T3-L1 preadipocytes, suggesting that insulin promotes adipogenesis through an INSR-dependent pathway (Accili and Taylor, 1991). Moreover, *in vivo* studies on transgenic mice with fat-specific disruption of the INSR and IGF1R genes have shown that selective deletion of INSR in adipocytes reduces white fat formation, while deletion of IGF1R has only modest effects on fat mass, clearly indicating the importance of INSR in white adipocyte development (Boucher et al., 2016).

At the molecular level, the binding of insulin to the extracellular α-subunit of the INSR results in autophosphorylation, whereby the intracellular β-subunit of the INSR becomes tyrosine-phosphorylated via its own activity. This preliminary tyrosine autophosphorylation of insulin receptor tyrosine residues provides docking sites for the recruitment of proteins known as insulin receptor substrates 1 - 4. (IRS1-4). Multiple tyrosine residues of IRS1 and IRS2 are phosphorylated by the INSR leading to binding and activation of phosphatidylinositol 3-kinase (PI3K), which converts phosphatidylinositol 3,4 bisphosphate (PIP2) to phosphatidylinositol 3,4,5 trisphosphate (PIP3). These phospholipids act as anchors, binding protein kinases to the plasma membrane and activating them. PIP3 bound to the plasma membrane recruits and activates PDK1, which, together with PI3K, activates major targets of insulin signaling, such as Akt (also known as protein kinase B, PKB) and atypical forms of protein kinase C (aPKC) (Haeusler et al., 2018; Tsatsoulis et al., 2013; Capurso and Capurso, 2012).

Activated Akt is thought to initiate many of the metabolic actions of insulin in responsive tissues: adipose tissue, muscle, liver, and pancreas. For example, Akt1 phosphorylates and inactivates GSK-3, which leads to activation of glycogen synthase and stimulation of glycogen synthesis. Akt1 also results in mammalian target of rapamycin (mTOR) activation and increased protein synthesis. Moreover, Akt phosphorylates and inhibits FOXO1, a key regulator of gluconeogenesis. Finally, Akt, together with aPKCs and other factors, promotes insulin stimulated glucose uptake via glucose transporter 4 (GLUT4) vesicle translocation to the plasma membrane (Haeusler et al., 2018).

Adipogenesis was found to be reduced by 60% or 15%, respectively, in embryonic fibroblasts obtained from IRS1-deficient or IRS2-deficient mice, compared to wild-type animals.

In addition, double IRS1/IRS2-deficient embryonic fibroblasts lacked the ability to differentiate into adipocytes. They also displayed a significant reduction in the expression of C/EBPα and PPARγ, further demonstrating the role of insulin signaling in efficient adipogenesis (Miki et al., 2001). Insulin stimulation was shown to be unable to promote adipogenesis upon treatment with a dominant-negative mutant form of PI3K or inhibitors of PI3K (wortmannin and LY-294002), indicating that insulin signaling plays a critical role in adipocyte differentiation (Gagnon et al., 1999). Insulin pathway-mediated pro-adipogenic signals are relayed to the nucleus through Akt-dependent phosphorylation and deactivation of the transcription factor, Forkhead box protein O1 (FOXO1), which is a potent inhibitor of PPARγ transcriptional activity (Nakae et al., 2003; Dowell et al., 2003). In addition to the signaling pathway mediated through INSR, insulin has also been shown to promote adipogenesis by stimulating the expression of another pro-adipogenic transcription factor, SREBP-1c (Kim et al., 1998).

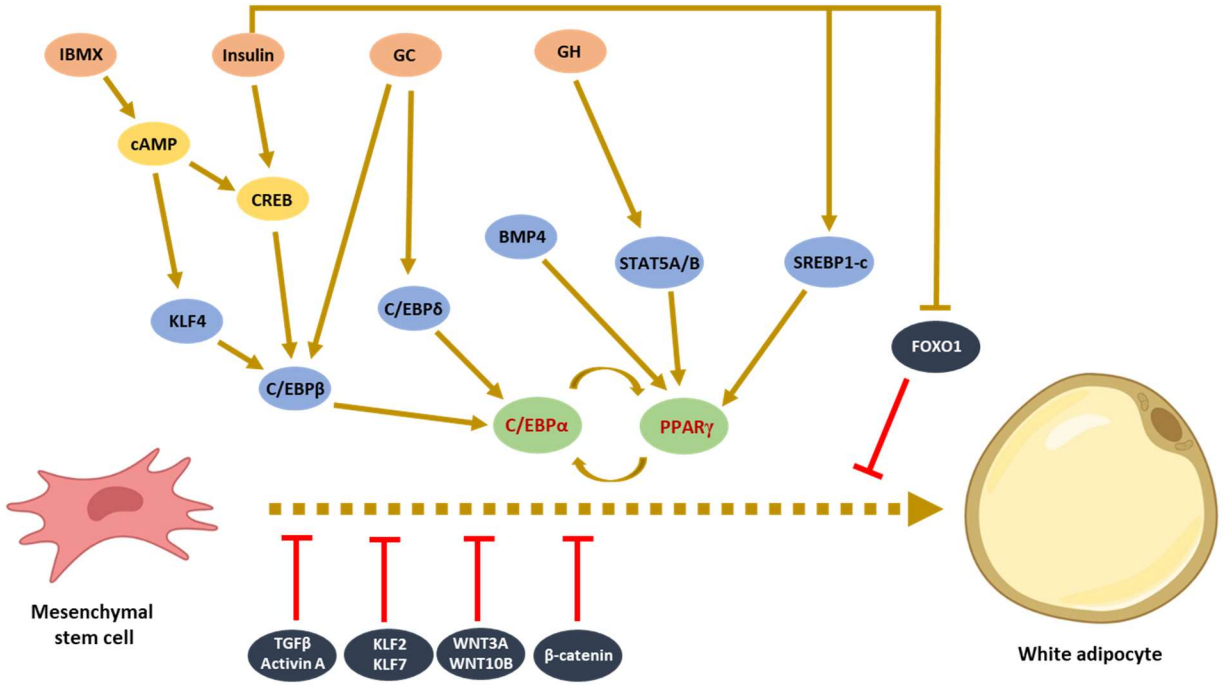

Fig. 3: Transcriptional and signaling factors controlling adipocyte differentiation. An adipogenic cocktail of inducers (i.e. insulin, glucocorticoids, a cAMP elevating agent (IBMX) and serum containing high levels of growth hormone) acts on their targets leading to the activation of C/EBPβ and C/EBPδ, which activate the master regulators of adipogenesis, C/EBPα and PPARγ. Once activated, C/EBPα and PPARγ can mutually induce the expression of each other and cooperatively activate the adipogenic gene program manifested by accumulation of lipid droplets as well as expression of multiple metabolic programs characteristic of a mature fat cells. BMP4 promotes adipogenesis by inducing the expression of PPARγ. In addition to activating C/EBPβ during the early phase of differentiation, insulin also induces PPARγ via SREBP1-c, and inhibits FOXO1, a potent inhibitor of adipogenesis.

1.8 Role of mitochondria in adipose tissue development

The role of mitochondria in adipocytes was long neglected, possibly because of their low abundance in these cells. However, recent evidence has shown that mitochondria in adipocytes are at the core of the energy metabolism of the cell. In a healthy state, mitochondria actively control the following: lipid turnover, apoptosis, generation of ATP and cell metabolism substrates, production of new adipocytes, and other essential cellular functions (Boudina and Graham, 2014; De Pauw et al., 2009).

1.8.1 Mitochondrial homeostasis and function

The term 'mitochondria' was first introduced by Carl Brenda in 1898 (Ernster and Schatz, 1981) and originates from the Greek 'mitos' (thread) and 'chondros' (granule), referring to the appearance of these structures during spermogenesis. Mitochondria have since become a central subject of research within numerous disciplines of experimental biology. Mitochondria in humans are the organelles essential for vital cellular functions, regulating many metabolic pathways by which chemical energy from various cellular fuel sources (carbohydrates, lipids and proteins) is converted into the energy-substrate ATP. Pyruvate oxidation, the tricarboxylic acid (TCA) cycle, fatty acid β-oxidation and oxidative phosphorylation (OxPhos) take place in mitochondria, and hence, they are aptly known as the "powerhouse" of the cell (Goldenthal and Marin-Garcia, 2004).

Mitochondria have two membranes: an outer membrane and an inner membrane that is folded into cristae. These membranes divide mitochondria into an intermembrane space and an inner matrix subcompartment. The folded inner membrane houses the respiratory chain complexes (I-IV) and ATP-synthase (complex V), which together make up the critical units of oxidative phosphorylation-dependent energy production in the cell.

The oxidative phosphorylation pathway consists of ~90 protein subunits that are assembled into five complexes: (1) complex I (NADH dehydrogenase, with 45 subunits); (2) complex II (succinate dehydrogenase, with 4 subunits); (3) complex III (cytochrome bc 1, with 11 subunits); (4) complex IV (cytochrome oxidase, COX, with 13 subunits); and (5) complex V (ATP synthase, with 17 subunits). In addition to these complexes, the respiratory chain has two mobile electron shuttles, ubiquinone (Coenzyme Q, CoQ), and cytochrome c (cyt c), a heme-containing small polypeptide (McKenzie et al., 2009; Kühlbrandt, 2015).

Mitochondria also possess their own multicopy genome, a 16.6 kb circular mitochondrial DNA (mtDNA) residing in the inner matrix, which contains 37 genes coding for two ribosomal RNAs (12S and 16S), 22 transfer RNAs, and 14 polypeptides. The 13 mtDNA-encoded proteins are the core catalytic components of the respiratory chain complexes I, III, IV, and V, and the remaining OxPhos proteins are encoded in the nucleus, with complex II being solely nuclear-encoded (Falkenberg et al., 2007; Asin-Cayuela and Gustafsson, 2007). The 14th mtDNA-encoded protein called humanin, a biologically active protein involved in stress resistance, was discovered in 2001 and was found to be encoded by the mitochondrial gene MT-RNR2 (Hashomoto et al., 2001).

Mitochondrial homeostasis is critical to determine bioenergetic responses to metabolic stress and is determined by a delicate balance between mitochondrial biogenesis, dynamics and mitophagy. Mitochondrial biogenesis, defined as the growth and division of pre-existing mitochondria, is regulated by tightly orchestrated induction of transcriptional regulators, activated by energy demands (Scarpulla, 2008). Peroxisome proliferator-activated receptor gamma coactivator1α (PGC1α), mitochondrial transcription factor A (TFAM), and nuclear respiratory

factors (Nrfs), Nrf1 and Nrf2, have been shown to be important regulators of mitochondrial biogenesis (Jornayvaz and Shulman, 2010).

PGC1α, by co-activating and controlling the expression of the mitochondrial biogenesis network, directly links external physiological stimuli to the regulation of mitochondrial production and function (Scarpulla, 2011). The activity of PGC1α is regulated by acetylation, and in a normal state, PGC1α is acetylated and silenced. However, in nutrient excess, sirtuin 1 (SIRT1) activates PGC1α and mitochondrial activity is enhanced (Houtkooper et al., 2010). PGC1α regulates the functions of TFAM. The TFAM promoter contains recognition sites for Nrf1 and/or Nrf2, thus allowing coordination between mitochondrial and nuclear activation during mitochondrial biogenesis and controling the transcription of mitochondrial proteins (Virbasius and Scarpulla, 1994; Wu et al., 1999). PGC1α also targets estrogen-related receptor α (ERRα) and GA repeat-binding protein α (GABPα) to regulate respiratory chain complexes including cytochrome c and ATP synthase (Schreiber et al., 2004; Mootha et al., 2004). The transcription factor, FOXO1, is another important mitochondrial regulator, which enhances the expression of genes involved in mitochondrial lipid oxidation and oxidative stress protection (Brunet et al., 2004).

An important aspect of proper mitochondrial function is the maintenance of healthy numbers of mitochondria through mitochondrial dynamics, fusion and fission, which enable mitochondria to divide and help ensure proper organization of the mitochondrial network during biogenesis (Green and Van Houten, 2011). Abnormal mitochondrial fusion induces the fragmentation of mitochondria from a tubular morphology into pieces, whereas disturbed mitochondrial fission results in the fusion of adjacent mitochondria (Chen, 2006). The processes of mitochondrial fission/fusion are controlled by GTPases, most of which were identified in

genetic screens in yeast (Hoppins et al., 2007). Mitochondrial fusion in mammals is mediated by mitofusins: MTF1 and MTF2, (Bach et al., 2003) and optic atrophy 1 (OPA1) (Cipolat et al., 2004), while mitochondrial fission is regulated by dynamin-related protein 1 (DRP1) (Smirnova et al., 2001).

A third process involved in mitochondrial homeostasis is called mitophagy, which is a mitochondrial-specific equivalent of autophagy that involves breakdown of damaged and malfunctioning mitochondria. Mitophagy is considered to be a beneficial metabolic event and is important for preserving mitochondrial quality and insulin sensitivity (Gomes et al., 2011). Specifically, defective mitochondria are sequestered into a double membrane phagosome that is later fused with lysosomes to form autolysosomes, where the contents are degraded and can be recycled (Ding and Yin, 2012).

1.8.2 Regulation of adipogenesis by mitochondrial metabolism

Compared to transcriptional and signaling pathway mediated modulation of adipogenesis, the role of cellular metabolism in the regulation of adipocyte differentiation has not received as much attention. Nevertheless, increased oxygen consumption of preadipocytes has been shown during adipogenic differentiation, which suggests an increase in mitochondrial biogenesis. Moreover, adipogenic differentiation of 3T3-L1 preadipocytes has been shown to be accompanied by an increase (several-fold) in the concentration of mitochondrial protein along with marked changes in mitochondrial morphology (Wilson-Fritch et al., 2003; Wilson-Fritch et al., 2004). Mitochondrial activity has been shown to be a prerequisite for differentiation of MSCs into adipocytes, with a significant increase in mitochondrial function observed during early stages of adipogenesis (Zhang et al., 2013; Drehmer et al., 2016). Coordination between adipogenesis and

mitochondrial biogenesis is supported by the fact that the same transcription factors are needed in both processes. PPARγ, C/EBPα, CREB, (Rosen and Spiegelman, 2001), ERRα (Ijichi et al., 2007) and PGC1α are all major regulators of mitochondrial biogenesis as well as adipogenesis and body energy balance (Spiegelman et al., 2000). However, it is not clear whether this increase in mitochondrial activity is a causal factor or a consequence of adipogenic differentiation, particularly in the case of metabolic disorders that exhibit altered adipogenesis.

The byproducts of mitochondrial metabolism, mitochondrial reactive oxygen species (ROS), have been shown to inhibit proliferation of 3T3-L1 mouse preadipocytes (Carriere et al., 2003) and to exhibit strong anti-adipogenic effects in murine 3T3-F442A preadipocytes (Carriere et al., 2004). ROS levels have also been shown to drop during early stages of adipogenesis in 3T3-L1 preadipocytes, with a concomitant increase in expression of antioxidant enzyme genes (Ducluzeau et al., 2011). On the contrary, ROS levels have been shown to increase during adipogenesis in 3T3-L1 preadipocytes, where N-acetylcysteine (NAC), a well-known antioxidant, inhibited ROS levels as well as fat accumulation in a concentration-dependent manner. NAC also inhibits the expression of adipogenic transcription factors C/EBPβ and PPARγ (Calzadilla et al., 2011). Similarly, ROS generated by mitochondrial complex III has been reported to be essential for the activation of adipogenic transcription factors in human MSCs, where treatment with specific mitochondrial antioxidants, such as Mitotempol or MitoCP, resulted in abrogation of adipogenesis (Tormos et al., 2011). Additional studies on adipogenesis using human MSCs have also shown ROS levels to go up during early stages of adipogenesis (Zhang et al., 2013; Drehmer et al., 2016). In addition, high ROS levels are associated with insulin resistance in 3T3-L1 adipocytes, where inducing ROS production has been shown to decrease adiponectin expression

and secretion. Adiponectin is an important protein for insulin sensitivity, exhibiting anti-atherogenic and anti-inflammatory effects (Wang et al., 2013a). Taken together, these selected representative studies suggest that the amount and duration of ROS effects are critical in the initiation of normal versus pathological responses in adipocyte differentiation (Fig. 4).

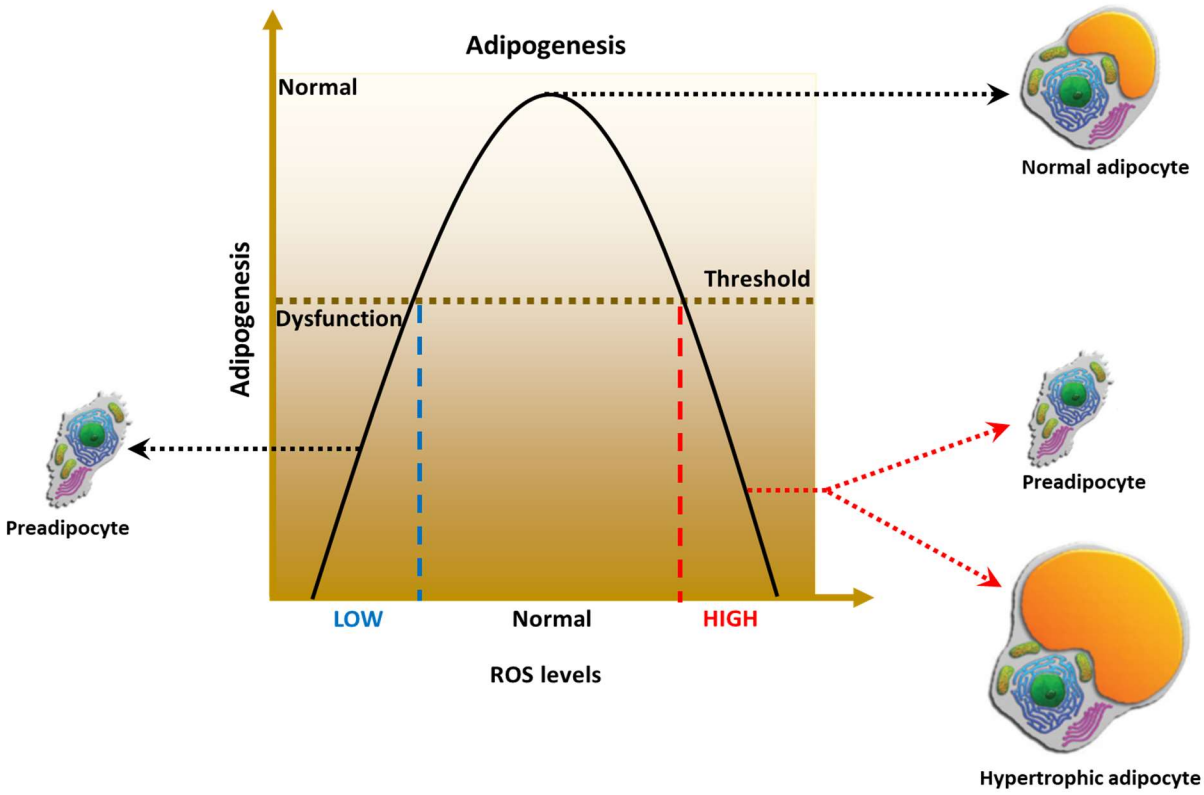

Fig. 4: The importance of physiological ROS levels for adipogenic differentiation. Several studies have suggested that ROS levels play a critical role in adipogenesis, where the timing and amount of ROS generation determine the initiation of a normal adipogenic process versus a pathological obese response. Normal ROS levels are obligate for adipogenesis and mediate a well-orchestrated process for the cell to become a mature adipocyte. However, below or above a certain ROS level adipogenesis fails to progress and/or is associated with adipocyte hypertrophy. (Adapted from: Castro et al., 2016).

To summarize, numerous studies suggest that normal mitochondrial function is needed to enable and drive adipogenesis in adipose tissue, and mitochondrial defects affect the differentiation capacity, and possibly, the expansion potential, of adipose tissue.

1.8.3 Metabolic checkpoints in determining stem cell differentiation and cell fate decisions

In addition to growth factors and extracellular matrix cues, cellular bioenergetics has also been shown to provide important signals for the self-renewal and differentiation potency of stem cells (Rehman, 2010). The metabolic profile distinguishes the undifferentiated state from the differentiated state of stem cells, with associated changes in mitochondrial morphology and a shift from glycolysis to mitochondrial oxidative phosphorylation (Wanet et al., 2015). Stem cells are particularly dependent upon glycolysis to support cellular growth and division and exhibit a high rate of glycolytic lactate production compared to differentiated cells. A high glycolysis rate in stem cells, together with reduced OxPhos, provides an essential supply of the cofactors and substrates necessary for the biosynthetic reactions underlying their expansion (Pereira et al., 2014). Moreover, reliance on glycolysis and circumventing OxPhos helps in maintaining low levels of ROS, thereby preventing oxidative damage to cellular lipids, proteins, and DNA associated with excessive ROS accumulation (Maryanovich and Gross, 2013). Further, it has also been proposed that mitochondria in undifferentiated stem cells are immature with lower transcription of electron transport chain components, and hence, are unable to fully execute oxidative phosphorylation (Chung et al., 2007; St John et al., 2007; Prigione et al., 2010). However, after specified lineage differentiation, mtDNA levels and emerging energy requirements are gradually increased in support of mitochondrial biogenesis (Cho et al., 2006). In differentiating stem cells, the development of the mitochondrial network precedes the loss of the pluripotency markers, OCT4

and Nanog (Mandal et al., 2011). Mitochondrial biogenesis and a metabolic shift toward OxPhos have been shown to be early events in the differentiation of stem cells towards osteogenic (Chen et al., 2008), neural (Calvo-Garrido et al., 2019; Zheng et al., 2016), and hepatogenic (Wanet et al., 2014) lineages.

Further, regulatory pathways that control stem cell/progenitor decisions to differentiate into specific lineages have been studied. For example, the transcriptional corepressor, p107 (Rbl1) has been shown to control a metabolic checkpoint occurring at growth arrest that affects progenitor cell fates between white and pro-thermogenic adipocytes, where p107-depleted progenitors were shown to undergo a metabolic state resembling aerobic glycolysis, which is required for commitment towards pro-thermogenic brown adipocytes (Scimé et al., 2005; Porras et al., 2017).

1.9 Mitochondrial and adipose tissue dysfunction in obesity and related metabolic complications

1.9.1 Adipose tissue dysfunction in obesity

To accommodate excess energy intake during the course of obesity, adipose tissue undergoes various cellular and structural remodeling processes including: (1) adipose tissue expansion through a coordinated combination of adipocyte hyperplasia involving the generation of new adipocytes from progenitors and adipocyte hypertrophy, where existing adipocytes become enlarged to accommodate more lipids (Wang et al., 2013b); (2) recruitment of inflammatory cells to adipose tissue (Lolmede et al., 2011); and (3) remodeling of the vasculature and the extracellular matrix (ECM) to allow effective adipose tissue expansion, oxygenation, and mobilization of nutrients (Cao, 2103). However, a sustained energy imbalance, together with an inflammatory microenvironment, results in the failure of these adaptive homeostatic mechanisms, leading to

adipose tissue dysfunction characterized by secretion of pro-atherogenic, pro-diabetogenic and pro-inflammatory adipokines, abnormal lipid storage and adipogenesis, impaired fibrosis deposition, and insulin resistance (Haczeyni et al., 2018) (Fig. 5).

Preadipocyte recruitment and subsequent adipogenic differentiation (hyperplasia) in subcutaneous adipose tissue, as a response to excess dietary fat, has been reported to be the metabolically healthy way to expand adipose tissue and to protect against metabolic disease (Gustafson et al., 2015; Laforest et al., 2015). Increased adipocyte size (hypertrophy), on the other hand, has been associated with insulin resistance (Kim et al., 2015; Hoffstedt et al., 2010; Andersson et al., 2014), dyslipidemia and hepatic steatosis (Larson-Meyer et al., 2006), and is shown to be a predictor of the onset of type 2 diabetes (Weyer et al., 2000; Lonn et al., 2010). Moreover, enlarged adipocyte size has been linked to cell death and has been suggested to be the determining factor of inflammatory macrophage infiltration in adipose tissue (Cinti et al., 2005; Strissel et al., 2007).

Smaller adipocytes have been shown to be associated with an insulin-sensitive phenotype, and accordingly, have been shown to be present in the visceral fat of obese individuals who are insulin sensitive (Kloting et al., 2010) and in individuals characterized as “metabolically healthy” obese (O'Connell et al., 2010). It has been demonstrated that after bariatric surgery, subjects with the largest reduction in adipocyte size gained most in insulin sensitivity (Andersson et al., 2014). Also, it has been shown that induction of hyperplastic changes in adipose tissue (adipogenesis) alleviates symptoms of insulin resistance (Hoffstedt et al., 2010; Lu et al., 2014).

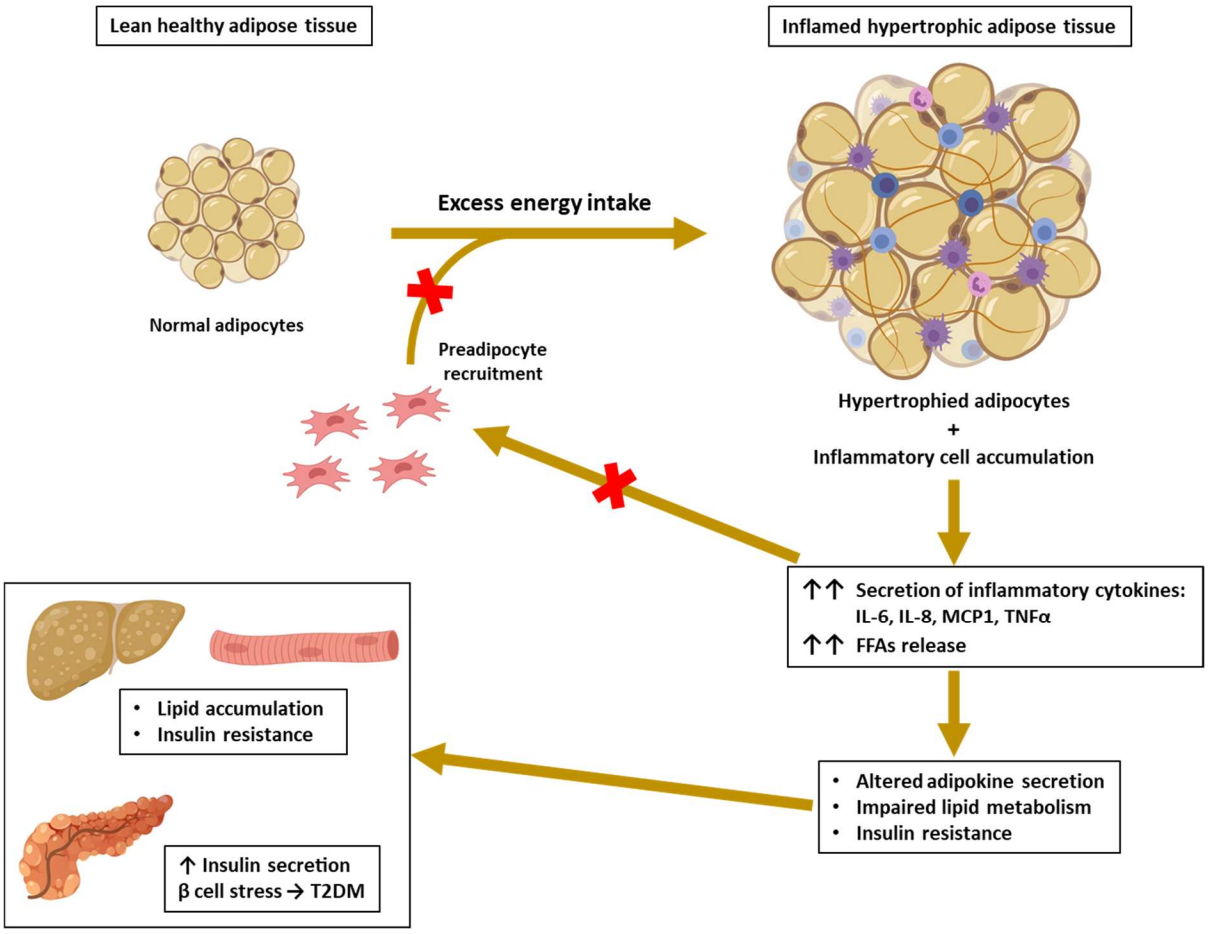

Fig. 5: Adipose tissue dysfunction in obesity. Long-term excess energy intake causes weight gain and adipocyte hypertrophy along with impaired lipid handling and altered adipokine secretion, resulting in a shift towards a pro-inflammatory state. The secreted adipokines further boost the infiltration of resident and circulating macrophages and inflammatory cells into the adipose tissue resulting in impaired preadipocyte recruitment and differentiation. Increased inflammatory adipokine secretion and aberrant lipid metabolism causes insulin resistance in the adipose tissue, which results in increased free fatty acids (FFAs) spillover, and accumulation in ectopic sites, thereby leading to whole-body metabolic complications. In muscle and liver, increased lipid content and insulin resistance is observed, with insulin-resistant adipose tissue contributing to a rise in blood glucose. In the pancreas, increased glucose concentrations cause overfunctioning of β-cells and subsequently, their exhaustion.

In addition to adipose tissue insulin resistance, hypertrophic adipocytes have also been associated with elevated levels of circulating inflammatory markers and an increased number of macrophages in adipose tissue (Skurk et al., 2007; Weisberg et al., 2003). Studies in mouse models of obesity have linked adipocyte hypertrophy with cell death (Cinti et al., 2005; Strissel et al., 2007; Gornicka et al., 2012). In one of the studies, it was shown that morphologically dying or dead adipocytes were surrounded by inflammatory macrophages, which fused to form syncytia that sequestered and scavenged residual "free" adipocyte lipid droplets and, ultimately, formed multinucleate giant cells, a hallmark of chronic inflammation.

The frequency of adipocyte death has been positively correlated with increased adipocyte size in adipose tissue of obese mice and humans. (Cinti et al., 2005). In rodents, large adipocytes secrete more inflammatory tumor necrosis factor α (TNFα) (Morin et al., 1998). Increased expression and secretion of proinflammatory adipokines such as interleukins 6 and 8 (IL-6, IL-8), TNFα, monocyte chemoattractant protein 1 (MCP1), C-reactive protein (CRP), chemerin, progranulin and granulocyte colony stimulating factor (G-CSF) have been related to adipocyte hypertrophy (Skurk et al., 2007; Jernas et al., 2006; Unamuno et al., 2018). Further, hypertrophied adipocytes have been shown to release large quantities of free fatty acids (FFAs) via macrophage-induced adipocyte lipolysis, which serve as naturally occurring ligands for Toll-like receptor 4 (TLR4), thereby inducing inflammatory changes in both adipocytes and macrophages via NF-kappaB activation (Suganami et al., 2007). Adipocyte apoptosis has also been suggested to be a key event that contributes to macrophage infiltration into adipose tissue and subsequent insulin resistance (Alkhouri et al., 2010).

Several studies have shown adipogenesis to be decreased in hypertrophic obesity (Perez et al., 2015; Gustafson et al., 2013; Isakson et al., 2009; van Harmelen et al., 2003), where ADSCs or preadipocytes isolated from SAT of obese individuals have been found to have significant reduction in their adipogenic differentiation potential. This suggests that hypertrophy of existing adipocytes, in response to chronic caloric excess, results from an inability to recruit progenitors for the formation of new adipocytes. Hence, adipocyte hyperplasia (adipogenesis) as a means of adipose tissue expansion seems to be a mechanism that could protect individuals from the metabolic complications of obesity.

Depot-specific differences in adipocyte hypertrophy have also been reported during adipose tissue expansion in response to a continued positive energy balance in high fat diet (HFD)-fed obese AdipoChaser mice. In this model, HFD-induced adipose tissue expansion occurred primarily by hypertrophy in both SAT and epididymal adipose tissue depots during the first month of HFD, whereas after prolonged HFD exposure, a wave of adipogenesis was initiated in the epididymal adipose tissue, while only negligible levels of adipogenesis occurred in SAT depots (Wang et al., 2013b).

1.9.2 Mitochondrial dysfunction in obese adipose tissue

Several animal studies using genetic or dietary models of obesity have shown a reduction in mitochondrial oxidative capacity in white adipose tissue (Wilson-Fritch et al., 2003; Choo et al., 2006). Mitochondrial number has been shown to be reduced by 50%, along with a decrease in the transcription of genes encoding mitochondrial proteins in white epididymal adipocytes obtained from *ob/ob* mice, when compared with lean mice (Wilson-Fritch et al., 2004). In another mouse model of obesity, a decrease in citrate synthase activity was accompanied by reduced

expression of PGC1α, together with a decrease in the abundance of several proteins in the mitochondrial respiratory chain. However, this didn't result in changes in mitochondrial mtDNA amounts or basal oxygen consumption levels, suggesting downregulation of mitochondrial activity at the nuclear level alone (Cummins et al., 2014).

Mitochondrial DNA content, and gene expression associated with mitochondrial respiration and transcription factors, PGC1α, PGC1β and ERRα, were found to be downregulated in *db/db* and high-fat diet fed mice compared with non-diabetic or lean mice (Rong et al., 2007). These defects were rescued upon treatment with the PPARγ agonist and insulin sensitizer, rosiglitazone, suggesting a relationship between mitochondrial function and insulin sensitivity. Similarly, 3T3-L1 adipocytes exhibited impaired insulin responsiveness due to impaired glucose transport (decreased GLUT4 translocation to the cell surface) upon induction of mitochondrial dysfunction by knockdown of a transcription factor involved in mitochondrial biogenesis, TFAM (Shi et al., 2008).

Mitochondrial dysfunction has also been associated with obese adipose tissue in human studies. Defects in mitochondrial function, in terms of reduced respiratory chain complex activity, mitochondrial membrane potential, and inorganic phosphate utilization, have been reported in SAT of obese and diabetic patients. Interestingly, non-obese diabetic individuals did not show any change in mitochondrial function, suggesting that obesity *per se* relates to impaired mitochondrial function (Chattopadhyay et al., 2011). Similarly, an inverse relationship between BMI and mitochondrial oxidative phosphorylation capacity has been shown in primary human subcutaneous adipocytes (Fischer et al., 2015). Moreover, n-3-polyunsaturated fatty acids, which are known to prevent obesity and insulin resistance, upregulate mitochondrial biogenesis and oxidative

metabolism in human adipose tissue (Flachs et al., 2005). Reduced mtDNA levels have been observed in genetically identical twins, when obese siblings are compared with their leaner counterparts, highlighting that environmentally acquired effects contribute to the regulation of mitochondrial mass and biogenesis (Pietilainen et al., 2008). Using *in vitro* differentiated human preadipocytes, it was shown that adipocytes from obese individuals have lower oxygen consumption rates after β-adrenergic stimulation compared with preadipocytes from lean subjects (Yehuda-Shnaidman et al., 2010).

1.9.3 Mitochondrial dysfunction in obesity and its associated complications: cause or consequence?

Despite ample evidence linking mitochondrial dysfunction with obesity and associated complications, like insulin resistance, in both mouse and human models, the cause and effect relationship between the changes in mitochondria and the development of metabolic complications of obesity has remained unclear. In adipose tissue, high-fat-fed mice have been shown to display mitochondrial dysfunction that was observed as a secondary feature occurring after the development of insulin resistance (Sutherland et al., 2008; Wang et al., 2014). Moreover, the inflammatory cytokine TNFα has been shown to impair mitochondrial biogenesis and function in adipose tissue in obese mice (Valerio et al., 2006). Similarly, in human preadipocytes, treatment with the inflammatory cytokine TNFα reduced the expression of respiratory chain pathway genes in healthy individuals, suggesting a role for inflammation in the development of mitochondrial dysfunction (Dahlman et al., 2006).

On the other hand, alternate studies have suggested that mitochondrial dysfunction is the underlying mechanism behind insulin resistance and inflammation. For instance, high levels of

FFAs and glucose have been reported to directly stimulate mitochondrial dysfunction in 3T3-L1 adipocytes (Gao et al., 2010). TNFα and other inflammatory cytokines can also be secreted because of dysfunctional mitochondria. Mitochondria are the sites of phospholipid synthesis for the adipocyte cell membrane (Vance, 1990), and adipocyte cell membrane lipid modifications have been shown to recruit inflammatory cells to adipose tissue (Pietilainen et al., 2011). It is thus plausible that mitochondria and their dysfunction might be involved in adipocyte cell membrane alterations and inflammatory processes of adipose tissue, potentially leading to inflammation observed in obesity.

Moreover, the mechanisms responsible for reduced mitochondrial function in adipose tissue in obesity are not yet known. It has been suggested that they involve alterations in mitochondrial life cycle, such as reduced mitochondrial biogenesis and impaired mitochondrial dynamics (fission and fusion), or defective clearance of damaged mitochondria (mitophagy), in combination with increased inflammation and damage caused by excess ROS accumulation in mitochondrial metabolism and endoplasmic reticulum (ER) stress (Boudina and Graham, 2014; Kusminski and Scherer, 2012; De Pauw et al., 2009).

1.10 Current treatment strategies for obesity and its related metabolic disturbances

Typically, the first option for weight loss is centered on a commitment to lifestyle changes, such as dietary restrictions to lower caloric intake, increased physical activity to promote higher energy expenditure, and behavior therapy to promote healthier eating habits and higher self-control (Wadden et al., 2012). The success of lifestyle modifications for obesity and avoidance of weight re-gain is only feasible if healthy routines are maintained in the long-term. Intense diet programs with meal replacement supplements and heavy exercise regimens, which may be practiced in initial

stages of weight loss, can be transitioned into practical routines that are better suited for continued maintenance of a healthy body weight. However, in most cases of obesity, the aforementioned lifestyle interventions are ineffective for long-term weight loss. In these cases, pharmacological treatments are used in tandem with dietary restrictions and physical activity to treat obesity.

According to guidelines from the Endocrine Society on the treatment of obesity, pharmacotherapy should only be used in conjunction with lifestyle changes for individuals with a BMI of 27 kg/m^2 or higher with comorbidity or for individuals with a BMI over 30 kg/m^2 (Apovian et al., 2015). In more extreme cases (BMI > 40 kg/m^2, or BMI > 35 kg/m^2 with comorbidities), patients are eligible for bariatric surgery, which is far more efficacious than the aforementioned interventions in sustaining long-term weight loss. However, due to associated surgical complications and frequent needs for re-operation, bariatric surgery is not intended for the majority of obese individuals (Choban et al., 2002).

1.10.1 Current pharmacotherapy options for the treatment of obesity

Existing anti-obesity pharmacological therapies largely act via either suppressing appetite or preventing fat absorption. There are currently five FDA-approved anti-obesity drugs and two Health Canada-approved drugs on the market (Srivastava and Apovian, 2018; Canadian obesity network, 2017).

The longest standing anti-obesity drug is orlistat, which is a gastrointestinal lipase inhibitor. By interfering with this enzyme's lipolytic function, to break down triglycerides into fatty acids, fat absorption is decreased by almost 30%. Nevertheless, there are several gastrointestinal side effects associated with this drug, such as flatulence, diarrhea and steatorrhea, but serious adversities have not been reported (Henness and Perry, 2006).

The second dual-approved medication is liraglutide, which is a long-acting human glucagon-like peptide-1 (GLP-1) agonist. Although this medication was first introduced for the treatment of type 2 diabetes, as it increases insulin secretion and decreases inappropriate glucagon secretion, it is also effective as a weight loss medication because it suppresses appetite and slows gastric emptying (Pi-Sunyer et al., 2015).

The last three drugs, lorcaserin, phentermine/topiramate and naltrexone/bupropion are only approved in the United States. Lorcaserin is an analog of 5-hydroxytryptamine (5-HT) and has properties of serotonin, a key mediator of food intake. It selectively binds to one type of serotonin receptor, 5-HT_{2C}, which results in appetite suppression and controlled caloric intake (Brashier et al., 2014). Phentermine/topiramate is a combination medication that also acts as an appetite suppressant. However, its exact mechanism of action is unknown. It is associated with the highest weight-loss results, in comparison to its competitors, but is associated with fetal harm in pregnancies, glaucoma, and adverse cognitive and psychiatric effects (Srivastava and Apovian, 2018). Naltrexone/Bupropion, a combination of an opioid antagonist and antidepressant respectively, reduces hunger in a mechanism that is not entirely understood. Due to its potential adverse effects, this medication is not advised for patients with a seizure history, high blood pressure, cardiac disease or hepatic disease (Tek, 2016).

These aforementioned pharmacological agents have been successful in weight reduction and counteracting obesity. However, each option has its limitations and is often suited for short-term use only. In addition, these on-market medications are all based on similar drug targets and modes of action. Hence, there is still a large clinical need for novel medications with minimal side effects, that are capable of creating long-term solutions for obese patients.

1.10.2 Current drug screening platforms for obesity and metabolic disorders

Healthy adipose tissue expansion occurs as a combination of hyperplasic and hypertrophic tissue expansion and maintenance of an overall anti-inflammatory state. By contrast, obesity is associated with unhealthy expansion dominated by adipocyte hypertrophy and dysfunctional adipose tissue due to increased insulin resistance, poor endocrine function, an overall pro-inflammatory state, defective mitochondrial function, and a higher degree of hypoxia and fibrosis (Ghaben and Scherer, 2019). Thus, targeting obese adipose tissue has recently gained attention for developing newer pharmacological interventions for obesity and its associated complications (Kusminski et al., 2016). To move forward in that direction, robust high-throughput primary drug screening platforms measuring adipocyte differentiation and/or unhealthy metabolic parameters are necessary.

Most current screening assays quantify adipogenesis by measuring lipid accumulation as the primary endpoint. Drug screening platforms using murine OP9 preadipocyte cells (Lane et al., 2014), human ADSCs (Foley et al., 2015), or induced pluripotent stem cells (iPSCs) (Yuan et al., 2019), based on high-throughput lipid and nuclear staining measurements to determine changes in adipogenesis, have been reported. Another high-throughput lipid stain-based microscopy assay has been developed for screening anti-obesity agents on miniaturized micro-cell patterned chips using murine 3T3-L1 preadipocytes (Kim et al., 2016). An siRNA screening assay utilizing lipid staining as an endpoint measurement has also been described for the identification of anti-obesity compounds (Sohle et al., 2012). Also, a luciferase reporter-based platform has been reported, where murine 3T3-F442A preadipocytes, stably expressing a luciferase reporter gene driven by the adipogenic specific promoter-adipocyte Protein 2 (aP2), were used to determine changes in

adipogenesis upon drug treatment (Waki et al., 2007). A similar drug screening system was developed by using human MSCs stably expressing a fluorescent reporter gene under the aP2 promoter to detect small molecule mediated changes in adipogenesis (Qin et al., 2010). Moreover, flow cytometry (Wolins et al., 2018) and image cytometry-based (Doan-Xuan et al., 2013) methods for the quantification of adipogenesis and lipid accumulation have also been described. However, they might not be amenable for use in a high-throughput drug-screening process.

The majority of these screening tools employ murine cell lines, and due to interspecies differences in physiology and metabolism, these models are not ideal for identifying anti-obesity drugs applicable to humans. Some of these platforms have used human cells, however they were of healthy origin and hence, are not a true representation of obese adipocyte differentiation that is the intended target. Thus, there appears to be a vital need to develop primary screening platforms that are more reflective of the actual drug target tissue, which is obese adipose tissue.

1.11 Summary of intent

Obesity is characterized by excessive storage of calories resulting from overnutrition in the form of triglycerides in adipose tissue, which leads to adipose tissue expansion. In response to overnutrition, adipose tissue expands primarily through a combination of: (1) hyperplasia, where the adipose tissue resident stem/progenitor cells give rise to new adipocytes, also known as adipogenesis; and (2) hypertrophy, where existing adipocytes enlarge in size to accommodate excessive triglycerides. The balance between these two modes of adipose tissue expansion has been shown to impact the overall metabolic state of an obese individual, where hyperplastic expansion has been associated with the maintenance of normal adipocyte function and is considered a metabolically healthy mechanism for adipose tissue expansion. Hypertrophic expansion on the other hand is accompanied by adipose tissue dysfunction and inflammation, where hypertrophic adipocytes have been shown to crosstalk with immune cells through cytokines, FFAs, and leukotrienes to enhance inflammation, thereby providing a metabolically unhealthy environment for adipose tissue expansion.

Adipogenesis has been studied in great detail using murine and human *in vitro* models and has been shown to be a tightly regulated process controlled by complex transcriptional and signaling cascades. However, the metabolic regulation of this process has not been studied in detail in human systems. Moreover, given the metabolic derangements observed in obesity, more studies are required to understand the metabolic control of adipogenesis in the context of obesity. A better understanding of human adipogenesis in the context of obesity would ultimately aid in the design of targeted pharmacological approaches aimed at increasing adipogenesis over adipocyte hypertrophy to treat metabolic disorders.

Studying adipogenesis *in vitro* in the context of metabolic disorders has been largely inconsistent primarily due to the failure to properly represent the metabolic intricacies experienced by a metabolically unhealthy obese patient. Thus, there remains a lack of *in vitro* models that are able to capture the details of molecular and metabolic landscape of an obese microenvironment. Therefore, **I hypothesize that resident stem cells isolated from morbidly obese individuals will provide an *in vitro* model that closely recapitulates the pathways uniquely regulating aberrant adipogenesis in human obesity, allowing for the identification of therapeutic targets for improving metabolic health in an obese setting**.

To address my hypothesis, I defined the following four specific objectives:

(1) Investigate metabolic pathways at molecular and functional levels by using ADSCs *in vitro* to create a comprehensive map of healthy human adipogenesis
(2) Develop a patient-derived cellular model for studying obesity *in vitro*
(3) Identify molecular and metabolic switches that can serve as markers for aberrant adipogenesis in obesity
(4) Develop a drug screening platform that targets aberrant adipogenesis

First, I needed to create a metabolic map of healthy human adipogenesis that would serve as a useful model to compare the pathways that are dysregulated in obese adipogenesis. Studying cellular bioenergetics by using molecular and functional techniques along the time course of human adipogenesis in ADSCs isolated from subcutaneous adipose tissue depots of healthy donors allowed me to create a complete metabolic map of human adipogenesis that captured both early and late stages of the process (Chapter 2).

I then isolated ADSCs from subcutaneous adipose tissue samples obtained from our cohort of patients, encompassing overweight and obesity classes over a wide spectrum of BMIs ranging from 27.1 to 52.4. Upon characterization of ADSCs isolated from across the BMI range, I identified that ADSCs from class III obese (morbidly obese) individuals were most reflective of an obese environment in terms of defects in adipogenesis and consistency across multiple patients. Utilizing this cellular model of obesity, with the help of transcriptomic, proteomic and functional bioenergetics tools, I identified signaling and metabolic defects underlying blocked adipogenic differentiation of obese cells that I could partially rescue upon improving their metabolic health. This provided a proof-of-concept that there is a potential to improve adipogenesis defects in obese cells with small molecule-mediated pharmacological intervention (Chapter 2).

Through functional metabolic and global transcriptomic analyses of obese versus healthy patient-specific ADSCs and developing adipocytes, I observed a dysregulation in both Wnt signaling and mitochondrial metabolic gene expression and sought to clarify how Wnt signaling regulates adipogenesis in my model system (Chapter 3). As my studies provided me with a more in-depth understanding of the pathophysiology of obesity with potential targetable pathways towards treatment of obesity, I proceeded to develop a novel high-throughput drug-screening platform to identify small molecule compounds that improve adipogenesis and metabolic health in an obese setting (Chapter 4).

Collectively, the studies presented in this thesis advance our understanding of the unique regulators of adipogenesis in an obesity-specific *in vitro* cellular model that can be tangibly targeted for developing disease-selective therapies.

CHAPTER 2

Morbid obesity impairs stem cell function by blocking early metabolic switches during adipocyte differentiation

Preface

This chapter is prepared as an unpublished manuscript, in preparation for submission. The authors include:

Kanwaldeep Singh, Brandon Law, Derek Auyeung, Sansi Xing, Arianna Dal-Cin, Yu Lu, Eva Szabo and Bradley Doble

I designed the study, conducted the experiments, analyzed the data, assembled the figures and wrote the manuscript together with Dr. Brad Doble. Brandon Law and Derek Auyeung performed western blotting experiments. Sansi Xing assisted with proteomics sample preparation. Dr. Arianna Dal-Cin collected and provided patient samples, patient data and clinical advice. Dr. Yu Lu designed proteomics analyses and helped with the proteomic bioinformatics. Dr. Eva Szabo helped with study design and interpretation of data.

Chronic caloric overload in obesity is associated with reduced adipogenesis. Adipose tissue in the context of obesity expands primarily through hypertrophic expansion of existing adipocytes. Adipocyte hypertrophy disrupts adipose tissue homeostasis, resulting in adipose tissue dysfunction, which is characterized by increased secretion of pro-inflammatory adipokines and

abnormal lipid storage thereby contributing to the development of insulin resistance. Adipogenesis is considered a metabolically healthy way for adipose tissue to expand, making it critical to study the molecular mechanisms that contribute to reduced adipogenesis in obesity and metabolic disorders. The primary goal of this study was to advance our understanding of molecular and metabolic factors regulating aberrant adipogenesis in the context of obesity.

In this manuscript, we examined, in depth, the molecular and functional differences between healthy versus obese patient-specific adipose tissue derived stem cells (ADSCs) over the time course of adipogenic differentiation. Our study has revealed that morbidly obese patient-specific ADSCs display blocked differentiation as a result of aberrant metabolic regulation, which limits their capacity to switch on metabolism-specific transcription and signaling pathways, thereby dysregulating mitochondrial metabolic pathways, insulin sensitivity, and fatty acid metabolism related genes. When compared to healthy counterparts, obese ADSCs remain immature, insulin insensitive, and metabolically quiescent. Our study provides proof-of-concept data in support of the development of new therapeutics by using obese patient-specific cell models that enable the targeting of aberrant metabolic pathways, towards the treatment of obesity.

Morbid obesity impairs stem cell function by blocking early metabolic switches during adipocyte differentiation

Highlights

- Adipocyte differentiation is significantly altered in morbid obesity
- Glycolytic and mitochondrial dysfunction is observed in morbid obesity resulting in failure to meet energy demand during adipocyte differentiation
- Insulin sensitization during adipocyte differentiation is impaired in obesity and is associated with blocked stem cell to preadipocyte conversion
- Adipocyte differentiation-specific pathway activation is delayed in obesity

Summary

Adipogenesis involves a complex interaction between cellular bioenergetics and insulin signaling. However, it is unclear how these processes are regulated in human obesity. In this study, by using human adipose tissue resident/derived stem cell (ADSCs), we explored the interplay between metabolic function and insulin signaling during metabolic switching in healthy versus morbidly obese settings. Obese ADSCs showed significantly decreased adipogenesis and impaired induction of insulin signaling compared to healthy cells. The severity of these alterations was found to be positively correlated with impaired metabolic triggers in both glycolysis and oxidative phosphorylation. The metabolic derangements, coupled with increased accumulation of reactive oxygen species (ROS), resulted in overall metabolic quiescence during adipocyte differentiation.

Induction of mitochondrial activity rescued adipogenic differentiation in obese ADSCs. Our findings demonstrate the importance of cellular bioenergetics during the early stages of adipogenesis and provide novel avenues for therapeutically targeting obese adipose tissue.

Introduction

We are in the midst of an obesity epidemic. As a consequence, interest in understanding the pathophysiology of obesity has gained tremendous momentum. Nevertheless, there is a gap in our understanding of factors that drive human adipocyte development (i.e. adipogenesis) and downstream obesity.

Adipogenesis, can be divided into two parts. The first step, termed the "commitment stage," involves generation of preadipocytes (adipocyte precursor cells) from ADSCs. The second step entails terminal differentiation of preadipocytes into mature adipocytes, the "terminal differentiation stage" (Henry et al., 2012). In humans, adipogenesis largely contributes to formation of white adipose tissue, which regulates energy homeostasis (balance, storage and expenditure of energy) and synthesis and release of a variety of adipokines, such as adiponectin and leptin (Hauner, 2005; Fu et al., 2005; Stern et al., 2016). These adipokines, in turn, promote cell proliferation and accelerate adipocyte differentiation by enhancing gene expression of adipocyte specific markers i.e. CCAAT-enhancer binding protein-alpha (C/EBPα), peroxisome proliferator-activated receptor gamma (PPARγ), sterol regulatory element-binding protein-1c (SREBP-1c). They also regulate insulin homeostasis and glucose and lipid metabolism, resulting in increased lipid content (Stephens, 2012; Rosen and Spiegelman, 2006; Rosen and MacDougald, 2006). Thus, dysregulation of energy homeostasis or pathways involved with adipocyte

differentiation can result in obesity (Arner et al., 2011; Bergen, 2017; Klöting et al., 2010).

While it is well established that mitochondrial biogenesis plays a major role in metabolism and energy homeostasis, the functional and molecular mechanisms underlying mitochondrial biogenesis during healthy and obese human adipogenesis remain to be fully delineated. Mitochondrial dysfunction and indications of mitophagy induction have been observed in high fat diet-induced obesity in mice (Kim et al., 2013). In murine models, the interaction between adipogenesis and mitochondrial biogenesis has also been examined through evaluation of the relationship between two transcription factors known to regulate both of these processes, namely PPARγ and its co-activator, peroxisome proliferator-activated receptor gamma coactivator 1 alpha (PGC1α) (De Pauw et al., 2009). Treatment of 3T3-L1 adipocytes with a PPARγ agonist increased the number of mitochondria in individual cells and altered mitochondrial structure and gene expression (Wilson-Fritch et al., 2003; Wilson-Fritch et al., 2004). In addition, higher oxidative capacity has been observed during differentiation of human mesenchymal stem cells (MSCs) and 3T3-L1 adipocytes, with oxygen consumption coupled to ATP synthesis in the early stages of differentiation and progressively uncoupled during maturation to adipocytes, with a concomitant increase in PGC1α levels (Ducluzeau et al., 2011, Zhang et al., 2013, Wilson-Fritch et al., 2003).

ROS production has been shown to play a regulatory role during 3T3-L1 adipocyte and human MSC differentiation (Ducluzeau et al., 2011), where ROS generation was required for adipogenesis (Tormos et al., 2011). The timing and the amount of ROS generation determines the initiation of a normal adipogenic process *versus* pathological obese responses (Frohnert et al., 2011; Galinier et al., 2006). For example, previous studies using murine obesity models showed that oxidative stress due to over production of ROS can inhibit insulin signaling and alter lipolysis,

resulting in insulin resistance in adipose tissue of obese mice (Curtis et al., 2010; Ruskovska and Bernlohr, 2013). Furthermore, studies utilizing a high-fat diet regime in mice revealed that mitochondrial dysfunction might result from the onset of insulin resistance and changes in glucose tolerance (Sutherland et al., 2008; Wang et al., 2014). However, whether these findings in rodents will hold true in humans requires further investigation, and the mechanisms of mitochondrial dysfunction and their impact on adipogenesis in the context of obesity remain unclear.

Previous studies have identified a functional link between metabolism and stem cell development (Shyh-Chang et al., 2013; Ochocki and Simon, 2013). As stem cells differentiate, their dependence on glycolysis decreases with a concomitant increase in their requirements for oxidative phosphorylation-driven pathways (Shyh-Chang et al., 2013). While the metabolic switches have been explored functionally and mechanistically in healthy and diseased settings for some adult stem cell types, such as hematopoietic and neural stem cells (Yu et al., 2013; Suda et al., 2011; Saito et al., 2015, Khacho et al., 2016, Hamilton et al., 2015), a similar in-depth understanding of the metabolic changes occuring during adipogenesis of ADSCs from healthy versus obese individuals remains to be elucidated. Only a few studies have explored metabolic switching during adipocyte differentiation, and these studies were focused on murine 3T3-L1 cell differentiation (Halama et al., 2016).

Here, we demonstrate that glycolytic and mitochondrial dysfunction is inherent to morbidly obese human ADSCs, and as a result these cells are refractory to metabolic triggers and show mitochondrial functional defects resulting in aberrant adipogenesis. While obese ADSCs express Insulin-like growth factor 1 receptor (IGFR1), the switch from IGFR1-dependent pathways to insulin receptor (INSR) signaling that takes place during the early stages of differentiation does

not occur, thus these cells also show hallmarks of insulin resistance during the early differentiation process. The block in obese ADSC adipogenesis could be rescued, in part, by improving mitochondrial function, which resulted in improved lipid accumulation and decreased ROS production. Our results indicate that metabolic check points during early differentiation steps are important for establishment of healthy adipogenesis. In addition, our study demonstrates that there are profound differences in healthy versus obese ADSCs and their adipocyte differentiation and maturation trajectories, suggesting that targeting obese ADSC and adipocyte mitochondrial biogenesis may provide an important avenue towards treatment of obesity.

Results

For this study, ADSCs were isolated by collagenase digestion of abdominal subcutaneous adipose tissue obtained from age- and gender-matched healthy and obese donors (Fig. S1). Prior to using the ADSCs for experiments, the cells were confirmed to be bona fide mesenchymal stem cells by performing characterization based on three criteria laid out by International society for cellular therapy (ISCT) (Dominici et al., 2006; Bourin et al., 2013): (1) examining their morphology and adherence to tissue-culture plasticware, (2) performing flow cytometry for surface MSC markers: CD73, CD90 and CD105, and (3) examining tri-lineage differentiation potential into adipocytes, chondrocytes and osteoblasts (Fig. S2). Fibroblast-Colony forming unit (CFU-F) assay was performed using stromal vascular fraction (SVF) and no significant differences in the colony forming efficiency were observed for the mesenchymal progenitors in the SVF across healthy, overweight and obese samples.

ADSCs from morbidly obese donors show significant reduction in adipogenesis

To investigate the effect of Body Mass Index (BMI) on adipogenic differentiation potential, ADSCs from our cohort of patients (n=28) with varying BMIs (healthy (BMI<25), overweight (BMI between 25.1 and 29.9), Class I obese (BMI between 30 and 34.9), Class II obese (BMI 35 to 40) and Class III obese (BMI over 40) were subjected to adipogenic differentiation over a 14 day timeline (Fig. 1A and 1B). The degree of adipogenesis was quantified by using Oil Red O (ORO) staining and extraction at days 7 and 14 of adipogenesis (Fig. 1C) and further confirmed by BODIPY (Boron-dipyrromethene) staining at day 14 of adipogenic differentiation (Fig. 1D and 1E). ADSCs from healthy (n=6) individuals showed highest adipogenic potential and the extent of ADSC adipogenesis decreased as donor BMIs increased, with morbidly obese (Class III-BMI over 40) ADSCs (n=6) showing the most significant reduction in adipogenesis as measured by ORO accumulation over the course of adipogenesis. This suggests that there is a negative correlation between increasing BMI and the adipogenic differentiation potential (Fig. 1A). Since morbidly obese (Class III) ADSCs showed the most significant reduction in adipogenesis, further experiments were focused on characterizing and elucidating the mechanisms underlying the severely impaired adipogenesis in these ADSCs. In subsequent experiments this subtype of obese cells will be simply referred to as "obese ADSCs."

Obese cells showed reduced mRNA expression (Fig. 1F) and protein levels (Fig. 1H, 1I) of master regulators of adipogenesis, PPARγ and C/EBPα during the adipogenesis timeline compared to healthy counterparts. Furthermore, obese ADSC-derived adipocytes, when compared to their healthy counterparts, showed significantly lower levels and delayed expression of mature adipocyte markers such as fatty acid transporter - CD36, PLIN1 (Perilipin), ACC (acetyl CoA

carboxylase), FABP4 (fatty acid binding protein 4), FASN (fatty acid synthase) at the mRNA (global gene expression analysis; Fig. 1F) and protein levels (Fig. 1G, 1J-M and Fig. S3A-B). These results suggest that there is a significant loss and shift in adipogenesis in obese ADSC derived adipocytes compared with healthy counterparts.

To further explore the lack of maturation of obese ADSC-derived adipocytes, we examined the expression of MSC markers, CD73 and CD105 in healthy and obese cells during the adipocyte differentiation timeline to determine if there were any defects in their differentiation and specification trajectory. Both healthy and obese ADSCs displayed high expression of MSC markers at Day 0, with marker levels over 95% (Fig. S2). However, healthy ADSCs lose MSC marker expression (CD73 and CD105) gradually over the differentiation timeline, while obese cells retain significantly higher levels of CD73 compared to healthy counterparts at mRNA and protein levels, as examined through global gene expression analysis and western blotting, respectively (Fig. S3C-E).

Moreover, healthy cells gradually switch from Insulin-like growth factor 1 receptor (IGF1R) to Insulin receptor (INSR) in order to be able to respond to insulin and initiate downstream insulin signaling in response to adipogenic stimulation during the course adipogenesis. Differentiated healthy ADSCs displayed a greater than 3-fold increase in INSR expression levels along with a decrease in IGF1R expression, a pattern that was lacking for differentiated obese ADSCs (Fig 1G, 1N and 1O). Therefore, obese cells fail to exhibit a switch from IGF1R to INSR expression for efficient insulin signaling, suggesting that the obese cells remain in an immature and insulin insensitive state during adipogenesis.

Overall, these results indicate that obese ADSCs have significantly limited adipogenic potential compared to healthy cells, which is evidenced by a pronounced attenuation of their adipogenic differentiation *in vitro*. Moreover, these results suggest that obese ADSCs retain obesity-associated insulin insensitivity during *in vitro* expansion and differentiation and show signs of insulin insensitivity in adipocytes derived from them.

Obese ADSCs show a distinct gene expression profile compared to healthy cells during adipogenesis *in vitro*

We performed global gene expression on healthy and obese cells at different timepoints over the differentiation time course to capture and identify differential gene expression at early (days 0, 1, 3) and late differentiation stages (days 7 and 14). We employed Clariom S human HT gene chip analysis for mRNA expression and tandem mass tag-mass spectrometry (TMT-MS) analysis for global protein expression.

Gene expression correlation among all the differentiation timepoints was examined by using Spearman's rank-order correlation matrix, and as expected, the timepoints with the highest correlation were observed on the diagonal of the matrix. Very high gene expression correlation was observed among early timepoints: days 0 and 1 (rho values between 0.9-1) and among late timepoints days 7 and 14 (rho values between 0.9-1). Interestingly, correlation among different timepoints along the differentiation time course (from days 0 to 14) showed a higher reduction in healthy cells (rho values from 1 to 0.75) as compared to obese cells (rho values from 1 to 0.85) suggesting a greater degree of similarity between obese ADSCs and obese adipocytes compared to similarities between healthy ADSCs and healthy adipocytes (Fig. 2A).

Protein expression correlation also showed a similar pattern between healthy and obese timepoints (Fig. 2B), where similarities among ADSCs and adipocytes were greater for the cells originating from obese patients versus healthy individuals. The similarities were reduced if the same comparison was made between cells of the same stage derived from healthy versus obese patients.

We correlated healthy and obese cells based on their mRNA expression and protein abundance across all the timepoints tested and observed that the overall correlation between gene expression and protein abundance was lower than gene-gene and protein-protein correlations. However, gene-protein comparisons also exhibited a similar pattern of higher correlation between ADSCs and adipocytes from obese donors as compared to correlation between ADSCs and adipocytes from healthy individuals. Moreover, later differentiation timepoints (days 7 and 14) showed better correlation between gene- and protein-expression in both healthy and obese conditions compared to early differentiation timepoints (days 0, 1 and 3) (Fig. 2C).

We also examined changes in mRNA and protein expression ratios between healthy and obese samples at different timepoints, which showed a positive correlation values (rho values 0.39 – 0.60) at all the timepoints suggesting a linear relationship between mRNA and protein changes, which further shows that transcript levels are indicative of protein expression, particularly at later differentiation timepoints (days 7 and 14 with rho values of 0.60 and 0.59 respectively) (Fig. 2D).

Principal component analysis (PCA) revealed that healthy samples had a gene expression pattern distinct from that observed for obese samples, collected throughout their transition from ADSCs (day 0) to mature adipocytes at day 14 of adipogenesis, at both mRNA (Fig. 3A) and protein expression levels (Fig. 4A). This pattern held across all the healthy and obese patients,

which indicates that it is independent of genetic background. At the ADSC stage (day 0), obese and healthy cells cluster together. However, they failed to show a similar trajectory along the adipogenesis timeline. PCA analysis and hierarchical gene clustering indicate that late differentiation stage obese cells (days 7 and 14) cluster together with early differentiation stage healthy cells (day 3) (Fig. 3A-B and Fig. 4A-B). These results, together with correlation analysis, suggest that obese ADSCs fail to initiate transcriptional pathways that are required for normal adipogenesis.

We then examined the transcript and protein expression patterns and pathways that are differentially regulated between healthy and obese samples. We evaluated the number of differentially expressed genes and proteins during healthy vs obese adipogenesis and performed functional clustering and enrichment of the genes upregulated during the healthy adipogenic differentiation timeline in Reactome 2016, Kyoto Encyclopedia of Genes and Genomes (KEGG) 2019, GO biological processes 2018 and GO cellular compartment 2018 databases (Fig. 3C-E and Fig. 4C-E). The healthy cells showed a striking difference in gene expression as early as day 1 of differentiation, showing upregulation in lipid biosynthesis, fatty acid metabolism, mitochondrial biogenesis and insulin signaling pathway genes. Days 3, 7 and 14 showed a similar pattern of upregulated genes at both mRNA and protein levels during the course of healthy ADSC adipogenesis (Fig. 3D and Fig. 4D). By day 3 of differentiation, healthy cells exhibited an enrichment of triglyceride synthesis and metabolism related gene clusters (i.e. lipid, fatty acid and glucose metabolism), with mitochondrial metabolism genes showing highest enrichment that continued into the late differentiation stages as well (days 7 and 14). Consequently, there is also a set of genes that is upregulated by day 3 of differentiation and remains upregulated through days

7 and 14 in healthy versus obese cells. This set of genes was also found to be enriched in mitochondrial metabolism pathway-specific factors (Fig. 3F). Accordingly, gene clustering of upregulated genes in healthy cells showed highest enrichment for mitochondria- and lipid droplet-localised genes by as early as day 3 of differentiation, and this enrichment was maintained until day 14 of differentiation (Fig. 3E and 4E).

These results show that lipid biosynthesis, insulin signaling and metabolic pathways that are essential for cellular transitions towards the formation of mature adipocytes fail to trigger in obese cells during the early differentiation stages.

Obese cells display a gene signature reflecting altered glucose metabolism and mitochondrial biogenesis during adipogenesis

Since our functional gene clustering and enrichment analyses from transcriptomics and proteomics identified metabolic pathways to be the most enriched cluster, we further looked at the gene expression of various enzymes involved in major cellular energy-generating pathways. We first looked at the expression of enzymes involved in glycolysis by global gene expression analysis and calculated log2 fold change in the expression of these genes with respect to day 0 of differentiation. Our analysis showed a significantly higher enrichment of glycolysis pathway genes in healthy cells versus obese cells along the adipogenesis timeline (Fig. 5A) These results were further confirmed at the protein level for glycolysis enzymes, including hexokinase 2 (HK2), Aldolase, fructose-bisphosphate A (ALDOA) and 6-phosphofructo-2-kinase/fructose-2,6-biphosphatase 3 (PFKFB3), which showed a similar increase in levels in healthy cells compared to obese cells during adipogenic differentiation (Fig. 5B-D). Moreover, the genes that were

upregulated in healthy adipocytes at day 14 of differentiation were mapped onto glycolysis pathway (Fig. 5E).

In addition, we examined the gene expression of various mitochondrial pathways over the time course of differentiation in healthy versus obese settings. Using the global gene expression dataset, we found an increase in mitochondrial pathways and genes associated with mitochondrial function (i.e. mitobiogenesis markers, mito-fission/fusion, TCA cycle, oxidative phosphorylation, fatty acid metabolism) over the timeline of healthy adipocyte differentiation, with several fold increase of these gene sets over the time course of differentiation (Fig. 6A). This pattern was minimal to absent during obese adipogenesis. Analysis of protein levels by Western blotting for mitochondrial markers (SDHA, COX IV, TFAM, TOMM20, IMMT) (Fig. 6B-F), mitochondrial-DNA encoded proteins, MT-ND1 and MT-ND5 (Fig. 6G and 6H) and respiratory chain complexes, complex I-V (Fig. 6I and 6J) throughout healthy vs obese adipogenesis further confirmed this enrichment at the protein level for healthy adipocytes and a lack of this increase for obese counterparts. Further, we mapped the genes upregulated in healthy adipocytes at differentiation endpoint (day 14) on TCA cycle, electron transport chain (ETC), fatty acid synthesis and lipid biosynthesis pathways (Figs. 6K, 6L, S4 and S5).

We examined the gene expression of some of the adipogenesis, glycolysis and mitochondrial function pathway associated genes in the healthy and obese ADSCs (day 0 of differentiation). ADSCs from healthy and obese patients did not exhibit any conclusive differences in the gene expression of any of these three pathways suggesting that the aberrations in glycolysis, adipogenesis and mitochondrial function are inherent in obese ADSCs, however they show up only upon adipogenic stimulation during the course of differentiation (Fig. S7).

Obese cells exhibit altered cellular bioenergetics during adipogenesis

Since our gene expression results identified alterations in metabolic pathways in early and late stages of differentiation in obese cells, our next aim was to confirm these transcriptomics and proteomics findings by performing functional cellular metabolism assays in healthy and obese settings. We measured oxygen consumption rate (OCR) as a measure of mitochondrial respiration in healthy and obese cells over the adipogenic differentiation time course and calculated four mitochondrial functional activity parameters: basal respiration, ATP production, maximal respiration and spare respiratory capacity.

Obese adipocytes showed a significant reduction in all four mitochondrial function parameters compared to the healthy counterparts (Fig. 7A-B). Once we analyzed these parameters over the time course of adipogenesis, we observed that healthy cells exhibited significantly higher basal and maximal respiration, ATP production and spare respiratory capacity by day 7 into the adipogenic differentiation as compared to obese cells, and this pattern was maintained up to day 14 of differentiation (Fig. 7C).

We also examined glycolysis over the timeline of adipogenesis by measuring proton efflux rate specific to glycolysis (glycoPER) in healthy and obese ADSCs and calculated glycolytic functional parameters: basal glycolysis and compensatory glycolysis. Glycolysis increased gradually in healthy cells during adipogenesis compared to obese cells (Fig. 7D-E). Healthy ADSCs showed significant increase in compensatory glycolysis compared to obese cells as early as day 3 of adipogenic differentiation (Fig. 7F). Furthermore, when plotted on an OCR vs glycoPER energy map, the day 14 differentiated obese adipocytes appeared to be in a metabolic quiescent state versus healthy counterparts, which were highly energetic (Fig. 7G). Taken together,

these results suggest a positive correlation between impaired adipogenesis and metabolic quiescence at the cellular level in obese ADSCs.

To reinforce this positive association between mitochondrial function and adipogenesis, we took a small molecule approach and inhibited mitochondrial activity using ETC complex inhibitors, Oligomycin A (complex V inhibitor), Antimycin A (complex III inhibitor), and Rotenone (complex I inhibitor), in healthy ADSCs. Upon inhibition of the individual ETC complexes in healthy ADSCs, we observed a dose dependent reduction in adipogenesis with all 3 inhibitors (Fig S6A), with a concomitant induction of mitochondrial dysfunction (Fig. S6B). This suggests that the lack of adipogenesis in an obese setting is due, in part, to the mitochondrial defects that we observed in morbidly obese patients.

Obese cells generate and accumulate more ROS during adipogenesis

We examined oxidative stress during adipogenesis in obese and healthy cells by measuring the accumulation of mitochondrial superoxide species and cellular ROS with MitoSox and CellRox DeepRed stains, respectively, followed by flow cytometry. Obese adipocytes (days 7 and 14 of adipogenic differentiation) generated and accumulated significantly more cellular ROS during adipogenesis than healthy cells (Fig 8A-B). Moreover, the cellular ROS accumulation gradually increased in healthy adipogenesis, peaking at day 7, followed by a decrease in ROS levels as the cells transitioned into mature adipocytes by day 14 differentiation. However, in obese samples, ROS levels plateaued at day 7 and remained high until day 14 differentiation (Fig. 8A-B). Similarly, mitochondrial superoxide accumulation was found to be significantly higher in obese adipocytes compared to healthy counterparts at the differentiation endpoint (day 14) (Fig. 8C-D).

Overall, these results indicate that obese cells have alterations in their molecular and functional metabolic profiles, which together with excessive cellular and mitochondrial ROS accumulation, results in altered adipogenic potential in an obese setting.

Promoting mitochondrial function rescues adipogenesis in obese cells

Given that the obese samples are exhibiting hallmarks of mitochondrial dysfunction at both the molecular (Fig. 3D-F, Fig. 4D-E and Fig. 6) and functional levels (Fig. 7A-C, G), we then aimed to determine if the impaired adipogenesis observed in obese ADSCs could be rescued by improving mitochondrial metabolism and function in these cells. Lipoamide has been shown to improve mitochondrial biogenesis and insulin resistance in murine 3T3-L1 adipocytes (Shen et al., 2011) and to alleviate oxidative stress in retinal pigment epithelial cells (Zhao et al., 2015; Li et al., 2008). RTA-408 (also known as omaveloxolone) is a Nrf2 inducer, shown to improve mitochondrial defects and oxidative stress in models of neurological disorders (Abeti et al., 2018). Hence, we treated obese ADSCs with 10 μM lipoamide and 100 nM RTA-408 in an effort to induce mitochondrial function along the adipogenesis timeline. Lipoamide and RTA-408 treatment resulted in improved adipogenesis as indicated by increased ORO staining (Fig. 9A). We also observed higher gene expression of adipogenesis (PPARγ, C/EBPα, FASN and FABP4) and mitochondrial markers (COXIV, TOMM20 and TFAM) versus control cells in both lipoamide (Fig. 9B) and RTA-408 (Fig. 9C) treated obese patient derived cells and further confirmed this upregulation at protein level (Fig. 9D) for PPARγ, CEBPα, ACC, FASN, PLIN1 and FABP4 (adipogenesis markers) and COXIV, TOMM20, TIMM23, TFAM, MT-ND1 (mitochondrial markers). Moreover, this increase in expression of adipogenesis and mitochondrial markers was accompanied by a concomitant decrease in the expression of MSC marker, CD73 (Fig. 9D).

These results provide additional evidence in support of disturbed cellular metabolism, specifically mitochondrial biogenesis, playing a critical role in the disrupted adipogenesis observed in obese ADSCs. Our results also suggest that targeting mitochondrial function may be an effective therapeutic intervention in obesity and insulin resistance.

Discussion

Obesity has been shown to influence cell proliferation, metabolism and 'stemness' in mouse and human adipose tissue derived stem cells (Perez et al., 2015; Frazier et al., 2013; Wu et al., 2013; Onate et al., 2013; Roldan et al., 2011). However, the overall results have been inconsistent across species and independent studies. This inconsistency may be due to several reasons including: 1. limited translation from murine models to humans; 2. differences in transgenic animal models used; 3. in the human studies, failure to segregate and analyze data for different classes of obesity; and 4. use of high and non-physiologically relevant concentrations of free fatty acids, TNFα, high glucose and insulin, which only partly mimics the *in vivo* obese environment to which these cells are exposed in an obese individual (Wu et al., 2013; Lo et al., 2013; Stephens et al., 1997). We used patient-specific ADSCs isolated from age-, gender- and adipose tissue depot-matched healthy, overweight and individuals from different obesity classes and showed that differences in adipogenic differentiation potential exist among different obesity classes, which provided us with a platform to study the effect of inherent metabolic derangements on adipogenic capacity across different obese patient cohorts.

In this study, using global transcriptomics, proteomics and functional cellular metabolic analyses, we identified a positive correlation between morbid obesity, metabolic derangements

and impaired adipogenesis, using obese ADSCs as a cellular model. Our data suggest that obese ADSCs fail to activate metabolic pathways and remain in an overall metabolically quiescent state. Moreover, our results show that adipogenic differentiation from ADSCs is accompanied by a several fold increase in the two major cellular energy producing pathways: glycolysis and mitochondrial respiration, which is contrary to differentiation to some other lineages, which is accompanied by a metabolic switch from glycolysis to oxidative phosphorylation (Hopkinson et al., 2017; Zheng et al., 2016; Chen et al., 2008; Hu et al., 2018), suggesting that adipogenic differentiation from ADSCs is a highly energy demanding and dynamic process.

Our analyses at early and late stages of adipogenic differentiation, show that both glycolytic and mitochondrial metabolism increases very early during adipogenic differentiation, concomitant with the enrichment for adipogenesis markers, and this metabolic pathway boost fails in an obese setting. Mitochondrial dysfunction observed in obese cells during adipogenesis could result from one or more defects in the mitochondrial life cycle, which starts with mitochondrial biogenesis, followed by mitochondrial fusion to facilitate distribution of mitochondrial DNA, lipids and proteins across all mitochondria.

Over the course of their life cycle, mitochondria accumulate damage from ROS, and to get rid of excessive ROS, they undergo fission to split into healthy and damaged mitochondria. Damaged mitochondria are then removed from the cell through mitophagy. Our results show that mitochondrial biogenesis programs do not initiate in obese cells during early phases of adipogenic differentiation, including lack of initiation of the fusion and fission related genes. This results in reduced mitochondrial function and turnover compared to healthy cells. Moreover, obese cells

exhibit oxidative stress in terms of higher generation and accumulation of mitochondrial and cellular ROS.

ROS have been shown to be required for adipogenesis (Tormos et al., 2011; Zhang et al., 2013), however, in obese ADSCs, excessive ROS accumulation, together with reduced mitochondrial turnover, results in the observed inhibition of adipogenesis. To this end, we were able to rescue the reduced adipogenesis phenotype in obese ADSCs upon treatment with lipoamide and RTA-408. Both lipoamide and RTA-408 are small molecules that induce mitochondrial biogenesis and improve oxidative stress. This suggests that development of novel small molecule drug screening platforms using morbid obese ADSCs is necessary to be able to target metabolic defects in obesity, with the goal of improving free fatty acid and lipid accumulation in obese adipose tissue and potentially alleviating insulin resistance.

Overall, in this study, we have demonstrated that the resident stem cells within adipose tissue, when isolated and differentiated *in vitro,* retain obesity-associated alterations in cellular metabolism, and hence, offer a good *in vitro* cellular model to study this disease. Moreover, we have shown that an altered metabolic landscape drives the adipogenic differentiation blockade and impaired insulin sensitivity observed in obese cells. Our study provides proof-of-concept that potential therapeutic interventions targeting cellular bioenergetics may be a viable strategy to improve adipogenesis and insulin sensitivity in morbidly obese patients. Specifically, targeting mitochondria in patients showing hallmarks of mitochondrial dysfunction provides an alternative personalized medicine approach towards treatment of morbid obesity.

Supplemental Information

Supplemental Figures S1-S7

Acknowledgements

This work was supported by Canadian Institutes of Health Research Grant and Canada Foundation for Innovation (CFI)-infrastructure fund (to Dr. Brad Doble and Dr. Eva Szabo). We thank the patients and donors for providing their consent to donate adipose tissue samples for this study. We acknowledge McMaster Genome Facility for performing the Clariom S transcriptomics. We thank Dr. Kennedy Makondo and Jamie McNicol for technical support, and all the lab members for experimental support and advice.

Materials and Methods

Human sub-cutaneous adipose tissue samples

Sub-cutaneous adipose tissue samples were obtained from healthy (BMI 21.5 ± 2.4; n=6), overweight (BMI 28.1 ± 1.4; n=2), class I obese (BMI 32.1 ± 1.0; n=3), class II obese (BMI 37.6 ± 0.6; n=2) and class III morbid obese (BMI 45.1 ± 4.3; n=6) individuals undergoing elective abdominoplasty surgery at Juravinski Hospital, Hamilton. All subjects were females aged 40-50 years. Samples were collected with consent, in accordance with the guidelines for research involving human subjects, and with the approval of the Research Ethics Board, McMaster University.

Adipose tissue samples were collected in 1X DPBS (Corning, Cat# 21-031-CV) containing 1X penicillin and streptomycin. ADSCs were isolated from adipose tissue samples as described

previously (Skurk and Hauner, 2012) (Fig. S1). Adipose tissue was minced into 1-2 mm pieces and media was filtered out using a 100 μm nylon filter. Minced adipose tissue was digested with 200 U/mL Collagenase I (ThermoFisher, Cat# 17100017) at 37°C in a shaking water-bath for 1 hour, and the degree of digestion was checked every 10 minutes. The digested tissue was filtered again using a 100 μm nylon filter to remove undigested tissue from liberated cells. Filtrate was centrifuged at 300xg for 10 minutes to pellet stromal vascular fraction (SVF) containing the ADSCs and cultured in ADSC growth media, which is composed of DMEM-F12 (Corning, Cat# 10-090-CV) supplemented with 10% FBS, 1mM L-Glutamine (Corning, Cat# 25-005-CI) and 10ng/mL bFGF (Peprotech, Cat# 100-18B). Cells were plated on standard tissue-culture plasticware at a density of 5000-7500 cells/cm^2. Cells were characterized based on minimal defined criteria (Dominici et al., 2006; Bourin et al., 2013) (Fig. S2). ADSCs were checked for fibroblast like morphology, adherence to regular cell culture plasticware and expression of mesenchymal stem cell (MSC) markers, CD73 (BD Biosciences, Cat# 561254), CD90 (BD Biosciences, Cat# 555596) and CD105 (BD Biosciences, Cat# 562408) by flow cytometry. ADSCs between passage 3 – 6 were used for all experimental procedures.

Adipogenic differentiation

ADSCs were plated at a density of 7500 cells/cm^2 and were grown until they reached confluency in ADSC growth media. Adipogenic differentiation was induced two days post confluency (day 0) with adipogenic differentiation medium composed of DMEM-F12 supplemented with 10% FBS, 1mM L-Glutamine, 250 μM isobutyl-methylxanthine (IBMX) (Sigma, Cat# I5879), 0.5μM dexamethasone (Sigma, Cat# D2915), 10 μg/mL insulin (Sigma, Cat# I9278), and 100 μM indomethacin (Sigma, Cat# I7378), followed by a complete media change

with fresh differentiation medium every other day until day 14. For lipoamide (Toronto Research Chemicals, Cat# L468710) and RTA-408 (Cayman Chemicals, Cat# 17854) treatments, cells were cultured in ADSC growth medium until confluency and differentiated in adipogenic differentiation media containing either 10μM lipoamide or 100nM RTA-408 until day 14.

ORO and BODIPY stainings

Cells were fixed with 4% paraformaldehyde (PFA) (Electron Microscopy Sciences, Cat# 15710) for 10 minutes at room temperature at days 0, 1, 3, 7 and 14 of differentiation. For ORO staining, cells were rinsed with 60% isopropanol for 2 minutes followed by staining with ORO working solution (6 parts 0.5% ORO (Sigma, Cat# O0625) in 100% isopropanol and 4 parts distilled water) for 30 minutes. Cells were washed under running water until water ran clear. Whole cell culture plate wells were scanned by using an Epson V700 photo scanner followed by imaging. For BODIPY (ThermoFisher, Cat# D3922) staining, cells were stained with 0.1 mg/mL BODIPY solution for 30 minutes at 37°C.

ORO Extraction and Quantification

ORO was extracted with 100% isopropanol for 30 minutes with gentle shaking at room temperature. Extracted ORO was quantified spectrophotometrically by measuring absorbance at 492nm against 100% isopropanol as background control.

Osteogenic differentiation

Osteogenic differentiation was performed using StemPro Osteogenesis differentiation kit (ThermoFisher, Cat# A10072-01). Briefly, ADSCs were plated at a density of 5000 cells/cm2 in ADSC growth media in 6-well plates and incubated at 37°C, 5% CO_2 for two days. Media was

replaced with pre-warmed complete osteogenesis differentiation media followed by a complete media change with fresh differentiation media every 3 days until day 21. After 21 days, cells were fixed with 4% PFA for 30 minutes at room temperature and rinsed twice with distilled water. Fixed cells were then stained 2% Alizarin Red solution (Sigma, Cat# TMS-008-C) for 3 minutes at room temperature, washed thrice with distilled water and imaged under light microscope.

Chondrogenic differentiation

Chondrogenic differentiation was performed on ADSC micromass cultures using StemPro Chondrogenesis differentiation kit (ThermoFisher, Cat# A10071-01). ADSCs were trypsin dissociated to generate cell solution of $1.6x10^7$ viable cells/ml. Micromass cultures were generated by seeding 5µL droplets of this cell solution in the center of 12-well plate wells followed by incubation for 2 hours at 37°C, 5% CO_2 under high humidity conditions. Pre-warmed complete chondrogenesis media was then added to the wells followed by a complete media change with fresh differentiation media every 2 days until day 7. At day 7, the developing chondrogenic pellets in the wells were fixed with 4% PFA for 30 minutes at room temperature and rinsed twice with DPBS. Fixed cell pellets were then stained 1% Alcian Blue solution (Sigma, Cat# TMS-008-C) for 30 minutes at room temperature, washed thrice with distilled water and imaged under light microscope.

Fibroblastoid colony-forming unit (CFU-F) assay

The CFU-F assay was used to evaluate the frequency of mesenchymal progenitors in the SVF as described (Samsonraj et al., 2015). Briefly, cells from the SVF were plated at $1x10^6$ cells in T75 tissue culture flasks in ADSC growth media and incubated at 37°C, 5% CO_2. After 2 weeks, the cells were washed with DPBS and stained with 0.5% crystal violet (Sigma, Cat# C0775).

Visible colonies were quantified only when they were greater than or equal to 50 cells, and not in contact with an adjacent colony. Efficiency was calculated by estimating the number of colonies formed per 10^5 cells plated.

Western blotting

Cell lysates for protein analysis were prepared at days 0, 1, 3, 7 and 14 of adipogenic differentiation by lysing the cells in lysis buffer containing 4% SDS, 20% glycerol in 125 mM Tris HCl, pH 6.8 and 1X protease inhibitor cocktail (ThermoFisher, Cat# 78441). Protein concentration in the cell lysates was determined by using the BCA method (ThermoFisher, Cat# 23225). Whole cell lysates (15µg/lane) were resolved on sodium dodecyl sulfate-polyacrylamide gel electrophoresis (SDS-PAGE) on 10% or 15% acrylamide/bisacrylamide gels (15% gels for detection of low molecular weight proteins: COXIV, TOMM20 and TIMM23) using a Mini Trans-Blot kit (Bio-Rad) and transferred to Immun-Blot polyvinylidene difluoride (PVDF) membranes (Bio-Rad, Cat# 1620177). Membranes were then incubated first with unconjugated primary antibodies against the protein of interest or for β-actin or Vinculin overnight at 4°C followed by incubation with horseradish peroxidase-conjugated anti-rabbit IgG or anti-mouse IgG secondary antibodies for 1 hour at room temperature. Signals were detected using a chemiluminescence horseradish peroxidase substrate (ThermoFisher, Cat# 34577) on a Bio-Rad ChemiDoc MP system.

Immunofluorescence staining

ADSCs were plated and differentiated as described above and were fixed at day 14 of differentiation using BD Cytofix/CytoPerm kit (BD Bioscience, Cat# 554714). Upon fixation, blocking was performed in 10% normal donkey serum for 1 hour at room temperature followed

by overnight incubation with primary unconjugated antibodies against CD36 (Abcam, Cat# ab133625), PLIN1 (Abcam, Cat# ab172907) and FABP4 (Abcam, Cat# ab92501) at 4 °C. The next day, cells were washed three times and stained with Alexa Fluor-647 conjugated secondary antibodies (ThermoFisher, Cat# A21244) at room temperature for 1 hour. Cells were washed three times, stained with DAPI (ThermoFisher, Cat# D3571), and then imaged.

RNA Extraction and quantitative RT-PCR

Total RNA was isolated at day 14 of adipogenic differentiation from control and lipoamide treated cells using an RNA Isolation kit (Norgen Total RNA Purification Plus Kit, Cat# 48400). Approximately 1 μg of total RNA was reverse transcribed into cDNA by using a Bioline SensiFast cDNA synthesis kit (Cat# BIO-65054) according to the manufacturer's protocol. 2μl of cDNA was used as template for each qRT-PCR reaction, using gene specific TaqMan expression assays (ThermoFisher, PPARγ assay id: Hs01115513_m1; CEBPα assay id: Hs00269972_s1; FASN assay id: Hs01005622_m1; FABP4 assay id: Hs01086177_m1; COX4I2 assay id: Hs00261747_m1; TOMM20 assay id: Hs00740685_sH; TFAM assay id: Hs00273372_s1; Cat# 4331182) and measured on QuantStudio3 Real-Time PCR detection system. Gene expression was normalized to the endogenous control, ribosomal protein lateral stalk subunit P0 (RPLP0) (ThermoFisher, assay id: Hs00420895_gH).

Glycolysis and Mitochondrial function assays

13000 cells/well were plated in Seahorse-Agilent 96-well plates (Agilent Technologies, Cat# 101085-004). For glycolysis and mitochondrial function assays on ADSCs, glycolytic rate assay (GRA) and mitochondrial stress test (MST) assays were performed a day after plating as per the manufacturer's protocol and were measured on an Agilent Seahorse XFe96 Analyzer using

GRA (Agilent Technologies, Cat# 103344-100) and MST (Agilent Technologies, Cat# 103015-100) kits respectively. For glycolysis and mitochondrial function assays conducted over the adipogenic differentiation timeline, adipogenesis was induced one day after cell plating and the GRA/MST assays were performed at days 1, 3, 7 and 14 of adipogenic differentiation. At specific time points, cells were rinsed twice with complete XF assay media, and MST and GRA assays were performed as per the instructions provided with the respective kits. XF assay media for the MST assay was XF DMEM base media without phenol red (Agilent Technologies, Cat# 103335-100) supplemented with 2.5 mM L-Glutamine, 1 mM sodium pyruvate, and 17.5 mM glucose. For the GRA assay, the same media was further supplemented with 5 mM HEPES, pH 7.4 (Agilent Technologies, Cat# 103337-100). Prior to use, the pH of all media was adjusted to 7.4 at 37 °C. The MST assay was performed using the optimized concentrations for Oligomycin (2 μM), FCCP (1 μM), and Antimycin/Rotenone (0.5 μM). The GRA assay was performed with Antimycin/Rotenone (0.5 μM) and 2-Deoxyglucose (50 mM). OCR (for the MST assay) and glycoPER (for the GRA assay) readouts were normalized to total cellular DNA content after GRA and MST assays to account for any differences in cell numbers. Cellular DNA content was measured using a CyQuant Cell Proliferation assay kit (ThermoFisher, Cat# C7026) following the manufacturer's protocol. Data analysis was performed by using Wave 2.6 desktop analysis software.

MitoSox and CellRox staining and quantification

Cells at indicated timepoints during adipogenesis were stained with 5 μM MitoSox Red (ThermoFisher, Cat# M36008) or 1 μM CellRox DeepRed (ThermoFisher, Cat# C10422) for 30

minutes at 37°C and quantified by flow cytometry on a BD LSR-II flow cytometer. Data analysis was performed by using FlowJo software.

Global Gene expression and functional gene enrichment analysis

RNA samples from 6 healthy and 6 morbidly obese cell samples were isolated at days 0, 1, 3, 7, and 14 of adipogenic differentiation, in duplicates, using an RNA Isolation kit (Norgen Total RNA Purification Plus Kit, Cat# 48400). Global gene expression analysis was performed by using Clariom S human HT gene chips at the McMaster Genome Facility and the CEL files generated were analyzed with Transcriptome Analysis Console Software (TAC version 4.0). Differentially expressed genes were identified between healthy and obese cells at the indicated timepoints, and those with fold-change >2 and $p<0.05$ were considered significant. To visualize similarity of gene expression patterns, we applied hierarchical clustering and principal component analyses methods using TAC4.0 software. To examine whether differentially expressed genes are biologically relevant, we performed functional enrichment analysis using the integrative web-based softwares, g:profiler and Enrichr, which enables the analysis of significant enrichment of genes/pathways in different databases including: Gene Ontology (GO) Consortium database, Kyoto Encyclopedia of Genes and Genomes (KEGG) database, and Reactome database (Chen et al., 2013; Kuleshov et al., 2016; Reimand et al., 2007).

Mass spectrometry and protein quantification

Proteomics analysis was performed at the Proteomics facility at Stem cell and cancer research institute, McMaster University. Briefly, whole cell lysates were prepared from cell samples were collected at days 0, 1, 3, 7 and 14 of adipogenic differentiation from 3 healthy and 3 morbid obese samples in the lysis buffer containing 8M urea and 100mM ammonium

bicarbonate. Lysates were spun down at 10000 rpm for 10 minutes and the supernatant was used for protein estimation. The proteins were reduced in 10mM tris(2-carboxyethyl) phosphine (TCEP) (10mM final) for 45min at 37°C followed by alkylation in 20mM iodoacetamide for 1 hour at room temperature and trypsin digested. The resulting peptides were labeled using tandem mass tag (TMT), and identified and quantified by Liquid chromatography–mass spectrometer (LC-MS).

Transcriptomics and proteomics integration, and gene function enrichment analysis

While transcripts were identified by official gene symbols, Uniprot IDs were used for proteins. To integrate the two, we mapped 8062 out of 8419 Uniprot IDs to official gene symbols present in the transcriptomics data using the id mapping file from the Uniprot website. Transcriptomics versus proteomics correlation analysis were performed on the log2 signal intensities for 8062 genes based on official gene symbols, for which we have matched mRNA and protein expression data in all the samples. log2 of protein expression ratios and mRNA expression ratios between healthy and obese samples at all the different timepoints (days 0, 1, 3, 7 and 14) were calculated and plotted to analyse correlation between these two datasets for all the timepoints. Differentially expressed genes were identified between healthy and obese cells at the indicated timepoints and those with fold-change >1.5 and $p< 0.05$ were considered significant. To visualize similarity of gene expression patterns, we applied hierarchical clustering and principal component analyses methods using BioVinci software. To examine whether differentially expressed genes are biologically relevant, we performed functional enrichment analysis using the integrative web-based softwares, g:profiler and Enrichr, which enable the analysis of significant enrichment of genes/pathways in different databases including: Gene Ontology (GO) Consortium database,

Kyoto Encyclopedia of Genes and Genomes (KEGG) database, and Reactome database (Chen et al., 2013; Kuleshov et al., 2016; Reimand et al., 2007).

Quantification and Statistical Analysis

Data are presented as means ± SEM. GraphPad Prism 8 was used to analyze the differences between two groups by multiple unpaired two-tailed Student's t-tests and two-way ANOVA corrected for multiple comparisons with Tukey's test as appropriate. The statistical test used and parameters (i.e. the exact n numbers and p values) can be found in the figure legends. For all experiments, a p-value less than 0.05 was considered significant.

Table 1: Key Resources Table

REAGENT or RESOURCE	SOURCE	IDENTIFIER
Antibodies		
Rabbit monoclonal anti-TIMM23	Abcam	Cat# ab116329; RRID: AB_10903878
Rabbit monoclonal anti-Vinculin	Abcam	Cat# ab129002; RRID: AB_11144129
Rabbit monoclonal anti-CD36	Abcam	Cat# ab133625; RRID: AB_2716564
Rabbit monoclonal anti-IGF1R beta	Cell Signaling Technology	Cat# 9750S; RRID: AB_10950969
Rabbit monoclonal anti-INSR beta	Cell Signaling Technology	Cat# 3025S; RRID: AB_2280448
Rabbit monoclonal anti-PLIN1	Abcam	Cat# ab172907
Rabbit monoclonal anti-FABP4	Abcam	Cat# ab92501; RRID: AB_10562486
Rabbit monoclonal anti-PPARgamma	Abcam	Cat# ab178860; RRID:
Rabbit monoclonal anti-CEBPalpha	Abcam	Cat# 40761; RRID: AB_726792
Rabbit monoclonal anti-TOMM20	Abcam	Cat# ab186734; RRID: AB_2716623
Rabbit monoclonal anti-IMMT (Mitofilin)	Abcam	Cat# ab137057
Mouse monoclonal anti-COXIV	Abcam	Cat# ab33985; RRID: AB_879754
Mouse monoclonal anti-β-Actin	Abcam	Cat# ab8224; RRID: AB_449644
Rabbit monoclonal anti-fatty acid synthase (FASN)	Cell Signaling Technology	Cat# 3180S; RRID: AB_2100796
Rabbit monoclonal anti-Acetyl CoA Carboxylase (ACC)	Cell Signaling Technology	Cat# 3676S; RRID: AB_10694239
Rabbit monoclonal anti-hexokinase 2 (HK2)	Cell Signaling Technology	Cat# 2867S; RRID: AB_2232946
Rabbit monoclonal anti-Aldolase A (ALDOA)	Cell Signaling Technology	Cat# 8060S
Rabbit monoclonal anti-PFKFB3	Cell Signaling Technology	Cat# 13123S
Rabbit monoclonal anti-SDHA	Cell Signaling Technology	Cat# 11998S
Rabbit monoclonal anti-CD73	Abcam	Cat# ab124725; RRID: AB_10976033
Mouse monoclonal anti-CD105	Abcam	Cat# ab44967; RRID: AB_726054
Rabbit monoclonal anti-mtTFA (TFAM)	Abcam	Cat# ab176558
Rabbit monoclonal anti MT-ND1	Abcam	Cat# ab181848; RRID: AB_2687504
Rabbit polyclonal anti MT-ND5	Abcam	Cat# ab138136
Total OXPHOS WB Antibody Cocktail	Abcam	Cat# ab110413; RRID: AB_2629281
Rabbit Anti-Mouse IgG H&L (HRP)	Abcam	Cat# ab97046; RRID: AB_10680920

Goat Anti-Rabbit IgG H&L (HRP)	Abcam	Cat# ab6721; RRID: AB_955447
Rabbit monoclonal anti-Vinculin	Abcam	Cat# ab129002; RRID: AB_11144129
Mouse monoclonal anti-beta actin antibody	Abcam	Cat# ab8224; RRID: AB_449644
Biological Samples		
Healthy weight patient subcutaneous adipose tissue	This paper	N/A
Overweight patient subcutaneous adipose tissue	This paper	N/A
Class I obese patient subcutaneous adipose tissue	This paper	N/A
Class II obese patient subcutaneous adipose tissue	This paper	N/A
Class III obese patient subcutaneous adipose tissue	This paper	N/A
Chemicals, Peptides, and Recombinant Proteins		
IBMX	Sigma	Cat# I5879; CAS: 28822-58-4
Dexamethasone	Sigma	Cat# D2915; CAS: 50-02-2
Indomethacin	Sigma	Cat# I7378; CAS: 53-86-1
Insulin	Sigma	Cat# I9278; CAS: 11061-68-0
basic Fibroblast growth factor (bFGF)	Peprotech	Cat# 100-18B
MitoSox Red	ThermoFisher	Cat# M36008
CellRox DeepRed	ThermoFisher	Cat# C10422
Lipoamide	Toronto Research Chemicals (TRC)	Cat# L468710; CAS: 940-69-2
RTA-408	Cayman chemicals	
Oil Red O (ORO)	Sigma	Cat# O0625; CAS: 1320-06-5
BODIPY	ThermoFisher	Cat# D3922
Critical Commercial Assays		
CyQUANT™ Cell Proliferation Assay Kit	ThermoFisher	Cat# C7026
Glycolytic Rate Assay (GRA) kit	Agilent Technologies	Cat# 103344-100
Mito Stress Test (MST) kit	Agilent Technologies	Cat# 103015-100
Deposited Data		
Raw and analyzed data (Clariom S transcriptomics)	This paper	
Raw and analyzed data (TMT-MS proteomics)	This paper	
Experimental Models: Cell Lines		
Healthy weight patient subcutaneous adipose tissue derived ADSCs	This paper	N/A
Overweight patient subcutaneous adipose tissue derived ADSCs	This paper	N/A
Class I obese patient subcutaneous adipose tissue derived ADSCs	This paper	N/A
Class II obese patient subcutaneous adipose tissue derived ADSCs	This paper	N/A
Class III obese patient subcutaneous adipose tissue derived ADSCs	This paper	N/A
Software and Algorithms		

Wave 2.6 Desktop	Agilent Technologies	https://www.agilent.com/en/products/cell-analysis/software-download-for-wave-desktop
GraphPad Prism 8	GraphPad Software	https://www.graphpad.com/scientific-software/prism/
Enrichr		http://amp.pharm.mssm.edu/Enrichr/
g:profiler		https://biit.cs.ut.ee/gprofiler/gost
Transcriptome Analysis Console (TAC) 4.0	ThermoFisher	https://www.thermofisher.com/ca/en/home/life-science/microarray-analysis/microarray-analysis-instruments-software-services/microarray-analysis-software/affymetrix-transcriptome-analysis-console-software.html
FlowJo 10.2	FlowJo, LLC	

References

Abeti, R., Baccaro, A., Esteras, N., and Giunti, P. (2018). Novel Nrf2-Inducer Prevents Mitochondrial Defects and Oxidative Stress in Friedreich's Ataxia Models. Frontiers in cellular neuroscience *12,* 188.

Arner, P., Bernard, S., Salehpour, M., Possnert, G., Liebl, J., Steier, P., Buchholz, B.A., Eriksson, M., Arner, E., Hauner, H., Skurk, T., Rydén, M., Frayn, K.N., and Spalding, K.L. (2011). Dynamics of human adipose lipid turnover in health and metabolic disease. Nature *478,* 110-113.

Bergen, W.G. (2017). Peptide-Based Regulation of Metabolism as Related to Obesity. Endocrinology *158,* 3081-3082.

Bourin, P., Bunnell, B. A., Casteilla, L., Dominici, M., Katz, A. J., March, K. L., Redl, H., Rubin, J. P., Yoshimura, K., and Gimble, J. M. (2013). Stromal cells from the adipose tissue-derived stromal vascular fraction and culture expanded adipose tissue-derived stromal/stem cells: a jointÂ statement of the International Federation for Adipose Therapeutics and Science (IFATS) and the International Society for Cellular Therapy (ISCT). Cytotherapy *15,* 641-648.

Chen, C. T., Shih, Y. R., Kuo, T. K., Lee, O. K., and Wei, Y. H. (2008). Coordinated changes of mitochondrial biogenesis and antioxidant enzymes during osteogenic differentiation of human mesenchymal stem cells. Stem cells (Dayton, Ohio) 26, 960-968.

Chen, E.Y., Tan, C.M., Kou, Y., Duan, Q., Wang, Z., Meirelles, G.V., Clark, N.R., and Ma'ayan, A. (2013). Enrichr: interactive and collaborative HTML5 gene list enrichment analysis tool. BMC bioinformatics *14,* 128.

Curtis, J.M., Grimsrud, P.A., Wright, W.S., Xu, X., Foncea, R.E., Graham, D.W., Brestoff, J.R., Wiczer, B.M., Ilkayeva, O., Cianflone, K., Muoio, D.E., Arriaga, E.A., and Bernlohr, D.A. (2010). Downregulation of adipose glutathione S-transferase A4 leads to increased protein carbonylation, oxidative stress, and mitochondrial dysfunction. Diabetes *59,* 1132-1142.

De Pauw, A., Tejerina, S., Raes, M., Keijer, J., and Arnould, T. (2009). Mitochondrial (dys)function in adipocyte (de)differentiation and systemic metabolic alterations. The American journal of pathology *175,* 927-939.

Dominici, M., Le Blanc, K., Mueller, I., Slaper-Cortenbach, I., Marini, F., Krause, D., Deans, R., Keating, A., Prockop, Dj., and Horwitz, E. (2006). Minimal criteria for defining multipotent mesenchymal stromal cells. The International Society for Cellular Therapy position statement. Cytotherapy *8,* 315-317.

Ducluzeau, P.H., Priou, M., Weitheimer, M., Flamment, M., Duluc, L., Iacobazi, F., Soleti, R., Simard, G., Durand, A., Rieusset, J., Andriantsitohaina, R., and Malthièry, Y. (2011). Dynamic regulation of mitochondrial network and oxidative functions during 3T3-L1 fat cell differentiation. Journal of physiology and biochemistry *67,* 285-296.

Frazier, T.P., Gimble, J.M., Devay, J.W., Tucker, H.A., Chiu, E.S., and Rowan, B.G. (2013). Body mass index affects proliferation and osteogenic differentiation of human subcutaneous adipose tissue-derived stem cells. BMC cell biology *14,* 34.

Frohnert, B.I., Sinaiko, A.R., Serrot, F.J., Foncea, R.E., Moran, A., Ikramuddin, S., Choudry, U., and Bernlohr, D.A. (2011). Increased adipose protein carbonylation in human obesity. Obesity (Silver Spring, Md.) *19,* 1735-1741.

Fu, Y., Luo, N., Klein, R.L., and Garvey, W.T. (2005). Adiponectin promotes adipocyte differentiation, insulin sensitivity, and lipid accumulation. Journal of lipid research *46,* 1369-1379.

Galinier, A., Carrière, A., Fernandez, Y., Carpéné, C., André, M., Caspar-Bauguil, S., Thouvenot, J.P., Périquet, B., Pénicaud, L., and Casteilla, L. (2006). Adipose tissue proadipogenic redox changes in obesity. The Journal of biological chemistry *281,* 12682-12687.

Halama, A., Horsch, M., Kastenmüller, G., Möller, G., Kumar, P., Prehn, C., Laumen, H., Hauner, H., Hrabě de Angelis, M., Beckers, J., Suhre, K, and Adamski, J. (2016). Metabolic switch during adipogenesis: From branched chain amino acid catabolism to lipid synthesis. Archives of biochemistry and biophysics *589,* 93-107.

Hamilton, L.K., Dufresne, M., Joppé, S.E., Petryszyn, S., Aumont, A., Calon, F., Barnabé-Heider, F., Furtos, A., Parent, M., Chaurand, P., and Fernandes, K.J. (2015). Aberrant Lipid Metabolism in the Forebrain Niche Suppresses Adult Neural Stem Cell Proliferation in an Animal Model of Alzheimer's Disease. Cell stem cell *17,* 397-411.

Hauner, H. (2005). Secretory factors from human adipose tissue and their functional role. The Proceedings of the Nutrition Society *64,* 163-169.

Henry, S.L., Bensley, J.G., Wood-Bradley, R.J., Cullen-McEwen, L.A., Bertram, J.F., and Armitage, J.A. (2012). White adipocytes: more than just fat depots. The international journal of biochemistry & cell biology *44,* 435-440.

Hopkinson, B.M., Desler, C., Kalisz, M., Vestentoft, P.S., Juel Rasmussen, L., and Bisgaard, H.C. (2017). Bioenergetic Changes during Differentiation of Human Embryonic Stem Cells along the Hepatic Lineage. Oxidative medicine and cellular longevity *2017,* 5080128.

Hu, D., Linders, A., Yamak, A., Correia, C., Kijlstra, J. D., Garakani, A., Xiao, L., Milan, D. J., van der Meer, P., Serra, M., Alves, P. M., and Domian, I. J. (2018). Metabolic Maturation of Human Pluripotent Stem Cell-Derived Cardiomyocytes by Inhibition of HIF1 and LDHA. Circulation research 123, 1066-1079.

Khacho, M., Clark, A., Svoboda, D.S., Azzi, J., MacLaurin, J.G., Meghaizel, C., Sesaki, H., Lagace, D.C., Germain, M., Harper, M.E., Park, D.S., and Slack, R.S. (2016). Mitochondrial Dynamics Impacts Stem Cell Identity and Fate Decisions by Regulating a Nuclear Transcriptional Program. Cell stem cell *19,* 232-247.

Kim, K.H., Jeong, Y.T., Oh, H., Kim, S.H., Cho, J.M., Kim, Y.N., Kim, S.S., Kim, D.H., Hur, K.Y., Kim, H.K., Ko, T., Han. J., Kim, H.L., Kim, J., Back, S.H., Komatsu, M., Chen, H., Chan, D.C., Konishi, M., Itoh, N., Choi, C.S., and Lee, M.S. (2013). Autophagy deficiency leads to protection from obesity and insulin resistance by inducing Fgf21 as a mitokine. Nature medicine *19,* 83-92.

Kloting, N., Fasshauer, M., Dietrich, A., Kovacs, P., Schon, M.R., Kern, M., Stumvoll, M., and Bluher, M. (2010). Insulin-sensitive obesity. American journal of physiology. Endocrinology and metabolism *299,* E506-E515.

Kuleshov, M.V., Jones, M.R., Rouillard, A.D., Fernandez, N.F., Duan, Q., Wang, Z., Koplev, S., Jenkins, S.L., Jagodnik, K.M., Lachmann, A., McDermott, M.G., Monteiro, C.D., Gundersen, G.W., and Ma'ayan, A. (2016). Enrichr: a comprehensive gene set enrichment analysis web server 2016 update. Nucleic acids research *44,* W90-97.

Li, X., Liu, Z., Luo, C., Jia, H., Sun, L., Hou, B., Shen, W., Packer, L., Cotman, C.W., and Liu, J. (2008). Lipoamide protects retinal pigment epithelial cells from oxidative stress and mitochondrial dysfunction. Free radical biology & medicine *44,* 1465-1474.

Lo, K.A., Labadorf, A., Kennedy, N.J., Han, M.S., Yap, Y.S., Matthews, B., Xin, X., Sun, L., Davis, R.J., Lodish, H.F., and Fraenkel, E. (2013). Analysis of in vitro insulin-resistance models and their physiological relevance to in vivo diet-induced adipose insulin resistance. Cell reports *5,* 259-270.

Ochocki, J.D., and Simon, M.C. (2013). Nutrient-sensing pathways and metabolic regulation in stem cells. The Journal of cell biology *203,* 23-33.

Onate, B., Vilahur, G., Camino-López, S., Díez-Caballero, A., Ballesta-López, C., Ybarra, J., Moscatiello, F., Herrero, J., and Badimon, L. (2013). Stem cells isolated from adipose tissue of obese patients show changes in their transcriptomic profile that indicate loss in stemcellness and increased commitment to an adipocyte-like phenotype. BMC genomics *14,* 625.

Perez, L.M., Bernal, A., de Lucas, B., San Martin, N., Mastrangelo, A., Garcia, A., Barbas, C., and Galvez, B. G. (2015). Altered metabolic and stemness capacity of adipose tissue-derived stem cells from obese mouse and human. PloS one *10,* e0123397.

Reimand, J., Kull, M., Peterson, H., Hansen, J., and Vilo, J. (2007). g:Profiler--a web-based toolset for functional profiling of gene lists from large-scale experiments. Nucleic acids research *35,* W193-200.

Roldan, M., Macias-Gonzalez, M., Garcia, R., Tinahones, F.J., and Martin, M. (2011). Obesity short-circuits stemness gene network in human adipose multipotent stem cells. FASEB journal: official publication of the Federation of American Societies for Experimental Biology *25,* 4111-4126.

Rosen, E.D., and Spiegelman, B.M. (2006). Adipocytes as regulators of energy balance and glucose homeostasis. Nature *444,* 847-853.

Rosen, E.D., and MacDougald, O.A. (2006). Adipocyte differentiation from the inside out. Nature reviews. Molecular cell biology *7,* 885-896.

Ruskovska, T., and Bernlohr, D.A. (2013). Oxidative stress and protein carbonylation in adipose tissue - implications for insulin resistance and diabetes mellitus. Journal of proteomics *92,* 323-334.

Saito, Y., Chapple, R.H., Lin, A., Kitano, A., and Nakada, D. (2015). AMPK Protects Leukemia-Initiating Cells in Myeloid Leukemias from Metabolic Stress in the Bone Marrow. Cell stem cell *17,* 585-596.

Samsonraj, R.M., Rai, B., Sathiyanathan, P., Puan, K. J., Rotzschke, O., Hui, J. H., Raghunath, M., Stanton, L. W., Nurcombe, V., and Cool, S. M. (2015). Establishing criteria for human mesenchymal stem cell potency. Stem cells *33,* 1878-1891.

Shen, W., Hao, J., Feng, Z., Tian, C., Chen, W., Packer, L., Shi, X., Zang, W., and Liu, J. (2011). Lipoamide or lipoic acid stimulates mitochondrial biogenesis in 3T3-L1 adipocytes via the endothelial NO synthase-cGMP-protein kinase G signalling pathway. British journal of pharmacology *162,* 1213-1224.

Skurk, T. and Hauner, H. (2012). Primary culture of human adipocyte precursor cells: expansion and differentiation. Methods in molecular biology (Clifton, N.J.) *806,* 215-226.

Smith, P.J., Wise, L.S., Berkowitz, R., Wan, C., and Rubin, C.S. (1988). Insulin-like growth factor-I is an essential regulator of the differentiation of 3T3-L1 adipocytes. The Journal of biological chemistry *263,* 9402-9408.

Stephens, J.M. (2012). The fat controller: adipocyte development. PLoS biology *10,* e1001436.

Stephens, J.M., Lee, J., and Pilch, P.F. (1997). Tumor necrosis factor-alpha-induced insulin resistance in 3T3-L1 adipocytes is accompanied by a loss of insulin receptor substrate-1 and GLUT4 expression without a loss of insulin receptor-mediated signal transduction. The Journal of biological chemistry *272,* 971-976.

Stern, J.H., Rutkowski, J.M., and Scherer, P.E. (2016). Adiponectin, Leptin, and Fatty Acids in the Maintenance of Metabolic Homeostasis through Adipose Tissue Crosstalk. Cell metabolism *23,* 770-784.

Suda, T., Takubo, K., and Semenza, G.L. (2011). Metabolic regulation of hematopoietic stem cells in the hypoxic niche. Cell stem cell *9,* 298-310.

Sutherland, L.N., Capozzi, L.C., Turchinsky, N.J., Bell, R.C., and Wright, D.C. (2008). Time course of high-fat diet-induced reductions in adipose tissue mitochondrial proteins: potential

mechanisms and the relationship to glucose intolerance. American journal of physiology. Endocrinology and metabolism *295,* E1076-1083.

Tormos, K.V., Anso, E., Hamanaka, R.B., Eisenbart, J., Joseph, J., Kalyanaraman, B., and Chandel, N.S. (2011). Mitochondrial complex III ROS regulate adipocyte differentiation. Cell metabolism *14,* 537-544.

Wang, P.W., Kuo, H.M., Huang, H.T., Chang, A.Y., Weng, S.W., Tai, M.H., Chuang, J.H., Chen, I.Y., Huang, S.C., Lin, T.K., and Liou, C.W. (2014). Biphasic response of mitochondrial biogenesis to oxidative stress in visceral fat of diet-induced obesity mice. Antioxidants & redox signaling *20,* 2572-2588.

Wilson-Fritch, L., Burkart, A., Bell, G., Mendelson, K., Leszyk, J., Nicoloro, S., Czech, M., and Corvera, S. (2003). Mitochondrial biogenesis and remodeling during adipogenesis and in response to the insulin sensitizer rosiglitazone. Molecular and cellular biology *23,* 1085-1094.

Wilson-Fritch, L., Nicoloro, S., Chouinard, M., Lazar, M.A., Chui, P.C., Leszyk, J., Straubhaar, J., Czech, M.P., and Corvera, S. (2004). Mitochondrial remodeling in adipose tissue associated with obesity and treatment with rosiglitazone. The Journal of clinical investigation *114,* 1281-1289.

Wu, C.L., Diekman, B.O., Jain, D., and Guilak, F. (2013). Diet-induced obesity alters the differentiation potential of stem cells isolated from bone marrow, adipose tissue and infrapatellar fat pad: the effects of free fatty acids. International journal of obesity (2005) *37,* 1079-1087.

Yu, W.M., Liu, X., Shen, J., Jovanovic, O., Pohl, E.E., Gerson, S.L., Finkel, T., Broxmeyer, H.E., and Qu, C.K. (2013). Metabolic regulation by the mitochondrial phosphatase PTPMT1 is required for hematopoietic stem cell differentiation. Cell stem cell *12,* 62-74.

Zhang, Y., Marsboom, G., Toth, P.T., and Rehman, J. (2013). Mitochondrial respiration regulates adipogenic differentiation of human mesenchymal stem cells. PLoS one *8,* e77077.

Zhao, L., Liu, Z., Jia, H., Feng, Z., Liu, J., and Li, X. (2015). Lipoamide Acts as an Indirect Antioxidant by Simultaneously Stimulating Mitochondrial Biogenesis and Phase II Antioxidant Enzyme Systems in ARPE-19 Cells. PLoS one *10,* e0128502.

Zheng, X., Boyer, L., Jin, M., Mertens, J., Kim, Y., Ma, L., Ma, L., Hamm, M., Gage, F.H., and Hunter, T. (2016). Metabolic reprogramming during neuronal differentiation from aerobic glycolysis to neuronal oxidative phosphorylation. eLife *5,* e13374.

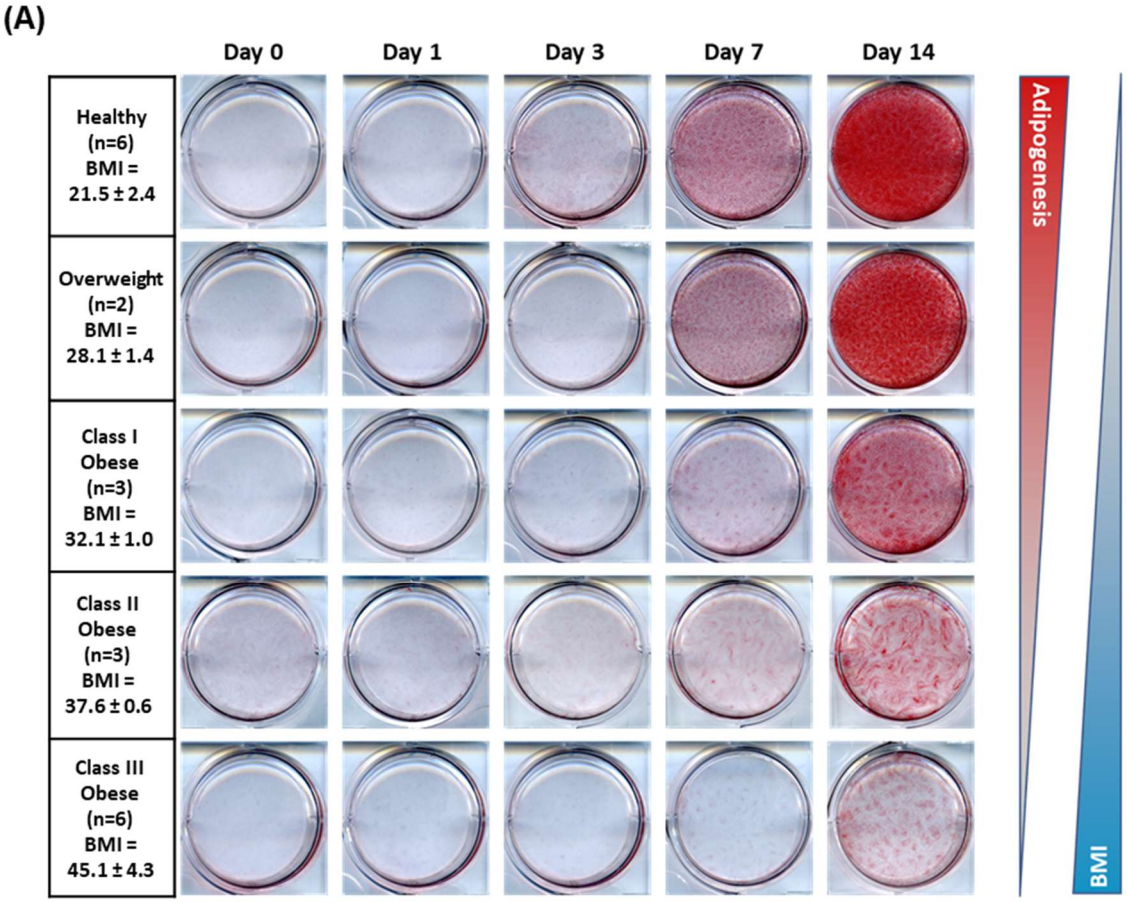
(A)
Day 0
Day 1
Day 3
Day 7
Day 14
Healthy (n=6) BMI = 21.5 ± 2.4
Overweight (n=2) BMI = 28.1 ± 1.4
Class I Obese (n=3) BMI = 32.1 ± 1.0
Class II Obese (n=3) BMI = 37.6 ± 0.6
Class III Obese (n=6) BMI = 45.1 ± 4.3
Adipogenesis
BMI

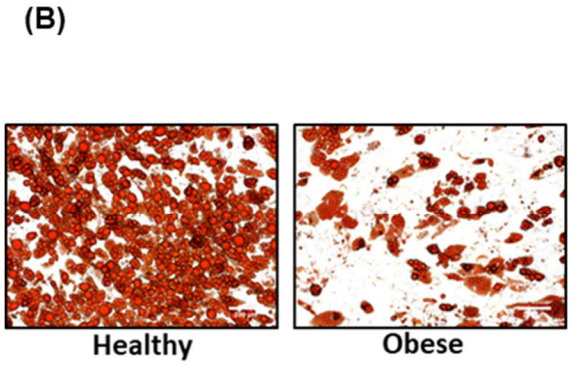
(B)
Healthy
Obese

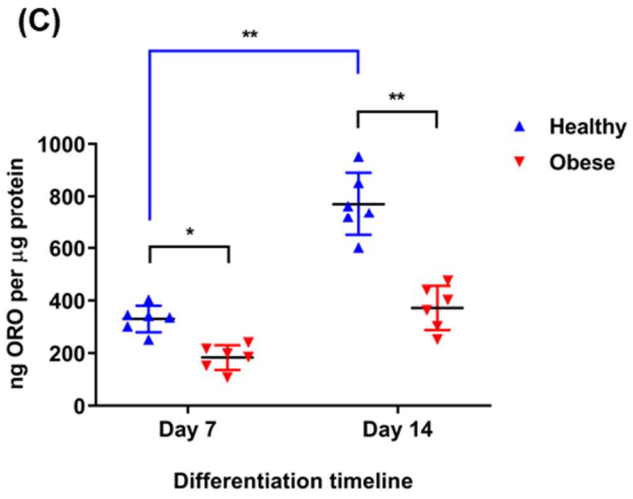
(C)
**
**
*
1000
800
600
400
200
0
ng ORO per µg protein
Day 7
Day 14
Differentiation timeline
Healthy
Obese

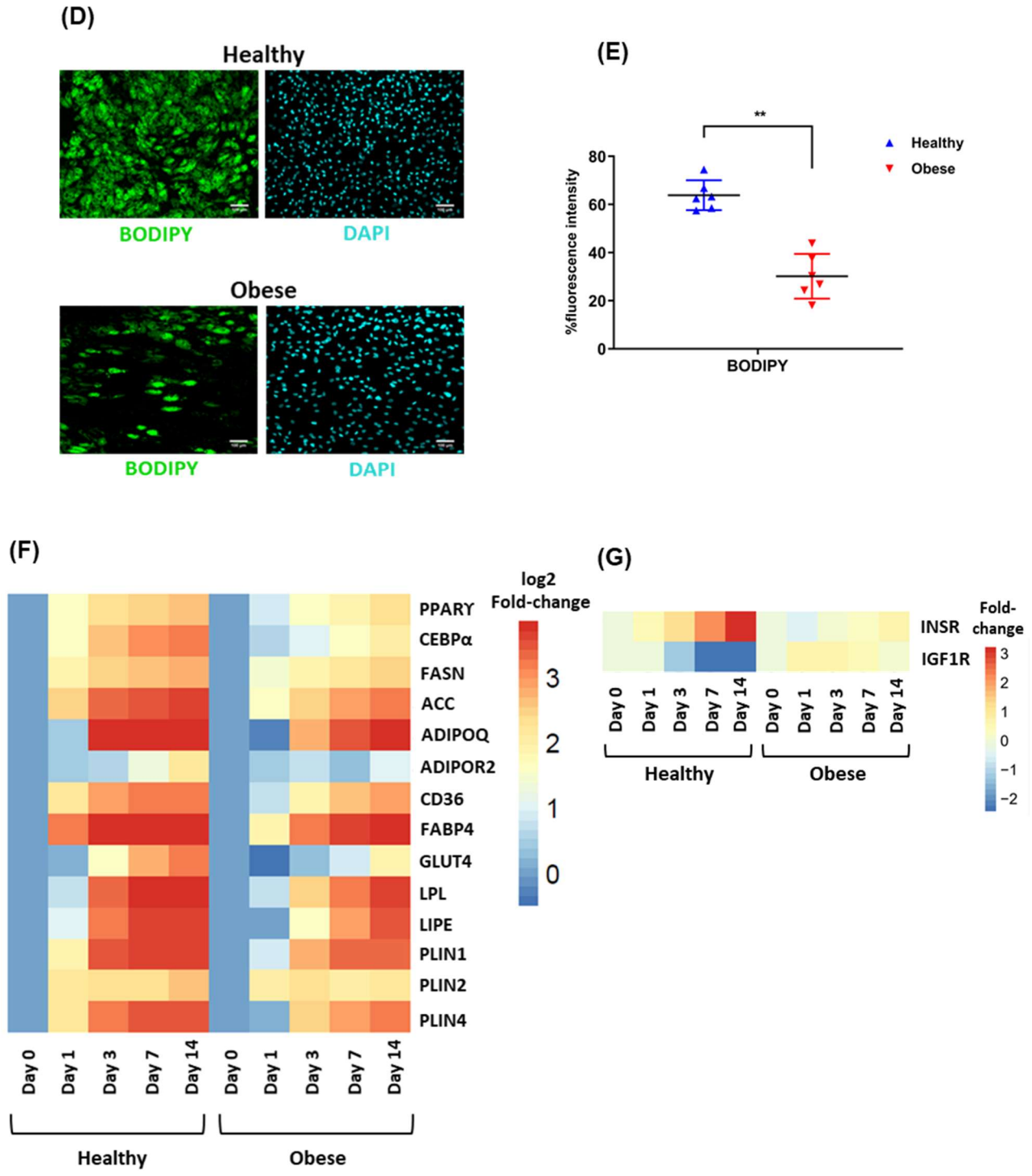
(D)
Healthy
BODIPY
DAPI
Obese
BODIPY
DAPI
(E)
**
Healthy
Obese
%fluorescence intensity
80
60
40
20
0
BODIPY
(F)
log2
Fold-change
3
2
1
0
PPARY
CEBPα
FASN
ACC
ADIPOQ
ADIPOR2
CD36
FABP4
GLUT4
LPL
LIPE
PLIN1
PLIN2
PLIN4
Day 0
Day 1
Day 3
Day 7
Day 14
Healthy
Obese
(G)
INSR
IGF1R
Fold-
change
3
2
1
0
−1
−2
Day 0
Day 1
Day 3
Day 7
Day 14
Healthy
Obese

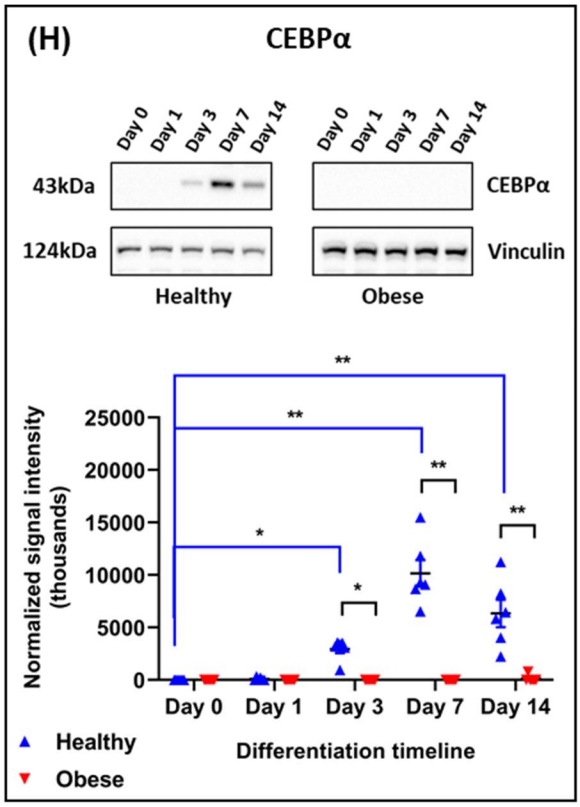
(H)
CEBPα
Day 0
Day 1
Day 3
Day 7
Day 14
43kDa
CEBPα
124kDa
Vinculin
Healthy
Obese
Normalized signal intensity (thousands)
25000
20000
15000
10000
5000
0
Day 0
Day 1
Day 3
Day 7
Day 14
Differentiation timeline
Healthy
Obese

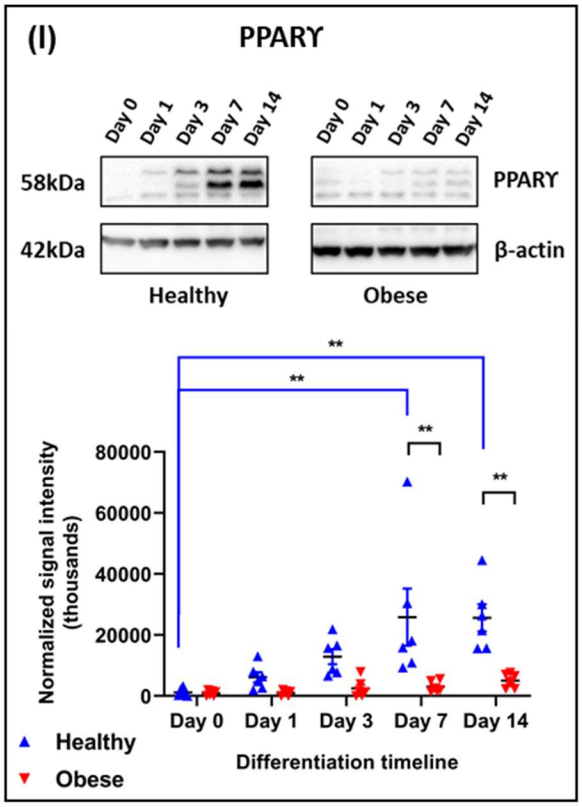
(I)
PPARϒ
Day 0
Day 1
Day 3
Day 7
Day 14
58kDa
PPARϒ
42kDa
β-actin
Healthy
Obese
Normalized signal intensity (thousands)
80000
60000
40000
20000
0
Day 0
Day 1
Day 3
Day 7
Day 14
Differentiation timeline
Healthy
Obese

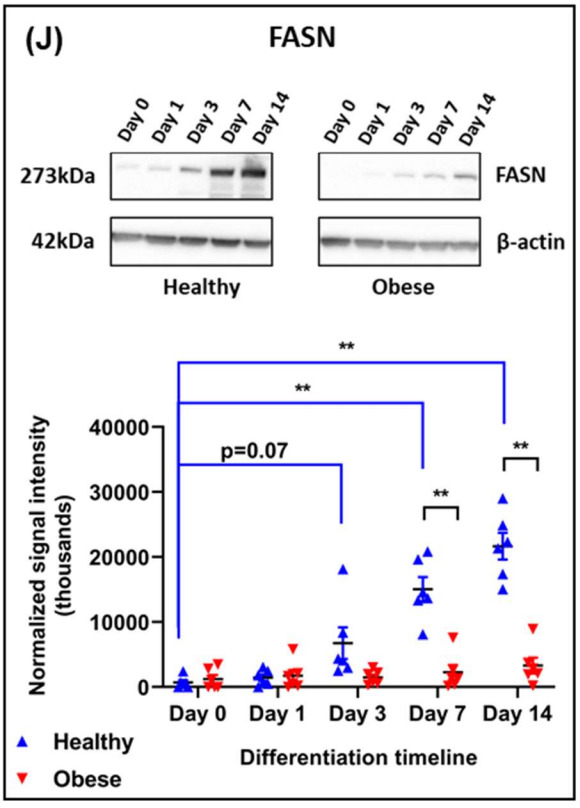
(J)
FASN
Day 0
Day 1
Day 3
Day 7
Day 14
273kDa
FASN
42kDa
β-actin
Healthy
Obese
Normalized signal intensity (thousands)
40000
30000
20000
10000
0
p=0.07
Day 0
Day 1
Day 3
Day 7
Day 14
Differentiation timeline
Healthy
Obese

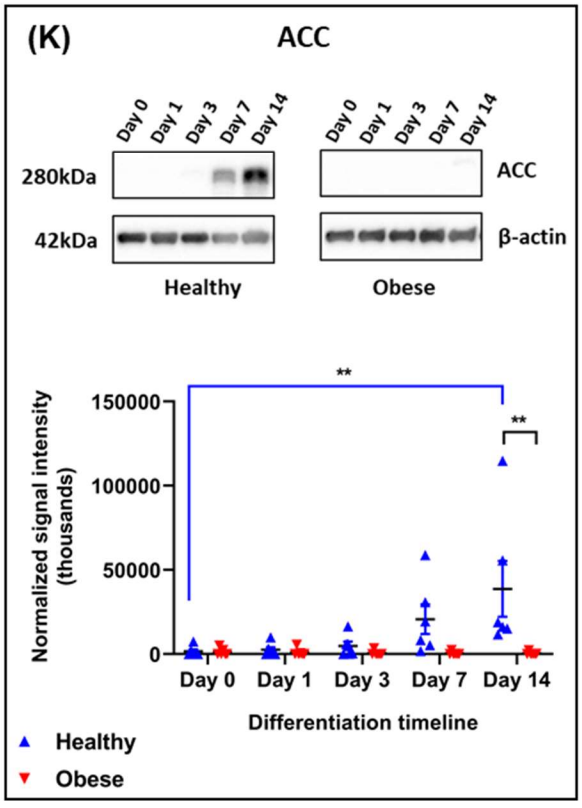
(K)
ACC
Day 0
Day 1
Day 3
Day 7
Day 14
280kDa
ACC
42kDa
β-actin
Healthy
Obese
Normalized signal intensity (thousands)
150000
100000
50000
0
Day 0
Day 1
Day 3
Day 7
Day 14
Differentiation timeline
Healthy
Obese

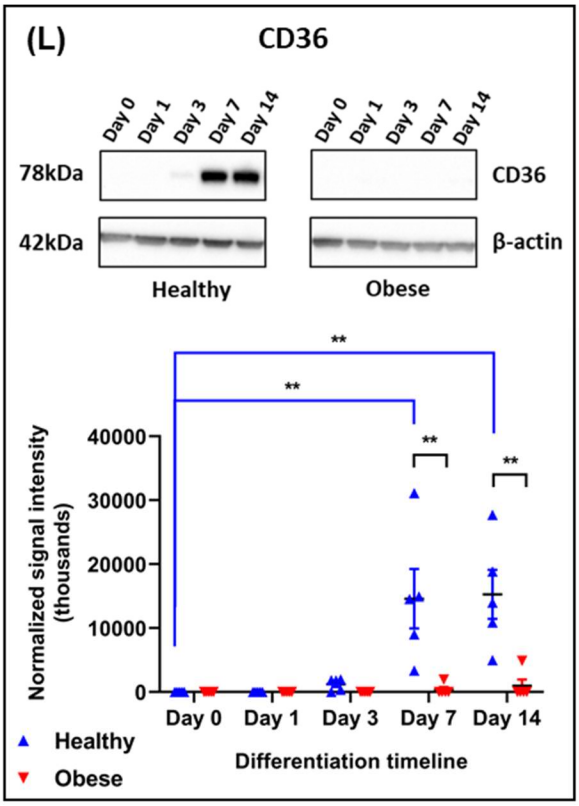
(L)
CD36
Day 0
Day 1
Day 3
Day 7
Day 14
78kDa
42kDa
CD36
β-actin
Healthy
Obese
Normalized signal intensity (thousands)
40000
30000
20000
10000
0
**
**
**
**
Day 0
Day 1
Day 3
Day 7
Day 14
Healthy
Obese
Differentiation timeline

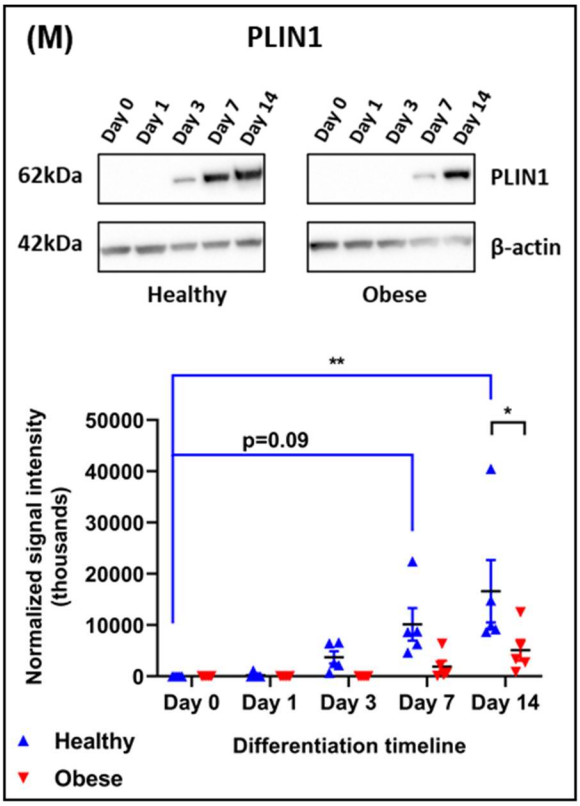
(M)
PLIN1
Day 0
Day 1
Day 3
Day 7
Day 14
62kDa
42kDa
PLIN1
β-actin
Healthy
Obese
Normalized signal intensity (thousands)
50000
40000
30000
20000
10000
0
**
p=0.09
*
Day 0
Day 1
Day 3
Day 7
Day 14
Healthy
Obese
Differentiation timeline

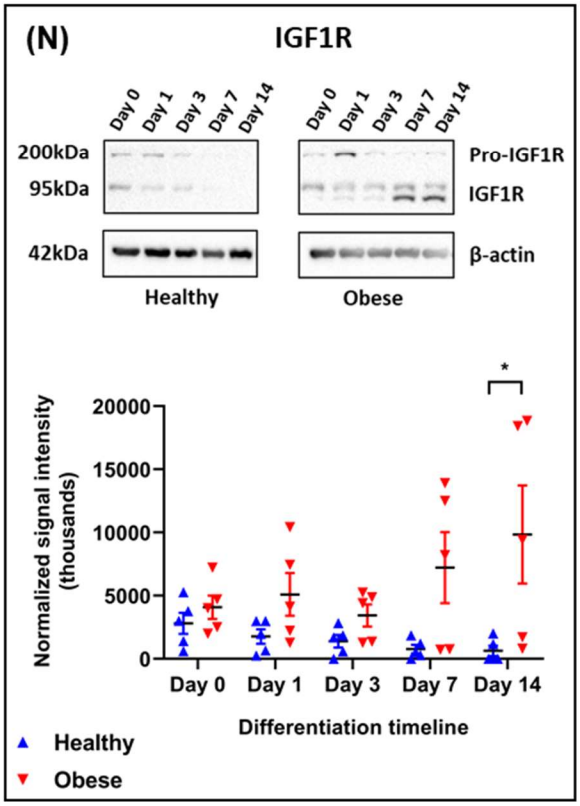
(N)
IGF1R
Day 0
Day 1
Day 3
Day 7
Day 14
200kDa
95kDa
42kDa
Pro-IGF1R
IGF1R
β-actin
Healthy
Obese
Normalized signal intensity (thousands)
20000
15000
10000
5000
0
*
Day 0
Day 1
Day 3
Day 7
Day 14
Healthy
Obese
Differentiation timeline

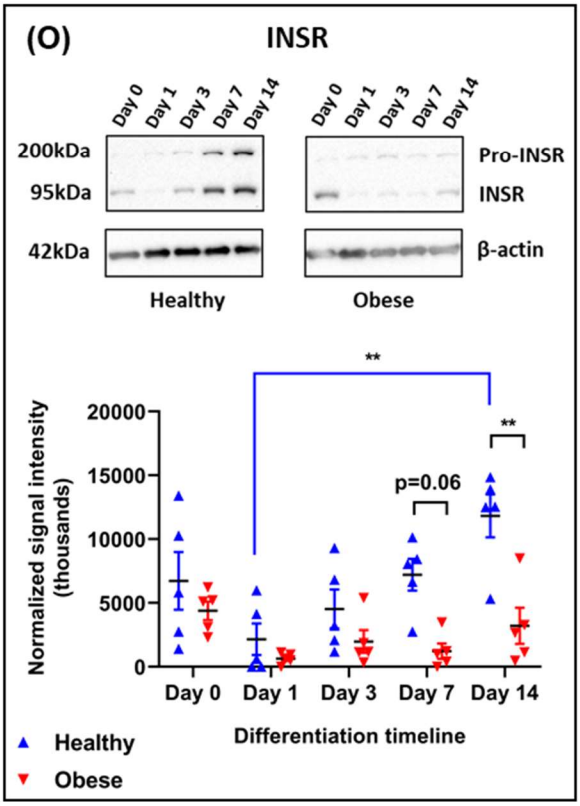
(O)
INSR
Day 0
Day 1
Day 3
Day 7
Day 14
200kDa
95kDa
42kDa
Pro-INSR
INSR
β-actin
Healthy
Obese
Normalized signal intensity (thousands)
20000
15000
10000
5000
0
**
**
p=0.06
Day 0
Day 1
Day 3
Day 7
Day 14
Healthy
Obese
Differentiation timeline

Fig. 1: ADSCs derived from obese donor tissue show significant reduction in adipogenesis. **(A)** Representative scanned ORO whole well images during adipogenic differentiation from ADSCs isolated from healthy, overweight and individuals from different obesity classes. **(B)** Representative images of ORO-stained morbidly obese (Class III obese, henceforth referred to as obese) and healthy ADSC-derived adipocytes. Scale bar represents 200μm. **(C)** Quantification of extracted ORO measured at 492nm by using a BioTek spectrophotometer. **(D)** Representative BODIPY-stained images of healthy and obese adipocytes. Scale bar represents 100 μm. **(E)** ImageJ quantification of BODIPY-positive cells, expressed as % fluorescence intensity normalized to cell numbers (DAPI). **(F)** Heat map showing log2 fold change in gene expression. **(G)** Heat map showing log2 fold change in INSR and IGF1R gene expression. **(H)** Representative western blots showing changes in CEBPα protein expression during adipogenesis and quantification of CEBPα expression upon normalization to vinculin (loading control). **(I)** Representative western blots showing changes in PPARγ, FASN **(J)**, ACC **(K)**, CD36 (n=5) **(L)**, PLIN1 (n=5) **(M)**, IGF1R (n=5) **(N)**, and INSR (n=5) **(O)** protein expression during adipogenesis and quantification of their expression upon normalization to β-actin (loading control).

Data is represented as mean±SEM, n=6 (except where indicated), where n represents biological replicates of healthy and obese ADSCs. Statistical significance was determined by using student's two-tailed t-test for panel **(E)** and two-way ANOVA corrected for multiple comparisons with Tukey's test for panels **(C)** and **(H) - (O)**. * $p<0.05$, * $p<0.01$.

See also Fig. S3.

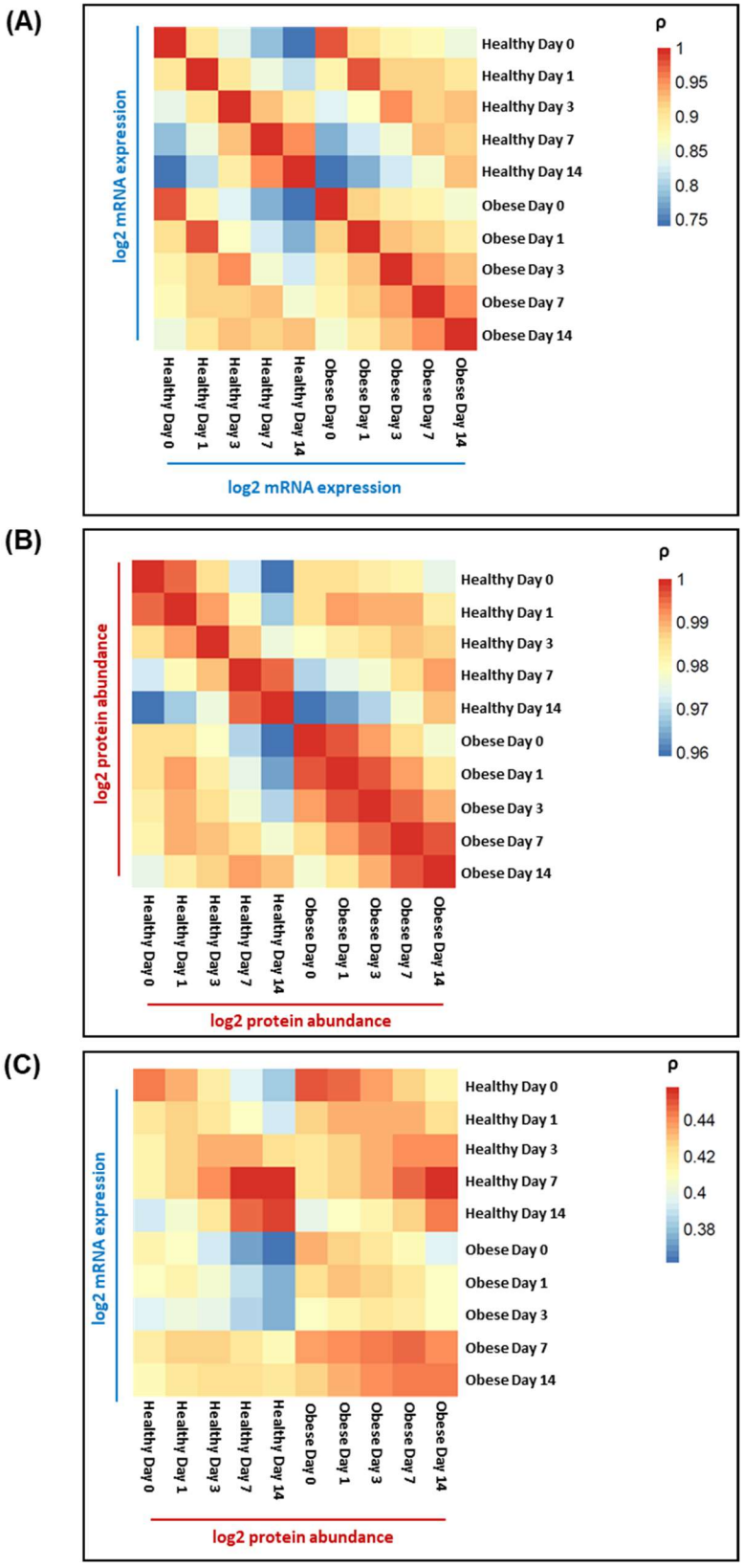
(A)
log2 mRNA expression
Healthy Day 0
Healthy Day 1
Healthy Day 3
Healthy Day 7
Healthy Day 14
Obese Day 0
Obese Day 1
Obese Day 3
Obese Day 7
Obese Day 14
log2 mRNA expression
ρ
1
0.95
0.9
0.85
0.8
0.75
(B)
log2 protein abundance
Healthy Day 0
Healthy Day 1
Healthy Day 3
Healthy Day 7
Healthy Day 14
Obese Day 0
Obese Day 1
Obese Day 3
Obese Day 7
Obese Day 14
log2 protein abundance
ρ
1
0.99
0.98
0.97
0.96
(C)
log2 mRNA expression
Healthy Day 0
Healthy Day 1
Healthy Day 3
Healthy Day 7
Healthy Day 14
Obese Day 0
Obese Day 1
Obese Day 3
Obese Day 7
Obese Day 14
log2 protein abundance
ρ
0.44
0.42
0.4
0.38

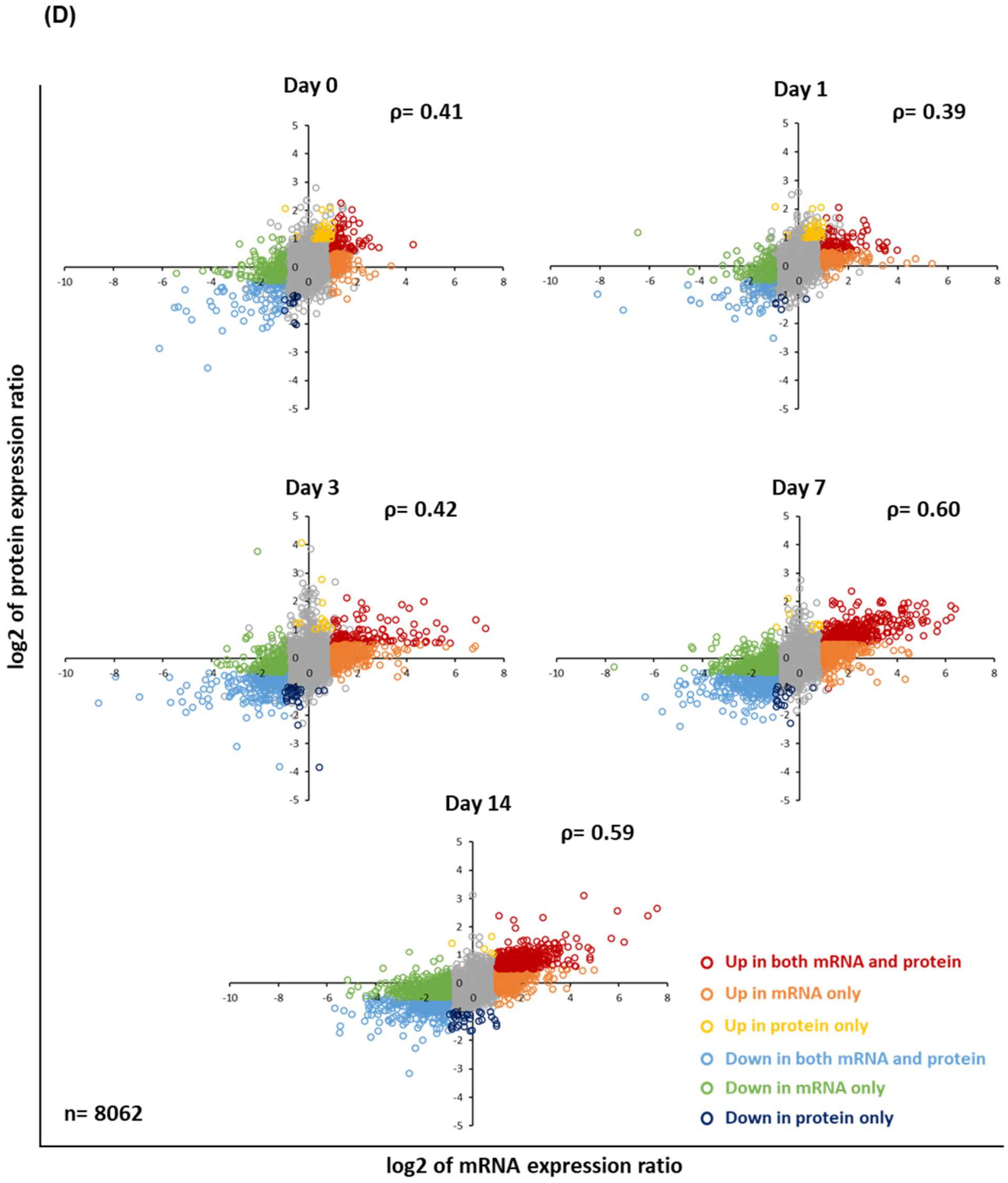
(D)
Day 0
ρ= 0.41
Day 1
ρ= 0.39
Day 3
ρ= 0.42
Day 7
ρ= 0.60
Day 14
ρ= 0.59
log2 of protein expression ratio
log2 of mRNA expression ratio
n= 8062
Up in both mRNA and protein
Up in mRNA only
Up in protein only
Down in both mRNA and protein
Down in mRNA only
Down in protein only

Fig. 2: Comparative analyses of transcriptomic and proteomic data at different timepoints during healthy and obese adipogenesis show positive correlation between gene and protein expression. (A) Heatmap showing correlation of transcriptomic data between different timepoints in healthy and obese adipogenesis. **(B)** Heatmap showing correlation of proteomic data between different timepoints in healthy and obese adipogenesis. **(C)** Heatmap showing correlation between transcriptomic and proteomic data along different timepoints in healthy and obese adipogenesis. **(D)** Correlation between changes in transcript (log2 mRNA expression ratio) and protein levels (log2 protein abundance ratio) of the gene products detected at both transcript and protein levels (n=8062) between healthy and obese samples at specified timepoints during adipogenesis.

ρ = Spearman's correlation coefficient.

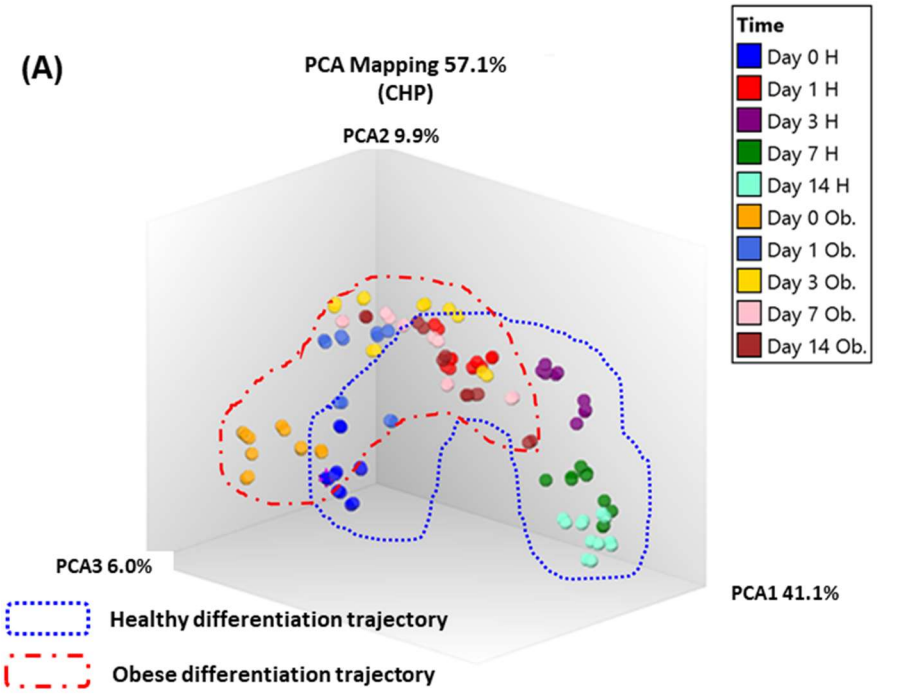
(A)
PCA Mapping 57.1%
(CHP)
PCA2 9.9%
Time
Day 0 H
Day 1 H
Day 3 H
Day 7 H
Day 14 H
Day 0 Ob.
Day 1 Ob.
Day 3 Ob.
Day 7 Ob.
Day 14 Ob.
PCA3 6.0%
PCA1 41.1%
Healthy differentiation trajectory
Obese differentiation trajectory

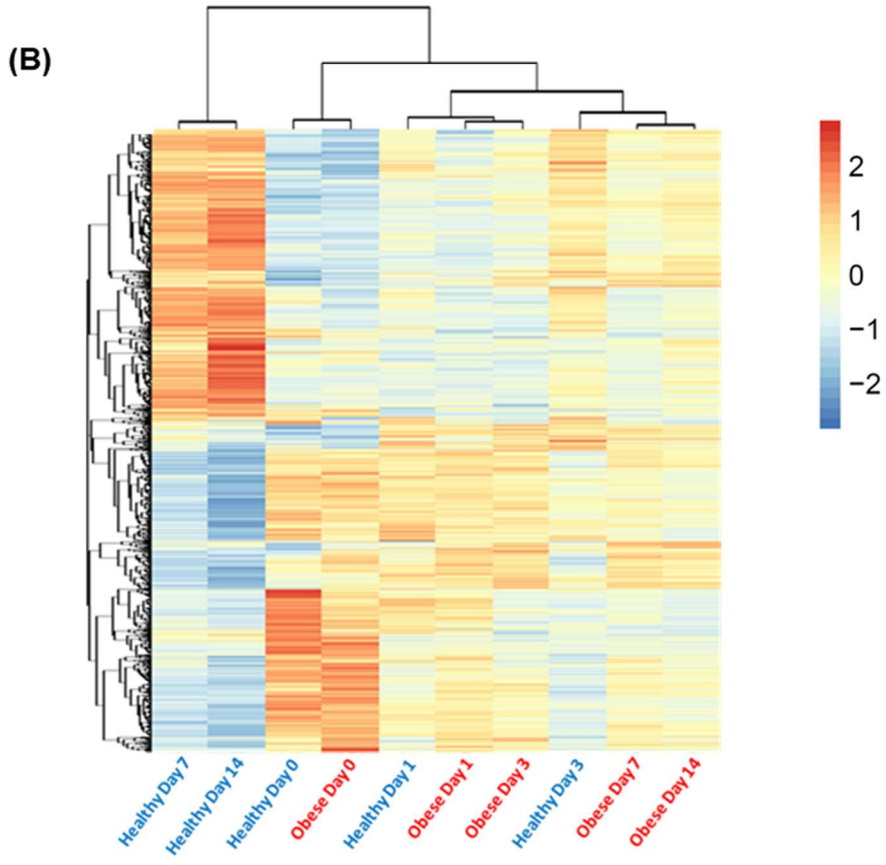
(B)
2
1
0
−1
−2
Healthy Day 7
Healthy Day 14
Healthy Day 0
Obese Day 0
Healthy Day 1
Obese Day 1
Obese Day 3
Healthy Day 3
Obese Day 7
Obese Day 14

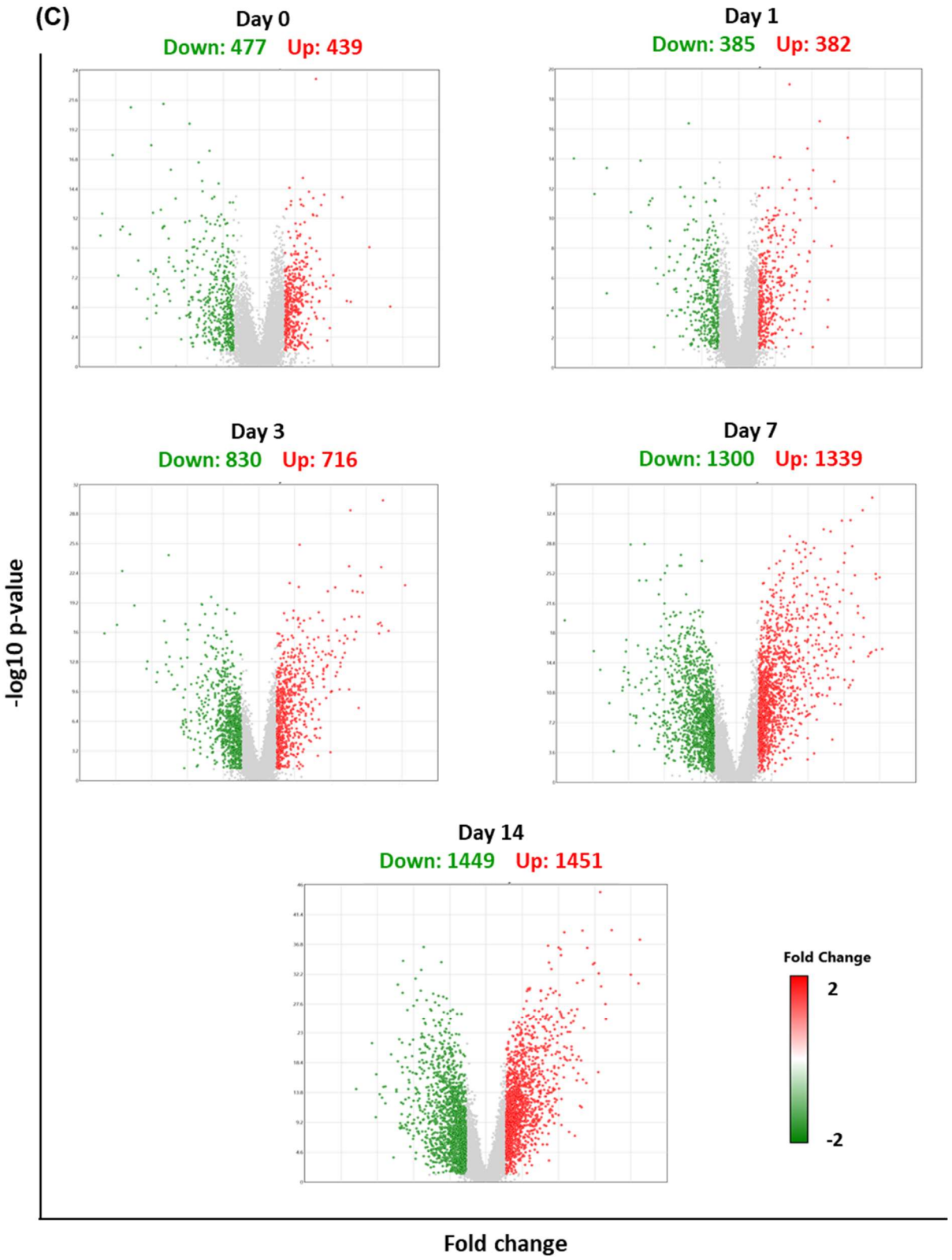
(C)
Day 0
Down: 477 Up: 439
Day 1
Down: 385 Up: 382
Day 3
Down: 830 Up: 716
Day 7
Down: 1300 Up: 1339
Day 14
Down: 1449 Up: 1451
-log10 p-value
Fold change
Fold Change
2
-2

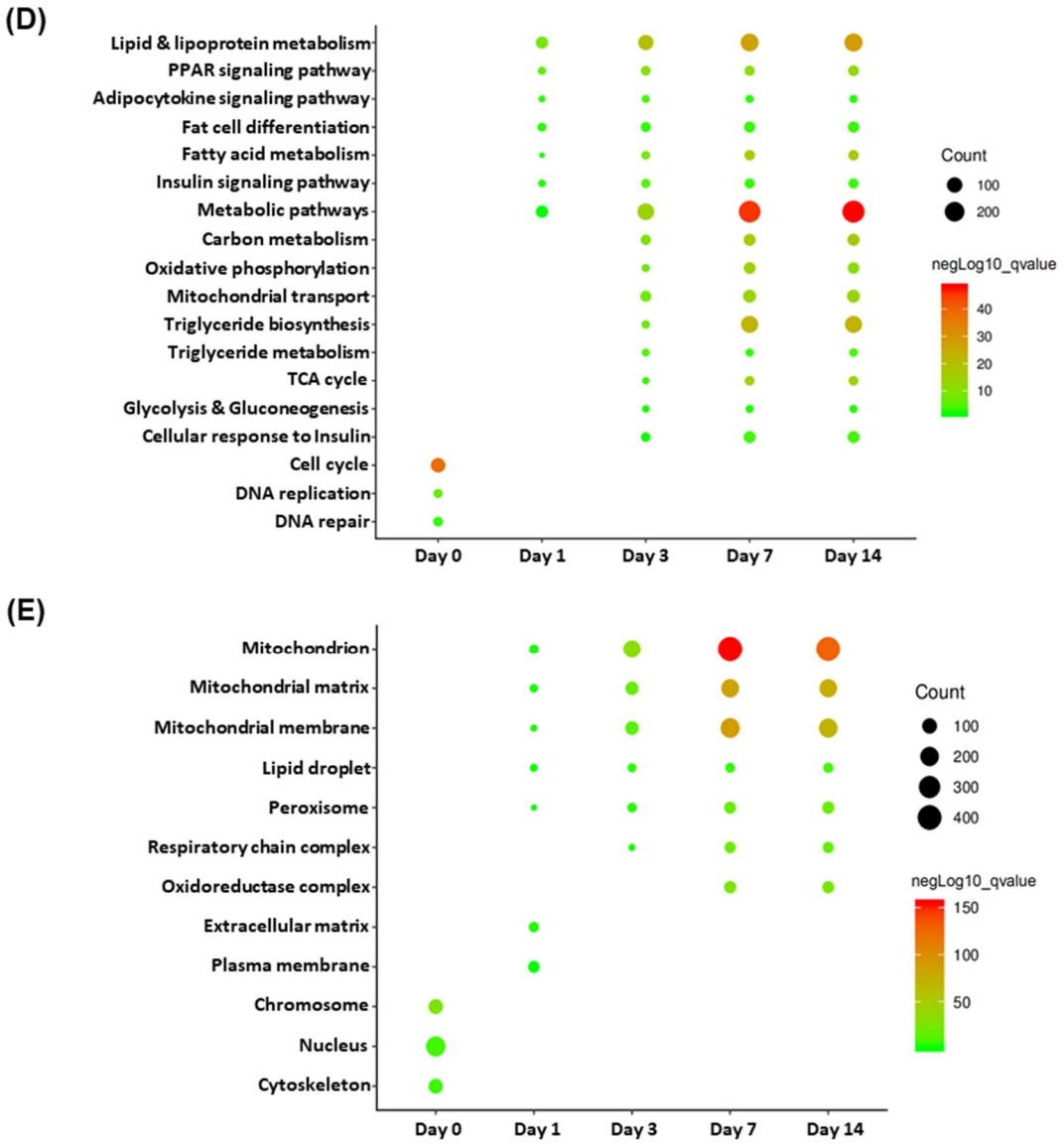
(D)
Lipid & lipoprotein metabolism
PPAR signaling pathway
Adipocytokine signaling pathway
Fat cell differentiation
Fatty acid metabolism
Insulin signaling pathway
Metabolic pathways
Carbon metabolism
Oxidative phosphorylation
Mitochondrial transport
Triglyceride biosynthesis
Triglyceride metabolism
TCA cycle
Glycolysis & Gluconeogenesis
Cellular response to Insulin
Cell cycle
DNA replication
DNA repair
Day 0
Day 1
Day 3
Day 7
Day 14
Count
100
200
negLog10_qvalue
40
30
20
10
(E)
Mitochondrion
Mitochondrial matrix
Mitochondrial membrane
Lipid droplet
Peroxisome
Respiratory chain complex
Oxidoreductase complex
Extracellular matrix
Plasma membrane
Chromosome
Nucleus
Cytoskeleton
Day 0
Day 1
Day 3
Day 7
Day 14
Count
100
200
300
400
negLog10_qvalue
150
100
50
(F)
Day 7
Day 14
Day 3
468
SLC2A4
PFKFB1
CEBPA
CD36
ACADM
SLC25A1
HK2
PPARG
PCK1
DECR1
ACOT2
ACAD5
PCCB
COX5B
MDH1
NDUFA9
COX4
PLIN1
CS
DGAT2
CYCS
FASN
LPIN1
LPL
LIPE
ACSL1
ACACA
ACO2
ATP5O
FH
HADHA
IDH2
FABP4
TCA & OXPHOS
Triglyceride biosynthesis
Fatty acid oxidation
Glucose metabolism
WAT differentiation
Mitochondrion
Lipid droplet

Fig. 3: Obese ADSCs present a distinct transcriptomic profile compared to healthy cells during adipogenesis over a 14-day time course. (A) PCA analysis and **(B)** Hierarchical clustering for healthy and obese samples at the indicated timepoints during adipogenesis. **(C)** Volcano plots showing number of differentially expressed genes in healthy and obese adipogenesis at indicated timepoints. **(D)** Functional gene clustering and enrichment analysis for upregulated genes in healthy cells at indicated timepoints during adipogenesis in REACTOME 2016, KEGG 2019, GO Biological Processes 2018. **(E)** GO Cellular component 2018 databases **(F)** Venn diagram showing upregulated genes common among days 3, 7 and 14 of adipogenic differentiation in healthy cells and functional gene clustering for these common upregulated genes.

All gene expression analyses (PCA, hierarchical clustering and volcano plots) were performed by using the TAC4.0 program from Thermo Scientific. Functional gene clustering was performed using the web-based gene clustering and enrichment tool, G:profiler. Enrichment of specific genes or pathways were considered statistically significant for p-values <0.05. $n=6$, where n represents healthy and obese biological replicates with two experimental replicates for each sample.

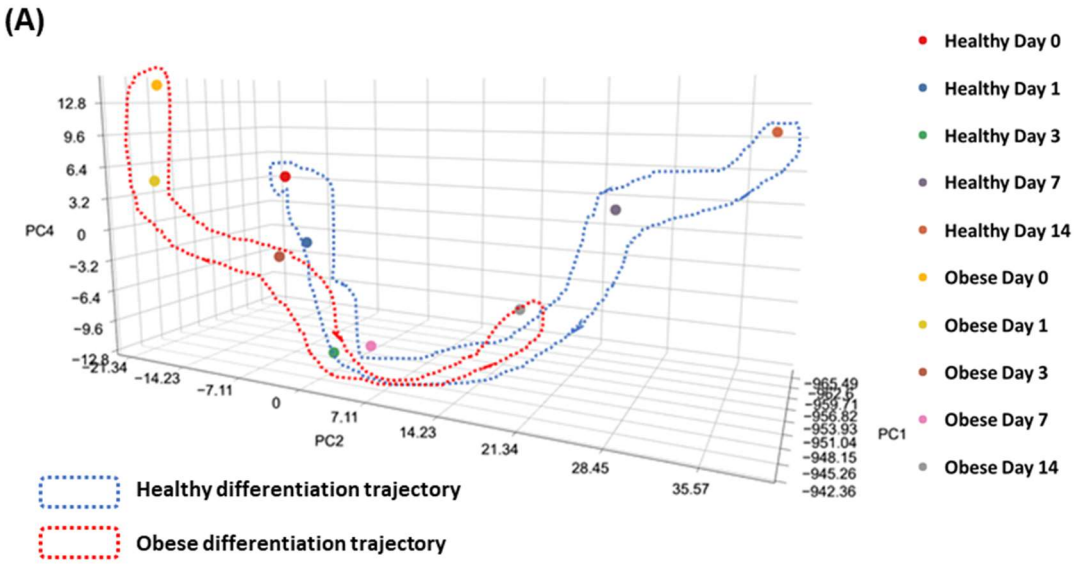
(A)
Healthy Day 0
Healthy Day 1
Healthy Day 3
Healthy Day 7
Healthy Day 14
Obese Day 0
Obese Day 1
Obese Day 3
Obese Day 7
Obese Day 14
PC4
PC2
PC1
Healthy differentiation trajectory
Obese differentiation trajectory

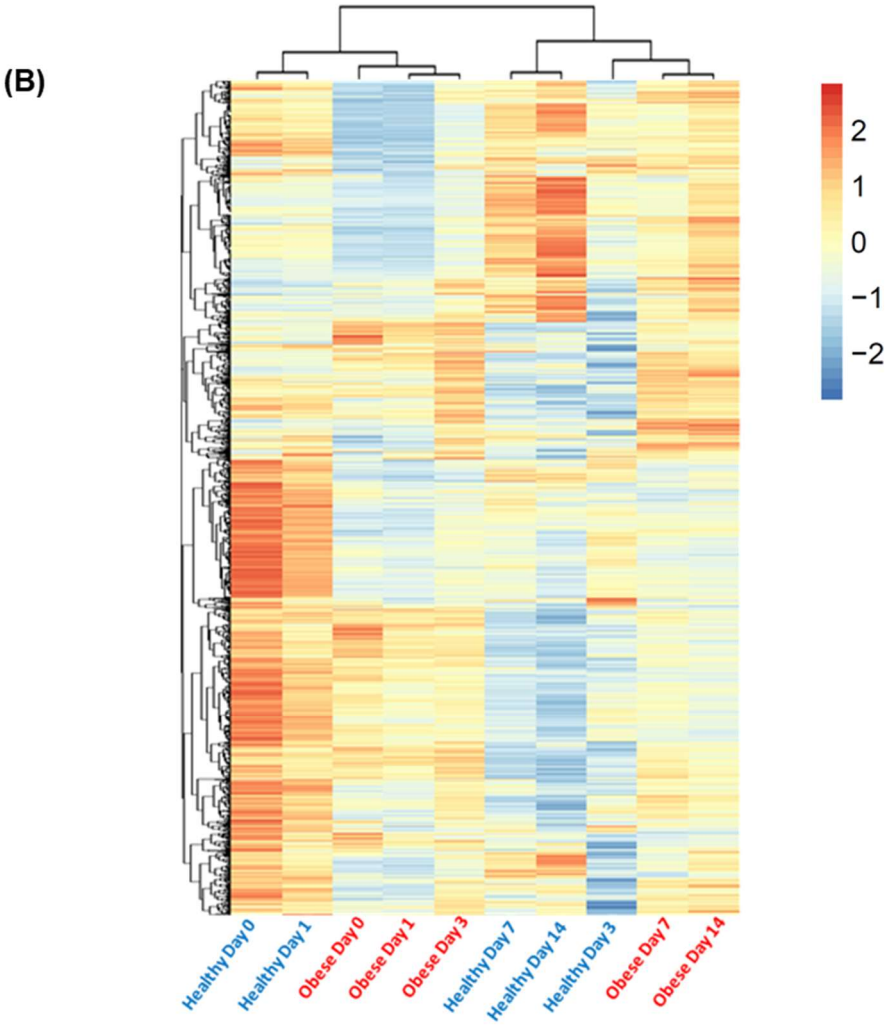
(B)
2
1
0
−1
−2
Healthy Day 0
Healthy Day 1
Obese Day 0
Obese Day 1
Obese Day 3
Healthy Day 7
Healthy Day 14
Healthy Day 3
Obese Day 7
Obese Day 14

(C)

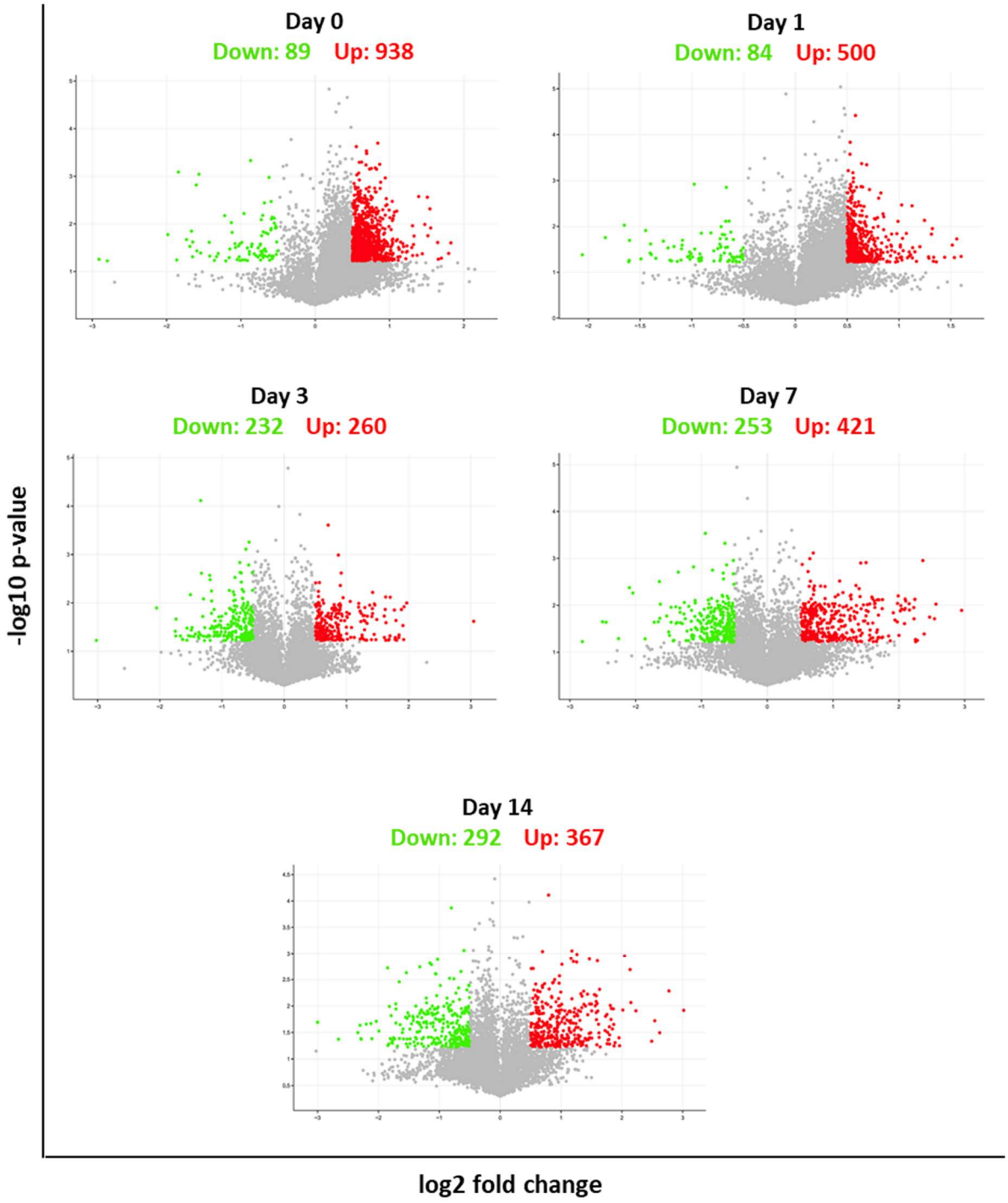
Day 0
Down: 89 Up: 938
Day 1
Down: 84 Up: 500
Day 3
Down: 232 Up: 260
Day 7
Down: 253 Up: 421
Day 14
Down: 292 Up: 367
-log10 p-value
log2 fold change

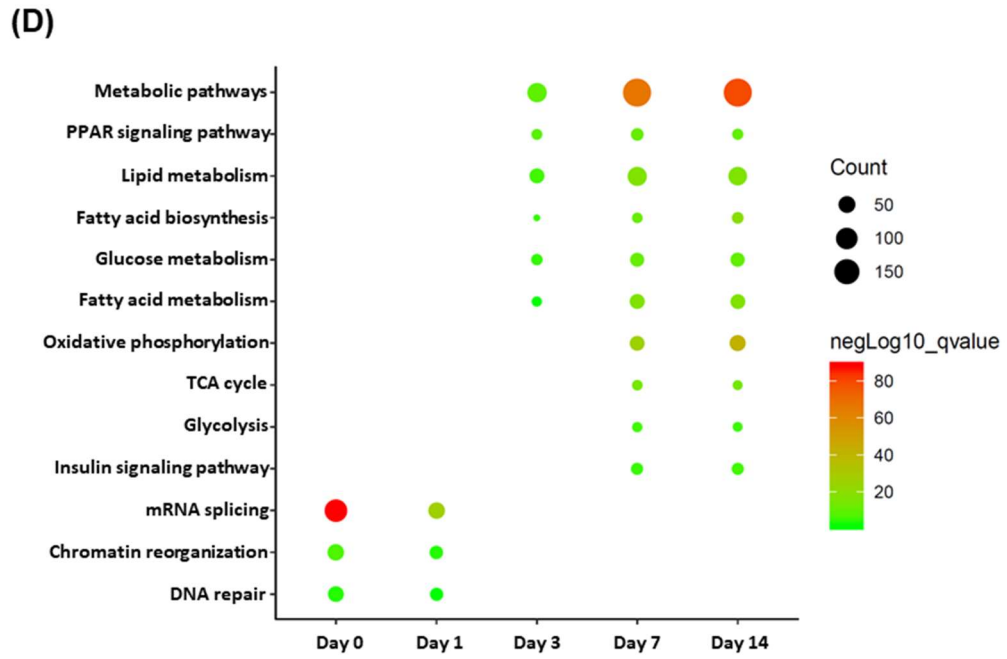
(D)
Metabolic pathways
PPAR signaling pathway
Lipid metabolism
Fatty acid biosynthesis
Glucose metabolism
Fatty acid metabolism
Oxidative phosphorylation
TCA cycle
Glycolysis
Insulin signaling pathway
mRNA splicing
Chromatin reorganization
DNA repair
Day 0
Day 1
Day 3
Day 7
Day 14
Count
50
100
150
negLog10_qvalue
80
60
40
20

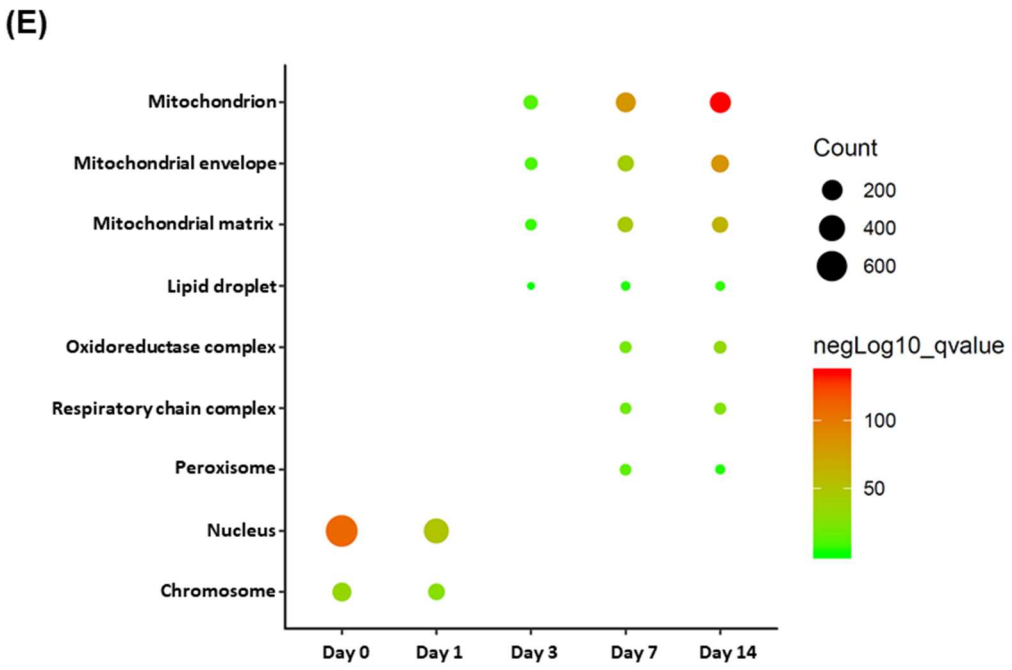
(E)
Mitochondrion
Mitochondrial envelope
Mitochondrial matrix
Lipid droplet
Oxidoreductase complex
Respiratory chain complex
Peroxisome
Nucleus
Chromosome
Day 0
Day 1
Day 3
Day 7
Day 14
Count
200
400
600
negLog10_qvalue
100
50

Fig. 4: Obese ADSCs display a distinct proteome profile compared to healthy cells during adipogenesis over a 14-day timespan. (A) PCA analysis and **(B)** Hierarchical clustering for healthy and obese samples at indicated timepoints during adipogenesis. **(C)** Volcano plots showing number of differentially expressed genes in healthy and obese adipogenesis at indicated timepoints. **(D)** Functional gene clustering and enrichment analysis for upregulated genes in healthy cells at indicated timepoints during adipogenesis in REACTOME 2016, KEGG 2019, GO Biological Processes 2018 and **(E)** GO Cellular component 2018 databases. n=3, where n represents healthy and obese biological replicates.

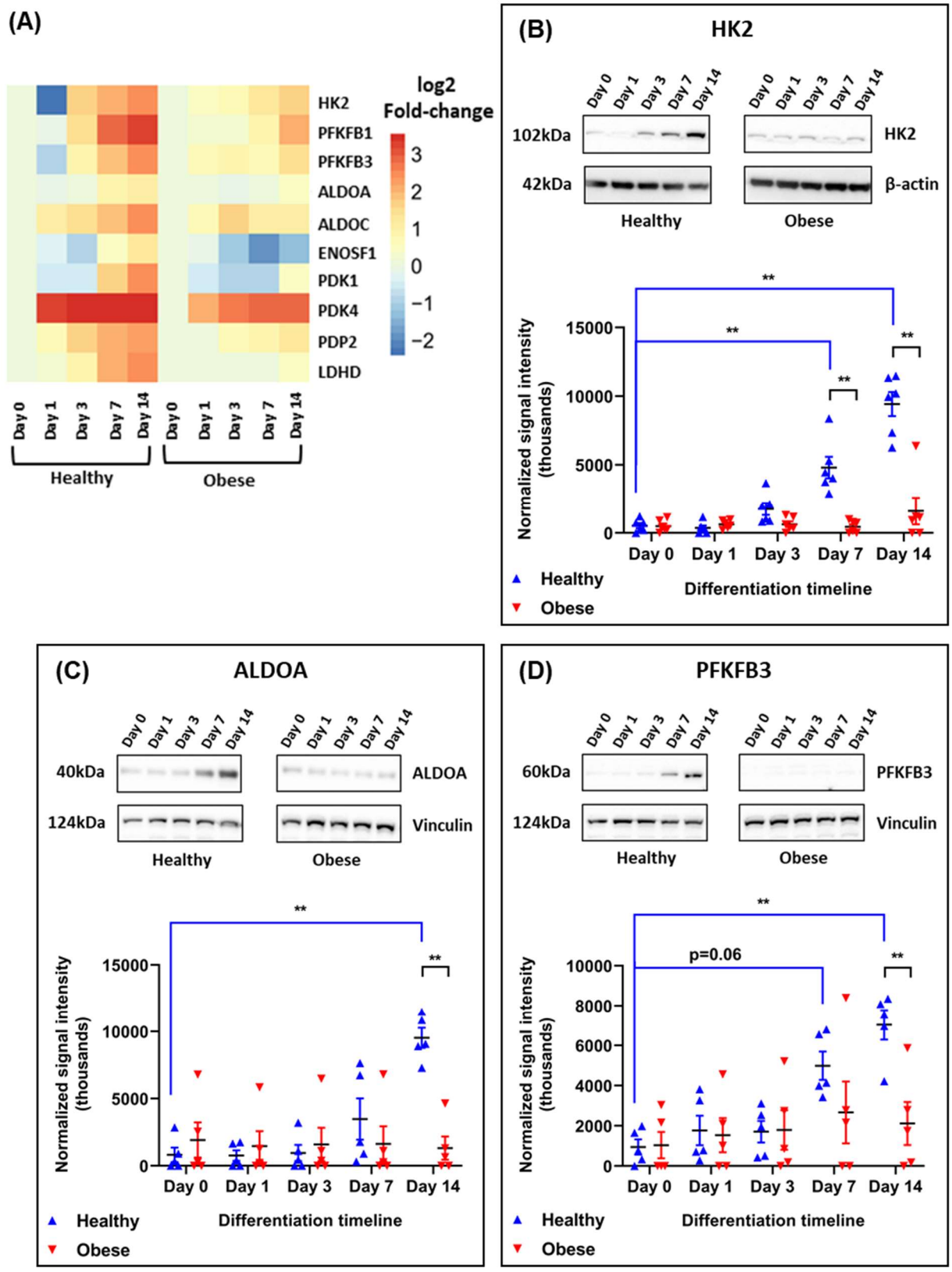
(A)
log2 Fold-change
3
2
1
0
−1
−2
HK2
PFKFB1
PFKFB3
ALDOA
ALDOC
ENOSF1
PDK1
PDK4
PDP2
LDHD
Day 0
Day 1
Day 3
Day 7
Day 14
Healthy
Obese
(B)
HK2
102kDa
42kDa
β-actin
Normalized signal intensity (thousands)
Differentiation timeline
Healthy
Obese
(C)
ALDOA
40kDa
124kDa
Vinculin
(D)
PFKFB3
60kDa
p=0.06

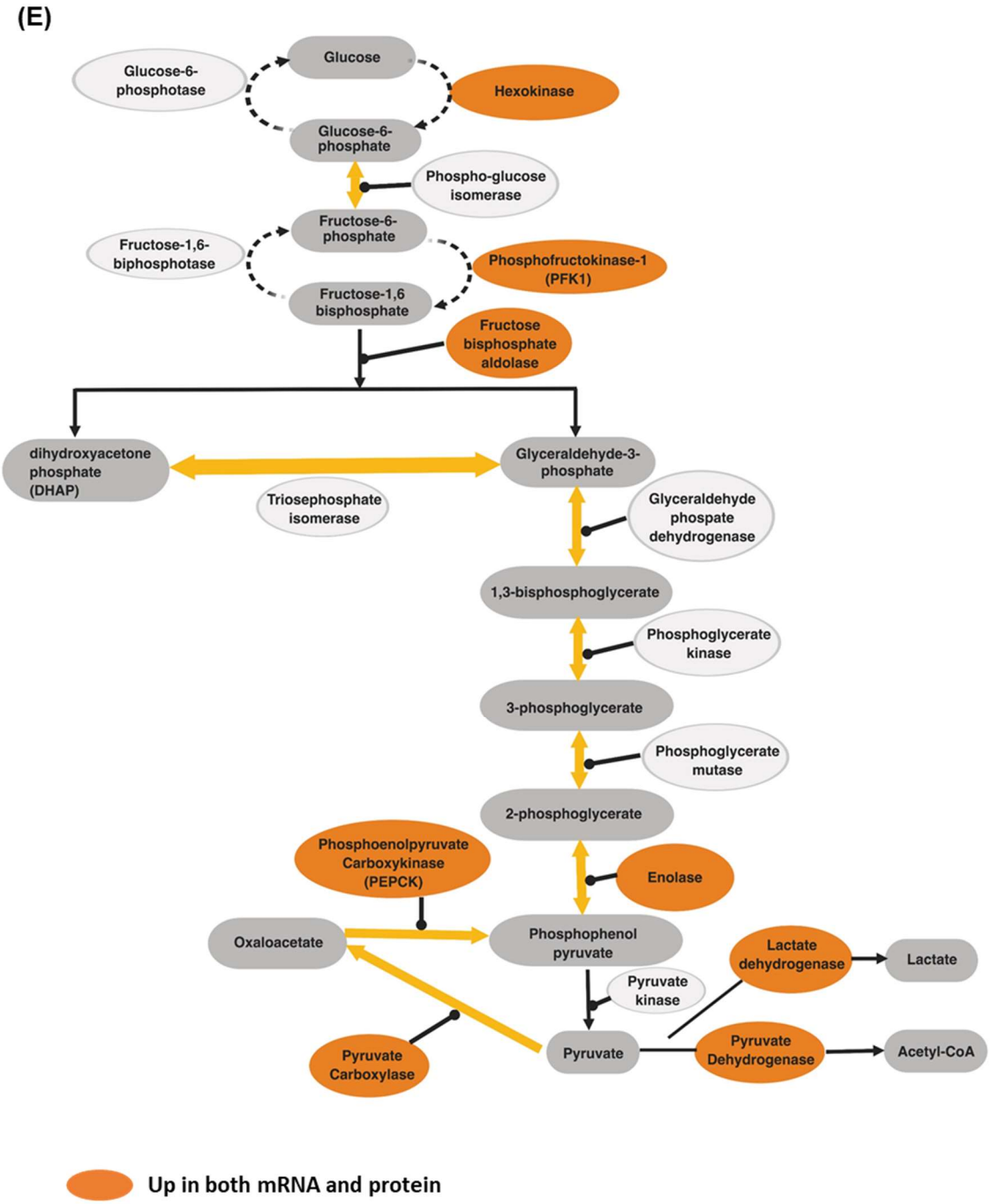
(E)
Glucose-6-phosphotase
Glucose
Hexokinase
Glucose-6-phosphate
Phospho-glucose isomerase
Fructose-6-phosphate
Fructose-1,6-biphosphotase
Phosphofructokinase-1 (PFK1)
Fructose-1,6 bisphosphate
Fructose bisphosphate aldolase
dihydroxyacetone phosphate (DHAP)
Triosephosphate isomerase
Glyceraldehyde-3-phosphate
Glyceraldehyde phospate dehydrogenase
1,3-bisphosphoglycerate
Phosphoglycerate kinase
3-phosphoglycerate
Phosphoglycerate mutase
2-phosphoglycerate
Phosphoenolpyruvate Carboxykinase (PEPCK)
Enolase
Oxaloacetate
Phosphophenol pyruvate
Lactate dehydrogenase
Lactate
Pyruvate kinase
Pyruvate Carboxylase
Pyruvate
Pyruvate Dehydrogenase
Acetyl-CoA
Up in both mRNA and protein

Fig. 5: Obese cells have an altered glucose metabolism gene signature during adipogenesis. **(A)** Heat map showing log2 fold change in gene expression of glycolysis markers in healthy and obese cells during adipogenic differentiation. **(B)** Representative western blots showing changes in HK2 protein expression during adipogenesis and quantification of HK2 expression upon normalization to β-actin (loading control). **(C)** Representative western blots showing changes in ALDOA protein expression during adipogenesis and quantification of ALDOA expression upon normalization to vinculin (loading control) (n=5). **(D)** Representative western blots showing changes in PFKFB3 protein expression during adipogenesis and quantification of PFKFB3 expression upon normalization to vinculin (loading control) (n=5). **(E)** Glycolysis pathway showing genes upregulated in day 14 healthy compared to obese adipocytes.

Data is represented as mean±SEM, n=6 (except where indicated), where n represents biological replicates of healthy and obese ADSCs. Statistical significance was determined by using two-way ANOVA corrected for multiple comparisons with Tukey's test. ** $p<0.01$.

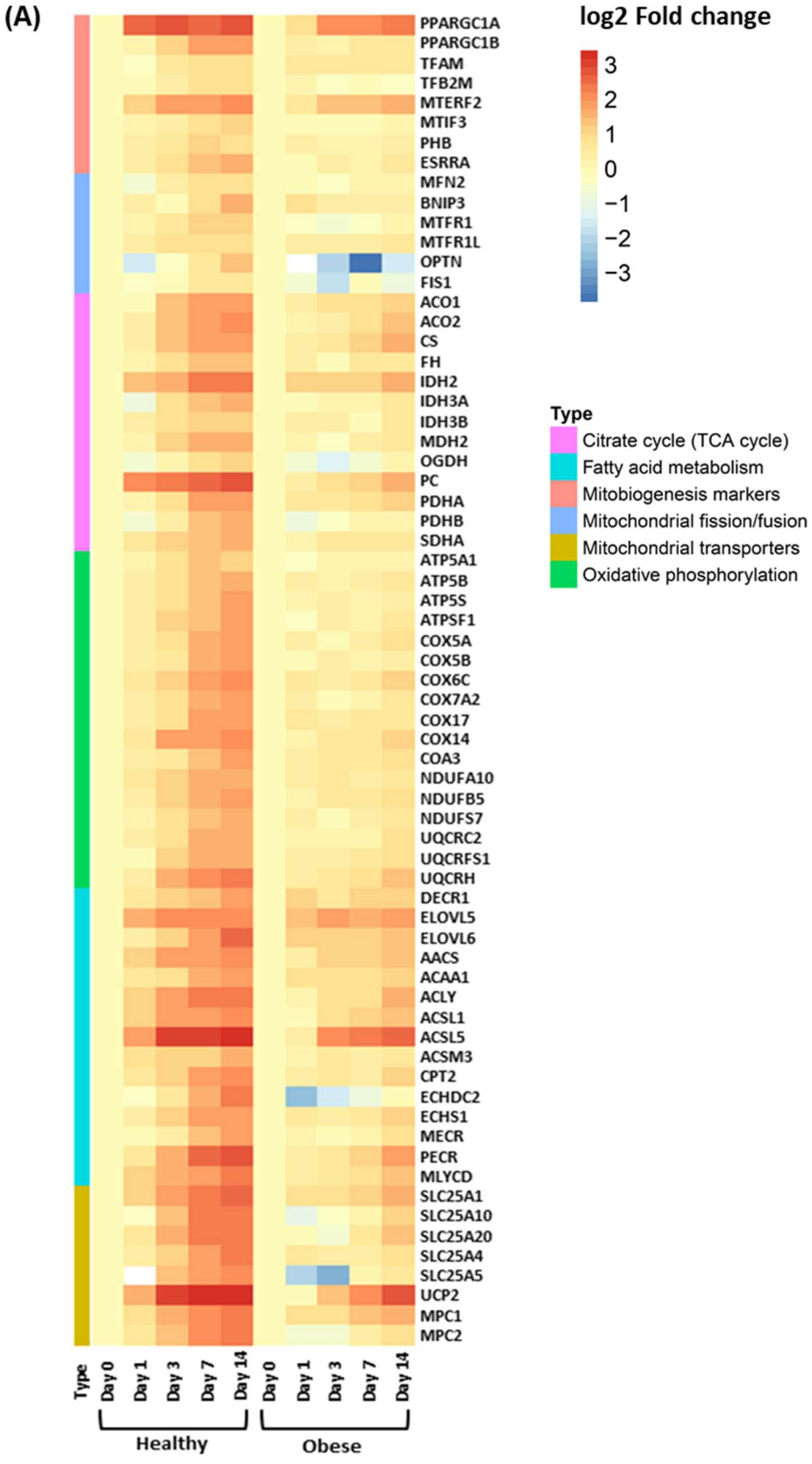
(A)
log2 Fold change
3
2
1
0
−1
−2
−3
PPARGC1A
PPARGC1B
TFAM
TFB2M
MTERF2
MTIF3
PHB
ESRRA
MFN2
BNIP3
MTFR1
MTFR1L
OPTN
FIS1
ACO1
ACO2
CS
FH
IDH2
IDH3A
IDH3B
MDH2
OGDH
PC
PDHA
PDHB
SDHA
ATP5A1
ATP5B
ATP5S
ATPSF1
COX5A
COX5B
COX6C
COX7A2
COX17
COX14
COA3
NDUFA10
NDUFB5
NDUFS7
UQCRC2
UQCRFS1
UQCRH
DECR1
ELOVL5
ELOVL6
AACS
ACAA1
ACLY
ACSL1
ACSL5
ACSM3
CPT2
ECHDC2
ECHS1
MECR
PECR
MLYCD
SLC25A1
SLC25A10
SLC25A20
SLC25A4
SLC25A5
UCP2
MPC1
MPC2
Type
Citrate cycle (TCA cycle)
Fatty acid metabolism
Mitobiogenesis markers
Mitochondrial fission/fusion
Mitochondrial transporters
Oxidative phosphorylation
Type
Day 0
Day 1
Day 3
Day 7
Day 14
Day 0
Day 1
Day 3
Day 7
Day 14
Healthy
Obese

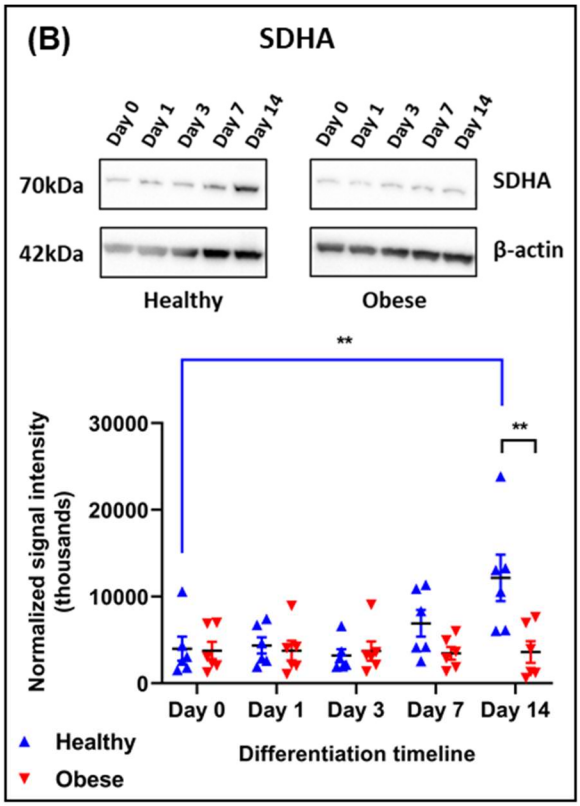
(B)
SDHA
Day 0
Day 1
Day 3
Day 7
Day 14
70kDa
SDHA
42kDa
β-actin
Healthy
Obese
Normalized signal intensity (thousands)
Healthy
Obese
Differentiation timeline

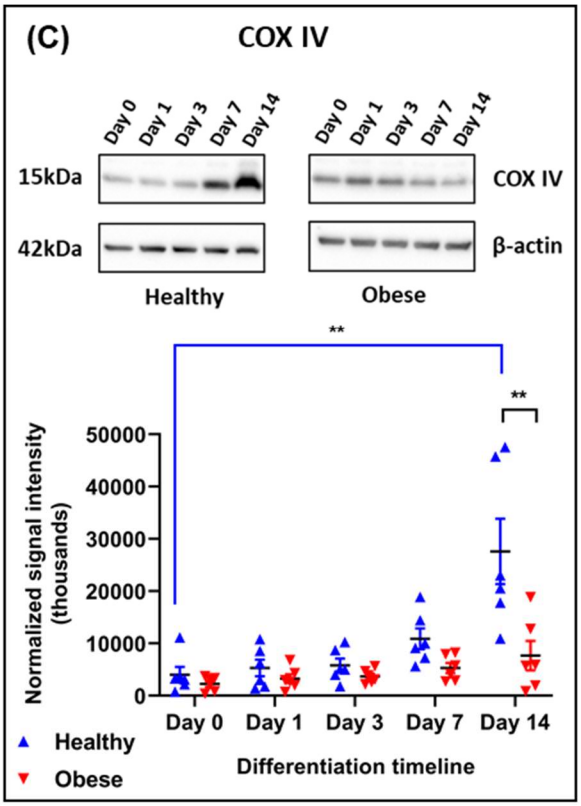
(C)
COX IV
Day 0
Day 1
Day 3
Day 7
Day 14
15kDa
COX IV
42kDa
β-actin
Healthy
Obese
Normalized signal intensity (thousands)
Healthy
Obese
Differentiation timeline

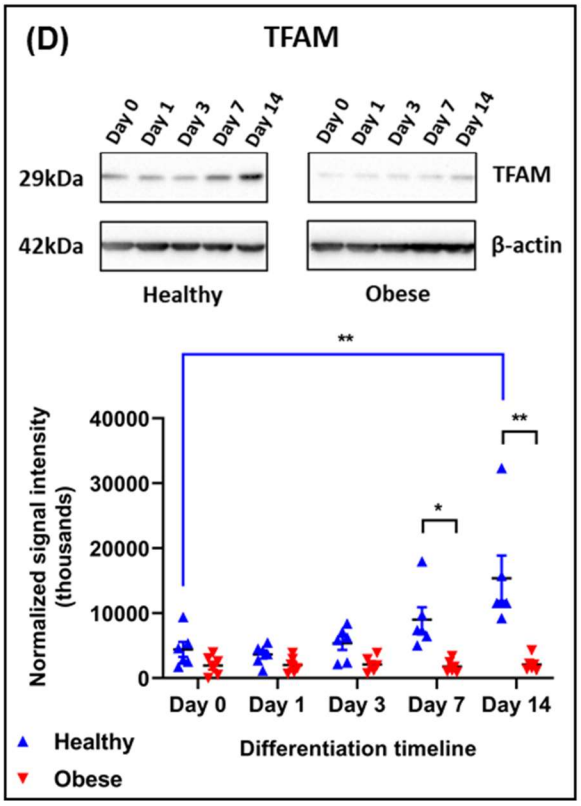
(D)
TFAM
Day 0
Day 1
Day 3
Day 7
Day 14
29kDa
TFAM
42kDa
β-actin
Healthy
Obese
Normalized signal intensity (thousands)
Healthy
Obese
Differentiation timeline

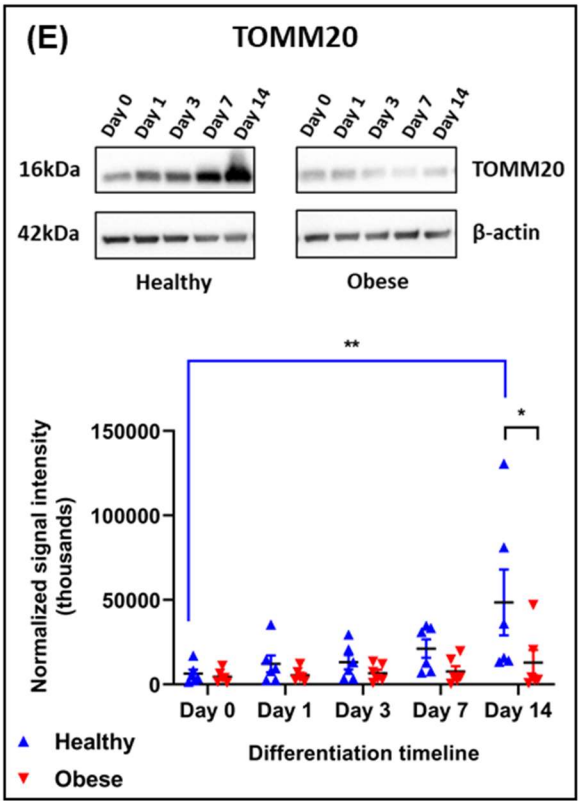
(E)
TOMM20
Day 0
Day 1
Day 3
Day 7
Day 14
16kDa
TOMM20
42kDa
β-actin
Healthy
Obese
Normalized signal intensity (thousands)
Healthy
Obese
Differentiation timeline

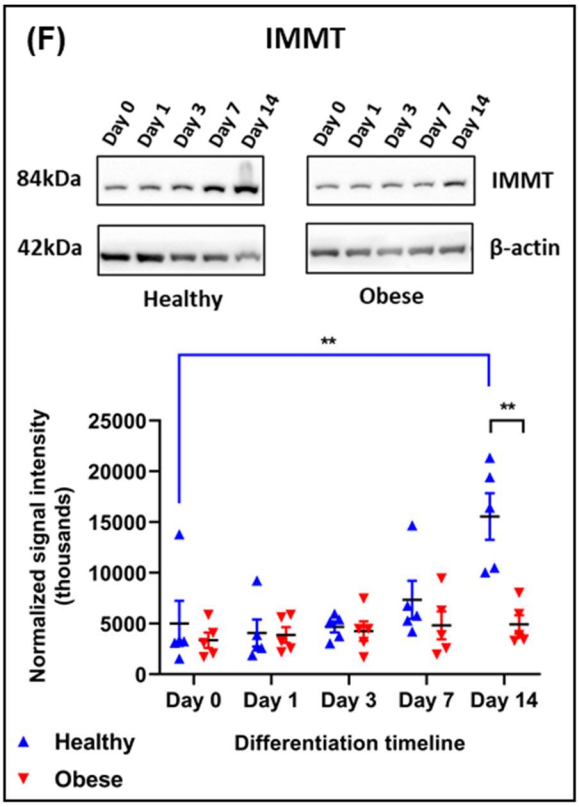
(F)
IMMT
Day 0
Day 1
Day 3
Day 7
Day 14
84kDa
42kDa
IMMT
β-actin
Healthy
Obese
Normalized signal intensity (thousands)
25000
20000
15000
10000
5000
0
**
Day 0
Day 1
Day 3
Day 7
Day 14
Healthy
Obese
Differentiation timeline

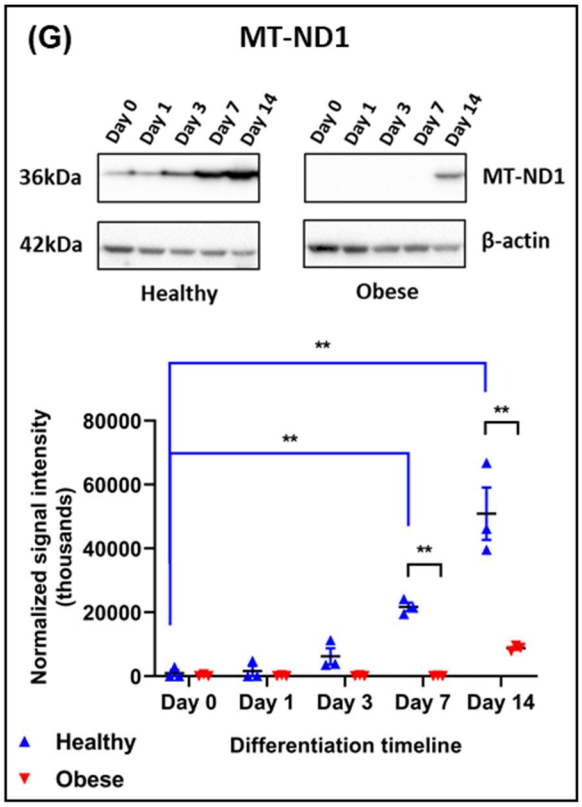
(G)
MT-ND1
Day 0
Day 1
Day 3
Day 7
Day 14
36kDa
42kDa
MT-ND1
β-actin
Healthy
Obese
Normalized signal intensity (thousands)
80000
60000
40000
20000
0
**
Day 0
Day 1
Day 3
Day 7
Day 14
Healthy
Obese
Differentiation timeline

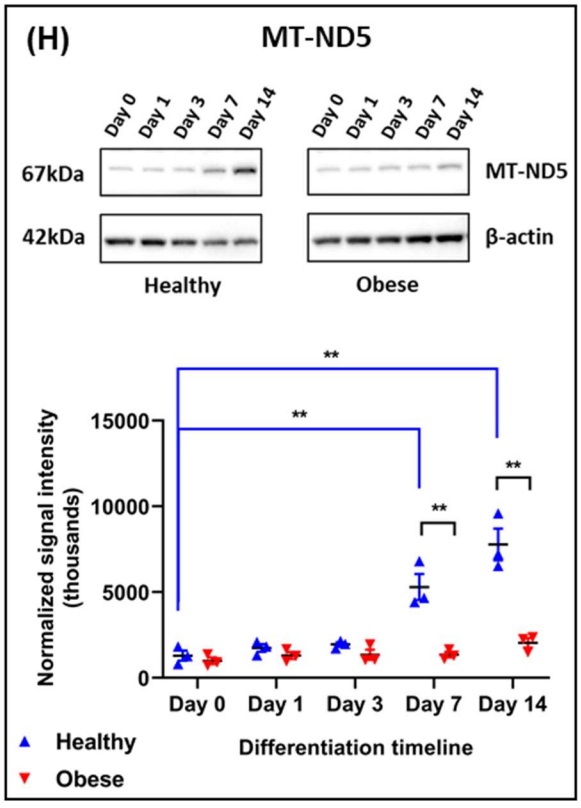
(H)
MT-ND5
Day 0
Day 1
Day 3
Day 7
Day 14
67kDa
42kDa
MT-ND5
β-actin
Healthy
Obese
Normalized signal intensity (thousands)
15000
10000
5000
0
**
Day 0
Day 1
Day 3
Day 7
Day 14
Healthy
Obese
Differentiation timeline

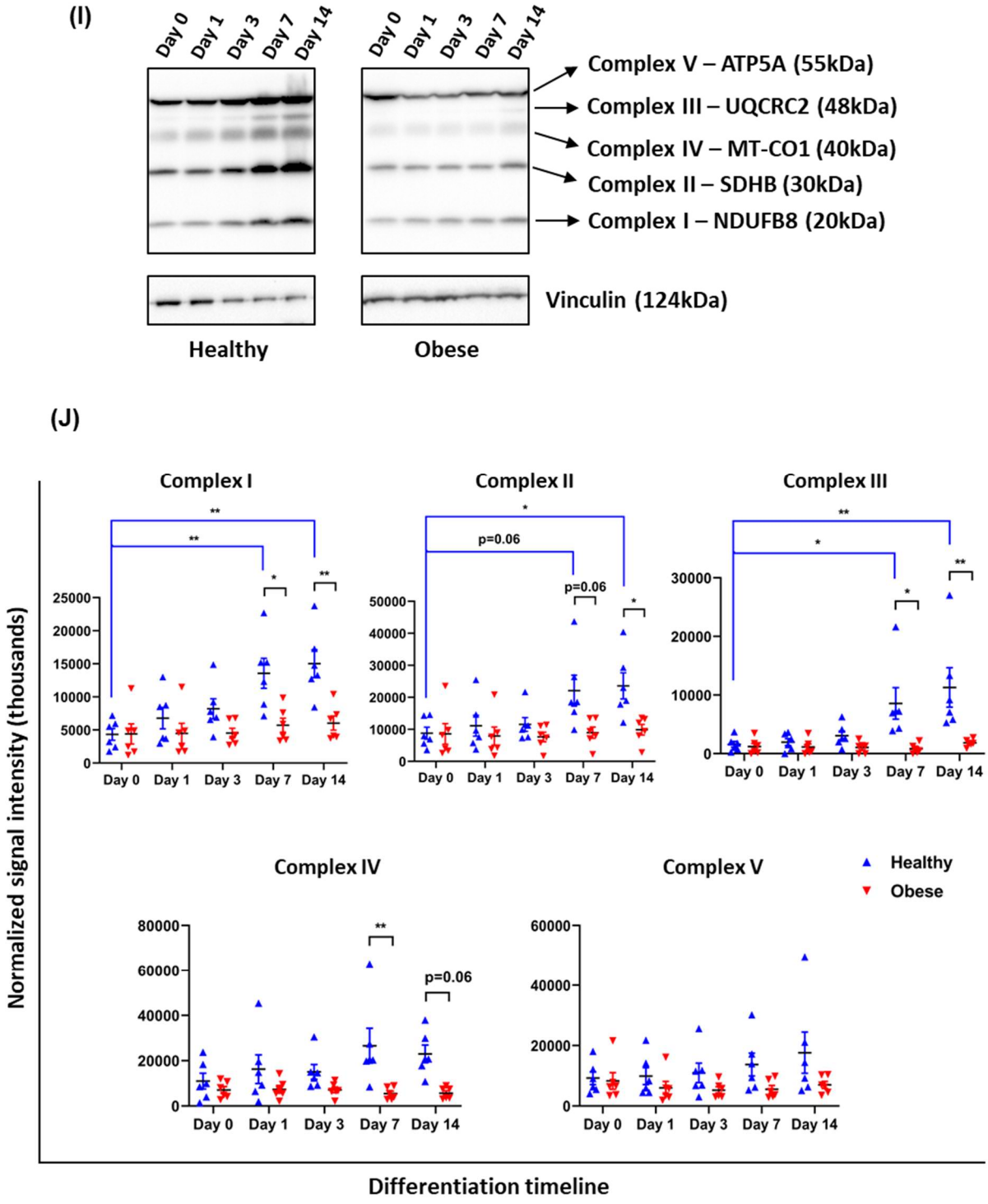
(I)
Day 0
Day 1
Day 3
Day 7
Day 14
Complex V – ATP5A (55kDa)
Complex III – UQCRC2 (48kDa)
Complex IV – MT-CO1 (40kDa)
Complex II – SDHB (30kDa)
Complex I – NDUFB8 (20kDa)
Vinculin (124kDa)
Healthy
Obese
(J)
Complex I
Complex II
Complex III
Complex IV
Complex V
p=0.06
Healthy
Obese
Normalized signal intensity (thousands)
Differentiation timeline

(K)

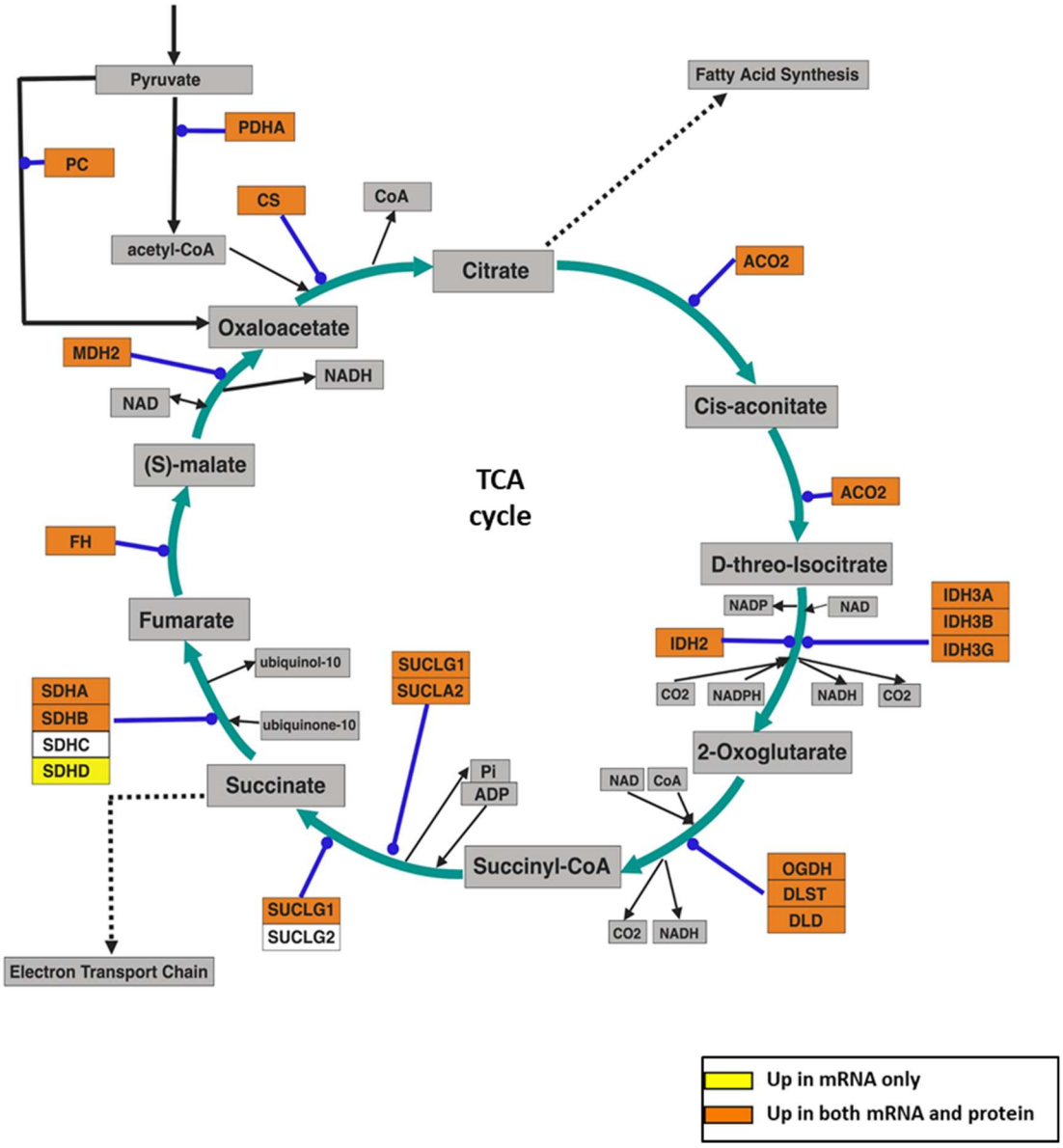
Pyruvate
PDHA
PC
CS
CoA
acetyl-CoA
Fatty Acid Synthesis
Citrate
ACO2
Oxaloacetate
MDH2
NADH
NAD
Cis-aconitate
(S)-malate
TCA cycle
ACO2
FH
D-threo-Isocitrate
NADP
NAD
IDH3A
IDH3B
IDH3G
IDH2
Fumarate
ubiquinol-10
SUCLG1
SUCLA2
SDHA
SDHB
SDHC
SDHD
ubiquinone-10
CO2
NADPH
NADH
CO2
2-Oxoglutarate
Pi
ADP
NAD
CoA
Succinate
Succinyl-CoA
OGDH
DLST
DLD
SUCLG1
SUCLG2
CO2
NADH
Electron Transport Chain
Up in mRNA only
Up in both mRNA and protein

(L)

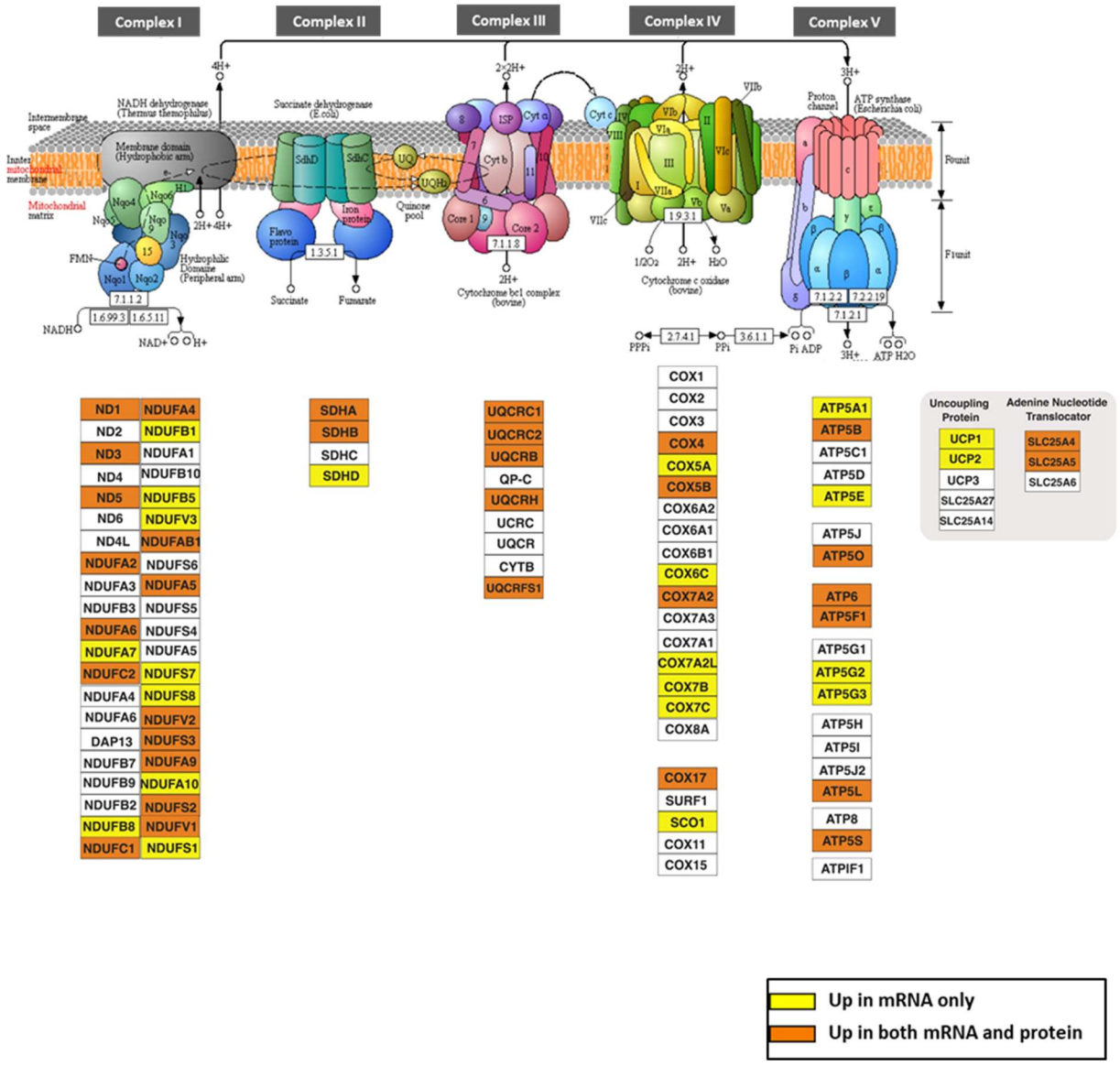
Complex I
Complex II
Complex III
Complex IV
Complex V
NADH dehydrogenase (Thermus thermophilus)
Succinate dehydrogenase (E.coli)
Membrane domain (Hydrophobic arm)
Hydrophilic Domain (Peripheral arm)
Flavo protein
Iron protein
Succinate
Fumarate
Quinone pool
Cytochrome bc1 complex (bovine)
Cytochrome c oxidase (bovine)
Proton channel
ATP synthase (Escherichia coli)
Intermembrane space
Mitochondrial matrix
NADH
NAD+
FMN
Fe-S
Cyt b
Cyt c1
Cyt c
Core 1
Core 2
ISP
SdhD
SdhC
UQ
UQH2
Fo unit
F1 unit
ATP H2O
Pi ADP
PPi
PPPi
ND1 NDUFA4
ND2 NDUFB1
ND3 NDUFA1
ND4 NDUFB10
ND5 NDUFB5
ND6 NDUFV3
ND4L NDUFAB1
NDUFA2 NDUFS6
NDUFA3 NDUFA5
NDUFB3 NDUFS5
NDUFA6 NDUFS4
NDUFA7 NDUFA5
NDUFC2 NDUFS7
NDUFA4 NDUFS8
NDUFA6 NDUFV2
DAP13 NDUFS3
NDUFB7 NDUFA9
NDUFB9 NDUFA10
NDUFB2 NDUFS2
NDUFB8 NDUFV1
NDUFC1 NDUFS1
SDHA
SDHB
SDHC
SDHD
UQCRC1
UQCRC2
UQCRB
QP-C
UQCRH
UCRC
UQCR
CYTB
UQCRFS1
COX1
COX2
COX3
COX4
COX5A
COX5B
COX6A2
COX6A1
COX6B1
COX6C
COX7A2
COX7A3
COX7A1
COX7A2L
COX7B
COX7C
COX8A
COX17
SURF1
SCO1
COX11
COX15
ATP5A1
ATP5B
ATP5C1
ATP5D
ATP5E
ATP5J
ATP5O
ATP6
ATP5F1
ATP5G1
ATP5G2
ATP5G3
ATP5H
ATP5I
ATP5J2
ATP5L
ATP8
ATP5S
ATPIF1
Uncoupling Protein
UCP1
UCP2
UCP3
SLC25A27
SLC25A14
Adenine Nucleotide Translocator
SLC25A4
SLC25A5
SLC25A6
Up in mRNA only
Up in both mRNA and protein

Fig. 6: Obese cells show aberrant mitochondrial biogenesis and function gene signature during adipogenesis. (A) Heat map showing log2 fold change in gene expression of mitochondrial biogenesis and function markers in healthy and obese cells during adipogenic differentiation. **(B)** Representative western blots showing changes in SDHA, COX IV **(C)**, TFAM **(D)**, TOMM20 **(E)**, IMMT (n=5) **(F)**, MT-ND1 (n=3) **(G)**, and MT-ND5 (n=3) **(H)** protein expression during adipogenesis and quantification of their expression upon normalization to β-actin (loading control). **(I)** Representative western blots showing protein expression of respiratory chain complexes I-V during adipogenesis in healthy and obese cells and quantification of their expression **(J)** upon normalization to vinculin (loading control). **(K)** Tricarboxylic acid (TCA) cycle and electron transport chain **(L)** pathways showing genes upregulated in day 14 healthy compared to obese adipocytes.

Data is represented as mean±SEM, n=6 (except where indicated), where n represents biological replicates of healthy and obese ADSCs. Statistical significance was determined by using two-way ANOVA corrected for multiple comparisons with Tukey's test. * $p<0.05$, * $p<0.01$.

See also Figs. S4 and S5.

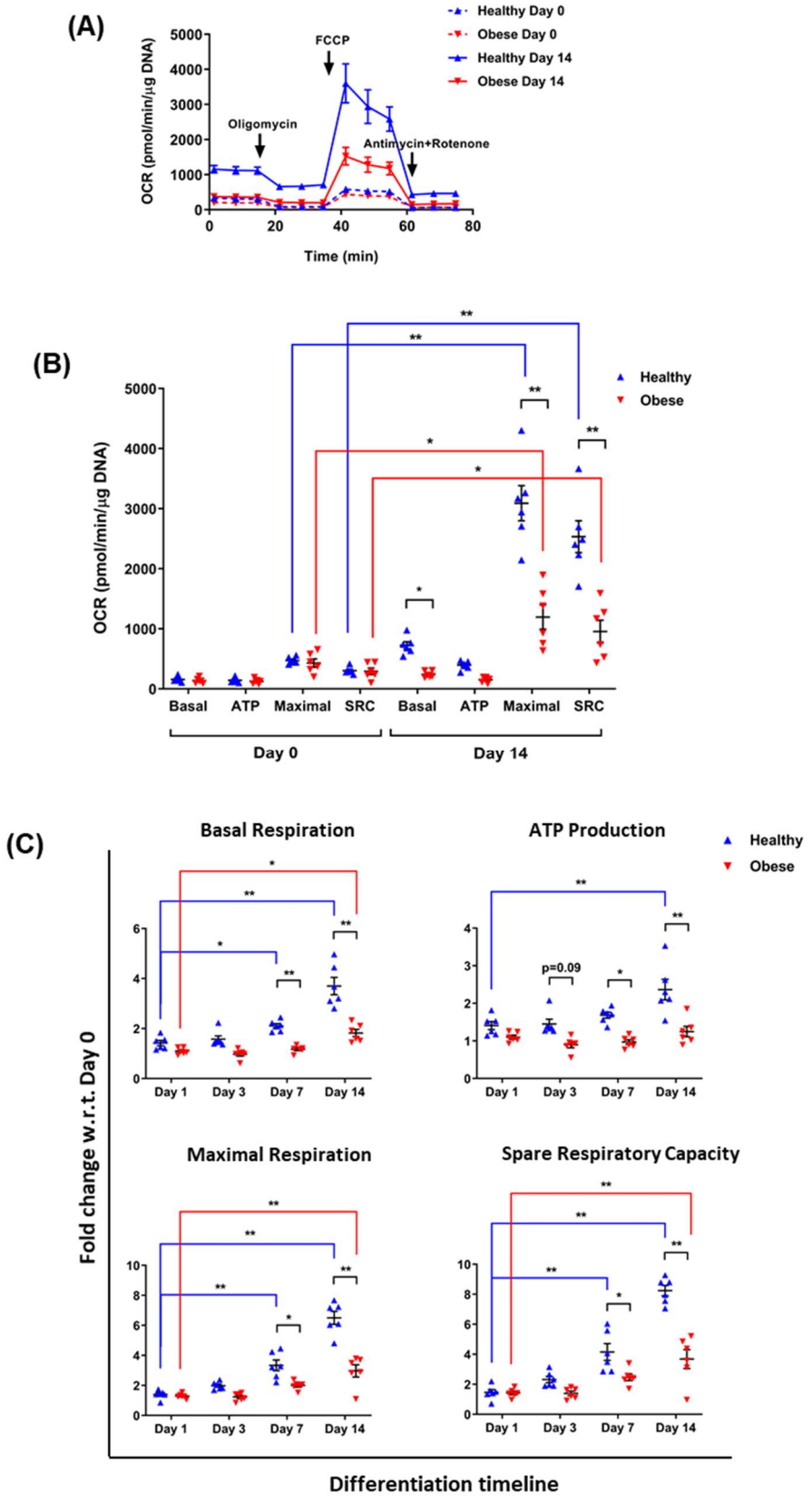
(A)
Healthy Day 0
Obese Day 0
Healthy Day 14
Obese Day 14
FCCP
Oligomycin
Antimycin+Rotenone
OCR (pmol/min/µg DNA)
Time (min)
(B)
Healthy
Obese
OCR (pmol/min/µg DNA)
Basal
ATP
Maximal
SRC
Day 0
Day 14
(C)
Basal Respiration
ATP Production
Maximal Respiration
Spare Respiratory Capacity
p=0.09
Day 1
Day 3
Day 7
Day 14
Fold change w.r.t. Day 0
Differentiation timeline

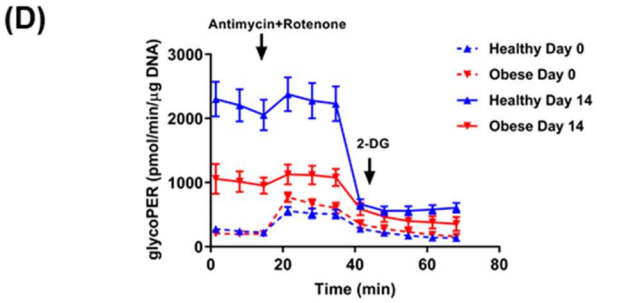
(D)
Antimycin+Rotenone
2-DG
Healthy Day 0
Obese Day 0
Healthy Day 14
Obese Day 14
glycoPER (pmol/min/µg DNA)
Time (min)

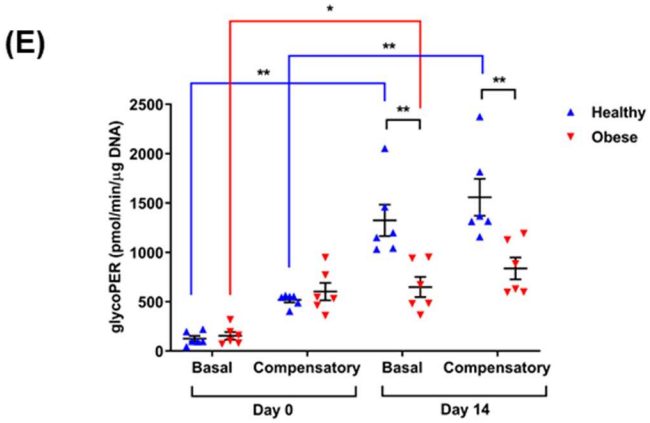
(E)
Healthy
Obese
glycoPER (pmol/min/µg DNA)
Basal
Compensatory
Basal
Compensatory
Day 0
Day 14

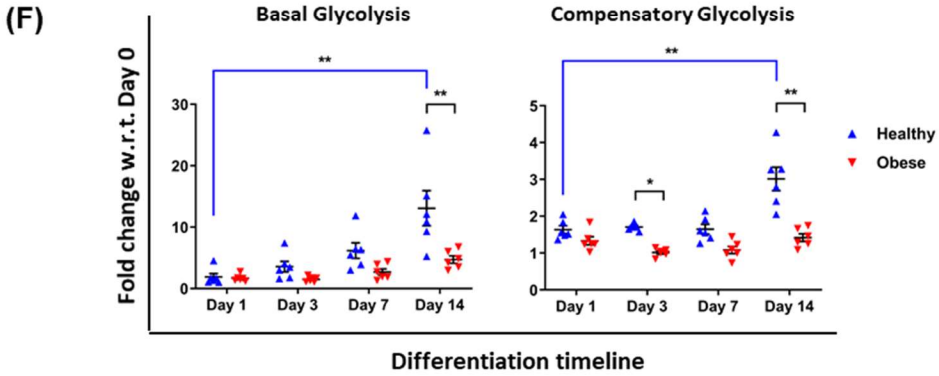
(F)
Basal Glycolysis
Compensatory Glycolysis
Fold change w.r.t. Day 0
Healthy
Obese
Day 1
Day 3
Day 7
Day 14
Differentiation timeline

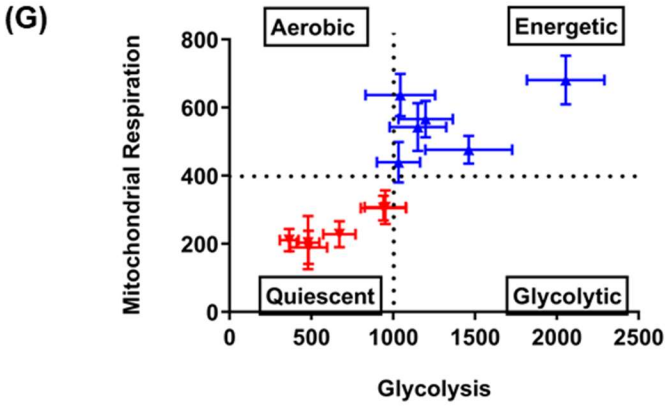
(G)
Aerobic
Energetic
Quiescent
Glycolytic
Mitochondrial Respiration
Glycolysis

Fig. 7: Obese cells exhibit altered cellular bioenergetics during adipogenesis. (A) Representative MST plots for healthy and obese cells at the start of adipogenic differentiation (day 0) and at the differentiation endpoint (day 14). **(B)** Mitochondrial function parameters: Basal respiration (Basal), ATP production (ATP), Maximal respiration (Maximal) and Spare respiratory capacity (SRC) calculated using the Agilent Seahorse Wave 2.6 desktop program at day 0 and 14 of differentiation in healthy and obese cells. **(C)** Fold change in mitochondrial function parameters in healthy and obese cells during adipogenesis. **(D)** Representative GRA plots for healthy and obese cells at the start of adipogenic differentiation (day 0) and at the differentiation endpoint (day 14). **(E)** Glycolytic function parameters: Basal glycolysis (Basal) and Compensatory glycolysis (Compensatory) calculated using the Agilent Seahorse Wave 2.6 desktop program at day 0 and 14 of differentiation in healthy and obese cells. **(F)** Fold change in glycolytic function parameters in healthy and obese cells during adipogenesis. **(G)** Energy map of healthy and obese cells at the differentiation endpoint (day 14).

Data is represented as mean±SEM, n=6, where n represents biological replicates of healthy and obese ADSCs. Statistical significance was determined by using two-way ANOVA corrected for multiple comparisons with Tukey's test. * $p<0.05$, * $p<0.01$.

See also Fig. S6.

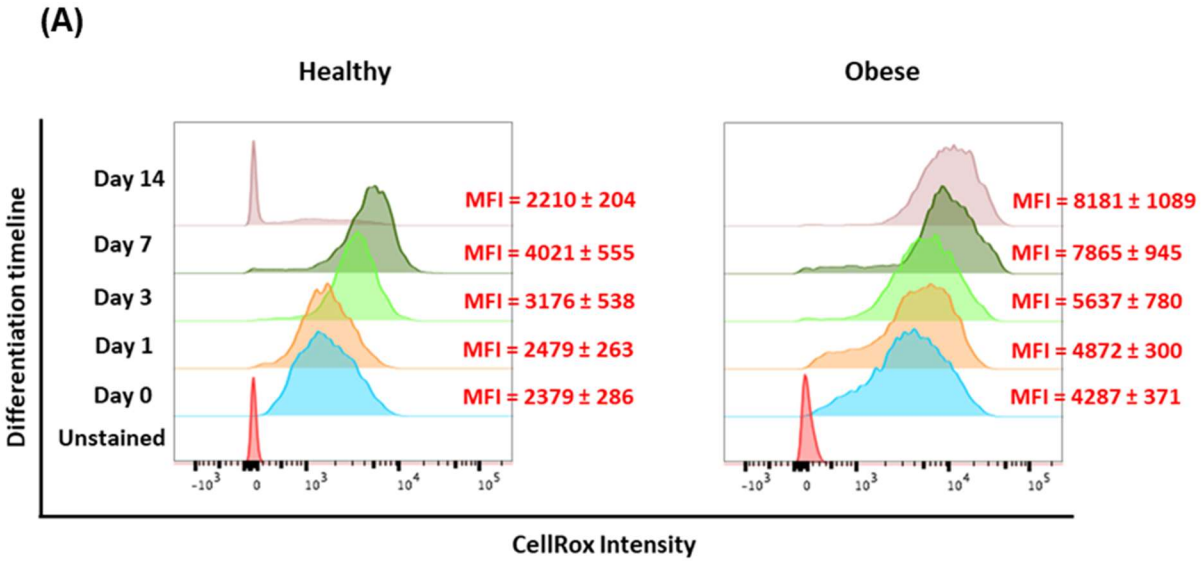
(A)
Healthy
Obese
Differentiation timeline
Day 14
Day 7
Day 3
Day 1
Day 0
Unstained
MFI = 2210 ± 204
MFI = 4021 ± 555
MFI = 3176 ± 538
MFI = 2479 ± 263
MFI = 2379 ± 286
MFI = 8181 ± 1089
MFI = 7865 ± 945
MFI = 5637 ± 780
MFI = 4872 ± 300
MFI = 4287 ± 371
CellRox Intensity

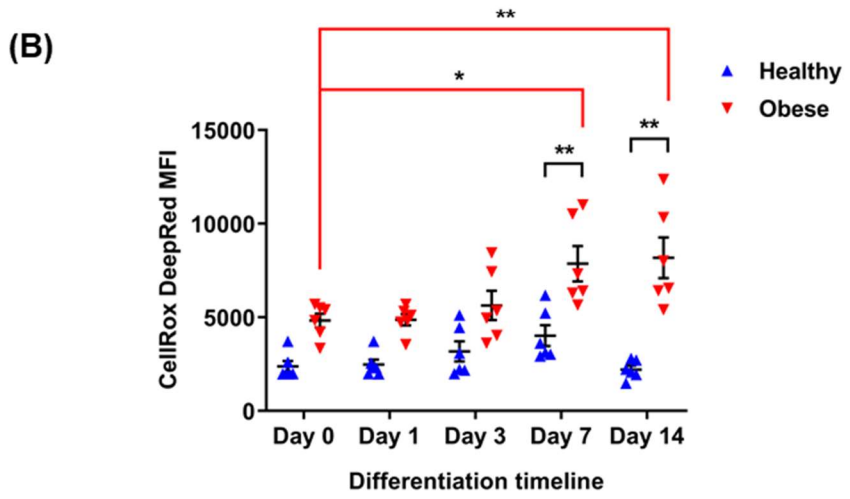
(B)
Healthy
Obese
CellRox DeepRed MFI
15000
10000
5000
0
Day 0
Day 1
Day 3
Day 7
Day 14
Differentiation timeline

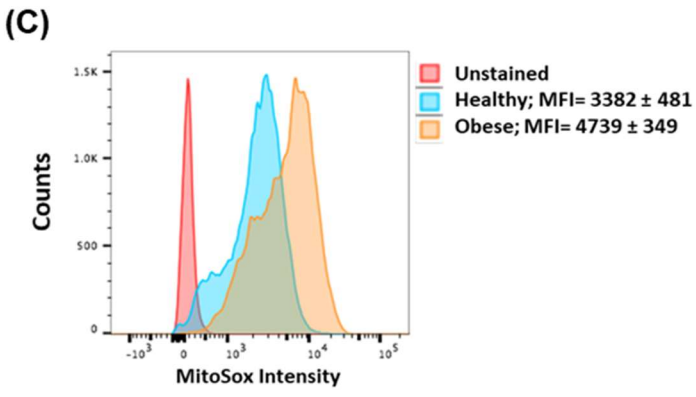
(C)
Counts
Unstained
Healthy; MFI= 3382 ± 481
Obese; MFI= 4739 ± 349
MitoSox Intensity

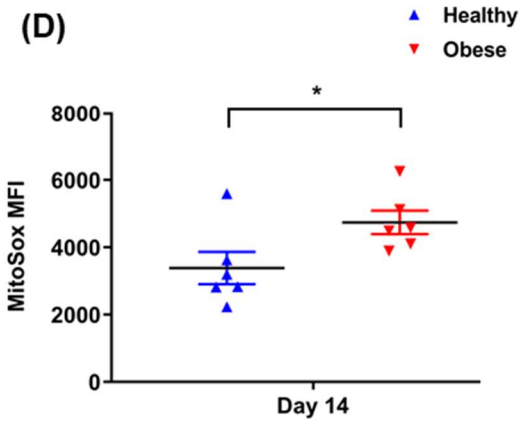
(D)
Healthy
Obese
MitoSox MFI
8000
6000
4000
2000
0
Day 14

Fig. 8: Obese cells generate and accumulate more ROS during adipogenesis. (A) Representative flow cytometry plots for CellRox DeepRed staining of healthy and obese cells at the indicated timepoints during adipogenesis. **(B)** Quantification of CellRox DeepRed staining of healthy and obese cells during adipogenesis by MFI calculated with FlowJo software. **(C)** Representative flow cytometry plots for MitoSox Red staining of healthy and obese cells at the differentiation endpoint (Day 14). **(D)** Quantification of MitoSox Red staining in Day 14 differentiated healthy and obese cells by MFI calculated with FlowJo software.

Data is represented as mean±SEM, n=6, where n represents biological replicates of healthy and obese ADSCs. Statistical significance was determined by using two-way ANOVA corrected for multiple comparisons with Tukey's test for panel (B) and student's two-tailed t-test for panel (D). * $p<0.05$, * $p<0.01$.

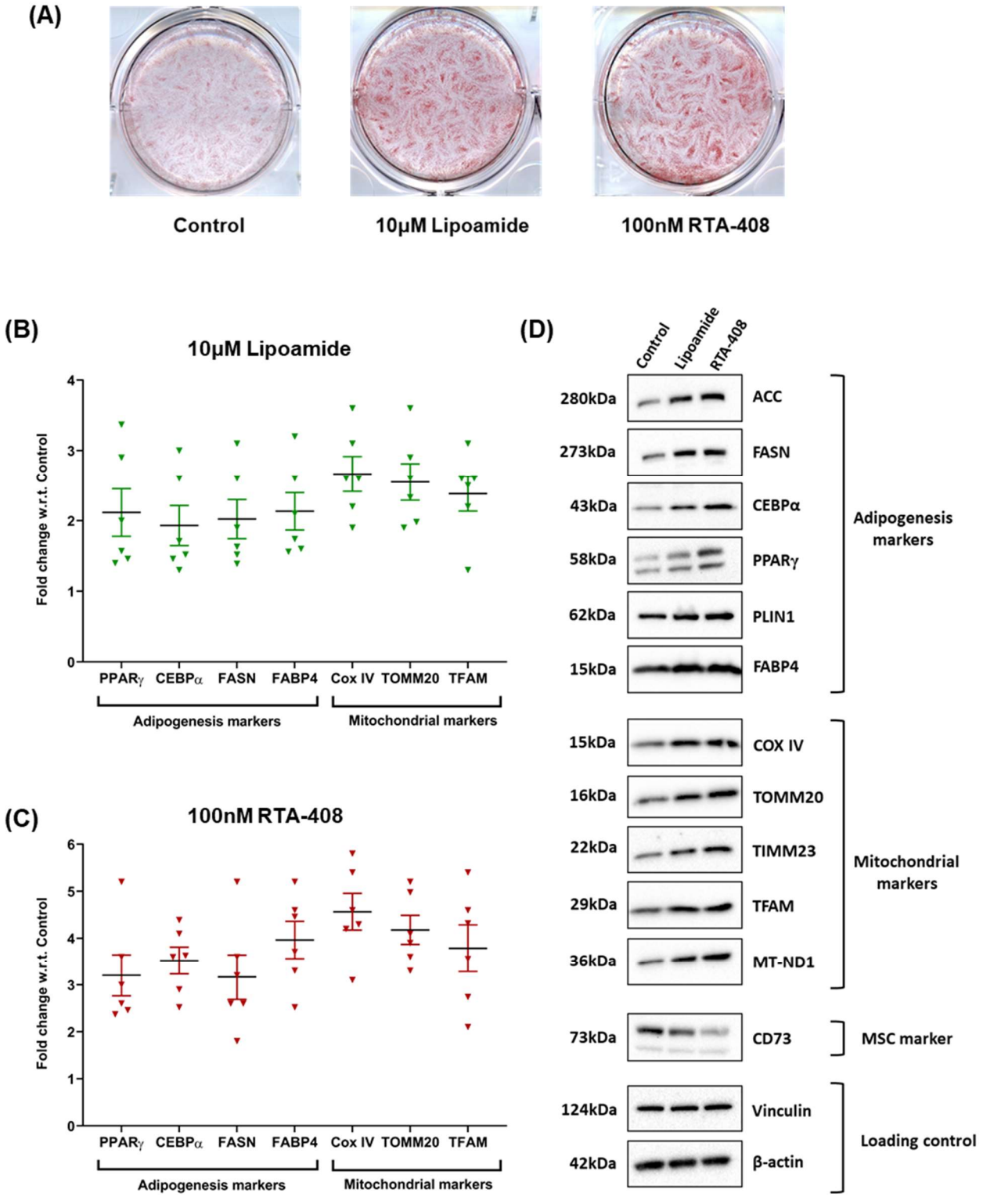
(A)
Control
10µM Lipoamide
100nM RTA-408
(B)
10µM Lipoamide
Fold change w.r.t. Control
PPARγ CEBPα FASN FABP4 Cox IV TOMM20 TFAM
Adipogenesis markers
Mitochondrial markers
(C)
100nM RTA-408
Fold change w.r.t. Control
PPARγ CEBPα FASN FABP4 Cox IV TOMM20 TFAM
Adipogenesis markers
Mitochondrial markers
(D)
Control
Lipoamide
RTA-408
280kDa ACC
273kDa FASN
43kDa CEBPα
58kDa PPARγ
62kDa PLIN1
15kDa FABP4
Adipogenesis markers
15kDa COX IV
16kDa TOMM20
22kDa TIMM23
29kDa TFAM
36kDa MT-ND1
Mitochondrial markers
73kDa CD73
MSC marker
124kDa Vinculin
42kDa β-actin
Loading control

Fig. 9: Small molecule-mediated rescue of adipogenesis in obese cells. (A) Representative scanned ORO whole well images of control, 10 μM Lipoamide- and 100 nM RTA408 treated obese cells. **(B)** Fold change in adipogenesis and mitochondrial marker gene expression by qPCR analysis of RNA isolated from 10 μM Lipoamide- and 100 nM RTA-408-treated **(C)** obese cells compared to control cells at the differentiation endpoint (day 14). **(D)** Representative western blots for adipogenesis, mitochondrial and MSC markers in lysates obtained from 10μM Lipoamide- and 100 nM RTA-408-treated obese cells compared to control cells at the differentiation endpoint (day 14) (n=1).

Data is represented as mean±SEM, n=6 (except where indicated), where n represents obese biological replicates.

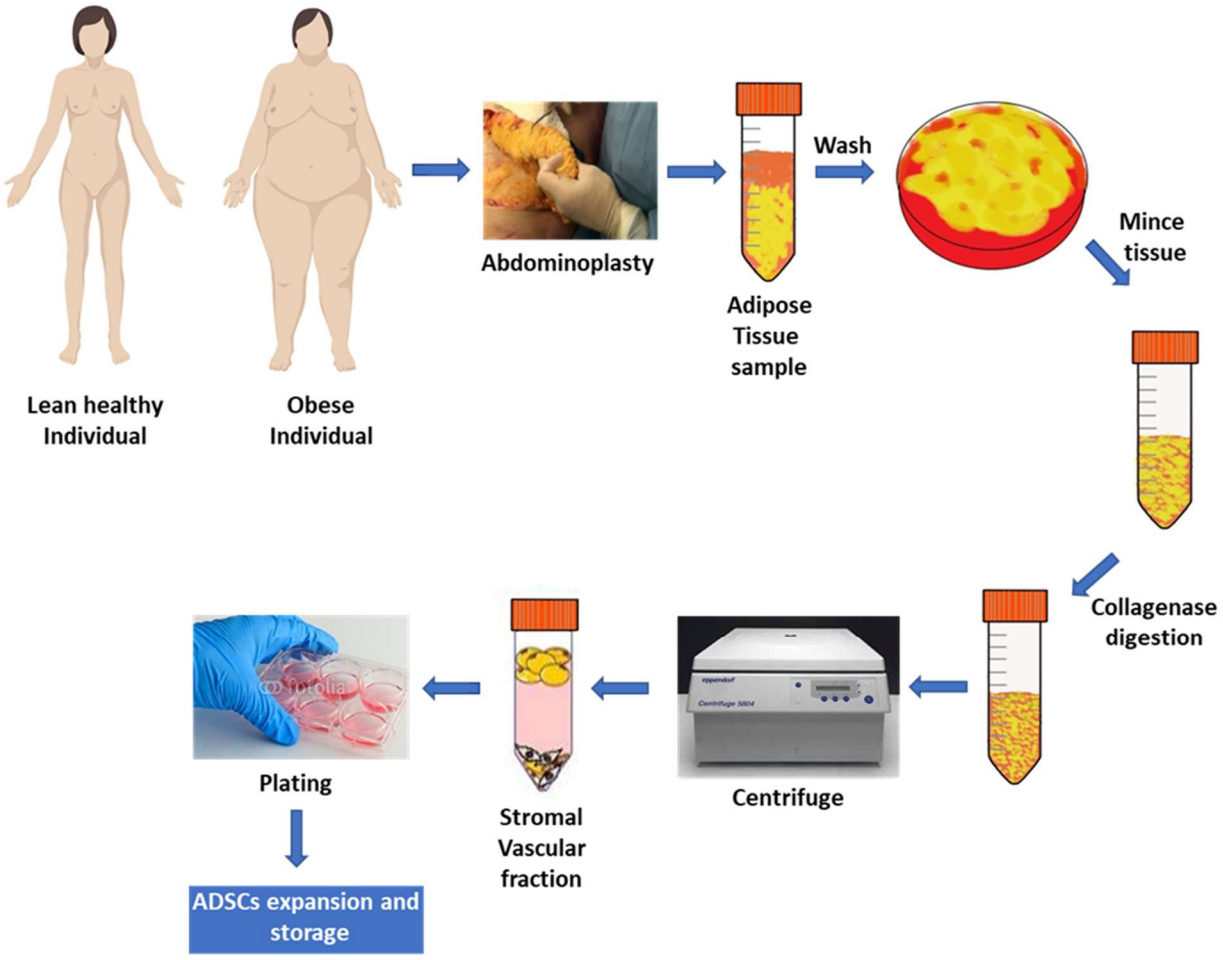

Fig. S1: Schematic showing collagenase-digestion protocol for the isolation of ADSCs from abdominal subcutaneous adipose tissue obtained from healthy and obese donors.

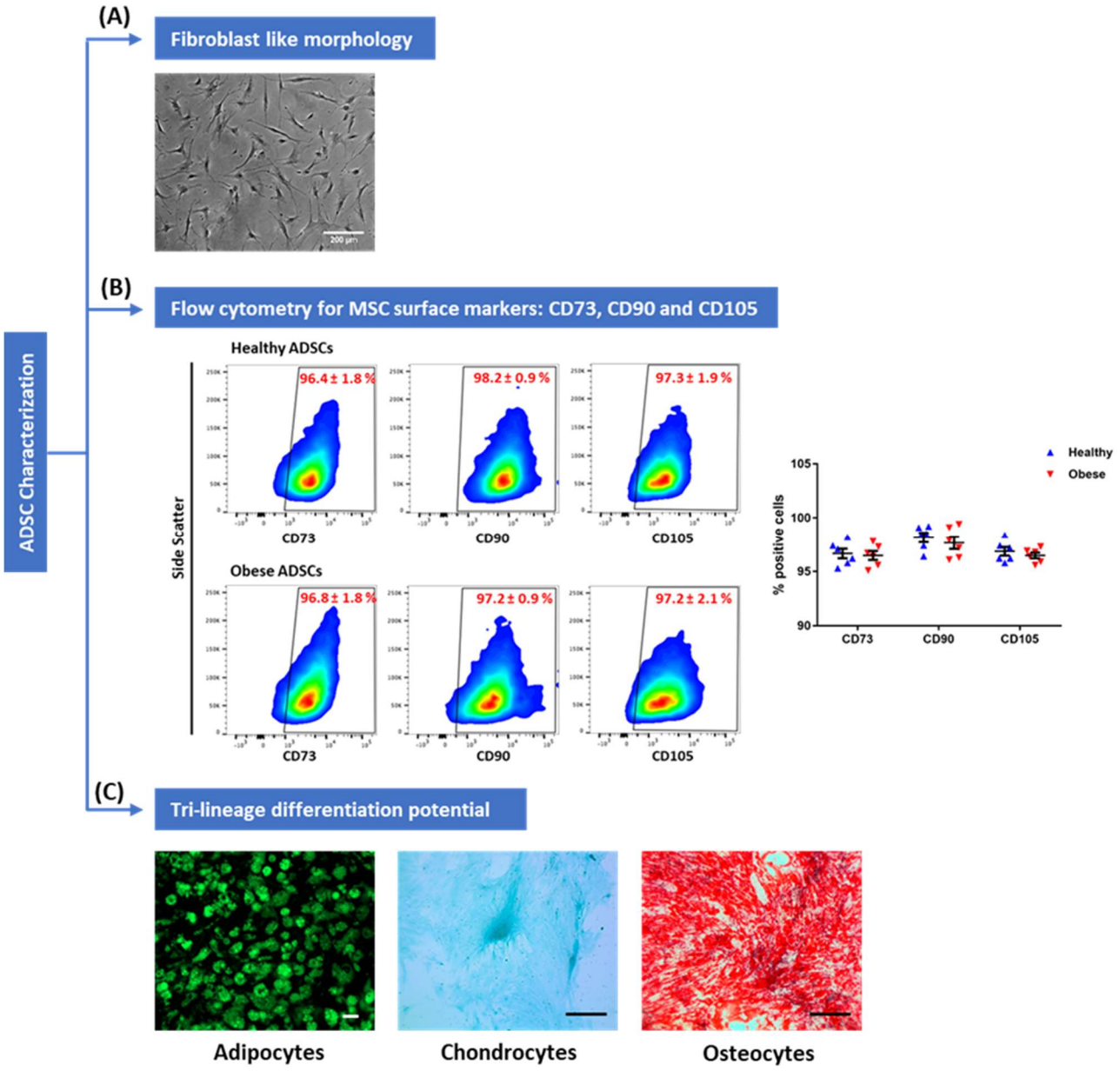
ADSC Characterization
(A)
Fibroblast like morphology
(B)
Flow cytometry for MSC surface markers: CD73, CD90 and CD105
Healthy ADSCs
96.4 ± 1.8 %
98.2 ± 0.9 %
97.3 ± 1.9 %
Side Scatter
CD73
CD90
CD105
Obese ADSCs
96.8 ± 1.8 %
97.2 ± 0.9 %
97.2 ± 2.1 %
CD73
CD90
CD105
Healthy
Obese
% positive cells
105
100
95
90
CD73
CD90
CD105
(C)
Tri-lineage differentiation potential
Adipocytes
Chondrocytes
Osteocytes

Fig. S2: Characterization of ADSCs based on ISCT criteria for MSCs. (A) Representative phase contrast image of ADSCs. **(B)** Representative flow cytometry plots showing CD73, CD90 and CD105 staining for healthy and obese ADSCs and their quantification. **(C)** Representative images of ADSCs differentiated into adipocytes (stained with BODIPY), chondrocytes (stained with Alcian blue) and osteocytes (stained with Alizarin Red). Scale bar represents 200μm.

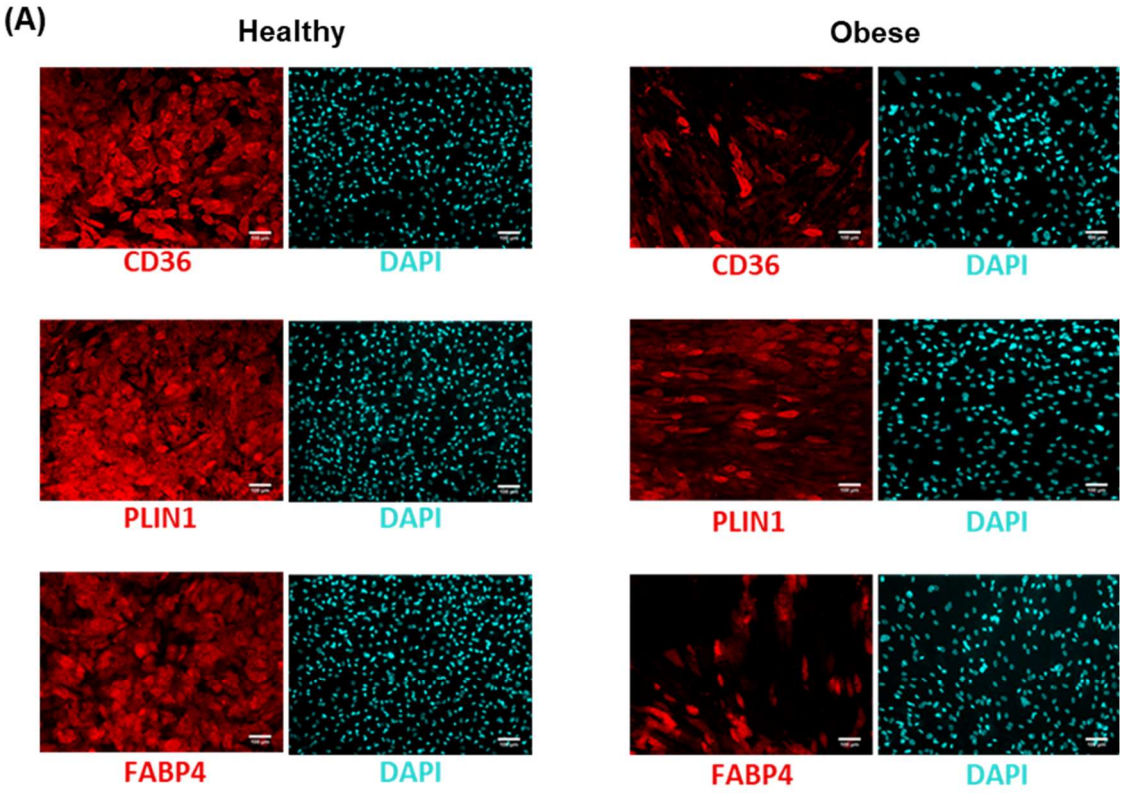
(A)
Healthy
Obese
CD36
DAPI
CD36
DAPI
PLIN1
DAPI
PLIN1
DAPI
FABP4
DAPI
FABP4
DAPI

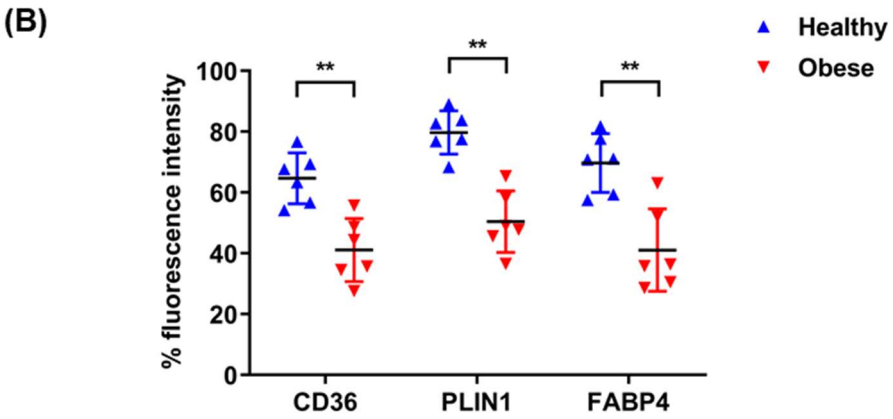
(B)
Healthy
Obese
% fluorescence intensity
100
80
60
40
20
0
**
**
**
CD36
PLIN1
FABP4

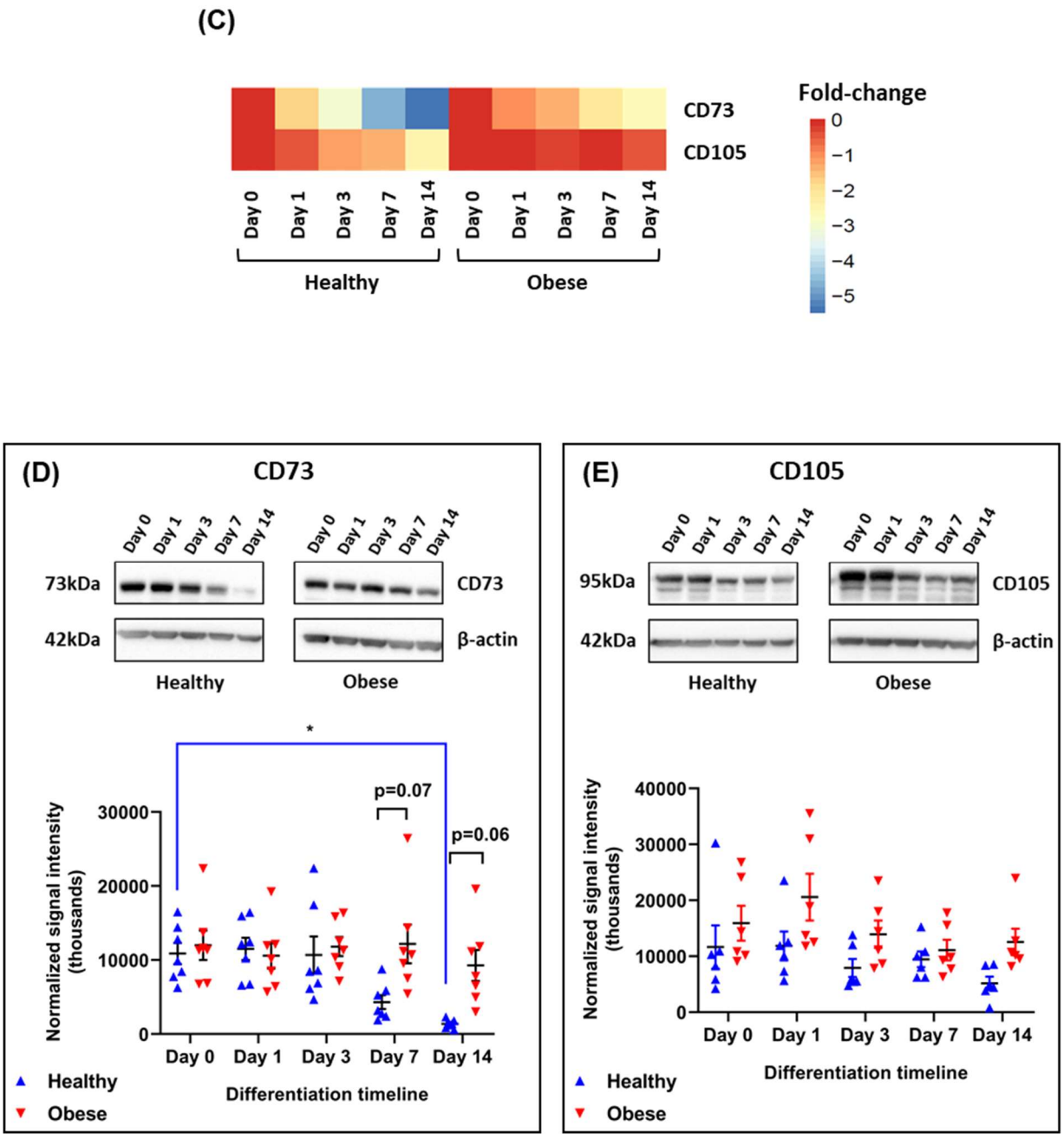
(C)
CD73
CD105
Fold-change
0
−1
−2
−3
−4
−5
Day 0
Day 1
Day 3
Day 7
Day 14
Healthy
Obese
(D)
CD73
73kDa
42kDa
β-actin
(E)
CD105
95kDa
Normalized signal intensity (thousands)
p=0.07
p=0.06
Differentiation timeline
Healthy
Obese

Fig. S3: Obese cells show significantly reduced adipogenic differentiation potential. (A) Immunofluorescence staining for adipocyte markers, CD36, PLIN1 and FABP4 on healthy and obese ADSC-derived adipocytes. **(B)** Quantification of fluorescent cells for CD36, PLIN1 and FABP4 stained cells, expressed as percent fluorescence intensity normalized to cell numbers (DAPI). (15 images analyzed for n=6 healthy and obese samples). Scale bar represents 100μm. **(C)** Heat map showing mRNA expression for MSC markers (CD73 and CD105) expression in healthy and obese cells during adipogenesis. **(D)** Representative western blots showing changes in CD73 (n=7) and CD105 **(E)** protein expression during adipogenesis and quantification of their expression upon normalization to β-actin (loading control).

Data is represented as mean±SEM, n=6 (except where indicated), where n represents biological replicates of healthy and obese ADSCs. Statistical significance was determined by using multiple unpaired student's two-tailed t-tests for panel (B) and two-way ANOVA corrected for multiple comparisons with Tukey's test for panels (D) and (E). * $p<0.05$, ** $p<0.01$.

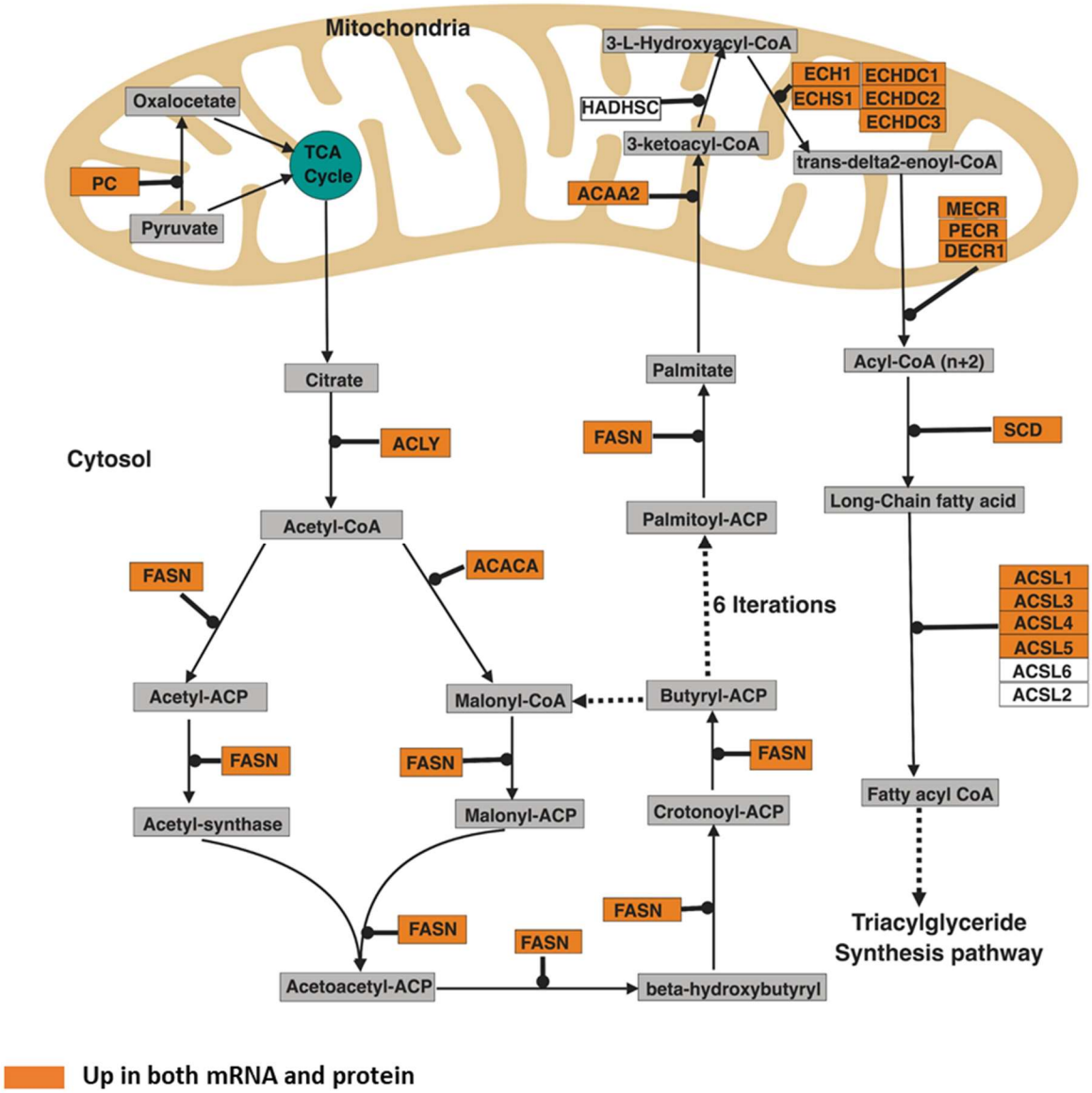

Fig. S4: Fatty acid synthesis pathway showing genes upregulated in day 14 differentiated healthy adipocytes as compared to obese adipocytes. Genes highlighted in orange are up in both mRNA and protein level.

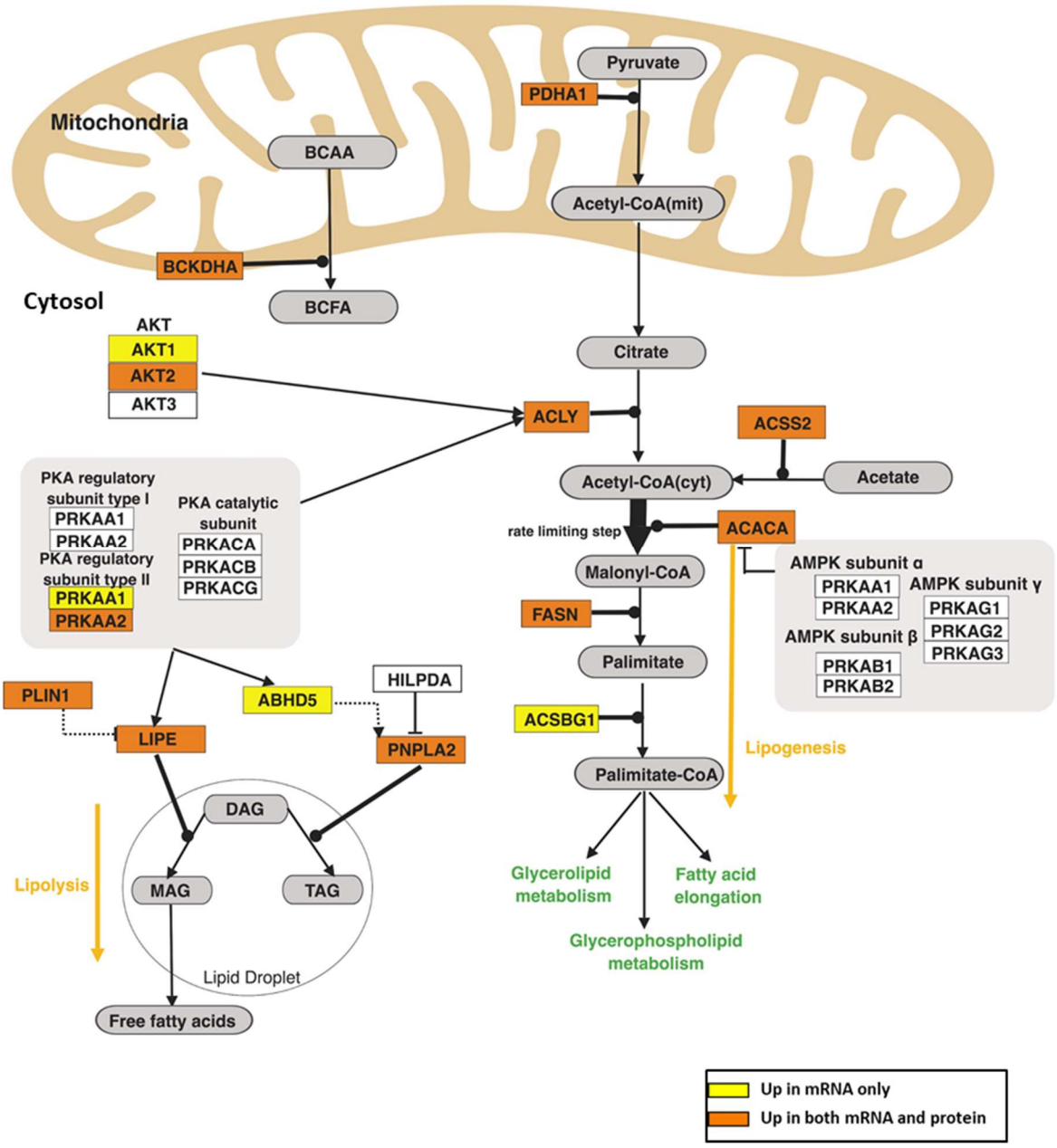

Fig. S5: Lipid biosynthesis pathway showing genes upregulated in day 14 differentiated healthy adipocytes as compared to obese adipocytes. Genes highlighted in orange are up in both mRNA and protein level.

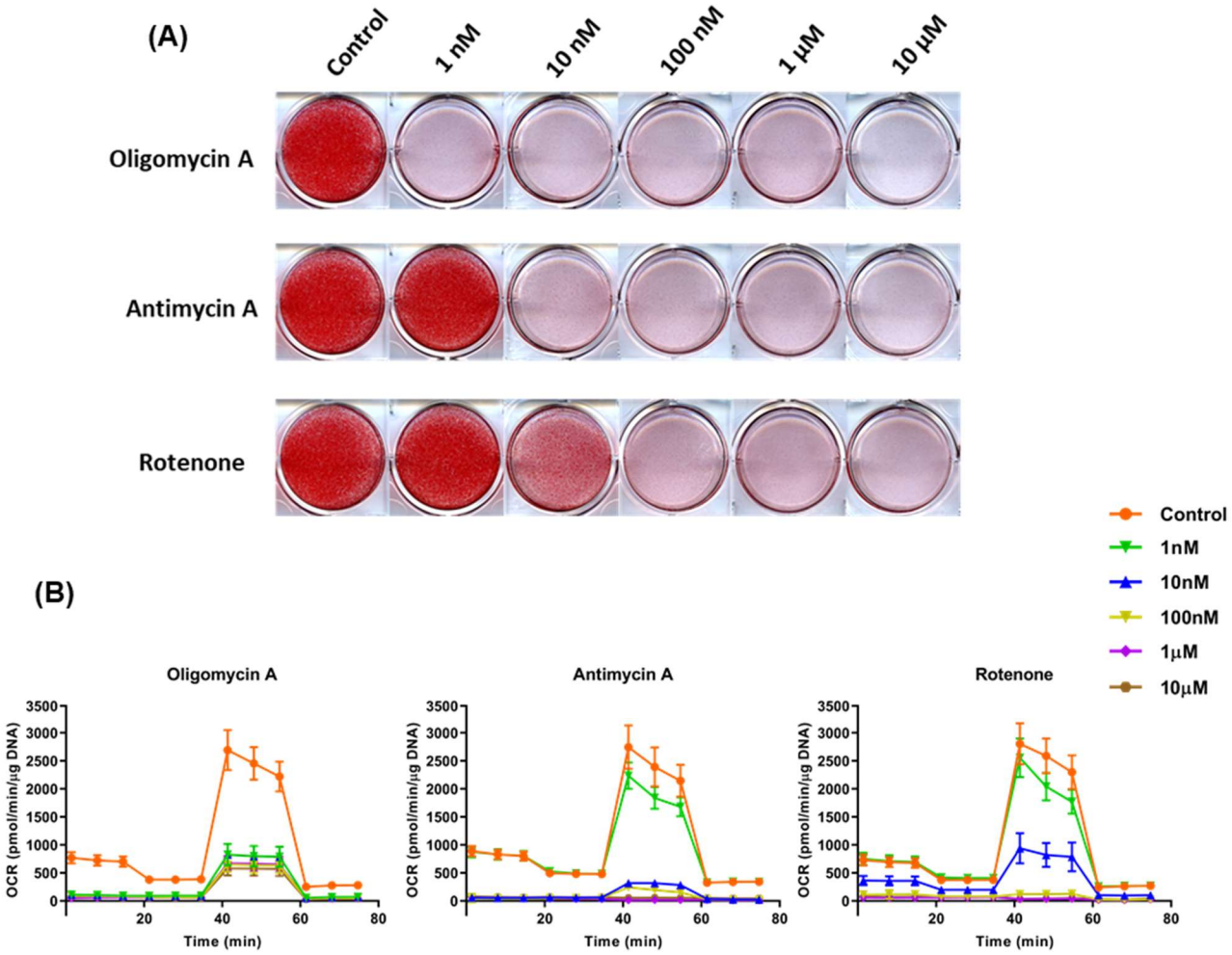

Fig. S6: Alterations in cellular bioenergetics result in reduced adipogenesis.

(A) Representative scanned whole well ORO images of healthy ADSCs differentiated with DMSO vehicle (control) and indicated concentrations of mitochondrial function inhibitors, Oligomycin A, Antimycin A and Rotenone at day 14 of adipogenic differentiation. **(B)** Representative traces of mitochondrial function parameters for healthy adipocytes differentiated with DMSO vehicle (control) and indicated concentrations of mitochondrial function inhibitors, Oligomycin A, Antimycin A and Rotenone at day 14 of adipogenic differentiation.

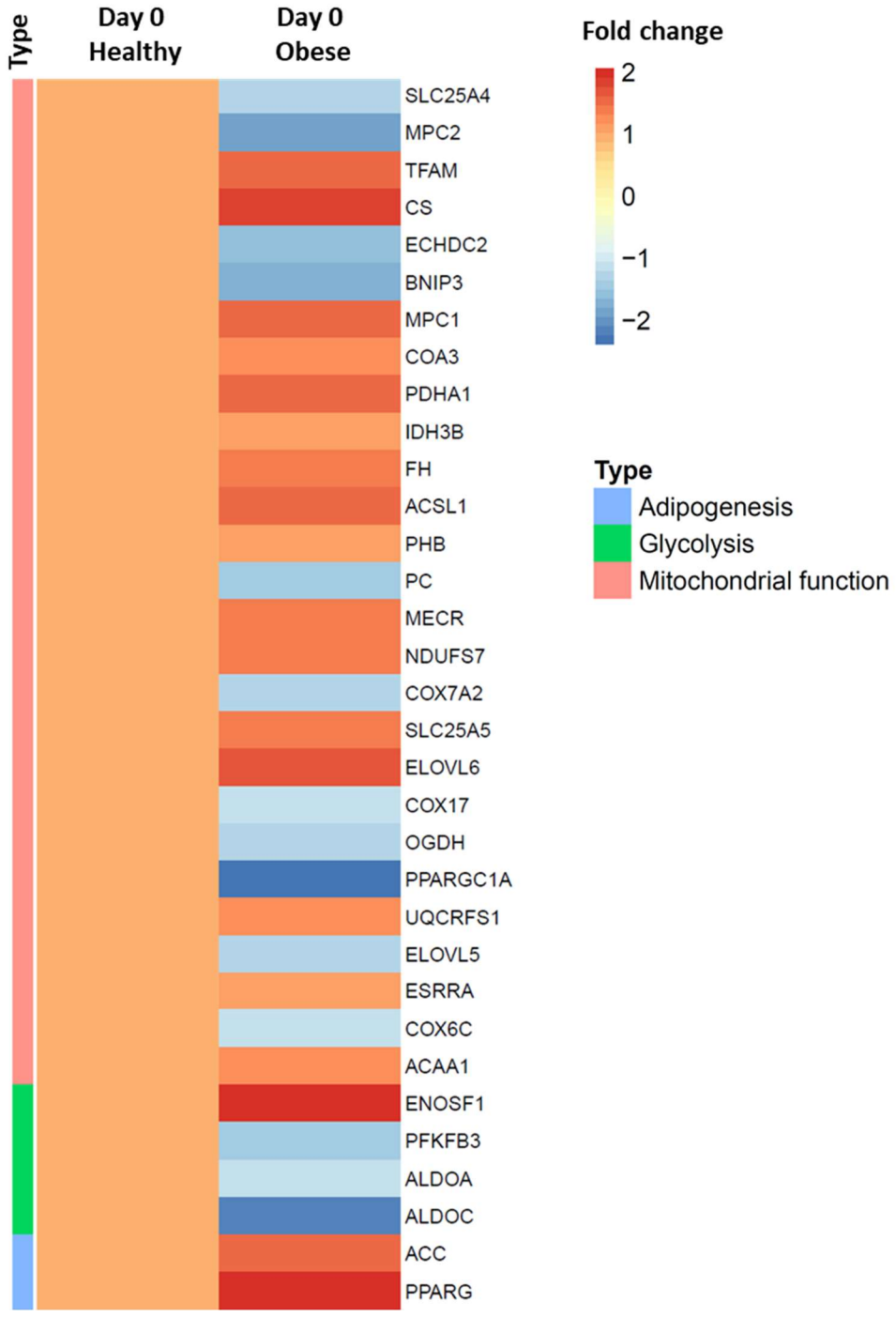

Fig. S7: Heatmap showing fold change in the gene expression of adipogenesis, glycolysis and mitochondrial function pathway genes in day 0 obese ADSCs compared to healthy ADSCs.

CHAPTER 3

Wnt signaling modulates adipogenesis and mitochondrial dysfunction in morbid obesity

Preface

This chapter is an original article in preparation for submission. The authors include:

Kanwaldeep Singh, Sansi Xing, Victor Gordon, Arianna Dal-Cin, Yu Lu, Eva Szabo and Bradley Doble

I designed the study, conducted the experiments, analyzed the data, assembled the figures and wrote the manuscript together with Dr. Brad Doble. Sansi Xing assisted with the proteomics experiments. Dr. Arianna Dal-Cin provided primary adipose tissue samples for isolation of ADSCs. Victor Gordon tested the biological activity of Wnt3A of prepared conditioned medium. Dr. Yu Lu designed proteomics analyses and helped with the proteomic bioinformatics. Dr. Eva Szabo helped with study design and interpretation of data.

Our results from Chapter 2 revealed significant disturbances in cellular metabolism and adipogenesis in obese cells. Previous observations linking abnormal Wnt signaling to obesity-associated pathologies led us to question whether there are aberrations in Wnt signaling in obese cells that are driving the defects in cellular bioenergetics we observed in them. Wnt signaling has been shown to be associated with obesity and associated metabolic disorders in *in vitro* as well as

genome-wide association studies (GWAS) (Gustafson and Smith, 2012; Christodoulides et al., 2006b). However, the exact molecular and cellular mechanisms that lead to metabolic derangements in response to deregulated Wnt signaling pathway are not known. Using our *in vitro* model of obesity, the studies in this chapter provide evidence supporting Wnt-mediated regulation of cellular metabolism and suggesting that alterations in Wnt signaling could contribute to the aberrant cellular bioenergetics and impaired adipose stem cell function observed in obesity.

Wnt signaling modulates adipogenesis and mitochondrial dysfunction in morbid obesity

Abstract

The increasing prevalence of obesity and metabolic syndrome has become a growing health concern with extensive socioeconomic consequences. One of the hallmarks of obesity is the inability of adipose-derived stem cells (ADSCs) in fat depots to generate new adipocytes in response to increased energy load, which leads to metabolic complications. Accordingly, studying how obesity regulates ADSC development and downstream adipogenesis is crucial to improving our understanding of the pathophysiology of the disease. To this end, ADSCs derived from obese patients offer an ideal platform to study molecular mechanisms involved in adipogenic differentiation, providing an opportunity to identify gene regulatory and signaling pathways that are aberrantly regulated in obesity.

In this study, ADSCs derived from healthy and morbidly obese patients were analyzed by using global transcriptomic and proteomic approaches across the adipogenesis timeline to identify differences in regulatory pathways that are driving adipogenesis. One of the pathways that was immediately evident to be dysregulated in obese ADSCs versus healthy cells was Wnt signaling. Wnt pathway components become enriched in our transcriptomic and proteomic analyses as ADSCs differentiate towards adipocytes in the obese setting, whereas the pathway is downregulated in healthy ADSCs within the first few days of differentiation.

This study also demonstrates a correlation between adipogenesis defects, mitochondrial dysfunction and aberrant Wnt signaling. By using Wnt ligands, Wnt antagonists, and small molecule modulators of the Wnt pathway, we present data suggesting that elevated Wnt signaling

is, in part, driving defects in adipogenesis and mitochondrial function observed in morbid obesity, providing a potential targetable pathway for the treatment of this physically and mentally debilitating disease.

Introduction

In normal conditions, white adipose tissue expands through a balance between formation of new adipocytes (adipogenesis) and storage of lipids in pre-existing adipocytes (adipocyte hypertrophy). In obesity, however, this balance shifts towards adipocyte hypertrophy and is accompanied by reduced adipogenesis, which is known to be associated with whole body insulin resistance (Hoffstedt et al., 2010; Andersson et al., 2014).

Adipose tissue resident mesenchymal stem cells, known as adipose tissue-derived stem cells (ADSCs), give rise to new adipocytes through adipogenesis, a process that is tightly regulated to ensure that adipogenic differentiation is strongly linked to the energy demands of the body. Among the regulatory networks that were previously shown to control this process is Wnt signaling network, which has been shown to negatively regulate adipogenesis in both murine and human cellular adipogenic models (Kang et al., 2007; Ross et al., 2000; Visweswaran et al., 2015).

Previous studies have shown that Wnt/β-catenin pathway activation plays a critical role in controlling mesenchymal stem cell fate and differentiation (Ling et al., 2008; Van Camp et al., 2014). For instance, Wnt activation in murine mesenchymal stem cells has been shown to impair their adipogenic differentiation, while promoting their differentiation towards osteogenic and myogenic lineages (Shang et al., 2007a; Shang et al., 2007b; Bennett et al., 2002; Kang et al., 2007; Ross et al., 2000; Bennet et al., 2005). Inhibition of Wnt signaling, on the other hand, has been shown to promote adipogenesis (Arango et al., 2005), whereas overexpression of Wnt10b or

β-catenin in adipose tissue has been shown to impair white and brown adipose tissue development and function *in vivo* (Longo et al., 2004). Moreover, secreted extracellular Wnt antagonists have been shown to stimulate adipogenic differentiation of murine 3T3-L1 preadipocytes, human MSCs (Christodoulides et al., 2006a; Visweswaran et al., 2015), and adipose tissue progenitors from obese individuals (Gustafson and Smith, 2012).

Obesity-induced inflammatory cytokines have been shown previously to mediate their anti-adipogenic functions through Wnt signaling. For example, two inflammatory cytokines, interleukin-6 (IL-6) and tumor necrosis factor alpha (TNFα), have been shown to exert anti-adipogenic action in 3T3-L1 pre-adipocytes by promoting Wnt/β-catenin signaling (Cawthorn et al., 2007; Gustafson et al., 2006).

Most of the evidence linking Wnt signaling and adipogenesis has been gained through the use of mouse models and from *in vitro* loss- and gain-of-function experiments, which might not be a true reflection of a relevant human disease environment. However, in one study, Wnt antagonism was shown to rescue adipogenesis in human hypertrophic obesity (Gustafson and Smith, 2012). Moreover, Wnt signaling has also been shown to modulate cellular energetics in a cell- and tissue-specific manner. For instance, Wnt3A/β-catenin signaling has been shown to enhance mitochondrial biogenesis and O_2 consumption in myoblasts (Yoon et al., 2010), whereas Wnt3A has also been shown to stimulate aerobic glycolysis independent of β-catenin, in bone-marrow stromal cells differentiating towards osteoblasts (Esen et al., 2013). Such studies provide direct evidence of the context-dependent nature of Wnt signaling in the regulation of cellular metabolism.

It is important to use physiologically relevant human disease models to further evaluate the role of Wnt signaling in obese adipogenesis. Hence, in this study, we used obesity-relevant disease models, comprising patient-specific ADSCs, and took a systematic approach to identify Wnt signaling as a target pathway that promotes the pathophysiology of obesity during adipocyte differentiation. The systematic analysis of temporal adipogenic differentiation in obese and healthy settings reveals that Wnt signaling is dysregulated in stem cells isolated from obese individuals and illustrates the consequences of aberrant Wnt signaling on adipogenesis and mitochondrial function in our cellular model of obesity.

Results

The major aim of this study was to identify the molecular mechanisms that potentially contribute to the defects in cellular metabolism in obese cells that were identified and detailed in Chapter 2 of this thesis.

Obese cells display a significant enrichment for Wnt signaling pathway genes during adipogenesis

Morbidly obese ADSC lines and healthy ADSC lines were differentiated towards adipocytes and were sampled at specific intervals (days 0, 1, 3, 7 and 14) during the differentiation timeline in order to identify differentially regulated pathways and gene networks. Days 0, 1, 3, 7 and 14 of adipocyte differentiation were compared in-depth in healthy versus obese cells by using Clariom S human HT gene chip transcriptomics (n=6) and tandem mass tag-mass spectrometry (TMT-MS) proteomics (n=3) datasets. Functional gene clustering and enrichment analyses were performed by using “The Panther Metabolic and Cell Signaling Pathway Database 2016” and “Kyoto Encyclopedia of Genes and Genomes (KEGG) database 2019” to identify functional gene

clusters that showed upregulation in obese cells compared to healthy counterparts during the adipogenesis timeline (days 0, 1, 3, 7 and 14).

Multiple signaling networks were found to be upregulated during the adipogenesis time course in obese cells versus healthy counterparts, namely the chemokine/cytokine mediated inflammatory network, integrin signaling, TGFβ signaling, interleukin signaling, and Wnt signaling (Fig. 1A). Some of the networks, such as TGFβ and interleukin signaling, were upregulated as differentiation progressed (day 3 onwards), indicating that these networks influence adipogenesis in the later stages of adipocyte development. By contrast, the apoptotic signaling pathway is already upregulated at the ADSC stage (day 0), which indicates that obese ADSCs have inherent aberrant regulation of apoptotic pathways.

Nevertheless, one of the most prominent pathways that showed enrichment at both gene and protein levels, across all differentiation time points, and which was enhanced as differentiation progressed, when compared to healthy counterparts, is the Wnt signaling pathway (Figure 1A and B). Accordingly, the gene expression of several mediators of Wnt signaling (*WNT3A*, *WNT5A*, *CTNNB1*, *FZD6*, *FZD7* and *PORCN*) was observed to be elevated, even in day 0 obese ADSCs, compared to healthy ADSCs (Fig. 1C). Functional clustering of the 114 genes commonly upregulated across days 0 to 14 during obese ADSC differentiation showed a clustering of Wnt pathway genes (Fig. 1C). Further, the upregulated genes in obese cells on days 0 and 14 of adipogenic differentiation were mapped onto the Wnt signaling pathway, showing an enrichment in Wnt/β-catenin pathway-specific genes (Fig. 2A and B). It is important to note that the majority of the upregulated Wnt components at day 0 and 14 are found upstream in the Wnt pathway (i.e.

ligands and receptors), suggesting that these would impact regulation of a wide number of downstream Wnt signaling axes.

Overall, our analyses suggest that Wnt signaling remains upregulated in obese ADSCs during the differentiation timeline, whereas in normal ADSCs, Wnt signaling is downregulated during the course of adipogenic differentiation.

Artificially enhanced Wnt signaling in healthy ADSCs results in reduced adipogenesis and mitochondrial dysfunction

Obese differentiating ADSCs showed an enrichment for Wnt pathway genes, which indicates a possible correlation between enhanced Wnt signaling and the impaired adipogenesis in these cells. Thus, to further evaluate the role of Wnt signaling in aberrant adipogenesis, healthy ADSCs were exposed to the Frizzled ligand, Wnt3A, during adipogenesis. Healthy ADSCs were differentiated in the presence of different amounts of Wnt3A-conditioned medium (Wnt3A-CM). That is, differentiation media were prepared with 25%, 50% and 100% Wnt3A-CM. Conditioned media from Wnt3A-expressing L-cells and control L- cells was prepared, and Wnt3A biological activity was assessed prior to use (Fig.S1). Healthy ADSCs treated with Wnt3A-CM exhibited a dose-dependent decrease in their adipogenic potential compared to control-CM-treated cells, as illustrated by Oil Red-O (ORO) staining, which is used to measure the lipid droplet accumulation that is a hallmark of adipocyte differentiation (Fig. 3A). To further confirm the negative effect of Wnt signaling on healthy adipogenesis, healthy ADSCs were differentiated in the presence of a small-molecule Wnt pathway activator, CHIR-99021 (1μM and 10μM). ORO staining of CHIR-treated healthy ADSCs showed that activation of Wnt signaling by CHIR results in a similar reduction in adipogenesis as that observed for Wnt3A (Fig. 3B).

Next, we evaluated mitochondrial activity at day 14 of differentiation in healthy ADSCs treated with control-CM, Wnt3A-CM or CHIR-99021, given that aberrant Wnt signaling has been previously associated with reduced adipogenesis in metabolic disorders such as obesity and type 2 diabetes (Gustafson and Smith, 2012; Gustafson et al., 2013; Chen and Wang, 2018), and our prior results (Chapter 2) also showed that there is mitochondrial dysfunction in obese ADSCs.

Significant mitochondrial dysfunction was observed in healthy ADSCs treated with Wnt ligand, Wnt3A and CHIR-99021 during differentiation (Fig. 3C and 3F). Treatment with Wnt-3A-CM in healthy ADSCs showed reduced levels of mitochondrial basal and maximal respiration in differentiated adipocytes (Fig. 3D-E), indicating that Wnts negatively regulate mitochondrial function and oxidative phosphorylation-dependent metabolism. Similarly, treatment with CHIR reduced mitochondrial function, as indicated by reduced basal and maximal respiration rates (Fig. 3G).

These results suggest that elevated Wnt signaling can drive reduced adipogenesis and mitochondrial dysfunction in healthy ADSC-derived adipocytes.

Wnt antagonism rescues adipogenesis and mitochondrial dysfunction in obese ADSCs

Our transcriptomic and proteomic datasets revealed that the expression of a Wnt signaling inhibitor, Dickkopf 1 (DKK1) spikes upwards significantly at day 1 of differentiation in healthy adipogenesis at the mRNA (~15-fold) and protein (~2-fold) levels (Fig. 4A and B). This suggests that effective antagonism of Wnt activity is required during early time points of adipogenesis for this process to proceed efficiently. Such Wnt antagonism fails to occur in obese cells. Hence, to further examine the role of Wnt signaling in adipogenesis and mitochondrial activity in the context

of obesity, Wnt signaling was antagonized during obese adipogenesis *in vitro* by treatment with DKK1 as well as a small molecule Wnt antagonist, PNU-74654.

Treatment of obese ADSCs with either DKK1 (250 ng/mL) or PNU-74654 (1 μM and 10 μM) resulted in increased adipogenesis as shown by ORO staining (Fig. 4C). Further, we observed that this rescue of adipogenesis upon Wnt antagonism with DKK1 or PNU-74654 was accompanied by an improvement in the mitochondrial function, as shown by significant improvement in both basal and maximal mitochondrial respiration in obese adipocytes (Fig. 4D-G).

Taken together, these results further suggest a link between Wnt activity and attenuated adipogenesis and mitochondrial function. Wnt signaling maintenance and upregulation during differentiation might be driving the observed defects in obese ADSC adipogenesis and metabolism, as enrichment of Wnt mediators precedes the impaired induction of adipogenesis and mitochondrial defects observed in the context of obesity.

Discussion

In this study, we observed a significant enrichment of Wnt signaling genes, particularly for the Wnt/β-catenin pathway (often referred to as the canonical Wnt pathway), in resting obese ADSC and during their blunted adipogenesis, compared to healthy counterparts. The expression of mediators of the Wnt/β-catenin pathway, including Wnt ligands, *Wnt3A* and *Wnt5A*, Frizzled receptors, *FZD5* and *FZD6*, and *CTNNB1* (β-catenin), was found to be higher in obese ADSCs. The expression of these Wnt pathway genes remained higher throughout the 14-day adipogenic

differentiation timeline, with further enrichment for other members of the pathway (*FZD6*, *FZD8*, *LRP6*, *ROR1/2*, *DVL1*) along the course of adipogenesis.

Canonical Wnt signaling is known to regulate mesenchymal cell fate towards different lineages *in vitro* and *in vivo*. Overexpression of Wnt10B has been associated with improved differentiation towards osteoblasts and myoblasts, while inhibiting adipogenesis (Bennet et al., 2002; Kang et al., 2007; Bennet et at., 2005; Longo et al., 2004). Similarly, Wnt3A-initiated signaling and β-catenin overexpression have been shown to decrease the expression of adipogenesis regulators, PPARγ and CEBPα, while simultaneously promoting the expression of pro-myogenic factors (Shang et al., 2007a; Shang et al., 2007b).

On the other hand, disruption of β-catenin expression in mesenchymal cells has been shown to be associated with a switch from myogenesis to adipogenesis *in vivo* (Arango et al., 2005). In our study, obese cells upregulated inflammatory mediators like IL-6 and TNFα at the ADSC stage and showed further enrichment in chemokine/cytokine mediated inflammation pathway genes at both mRNA and protein levels during the course of adipogenesis. This inflammatory environment is likely contributing further to the inhibition of adipogenic differentiation in obese cells through Wnt signaling, as inflammatory mediators are known to exert their anti-adipogenic effects through β-catenin-dependent Wnt signaling (Cawthorn et al., 2007; Gustafson and Smith, 2006). Thus, our study provides evidence that there is an inherent elevation in Wnt signaling in morbidly obese ADSCs, which ultimately impacts their differentiation potential and adipocyte function.

The extracellular Wnt antagonists, Secreted frizzled-related proteins (SFRPs) and Dickkopf (DKK) family members, modulate Wnt signaling by directly binding and sequestering Wnts from their receptors or by binding to LRP co-receptors as high-affinity antagonists,

respectively. These Wnt signaling antagonists also play an important regulatory role during adipogenic differentiation (Park et al., 2008). *DKKI* expression is shown to be transiently upregulated in human adipogenesis, while constitutive *DKK1* expression in 3T3-L1 preadipocytes has been shown to inhibit Wnt/β-catenin signaling and promote adipogenesis (Christodoulides et al., 2006a). Similarly, we observed a spike in *DKK1* gene and protein expression during early stages (day 1) of healthy ADSC adipogenesis, whereas obese cells failed to exhibit any increase in *DKK1* expression at any time point in the differentiation time course.

Overall, obese ADSCs lack coordinated regulation of Wnt signaling mediators and Wnt antagonists during the early and late stages of differentiation, resulting in significantly reduced adipogenic capacity in the obese setting. This understanding of a mechanism underlying the pathophysiology of obesity provides a novel targetable pathway, the Wnt/β-catenin pathway, for the treatment of obesity.

We also observed enrichment for other pathways, such as the TGF-β signaling pathway, in later stages of the differentiation timeline for obese ADSCs, which together with Wnt signaling, has been primarily associated with differentiation of mesenchymal stem cells towards osteogenic lineages (Zhao et al., 2009; Kulterer et al., 2007). This enrichment in TGF-β signaling pathway components could potentially be either another consequence of enhanced Wnt signaling or a completely separate axis that also negatively regulates adipogenesis in obese cells. Hence, it is important to note that while Wnt signaling has a negative impact on adipogenesis, the coordinated effects of multiple signaling pathways dysregulated during obesity could have an additive impact on adipocyte development and function in obesity.

Nevertheless, Wnt signaling is one of the only pathways that is inherently dysregulated in obese ADSCs and early adipogenesis. Thus, to confirm the association between Wnt pathway enrichment and reduced adipogenesis, and to evaluate the potential metabolic phenotype that results from Wnt stimulation, we induced Wnt signaling in healthy ADSCs during the course of adipogenesis via the Wnt ligand, Wnt3A, or the small molecule Wnt agonist, CHIR-99021 (Bennett et al., 2002; Qin et al., 2010). Both treatments resulted in reduced adipogenesis and significant reduction in mitochondrial activity, indicating that Wnt signaling can impact metabolism in developing adipocytes. As a counter experiment, we antagonized Wnt signaling in obese ADSCs with the Wnt antagonist, DKK1, and a small molecule canonical Wnt inhibitor, PNU-74654, which blocks β-catenin/TCF/LEF interactions (Trosset et al., 2006). This resulted in enhanced adipogenesis and improved mitochondrial function in obese ADSCs. These data provide preliminary evidence of an association between Wnt signaling and metabolism (mitochondrial function) in the context of human adipogenesis in the healthy vs obese state.

Wnt signals have been previously shown to be associated with metabolic disorders such as obesity and diabetes in human and transgenic animal models, where they have been shown to play an important role in the pathophysiology of these diseases. Wnt5A expression has been reported to be upregulated in murine models of obesity and type 2 diabetes, where increased expression of Wnt5A, together with reduced expression of SFRP5, was shown to contribute to insulin resistance and metabolic dysfunction observed in obesity (Ouchi et al., 2010).

In addition, fat metabolism defects as a result of hyperactive Wnt signaling, along with pharmacological mitigation of these defects by attenuating Wnt pathway, have been reported in *Drosophila* larvae models (Zhang et al., 2017). Moreover, Wnt antagonism has been shown to

rescue adipogenesis defects in hypertrophic obesity (Gustafson and Smith, 2012). However, our study provides the first evidence that enhanced Wnt signaling attenuates adipocyte development and promotes an aberrant metabolic phenotype in ADSCs from morbidly obese patients.

Our study provides the foundation for further in-depth experiments aimed at understanding how altered Wnt signaling drives mitochondrial dysfunction (and potentially, insulin resistance) observed in morbidly obese cells. Given the association of Wnt hyperactivity with metabolic disorders and our data showing upregulated Wnt signaling in stem cells isolated from obese individuals, stabilizing Wnt activity in a tissue-specific manner represents an attractive pharmacological strategy for designing newer therapeutic interventions for metabolic diseases such as obesity.

Supplemental Information

Supplemental Figure S1

Acknowledgements

This work was supported by Canadian Institutes of Health Research Grant and Canada Foundation for Innovation (CFI)-infrastructure fund (to Dr. Brad Doble and Dr. Eva Szabo). We thank the patients and donors for providing their consent to donate adipose tissue samples for this study. We acknowledge McMaster Genome Facility for performing the Clariom S transcriptomics.

Materials and Methods

Cell culture and adipogenic differentiation

Age-, gender- and adipose tissue depot-matched healthy (n=3; BMI = 22.4 ± 1.4) and morbidly obese ADSC (n=3; BMI = 44.8 ± 2.5) samples from our previously characterized biobank developed from a cohort of healthy, overweight and obese patient-derived ADSCs, (unpublished, Chapter 2 of this thesis) were used in this study. All ADSC lines have previously been characterized according to mesenchymal stem cell (MSC) guidelines issued by the International Society for Cellular Therapy (ISCT) (Dominici et al., 2006; Bourin et al., 2013).

ADSCs were cultured in DMEM-F12 (Corning, Cat# 10-090-CV) supplemented with 10% FBS, 1 mM L-Glutamine (Corning, Cat# 25-005-CI) and 10 ng/mL bFGF (Peprotech, Cat# 100-18B). For adipogenic differentiation, ADSCs were plated at a density of 7500 cells/cm^2 and grown until they reached confluency in ADSC growth medium, and differentiation was induced two days post confluency (day 0) with adipogenic differentiation medium composed of DMEM-F12 supplemented with 10% FBS, 1 mM L-Glutamine, 250 µM isobutyl-methylxanthine (IBMX) (Sigma, Cat# I5879), 0.5 µM dexamethasone (Sigma, Cat# D2915), 10 µg/mL Insulin (Sigma, Cat# I9278), and 100 µM indomethacin (Sigma, Cat# I7378), followed by a complete medium change with fresh differentiation medium every other day until day 14. For CHIR-99021 (Stem cell technologies, Cat# 72054), DKK1 (Peprotech, Cat# 120-30) and PNU-74654 (Cayman Chemicals, Cat# 16349) treatments, cells were cultured in ADSC growth medium until confluency and were differentiated in adipogenic differentiation media containing either CHIR-99021 (1 and 10µM), DKK1 (250ng/mL) or PNU-74654 (1 and 10µM), followed by a complete medium change every other day until day 14. For differentiation in Wnt3A and control L-cell-conditioned media,

the respective conditioned media were diluted in ADSC growth medium to 25% and 50% strengths. Differentiation media were then made in 25%, 50% and 100% conditioned media by adding the adipogenesis inducers (IBMX, dexamethasone, indomethacin and insulin), as described above. Differentiation was induced in healthy ADSCs two days post-confluency in differentiation media prepared in Wnt3A- or control-L-cell-CM followed by respective media changes every other day until day 14.

ORO staining

Cells were fixed with 4% PFA (Electron Microscopy Sciences, Cat# 15710) for 10 minutes at room temperature at days 0, 1, 3, 7 and 14 of differentiation. For ORO staining, cells were rinsed with 60% isopropanol for 2 minutes, followed by staining with ORO working solution (6 parts 0.5% ORO (Sigma, Cat# O0625) in 100% isopropanol and 4 parts distilled water) for 30 minutes. Cells were washed under running water until water ran clear. Whole cell culture plate wells were scanned on an Epson V700 photo scanner followed by imaging by light microscopy.

Wnt3A-conditioned and control L-cell-conditioned media

L-cells producing and secreting biologically active mouse Wnt3A protein (LWnt3A cells, ATCC Cat#CRL-2647) and control L-cells (ATCC Cat# CRL2648) were used for making Wnt3A- and control-conditioned media respectively. Briefly, a confluent monolayer of the cells was split 1:10 in ten T75 flasks in 10 mL culture medium (DMEM-F12 + 10% FBS + 2.5mM L-glutamine) and grown for 4 days. The media was then collected from the flasks, filter sterilized and stored at 4°C. Additional fresh medium (10 mL) was added to each flask and incubated for another 3 days. The second batch of media was collected after the additional 3 days and was filter sterilized and

mixed with the first batch of conditioned medium at a 1:1 ratio, resulting in the final Wnt3A or control conditioned media.

Wnt3A biological activity assay

Mouse embryonic stem cells (mESCs) transfected with a fluorescence-based TCF/LEF reporter construct based on the plasmid 7TGP were used to analyse the biological activity of Wnt3A in the conditioned media. 7TGP was a gift from Roel Nusse (Addgene plasmid # 24305). mESCs were exposed to Wnt3A- or control L-cell-conditioned media for 24 hours followed by imaging for expression of the fluorescent reporter. 10μM CHIR-99021 was used as a positive control.

Mitochondrial function assay

Mitochondrial respiration assays were performed on a XFe96 extracellular flux analyzer (Seahorse-Agilent). 13000 cells/well were plated in Seahorse-Agilent 96-well plates (Agilent Technologies, Cat# 101085-004). Adipogenesis was induced with or without indicated compounds the following day, as described above. At day 14 of the differentiation, cells were rinsed twice with complete XF assay medium pH 7.4 (XF DMEM base medium without phenol red (Agilent Technologies, Cat# 103335-100) supplemented with 2.5 mM L-Glutamine, 1 mM sodium pyruvate, and 17.5 mM glucose) and a mitochondrial stress test (MST) was performed as per the instructions provided with the MST kit (Agilent technologies, Cat# 103015-100). The MST assay was performed using the recommended/optimized concentrations of oligomycin (2 μM), FCCP (1 μM) and antimycin+rotenone (0.5 μM each). Oxygen consumption rate (OCR) readouts were normalized to total cellular DNA content after the MST assays, to account for any differences in cell number. Cellular DNA content was measured by using a CyQuant Cell

Proliferation assay kit (ThermoFisher, Cat# C7026) following the manufacturer's protocol. Data analysis was performed with Wave 2.6 desktop analysis software.

Functional gene and protein enrichment analysis

Transcriptomic and proteomic datasets for the adipogenesis timeline (days 0, 1, 3, 7 and 14) from healthy and morbidly obese ADSCs (unpublished, Chapter 2 of this thesis) were utilized to study the gene and protein networks that show upregulation in obese ADSCs and during the course of obese adipogenesis. Upregulated genes from both datasets were analyzed for functional clustering and enrichment using the integrative web-based software packages, g:profiler and Enrichr, which enable the analysis of significant enrichment of genes/pathways in different databases including: Gene Ontology (GO) Consortium database, Kyoto Encyclopedia of Genes and Genomes (KEGG) database, and The Panther Metabolic and Cell Signaling Pathway Database 2016 (Chen et al., 2013; Kuleshov et al., 2016; Reimand et al., 2007).

Statistical Analysis

Data are presented as means ± SEM. GraphPad Prism 8 was used to analyze the differences between two groups by multiple unpaired two-tailed Student's t-tests. The statistical parameters (i.e. the exact n numbers and p values) can be found in the figure legends. For all experiments, a p-value less than 0.05 was considered significant.

References

Andersson, D. P., Eriksson Hogling, D., Thorell, A., Toft, E., Qvisth, V., Naslund, E., Thorne, A., Wiren, M., Lofgren, P., Hoffstedt, J., Dahlman, I., Mejhert, N., Ryden, M., Arner, E., and Arner, P. (2014). Changes in subcutaneous fat cell volume and insulin sensitivity after weight loss. Diabetes care *37,* 1831-1836.

Arango, N.A., Szotek, P.P., Manganaro, T.F., Oliva, E., Donahoe, P.K., and Teixeira, J. (2005). Conditional deletion of beta-catenin in the mesenchyme of the developing mouse uterus results in a switch to adipogenesis in the myometrium. Developmental biology *288,* 276-283.

Bennett, C.N., Longo, K.A., Wright, W.S., Suva, L.J., Lane, T.F., Hankenson, K.D., and MacDougald, O.A. (2005). Regulation of osteoblastogenesis and bone mass by Wnt10b. Proceedings of the National Academy of Sciences of the United States of America *102,* 3324-3329.

Bennett, C.N., Ross, S.E., Longo, K.A., Bajnok, L., Hemati, N., Johnson, K.W., Harrison, S.D., and MacDougald, O.A. (2002). Regulation of Wnt signaling during adipogenesis. The Journal of biological chemistry *277,* 30998-31004.

Bourin, P., Bunnell, B. A., Casteilla, L., Dominici, M., Katz, A. J., March, K. L., Redl, H., Rubin, J. P., Yoshimura, K., and Gimble, J. M. (2013). Stromal cells from the adipose tissue-derived stromal vascular fraction and culture expanded adipose tissue-derived stromal/stem cells: a joint statement of the International Federation for Adipose Therapeutics and Science (IFATS) and the International Society for Cellular Therapy (ISCT). Cytotherapy *15,* 641-648.

Cawthorn, W.P., Heyd, F., Hegyi, K., and Sethi, J.K. (2007). Tumour necrosis factor-alpha inhibits adipogenesis via a beta-catenin/TCF4(TCF7L2)-dependent pathway. Cell death and differentiation *14,* 1361-1373.

Chen, N., and Wang, J. (2018). Wnt/β-Catenin Signaling and Obesity. Frontiers in physiology *9,* 792.

Christodoulides, C., Laudes, M., Cawthorn, W.P., Schinner, S., Soos, M., O'Rahilly, S., Sethi, J.K., and Vidal-Puig, A. (2006a). The Wnt antagonist Dickkopf-1 and its receptors are coordinately regulated during early human adipogenesis. Journal of cell science *119,* 2613-2620.

Christodoulides, C., Scarda, A., Granzotto, M., Milan, G., Dalla Nora, E., Keogh, J., De Pergola, G., Stirling, H., Pannacciulli, N., Sethi, J. K., Federspil, G., Vidal-Puig, A., Farooqi, I. S., O'Rahilly, S., and Vettor, R. (2006b). Wnt10B mutations in human obesity. Diabetologia *49,* 678-684.

Dominici, M., Le Blanc, K., Mueller, I., Slaper-Cortenbach, I., Marini, F., Krause, D., Deans, R., Keating, A., Prockop, D. j., and Horwitz, E. (2006). Minimal criteria for defining multipotent mesenchymal stromal cells. The International Society for Cellular Therapy position statement. Cytotherapy *8,*315-317.

Esen, E., Chen, J., Karner, C. M., Okunade, A. L., Patterson, B. W., and Long, F. (2013). Wnt-LRP5 signaling induces Warburg effect through mTORC2 activation during osteoblast differentiation. Cell metabolism *17,* 745-755.

Gustafson, B., and Smith, U. (2006). Cytokines promote Wnt signaling and inflammation and impair the normal differentiation and lipid accumulation in 3T3-L1 preadipocytes. The Journal of biological chemistry *281,* 9507-9516.

Gustafson, B., and Smith, U. (2012). The Wnt inhibitor Dickkopf 1 and bone morphogenetic protein 4 rescue adipogenesis in hypertrophic obesity in humans. Diabetes *61,* 1217-1224.

Gustafson, B., and Smith, U. (2012). The Wnt inhibitor Dickkopf 1 and bone morphogenetic protein 4 rescue adipogenesis in hypertrophic obesity in humans. Diabetes *61,* 1217-1224.

Gustafson, B., Hammarstedt, A., Hedjazifar, S., and Smith, U. (2013). Restricted adipogenesis in hypertrophic obesity: the role of WISP2, Wnt, and BMP4. Diabetes *62,* 2997-3004.

Hoffstedt, J., Arner, E., Wahrenberg, H., Andersson, D. P., Qvisth, V., Lofgren, P., Ryden, M., Thorne, A., Wiren, M., Palmer, M., Thorell, A., Toft, E., and Arner, P. (2010). Regional impact of adipose tissue morphology on the metabolic profile in morbid obesity. Diabetologia *53,* 2496-2503.

Kang, S., Bennett, C.N., Gerin, I., Rapp, L.A., Hankenson, K.D., and Macdougald, O.A. (2007). Wnt signaling stimulates osteoblastogenesis of mesenchymal precursors by suppressing CCAAT/enhancer-binding protein alpha and peroxisome proliferator-activated receptor gamma. The Journal of biological chemistry *282,* 14515-14524.

Kulterer, B., Friedl, G., Jandrositz, A., Sanchez-Cabo, F., Prokesch, A., Paar, C., Scheideler, M., Windhager, R., Preisegger, K.H., and Trajanoski, Z. (2007). Gene expression profiling of human mesenchymal stem cells derived from bone marrow during expansion and osteoblast differentiation. BMC genomics *8,* 70.

Ling, L., Nurcombe, V., and Cool, S. M. (2008). Wnt signaling controls the fate of mesenchymal stem cells. Gene *433,* 1-7.

Longo, K.A., Wright, W.S., Kang, S., Gerin, I., Chiang, S.H., Lucas, P.C., Opp, M.R., and MacDougald, O.A. (2004). Wnt10b inhibits development of white and brown adipose tissues. The journal of biological chemistry *279,* 35503-35509.

Ouchi, N., Higuchi, A., Ohashi, K., Oshima, Y., Gokce, N., Shibata, R., Akasaki, Y., Shimono, A., and Walsh, K. (2010). Sfrp5 is an anti-inflammatory adipokine that modulates metabolic dysfunction in obesity. Science *329,* 454-457.

Park, J.R., Jung, J.W., Lee, Y.S., and Kang, K.S. (2008). The roles of Wnt antagonists Dkk1 and sFRP4 during adipogenesis of human adipose tissue-derived mesenchymal stem cells. Cell proliferation *41,* 859-874.

Qin, J., Li, W.Q., Zhang, L., Chen, F., Liang, W.H., Mao, F.F., Zhang, X.M., Lahn, B.T., Yu, W.H., and Xiang, A.P. (2010). A stem cell-based tool for small molecule screening in adipogenesis. PloS one *5,* e13014.

Ross, S.E., Hemati, N., Longo, K.A., Bennett, C.N., Lucas, P.C., Erickson, R.L., and MacDougald, O.A. (2000). Inhibition of adipogenesis by Wnt signaling. Science *289,* 950-953.

Shang, Y.C, Zhang, C., Wang, S., Xiong, F., Zhao, C., Peng, F., Feng, S., Yu, M., Li, M., and Zhang, Y. (2007a). Activated beta-catenin induces myogenesis and inhibits adipogenesis in BM-derived mesenchymal stromal cells. Cytotherapy *9,* 667-681.

Shang, Y.C., Wang, S.H., Xiong, F., Zhao, C.P., Peng, F.N., Feng, S.W., Li, M.S., Li, Y., and Zhang, C. (2007b). Wnt3a signaling promotes proliferation, myogenic differentiation, and migration of rat bone marrow mesenchymal stem cells. Acta pharmacologica Sinica *28,* 1761-1774.

Trosset, J.Y., Dalvit, C., Knapp, S., Fasolini, M., Veronesi, M., Mantegani, S., Gianellini, L.M., Catana, C., Sundström, M., Stouten, P.F., and Moll, J.K. (2006). Inhibition of protein-protein interactions: the discovery of druglike beta-catenin inhibitors by combining virtual and biophysical screening. Proteins *64,* 60-67.

Van Camp, J. K., Beckers, S., Zegers, D., and Van Hul, W. (2014). Wnt signaling and the control of human stem cell fate. Stem cell reviews *10,* 207-229.

Visweswaran, M., Schiefer, L., Arfuso, F., Dilley, R.J., Newsholme, P., and Dharmarajan, A. (2015). Wnt antagonist secreted frizzled-related protein 4 upregulates adipogenic differentiation in human adipose tissue-derived mesenchymal stem cells. PloS one *10,* e0118005.

Yoon, J. C., Ng, A., Kim, B. H., Bianco, A., Xavier, R. J., and Elledge, S. J. (2010). Wnt signaling regulates mitochondrial physiology and insulin sensitivity. Genes & development *24,* 1507-1518.

Zhang, T., Hsu, F.N., Xie, X.J., Li, X., Liu, M., Gao, X., Pei, X., Liao, Y., Du, W., and Ji, J.Y. (2017). Reversal of hyperactive Wnt signaling-dependent adipocyte defects by peptide boronic acids. Proceedings of the National Academy of Sciences of the United States of America *114,* E7469-E7478.

Zhao, L., Jiang, S., and Hantash, B.M. (2010). Transforming growth factor beta1 induces osteogenic differentiation of murine bone marrow stromal cells. Tissue engineering. Part A *16,* 725-733.

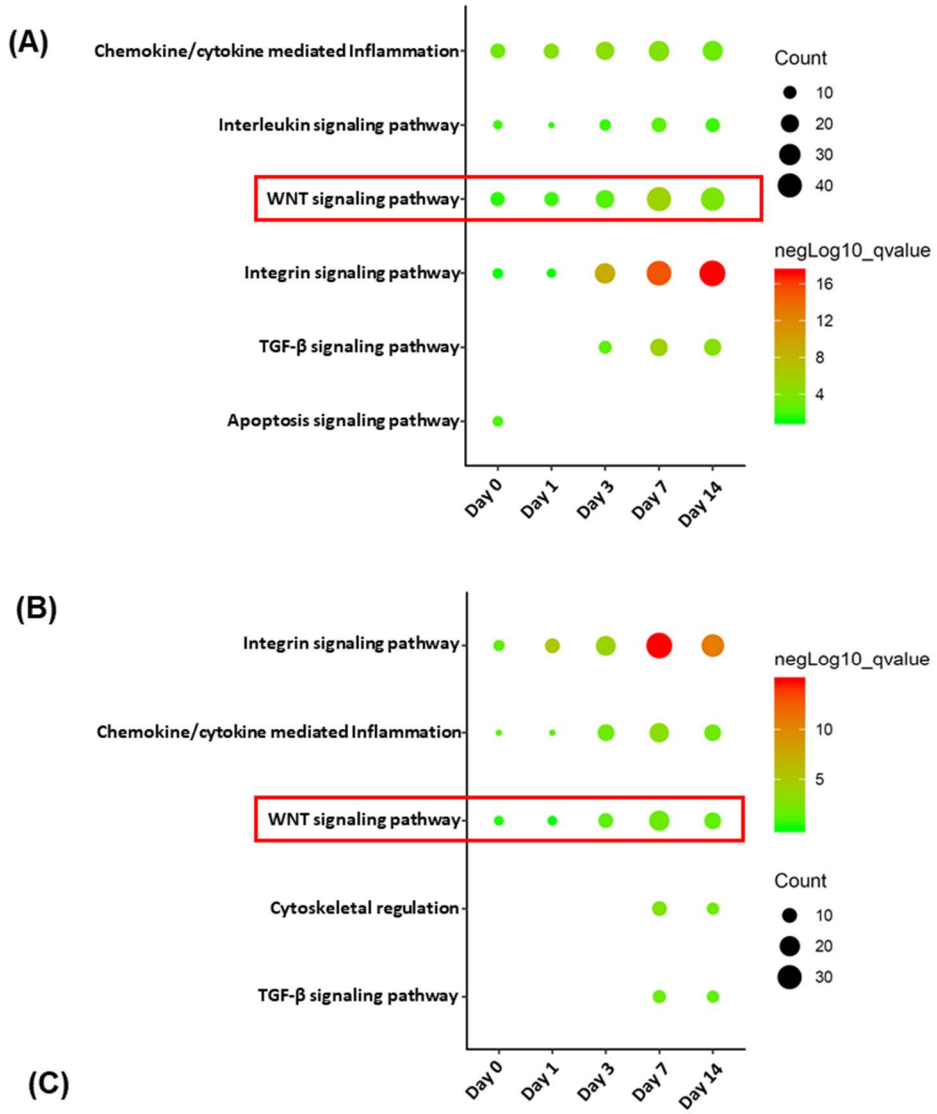
(A)
Chemokine/cytokine mediated Inflammation
Interleukin signaling pathway
WNT signaling pathway
Integrin signaling pathway
TGF-β signaling pathway
Apoptosis signaling pathway
Day 0
Day 1
Day 3
Day 7
Day 14
Count
10
20
30
40
negLog10_qvalue
16
12
8
4
(B)
Integrin signaling pathway
Chemokine/cytokine mediated Inflammation
WNT signaling pathway
Cytoskeletal regulation
TGF-β signaling pathway
Day 0
Day 1
Day 3
Day 7
Day 14
negLog10_qvalue
10
5
Count
10
20
30
(C)
Day 3 (830)
Day 1 (385)
Day 0 (477)
(114)
Day 14 (1449)
Day 7 (1300)
TGF-β signaling pathway
WNT signaling pathway
Chemokine/cytokine mediated inflammation
Interleukin signaling pathway
TGFBR1
CCL2
CTNNB1
PF4V1
IL6
WNT3A
INHBA
TNFA
FZD6
PORCN
CXCL8
PF4
FZD7
PTGS2
CXCL1
WNT5A

Fig. 1: Obese cells show significant enrichment of Wnt signaling pathway genes during adipogenesis. (A) Functional gene clustering and enrichment analysis for upregulated genes in obese cells at indicated time points during adipogenesis using The Panther Metabolic and Cell Signaling Pathway Database 2016 and KEGG database 2019 (n=6). **(B)** Functional gene clustering and enrichment analysis for upregulated genes in obese cells derived from proteomics datasets at indicated time points during adipogenesis in The Panther Metabolic and Cell Signaling Pathway Database 2016 and KEGG database 2019. (n=3). **(C)** Venn diagram showing 114 upregulated genes common among days 0, 1, 3, 7 and 14 of adipogenic differentiation in obese cells, and functional clustering of these 114 genes showing clusters for Interleukin, Wnt, TGFβ and chemokine-mediated inflammatory signaling pathways.

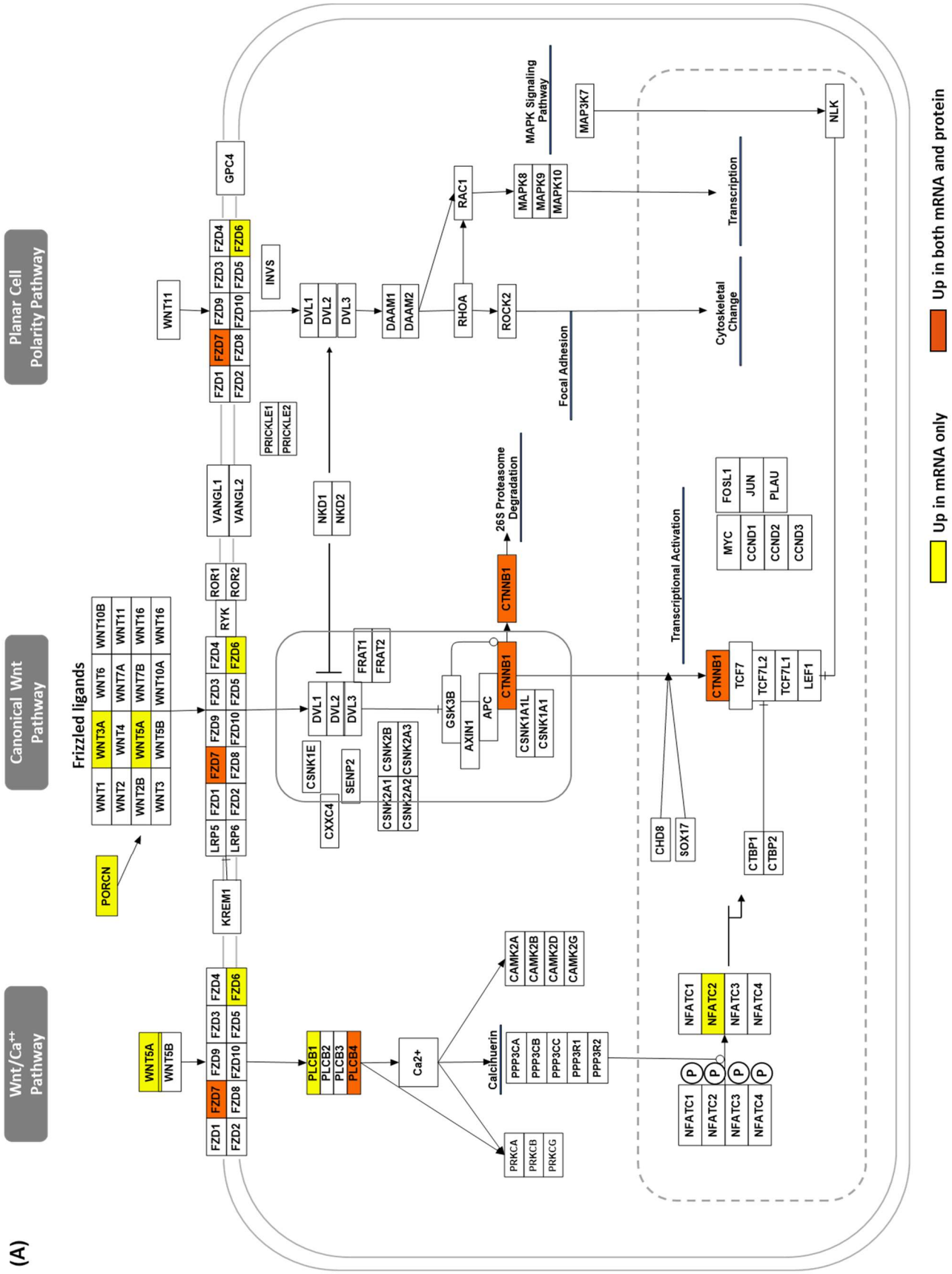
(A)
Wnt/Ca++ Pathway
Canonical Wnt Pathway
Planar Cell Polarity Pathway
Frizzled ligands
WNT1
WNT2
WNT2B
WNT3
WNT3A
WNT4
WNT5A
WNT5B
WNT6
WNT7A
WNT7B
WNT10A
WNT10B
WNT11
WNT16
WNT16
PORCN
KREM1
LRP5
LRP6
FZD1
FZD2
FZD7
FZD8
FZD9
FZD10
FZD3
FZD5
FZD4
FZD6
RYK
ROR1
ROR2
VANGL1
VANGL2
GPC4
PRICKLE1
PRICKLE2
WNT11
INVS
DVL1
DVL2
DVL3
NKD1
NKD2
DAAM1
DAAM2
RHOA
ROCK2
RAC1
MAPK8
MAPK9
MAPK10
MAPK Signaling Pathway
MAP3K7
NLK
Cytoskeletal Change
Transcription
Focal Adhesion
FRAT1
FRAT2
CSNK1E
CXXC4
SENP2
CSNK2A1
CSNK2A2
CSNK2B
CSNK2A3
GSK3B
AXIN1
APC
CSNK1A1L
CSNK1A1
CTNNB1
26S Proteasome Degradation
Transcriptional Activation
CHD8
SOX17
CTBP1
CTBP2
TCF7
TCF7L2
TCF7L1
LEF1
MYC
CCND1
CCND2
CCND3
FOSL1
JUN
PLAU
PLCB1
PLCB2
PLCB3
PLCB4
Ca2+
Calcineurin
PPP3CA
PPP3CB
PPP3CC
PPP3R1
PPP3R2
CAMK2A
CAMK2B
CAMK2D
CAMK2G
PRKCA
PRKCB
PRKCG
NFATC1
NFATC2
NFATC3
NFATC4
P
Up in mRNA only
Up in both mRNA and protein

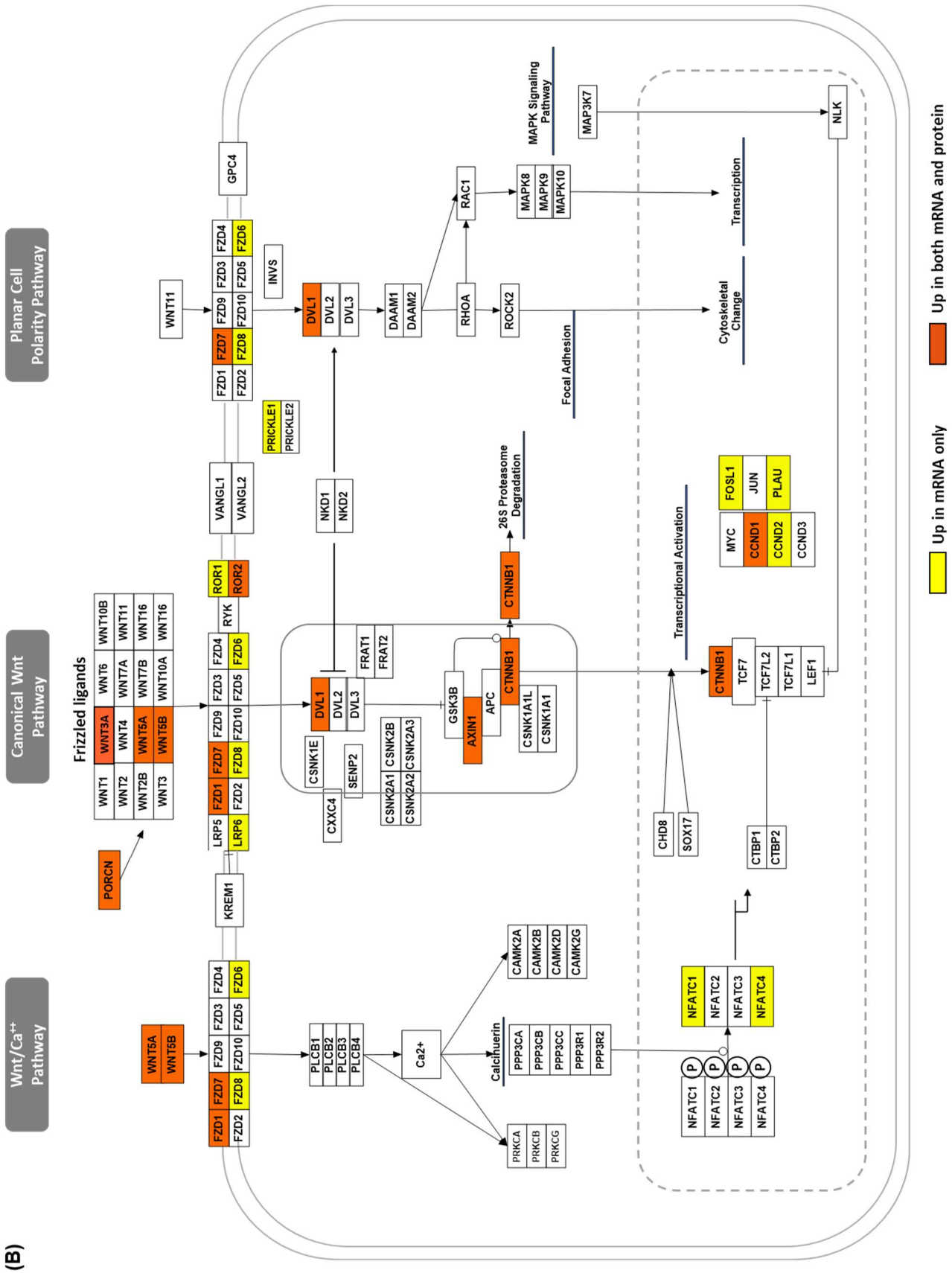
(B)
Wnt/Ca++ Pathway
Canonical Wnt Pathway
Planar Cell Polarity Pathway
Frizzled ligands
WNT1
WNT2
WNT2B
WNT3
WNT3A
WNT4
WNT5A
WNT5B
WNT6
WNT7A
WNT7B
WNT10A
WNT10B
WNT11
WNT16
PORCN
LRP5
LRP6
KREM1
FZD1
FZD2
FZD7
FZD8
FZD9
FZD10
FZD3
FZD5
FZD4
FZD6
RYK
ROR1
ROR2
VANGL1
VANGL2
GPC4
PRICKLE1
PRICKLE2
INVS
DVL1
DVL2
DVL3
NKD1
NKD2
CSNK1E
CXXC4
SENP2
FRAT1
FRAT2
CSNK2A1
CSNK2A2
CSNK2B
CSNK2A3
GSK3B
AXIN1
APC
CTNNB1
CSNK1A1L
CSNK1A1
26S Proteasome Degradation
DAAM1
DAAM2
RHOA
ROCK2
RAC1
MAPK8
MAPK9
MAPK10
MAPK Signaling Pathway
MAP3K7
NLK
Focal Adhesion
Cytoskeletal Change
Transcription
Transcriptional Activation
CHD8
SOX17
CTNNB1
TCF7
TCF7L2
TCF7L1
LEF1
MYC
CCND1
CCND2
CCND3
FOSL1
JUN
PLAU
CTBP1
CTBP2
PLCB1
PLCB2
PLCB3
PLCB4
Ca2+
Calcineurin
PPP3CA
PPP3CB
PPP3CC
PPP3R1
PPP3R2
CAMK2A
CAMK2B
CAMK2D
CAMK2G
PRKCA
PRKCB
PRKCG
NFATC1
NFATC2
NFATC3
NFATC4
P
Up in mRNA only
Up in both mRNA and protein

Fig. 2: Wnt signaling pathway showing genes upregulated at mRNA and protein levels in obese ADSCs (day 0 of differentiation) (A) obese adipocytes (day 14 of differentiation) (B) compared to healthy cells.

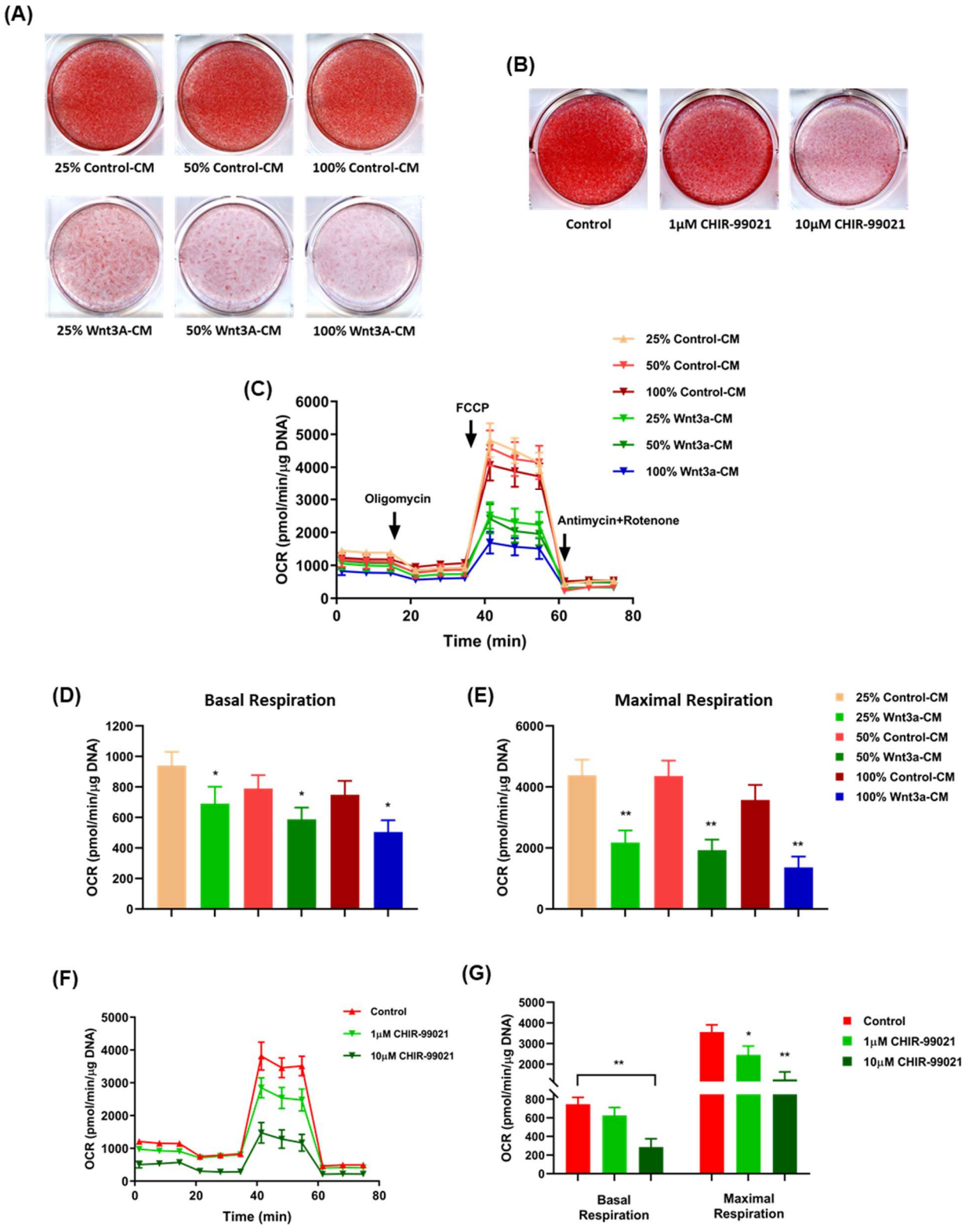
(A)
25% Control-CM
50% Control-CM
100% Control-CM
25% Wnt3A-CM
50% Wnt3A-CM
100% Wnt3A-CM
(B)
Control
1μM CHIR-99021
10μM CHIR-99021
(C)
25% Control-CM
50% Control-CM
100% Control-CM
25% Wnt3a-CM
50% Wnt3a-CM
100% Wnt3a-CM
FCCP
Oligomycin
Antimycin+Rotenone
OCR (pmol/min/μg DNA)
Time (min)
(D)
Basal Respiration
OCR (pmol/min/μg DNA)
(E)
Maximal Respiration
OCR (pmol/min/μg DNA)
(F)
Control
1μM CHIR-99021
10μM CHIR-99021
OCR (pmol/min/μg DNA)
Time (min)
(G)
Control
1μM CHIR-99021
10μM CHIR-99021
OCR (pmol/min/μg DNA)
Basal Respiration
Maximal Respiration

Fig. 3: Promoting Wnt signaling in healthy ADSCs results in reduced adipogenesis and induces mitochondrial dysfunction. (A) Representative whole well ORO (Oil Red-O stained) scans of healthy ADSCs treated with different concentrations: 25%, 50% and 100% of Wnt3A-CM (Wnt3A-conditioned media) or control-CM (control L-cell-conditioned media) at day 14 of differentiation. **(B)** Representative whole well ORO scans at day 14 of differentiation for healthy ADSCs differentiated in the presence of vehicle control or CHIR-99021 (1 μM and 10 μM). **(C)** Representative mitochondrial respiration traces at day 14 of adipogenic differentiation for healthy ADSCs treated with Wnt3A-CM (Wnt3A-conditioned media) or control-CM (control L-cell-conditioned media). Mitochondrial function parameters: basal **(D)** and maximal **(E)** respiration calculated from mitochondrial respiration specific oxygen consumption rates (OCR) values at day 14 of differentiation in control-CM or Wnt3A-CM differentiation media. **(F)** Representative mitochondrial respiration traces at day 14 of adipogenic differentiation of healthy ADSCs differentiated in the presence of vehicle control or CHIR-99021 (1μM and 10μM). **(G)** Mitochondrial function parameters: basal and maximal respiration calculated from mitochondrial respiration OCR values at day 14 of healthy differentiation in control or CHIR-99021-treated cells. (n=3; *$p<0.05$ and **$p<0.01$)

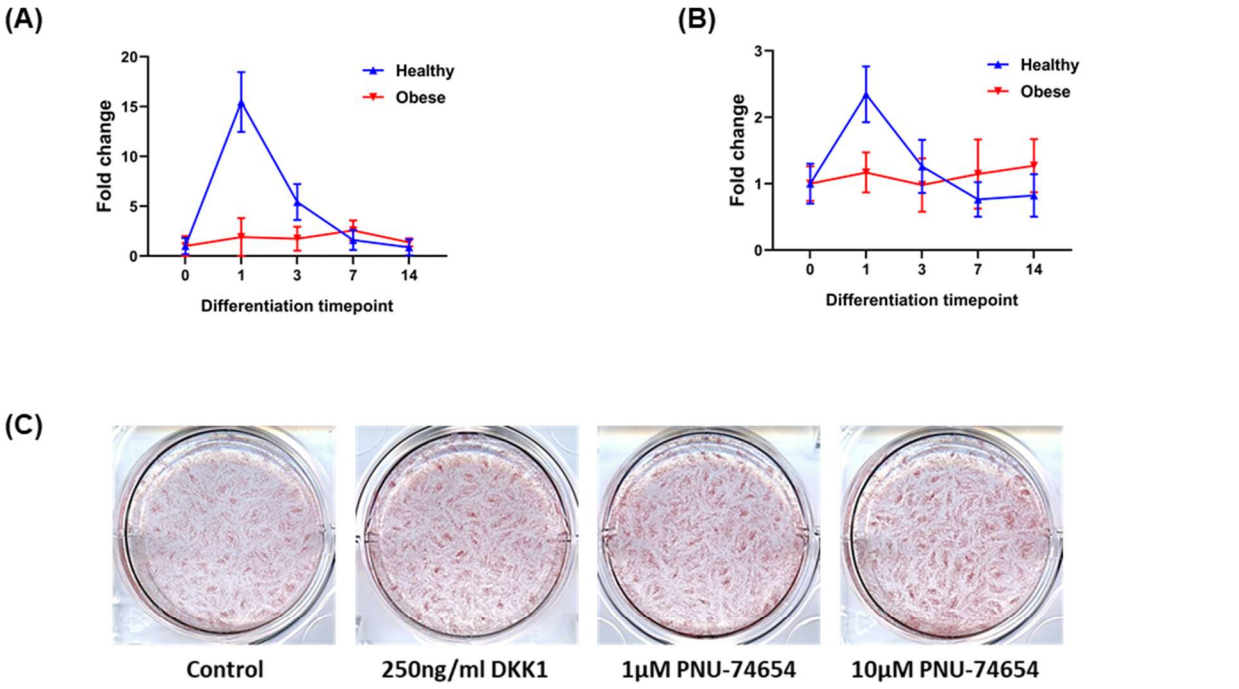
(A)
Healthy
Obese
Fold change
Differentiation timepoint
(B)
Healthy
Obese
Fold change
Differentiation timepoint
(C)
Control
250ng/ml DKK1
1µM PNU-74654
10µM PNU-74654
(D)
Control
250ng/ml DKK1
OCR (pmol/min/µg DNA)
Time (min)
(E)
Control
250ng/ml DKK1
OCR (pmol/min/µg DNA)
Basal Respiration
Maximal Respiration
(F)
Control
1µM PNU-74654
10µM PNU-74654
OCR (pmol/min/µg DNA)
Time (min)
(G)
Control
1µM PNU-74654
10µM PNU-74654
OCR (pmol/min/µg DNA)
Basal Respiration
Maximal Respiration

Fig. 4: Wnt antagonism rescues adipogenesis and mitochondrial dysfunction in obese ADSCs. Fold change in DKK1 expression at mRNA (n=6) **(A)** and protein (n=3) **(B)** levels in healthy and obese cells compared to their respective day 0 ADSCs, calculated from transcriptomic and proteomic datasets, respectively. **(C)** Representative whole well ORO scans at day 14 of differentiation for obese ADSCs differentiated in the presence of vehicle control, DKK1 (250 ng/mL) or PNU-74654 (1 μM and 10 μM). **(D)** Representative mitochondrial respiration traces at day 14 of adipogenic differentiation for obese ADSCs differentiated in the presence of vehicle control or DKK1 (250 ng/mL). **(E)** Mitochondrial function parameters: basal and maximal respiration calculated from mitochondrial respiration OCR values at day 14 of obese differentiation in control or DKK1-treated cells. **(F)** Representative mitochondrial respiration traces at day 14 of adipogenic differentiation for obese ADSCs differentiated in the presence of vehicle control or PNU-74654 (1 μM and 10 μM). **(G)** Mitochondrial function parameters: basal and maximal respiration calculated from mitochondrial respiration OCR values at day 14 of obese differentiation in control or PNU-74654 (1μM and 10μM) treated cells. (n=3; *$p<0.05$ and **$p<0.01$)

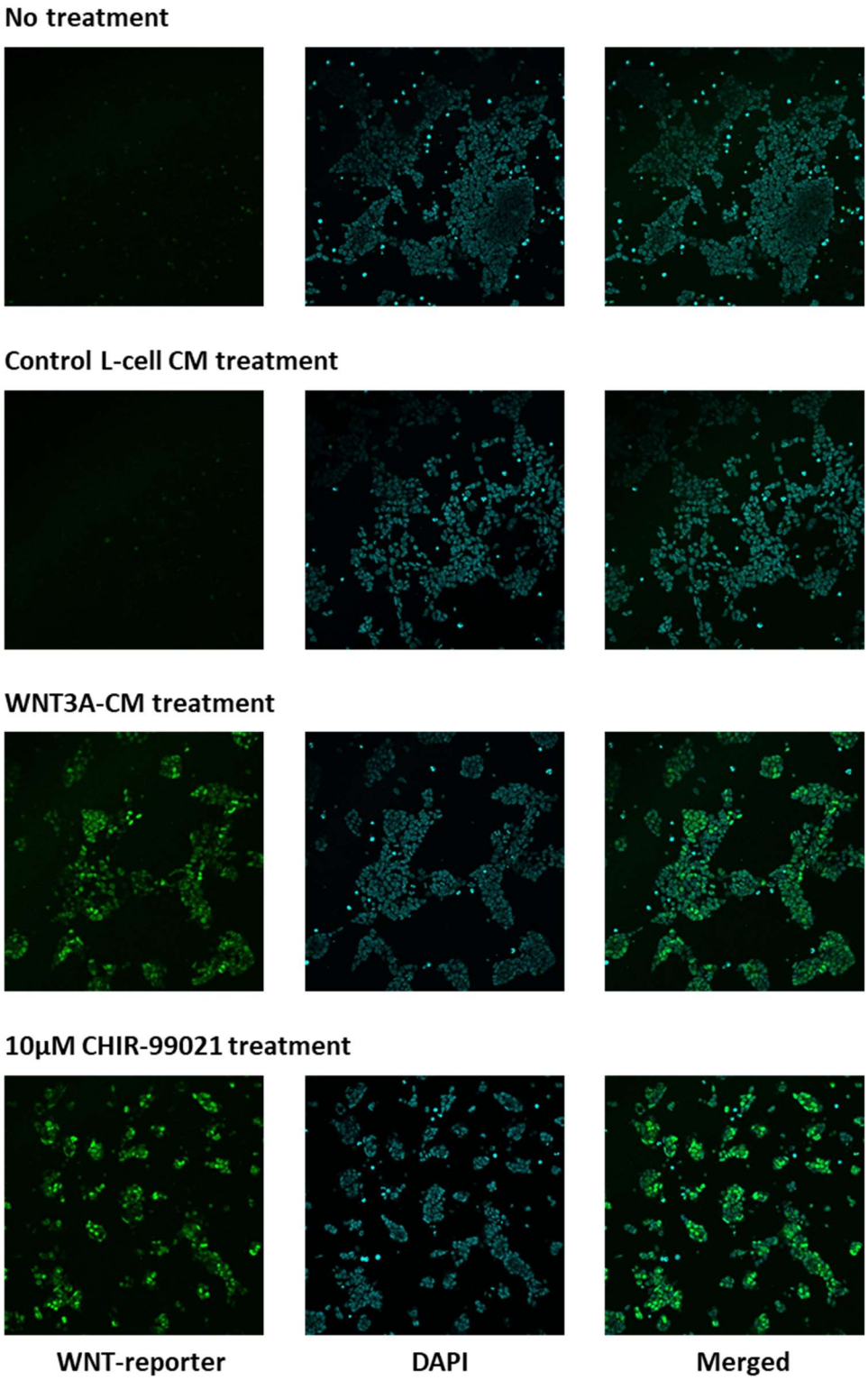
No treatment
Control L-cell CM treatment
WNT3A-CM treatment
10µM CHIR-99021 treatment
WNT-reporter
DAPI
Merged

Fig. S1: Wnt3A-CM contains biologically active Wnt3A. Representative fluorescent images showing Wnt reporter expression after 24 hours of stimulation with Wnt3A-CM, control L-cell-CM or 10μM CHIR-99021 in mESCs cells transfected with a fluorescence-based TCF/LEF reporter construct.

CHAPTER 4

A novel functional high-throughput drug-screening platform for the identification of compounds that target aberrant adipogenesis in an obese setting

Preface

This chapter is an original article in preparation for submission. It is presented in its pre-submission format. The authors include:

Kanwaldeep Singh, Brandon Law, Eva Szabo and Bradley Doble

I designed the study, conducted the experiments, analyzed the data, assembled the figures and wrote the manuscript together with Dr. Brad Doble. Brandon Law performed BODIPY stainings and image quantification. Dr. Eva Szabo helped with study design and interpretation of data.

Current drug screening platforms for adipogenesis modulators largely quantify adipogenesis based on lipid accumulation, which is measured by using high content image analyses of stained lipid droplets. However, these strategies are tedious to perform, suffer from reproducibility issues, provide little/no functional readouts, and employ cellular models that are not reflective of the target disease. Thus, there is a need to develop more robust drug screening assays in clinically relevant disease models to improve the clinical translation potential of identified candidate drugs. Previous work (Zhang et al., 2013; Wilson-Fritch et al., 2003) and our

results from Chapter 2 revealed a strong correlation between mitochondrial activity and adipogenesis. Moreover, stem cells derived from obese patients exhibited reduced adipogenesis, which could be rescued by improving their cellular metabolism and increasing their mitochondrial activity. This chapter describes how we used the positive association between these processes to develop and validate a novel functional drug screening platform targeting adipogenesis in obesity.

A novel functional high-throughput drug-screening platform for the identification of compounds that target aberrant adipogenesis in an obese setting

Abstract

Obesity is a worldwide epidemic, affecting over 39% of the global population. Thus, given its socioeconomic and health severity, numerous weight management programs have been proposed, including pharmacologic treatments. However, most of the current pharmaceuticals/drugs have severe side effects, minimal efficacy, and do not target obese adipose tissue. Accordingly, they have had limited success in reducing fat mass. There is an urgent need for therapeutics that directly target adipose tissue mass in an obese context, a treatment strategy that is currently unavailable in a clinical setting. Our study established a functional drug-screening platform that identifies small molecules/drugs which impact the pathways specifically dysregulated in obese adipocytes. Recent studies, as well as our work, have demonstrated that the molecular and functional pathways are differentially regulated in an obese versus healthy setting, and that these pathways impact mitochondrial bioenergetics, lipid accumulation and insulin responsiveness. Our proposed screening platform employs a live cell screening assay using patient-specific obese adipose tissue-derived stem cells (ADSCs) and allows for the discovery of drugs that influence mitochondrial function, lipid accumulation, and induction of brown adipogenesis. Overall, our study provides a screening platform that identifies drugs that directly target obese adipose tissue, with the potential to correct defects specific to diseased adipocytes, thereby offering a novel treatment for obesity.

Introduction

The process of adipocyte development/differentiation from precursors/preadipocytes derived from mesenchymal stem cells (MSCs) and adipose derived stem cells (ADSCs) is commonly referred to as adipogenesis. Adipocyte development encompasses both white and brown/beige adipogenesis, resulting in three distinct pools of adipose tissues: 1. white adipocyte tissue (WAT), 2. brown adipocyte tissue (BAT) and 3. brite/beige adipocyte tissue (b/bAT) (Billon and Dani, 2012). WAT is the main type of adipose tissue found in adult humans and is the primary site of energy storage. It synthesizes and releases a variety of adipokines (cytokines and hormones) such as adiponectin and leptin (Rosen and MacDougald, 2006), which promote cell proliferation and accelerate adipocyte differentiation. Dysregulation of energy homeostasis or pathways involved with WAT development can result in obesity (Derecka et al., 2012). BAT, on the other hand, plays an important role in the regulation of energy expenditure (Virtanen et al., 2009; Cypess et al., 2009; Zingaretti et al., 2009), and its activity is inversely correlated with severity of obesity and age. Several recent studies have shown that there is another type of fat called brite/beige adipose tissue (b/bAT), which resides in WAT depots (Wu et al., 2012). b/bAT is similar to BAT in that it can be induced to have a thermogenic phenotype. Thus, induction of b/bAT programs in WAT depots offers a unique opportunity to increase energy expenditure via burning fat, versus storing it, providing a potential strategy to combat obesity.

Over the past decade, numerous programs have been proposed for management of obesity. However, the long-term success of these programs is limited because of significant barriers influencing affected individuals (i.e. maintaining lifestyle changes) (Lau et al., 2006), limited efficacy, and severe side effects of treatments (Yanovski and Yanovski, 2002). For most obese

individuals, only 5-10% of weight can be managed by the current pharmacotherapies, which may be due to the fact that the drugs employed do not act on the physiological pathways specific for fat tissue mass regulation in obesity.

Current screening strategies that are used to identify potential drugs are mainly focused on identifying inhibitors of adipogenesis and/or are mostly conducted in mouse models. Assays using murine preadipocyte cell lines, such as 3T3-L1 and 3T3-F442A, involve staining and quantifying lipid content and measuring the activity of mature adipocyte markers (Choi et al., 2005; Sottile and Seuwen, 2001; Qin et al., 2010; Waki et al., 2007; Lane et al., 2014; Kim et al., 2016). However, due to inherent differences between human and murine adipogenesis (Mikkelsen et al., 2010) identification and subsequent translation of the drugs identified in mouse models to human obesity has been largely unsuccessful and is one of the main reasons for the lack of efficacious drugs/treatments available for human obesity. To date, only one drug screen has been performed in a human system (Moisan et al., 2015). It used a luminescence UCP1 mRNA capture assay to identify compounds that induce browning of white adipocytes from MSCs.

Notably, all existing screening platforms and protocols are optimized for healthy adipocytes and do not take into account the disease state. It has been shown that adipogenesis is differentially regulated in obese versus healthy states, resulting in functionally different adipocytes (Perez et al., 2013; De Girolamo et al., 2013). Hence, it is critical to study and identify adipogenesis modulators that specifically target obese adipocytes. In addition, present screening methods are only capable of identifying "hits" based on a single criterion/readout, either modulation of adipogenesis or induction of browning. They do not measure effects on insulin resistance and/or mitochondrial dysfunction, which drive development of obesity (Gustafson et al., 2015; Boudina

and Graham, 2014). Our present study demonstrates that it is possible to develop functional screening strategies that are capable of measuring multiple parameters, such as inhibition or induction of white adipogenesis, induction of brown adipogenesis and improving mitochondrial function, in a single assay using human obese adipocytes. Our screening assay represents a major improvement over previous assays and has the potential to identify novel compounds that could directly target obese adipose tissue towards treatment of obesity.

Results

We have previously shown a positive correlation between mitochondrial dysfunction and reduced adipogenic differentiation potential in obese ADSCs, along with proof-of-concept experiments suggesting that the defects in adipogenesis observed in obese ADSCs could be rescued by using small molecule-mediated improvement in mitochondrial function (unpublished, Chapter 2 of this thesis). Here, we have developed a novel drug screening strategy to identify compounds that promote adipogenesis based on their ability to stimulate mitochondrial function in obese ADSCs.

Mitochondrial functional assay optimization using obese ADSCs

We first optimized the mitochondrial stress test (MST) for obese ADSCs by using the XFe96 extracellular flux analyzer. This assay measures the oxygen consumption rate of cells, plated at optimal cell density, with sequential addition of Oligomycin (electron transport chain (ETC) complex V - ATP synthase inhibitor), FCCP (mitochondrial respiration uncoupler) and a mixture of Antimycin and Rotenone (inhibitors of ETC complexes I and III). It provides a complete

picture of the mitochondrial function under both basal and stressed conditions, including basal respiration, ATP production and maximal respiration capacity of the cells. One of the most important parameters that needs to be optimized for a successful MST assay capable of obtaining a robust and accurate measurement for OCR, is the concentration of FCCP to which the cells are exposed during the assay. OCR was thus measured with different FCCP concentrations (0, 0.25, 0.5, 1 and 2 μM) and was found to peak at 1 μM FCCP (Fig. S1). Therefore, 1 μM FCCP was determined to be the optimal FCCP concentration for all subsequent experiments.

Mitochondrial functional screening assay validation using mitochondrial biogenesis/function inducers

As the first step of validating a screening strategy using an optimized MST assay, obese ADSCs were pre-treated with known mitochondrial biogenesis inducers, RTA-408 and lipoamide, at two different concentrations during differentiation. Both compounds elicited a significant increase in OCR, compared to vehicle treated cells, in the MST assay performed at the differentiation endpoint (day 14). RTA-408 induced the highest increase in both basal and maximal respiration rates (~ 4 to 5-fold increase) (Fig. 1A-D). Cells were stained with BODIPY (lipid stain) to confirm that this increase in mitochondrial function in obese ADSCs was accompanied by an increase in adipogenic potential, as indicated by increased lipid accumulation per cell. An increase in BODIPY staining was observed following treatment with both compounds (Fig. 1E-F), indicative of an increased capacity to accumulate lipids. Overall, these results suggest that this platform can identify drugs that are able to regulate mitochondrial activity in differentiating adipocytes, which translates into changes in adipogenesis, as a result of improved mitochondrial biogenesis and function, in obese ADSCs.

Mitochondrial functional screening assay validation using known stimulators and inhibitors of adipogenesis

To evaluate the robustness of a screening platform, it is necessary to validate the platform by using known inhibitors or stimulators of the pathways that are being assayed. Thus, to validate our screening platform, obese ADSCs were pre-treated with known adipogenesis inducers and insulin sensitizer compounds (AM-251, rosiglitazone, harmine and adiporon) during the course of adipogenic differentiation, followed by readout of mitochondrial activity at the end of the differentiation timeline (day 14). AM-251 (100 nM and 1 μM) and rosiglitazone (50 μM) showed significant improvement in mitochondrial functional parameters, basal and maximal respiration, in differentiated adipocytes compared to vehicle treated cells (Fig. 2A-B and 2E-F). Similarly, treatment with harmine (1 μM and 10 μM) and adiporon (1 μM and 10 μM) also showed significant increase in mitochondrial function (Fig. 2C-F) by day 14 of differentiation. Compound- and vehicle-treated differentiated cells were stained with BODIPY to confirm that compound pre-treatment resulted in an increase in lipid accumulation, which is indicative of enhanced adipogenesis. Differentiation in presence of all four compounds, AM-251, rosiglitazone, harmine, and adiporon, showed an increased BODIPY staining, indicating an increase in adipogenic capacity (Fig. 2G-H). These results show that the high-throughput mitochondrial function assay is able to detect upregulation of mitochondrial activity, which translates to improved adipogenesis in obese ADSCs.

The screening assay was also validated for adipogenesis inhibitors, MK-2206 and wortmannin. MK-2206 (1μM and 10μM) and wortmannin (1μM and 10μM) both showed significant decreases in mitochondrial maximal respiration (Fig. 3A-C).

Taken together, these results show that a mitochondrial function-based screening assay can efficiently detect compounds that modulate adipogenesis in obese ADSCs.

Secondary screening assay for identification of "browning" inducers

This screening platform is aimed to identify "hits" based on changes in functional mitochondrial activity upon treatment with test compounds during the course of adipogenesis. However, the increase in mitochondrial activity during adipogenesis could be attributed to improvement in either white adipogenesis and/or induction of "browning" during adipogenesis. To determine whether the "hits" obtained from the primary mitochondrial function screen are white adipogenesis promoting agents or browning inducers, we developed a high-throughput brown adipocyte function-specific secondary screening assay based on β-adrenergic receptor agonist stimulated UCP1-dependent respiration on the XFe 96 extracellular flux analyzer.

We induced "browning" during adipogenesis of healthy ADSCs upon treatment with known browning inducers, R406 and tofacitinib (Moisan et al., 2015), during the course of adipogenesis. Changes in adipocyte morphology were evaluated by phase-contrast microscopy followed by BODIPY and ORO staining. The presence of unilocular lipid droplets in individual cells is characteristic of white adipocytes, while the presence of multiple lipid droplets is indicative of induction of brown adipogenesis. Therefore, when these parameters were measured, control adipocytes appeared as cells containing a single lipid droplet, while R406- and tofacitinib-treated adipocytes were all multilocular, a characteristic of brown adipocytes (Fig. 4A). Further, R406 and tofacitinib treatments resulted in ~3-fold increase in mRNA expression of UCP1, a known brown adipocyte marker, thereby further supporting "browning" of the compound-treated adipocytes (Fig. 4B).

Changes in OCR were measured upon stimulation with isoproterenol, a β-adrenergic receptor agonist, which has been shown to stimulate respiration in brown adipocytes via UCP1-dependent β-adrenergic receptor agonism (Li et al., 2014; Schnabl et al., 2019). Both R406 (0.5 μM) and tofacitinib (2.5 μM) treatments resulted in efficient browning of ADSCs obtained from white adipose depots, as suggested by ~ 2-fold increase in OCR upon isoproterenol stimulation compared to control (Fig. 4C). These results suggest that this secondary assay can efficiently detect brown adipocyte emergence and activity.

The effect on adipogenesis observed in the primary screen, using a panel of known mitochondrial biogenesis/function inducers (RTA-408 and lipoamide) and adipogenesis inducers/insulin sensitizers (AM-251, rosiglitazone, harmine and adiporon), was further evaluated in a secondary screening assay, to determine whether the adipogenesis improvement shown by these compounds was due to enhanced white adipogenesis and/or browning of the adipocytes. Among the compounds tested, only harmine (10 μM) and rosiglitazone (50 μM) exhibited a significant increase in OCR upon isoproterenol stimulation in this assay, suggesting that, in addition to increasing overall adipogenesis, these compounds lead to the browning of adipocytes as well (Fig. 4D).

Discussion

Obesity is characterized by limited adipogenesis, with adipose tissue expansion occurring almost exclusively through adipocyte hypertrophy, which results in increased lipid accumulation and ultimately leads to an insulin resistant state. Current efforts to identify compounds capable of rescuing adipogenesis and metabolic symptoms are restricted primarily due to limitations in cell

culture models used for the studies. Most studies utilize murine cell lines (Waki et al., 2007; Lane et al., 2014; Kim et al., 2016; Sohle et al., 2012), however this approach is highly limiting, as there is low translation between murine and human models in molecular events that drive adipogenesis (Mikkelsen et al., 2010). Furthermore, all current human and mouse cell models used in screening platforms are of healthy origin (Foley et al., 2015; Qin et al., 2010). The adipogenic deficiencies are generated by removing critical components of the differentiation media, which do not accurately reflect the etiology of obesity (Qin et al., 2010). Hence, compounds identified via these approaches would have unclear efficacy regarding their effects on adipogenesis, casting doubts over their translation potential in a clinical setting.

Our group (unpublished, chapter 2 of this thesis), and other preceding research, have shown a strong correlation between mitochondrial biogenesis and adipogenesis. Differentiation from ADSCs to adipocytes is accompanied by stimulation of mitochondrial proteins and an increase in mitochondrial functional activity (Wilson-Fritch et al., 2003; Zhang et al., 2013; Drehmer et al., 2016). We have used this strong correlation between these two cellular conditions to develop a novel high-throughput drug screening platform to identify compounds that promote adipogenesis in an obese setting by using a Seahorse XFe96 extracellular flux analyzer. Further, we developed a secondary screening method to categorize the "hits" obtained from the primary screening assay into white and/or brown adipogenesis inducers. We differentiated healthy ADSCs into brown adipocytes upon treatment with JAK3 inhibitor, tofacitinib, and SYK inhibitor, R406, both of which have been shown to efficiently induce browning of white adipocytes. Tofacitinib and R406 have been shown to inhibit the JAK-STAT pathway in human adipocytes, leading to downregulation of the interferon alpha (IFN), beta and gamma responses, thereby relieving

inhibition of the sonic hedgehog (SHH) pathway, thereby leading to accumulation of UCP1 and browning of adipocytes (Moisan et al., 2015). BAT program induction in our adipocytes was further confirmed by development of a high-throughput functional brown adipocyte activity assay based on isoproterenol (β-adrenergic receptor agonist)-stimulated UCP1-dependent mitochondrial respiration (Fig. 5).

The screening platform presented here improves on current methods in several ways: (1) It uses human cellular models of obesity, specifically, morbidly obese ADSCs instead of healthy cell lines, leading to a more accurate representation of "obesity in a dish"; (2) It provides multiparametric and functional readouts for both white and brown adipogenesis, compared to methods using single parameters (i.e. BODIPY or ORO stained lipid-droplet imaging), which do not provide any evidence of functional activity of the adipocytes; and (3) It provides a more economical platform than traditional 96-well screening assays, as the well area for a Seahorse XF96-well plate is ~ 3 times smaller than regular tissue-culture 96-well plates, thereby requiring significantly fewer cells and costly reagents/human growth factors for running the screening assay.

The ability of this screening platform to capture potential "hits" was further verified by testing eight different adipogenesis and mitochondrial function modulators across three different compounds categories: (1) mitochondrial biogenesis/function inducers, RTA-408 and lipoamide; (2) adipogenesis inducers and insulin sensitizers, AM-251, rosiglitazone, harmine and adiporon; and (3) adipogenesis inhibitors, MK-2206 and wortmannin. RTA-408 (also known as omaveloxolone) is a potent Nrf2 (a key transcription factor in mitochondrial biogenesis) activator that has been shown to improve mitochondrial bioenergetics in models of neurological disorders (Abeti et al., 2018). Our group has previously shown the pro-adipogenic effects of this compound

in an *in vitro* obesity model (unpublished, Chapter 2 of this thesis). Lipoamide has been shown to stimulate mitochondrial biogenesis, where lipoamide-treated 3T3-L1 adipocytes exhibited increased mitochondrial DNA copy number, protein levels, and expression of transcription factors involved in mitochondrial biogenesis (Shen et al., 2011). Among the adipogenesis modulators tested, rosiglitazone is a PPARγ agonist that is known to stimulate adipogenesis in a number of *in vitro* models (Benvenuti et al., 2007; Lu et al., 2016; Crossno et al., 2006). It has also been shown to induce browning of adipocytes *in vitro* (Merlin et al., 2017). AM-251 is a type I cannabinoid (CB1) receptor antagonist that has been reported to improve adipogenesis from MSCs *in vitro* (Idris et al., 2009). Harmine has been reported to have a dual mode of action and exerts its pro-adipogenic effects via PPARγ agonism, together with inhibition of the Wnt signaling pathway (Waki et al., 2007). In addition, it has been shown to promote browning of white adipocytes *in vitro* and *in vivo* (Nie et al., 2016). AdipoRon is a small molecule activator of adiponectin receptors, AdipoR1 and AdipoR2, that has been shown to ameliorate obesity-associated insulin resistance in mouse models (Okada-iwabu et al., 2013). MK-2206 and wortmannin inhibit adipogenesis by targeting key proteins involved in insulin-mediated signal transduction, Akt and phosphatidylinositol 3-kinase (PI3K), respectively (Kajno et al., 2015; Tomiyama et al., 1995; Tomiyama et al., 1999). Using these known compounds, our screening platform demonstrated sensitivity to increased adipogenesis and mitochondrial biogenesis in obese cells, providing validation of this tool for use in a high throughput screening setting for anti-obesity drugs.

Overall, our screening method provides a proof of concept for using “obese ADSCs” as a screening tool to identify novel compounds that specifically target obese fat depots. Moreover, this platform has illustrated the ability to identify “hits” that act through various mechanisms of action

to improve metabolic function, enabling this screening platform to be an effective tool to interrogate libraries composed of diverse classes of molecules, towards identification of new therapeutic approaches for obesity.

Supplemental Information

Supplemental Figure S1

Acknowledgements

This work was supported by Canadian Institutes of Health Research Grant and Canada Foundation for Innovation (CFI)-infrastructure fund (to Dr. Brad Doble and Dr. Eva Szabo). We thank Dr. Tony Collins (SCCRI, McMaster University) and Dr. Yoonseok Kam (Agilent Technologies) for valuable comments.

Materials and Methods

ADSC culture, compound treatments and adipogenic differentiation

Healthy ADSCs (n=1, BMI = 22.6) and morbidly obese ADSCs (n=1, BMI = 45.4) from our previously characterized cohort of age-, gender- and adipose tissue depot matched healthy, overweight and obese patient-derived ADSC biobank (unpublished, Chapter 2 of this thesis) were used in this study. Cells were cultured in DMEM-F12 (Corning, Cat# 10-090-CV) supplemented with 10% FBS, 1 mM L-Glutamine (Corning, Cat# 25-005-CI) and 10

ng/mLbFGF (Peprotech, Cat# 100-18B). For adipogenic differentiation, ADSCs were plated at a density of 7500 cells/cm^2 and were grown until they reached confluency in the ADSC growth medium, Differentiation was induced two days post confluency (day 0), with adipogenic differentiation medium composed of DMEM-F12 supplemented with 10% FBS, 1 mM L-Glutamine, 250 µM isobutyl-methylxanthine (IBMX) (Sigma, Cat# I5879), 0.5 µM dexamethasone (Sigma, Cat# D2915), 10 µg/mL Insulin (Sigma, Cat# I9278), and 100 µM indomethacin (Sigma, Cat# I7378), followed by a complete medium change with fresh differentiation medium every other day until day 14. RTA-408 (Cayman chemicals, Cat# 17854), lipoamide (Toronto Research Chemicals, Cat# L468710), AM-251 (Cayman chemicals, Cat# 71670), rosiglitazone (Cayman chemicals, Cat# 71740), harmine (Cayman chemicals, Cat# 10010324), adiporon (Cayman chemicals, Cat# 15941), MK-2206 (Cayman chemicals, Cat# 11593), and wortmannin (Cayman chemicals, Cat# 10010591) were used for treatments and adipogenic differentiation in obese cells, as indicated. For compound treatments, obese ADSCs were cultured in ADSC growth medium until confluency and were differentiated in adipogenic differentiation medium containing either RTA-408 (10 and 100 nM), lipoamide (1 and 10 µM), AM-251 (100 nM and 1 µM), rosiglitazone (10 and 50 µM), harmine (1 and 10 µM), adiporon (1 and 10 µM), MK-2206 (100 nM, 1 µM and 10 µM) or wortmannin (100 nM, 1 µM and 10 µM), followed by a complete medium change every other day until day 14.

BODIPY staining and image quantification

At day 14 of adipogenic differentiation, cells were stained with 0.1 mg/mL BODIPY (ThermoFisher, Cat# D3922) solution for 30 minutes at 37°C, washed thrice with DPBS, and imaged under fluorescent microscope. BODIPY intensity for the images was quantified by

using ImageJ software. Image quantification results are expressed as average fold increase in the BODIPY intensity normalized to cell numbers (DAPI) from 15 images for each treatment.

Mitochondrial function assay

Mitochondrial respiration assays were performed on an XFe96 extracellular flux analyzer (Seahorse-Agilent). 13000 obese ADSCs/well were plated in Seahorse-Agilent 96-well plates (Agilent Technologies, Cat# 101085-004). Adipogenesis was induced with, or without, indicated compounds the following day, as described above. At day 14 of differentiation, cells were rinsed twice with complete XF assay medium pH 7.4 (XF DMEM base medium without phenol red (Agilent Technologies, Cat# 103335-100) supplemented with 2.5 mM L-Glutamine, 1 mM sodium pyruvate, and 17.5 mM glucose), and the mitochondrial stress test (MST) was performed as per the instructions provided with the MST kit (Agilent technologies, Cat# 103015-100). FCCP concentration was optimized by using 0, 0.25, 0.5, 1 and 2 μM concentrations. All subsequent MST assays were performed by using the optimized concentration of FCCP (1 μM) along with recommended concentrations of oligomycin (2 μM) and antimycin+rotenone (0.5 μM each). Oxygen consumption rate (OCR) readouts were normalized to total cellular DNA content, after the MST assays, to account for any differences in cell number. Cellular DNA content was measured using the CyQuant Cell Proliferation assay kit (ThermoFisher, Cat# C7026) following the manufacturer's protocol. Data analysis was performed by using Wave 2.6 desktop analysis software.

Differentiation towards brown adipocytes

Healthy ADSCs were plated were plated at a density of 7500 cells/cm^2 and were grown until they reached confluency in ADSC growth medium. Differentiation was induced two days

post confluency (day 0) with adipogenic differentiation medium containing either 0.5 μM R406 (Cayman chemicals, Cat# 11422) or 2.5 μM tofacitinib (Cayman chemicals, Cat# 11598), followed by a complete medium change with fresh differentiation medium every other day until day 14. At day 14 of differentiation, cells were imaged by phase contrast microscopy followed by ORO and BODIPY staining. Cells were fixed with 4% PFA (Electron Microscopy Sciences, Cat# 15710) for 10 minutes at room temperature, followed by a rinse with 60% isopropanol for 2 minutes and staining with ORO working solution (6 parts 0.5% ORO (Sigma, Cat# O0625) in 100% isopropanol and 4 parts distilled water) for 30 minutes. Cells were washed under running water until the water ran clear. Cells were then imaged by light microscopy. For BODIPY (ThermoFisher, Cat# D3922) staining, cells were stained with 0.1 mg/mL BODIPY solution for 30 minutes at 37°C, washed thrice with DPBS, and imaged by epifluorescence microscopy.

RNA isolation, cDNA synthesis and qPCR

Total RNA from control and lipoamide treated cells was isolated at day 14 of adipogenic differentiation by using an RNA Isolation kit (Norgen Total RNA Purification Plus Kit, Cat# 48400). Approximately 1 μg of total RNA was reverse transcribed into cDNA by using a Bioline SensiFast cDNA synthesis kit (Cat# BIO-65054) according to the manufacturer's protocol. 2 μL of cDNA was used as template for each qRT-PCR reaction using a UCP1 TaqMan gene expression assay (ThermoFisher, assay id: Hs01084772_m1, Cat# 4331182), which was evaluated by using the QuantStudio3 Real-Time PCR detection system. UCP1 expression was normalized to that of an endogenous control RPLP0 (ThermoFisher, assay id: Hs00420895_gH).

Isoproterenol-stimulated respiration assay for "browning" of adipocytes

13000 healthy ADSCs/well were plated on Seahorse-Agilent 96-well plates (Agilent Technologies, Cat# 101085-004). Adipogenesis was induced with or without indicated compounds the following day, as described above. At day 14 of the differentiation, cells were rinsed twice with complete XF assay medium pH 7.4 (XF DMEM base media without phenol red (Agilent Technologies, Cat# 103335-100) supplemented with 2.5 mM L-Glutamine, 1 mM sodium pyruvate, 17.5 mM glucose, and 2% BSA). BSA scavenges extracellular free fatty acids and allows to specifically measure UCP1-mediated uncoupled respiration. A mitochondrial stress test (MST) was performed with the following sequential drug injections: isoproterenol (1 μM) to investigate UCP1-dependent uncoupled respiration, followed by oligomycin (2 μM) and antimycin+rotenone (0.5 μM each). OCR readouts were normalized to total cellular DNA content after the assays to account for any differences in cell numbers. Cellular DNA content was measured by using the CyQuant Cell Proliferation assay kit (ThermoFisher, Cat# C7026) following the manufacturer's protocol. Data analysis was performed by using Wave 2.6 desktop analysis software. Results are expressed as stimulated respiration, which is calculated as fold increase of basal respiration.

Statistical Analysis

Data are presented as means ± SEM. All experiments were conducted at least three times with similar results. GraphPad Prism 8 was used to analyze the differences between two groups by multiple unpaired two-tailed Student's t-tests. The statistical parameters (i.e. the exact n numbers and p values) can be found in the figure legends. For all experiments, a p-value less than 0.05 was considered significant.

References

Abeti, R., Baccaro, A., Esteras, N., and Giunti, P. (2018). Novel Nrf2-Inducer Prevents Mitochondrial Defects and Oxidative Stress in Friedreich's Ataxia Models. Frontiers in cellular neuroscience *12*, 188.

Benvenuti, S., Cellai, I., Luciani, P., Deledda, C., Baglioni, S., Giuliani, C., Saccardi, R., Mazzanti, B., Dal Pozzo, S., Mannucci, E., Peri, A., and Serio, M. (2007). Rosiglitazone stimulates adipogenesis and decreases osteoblastogenesis in human mesenchymal stem cells. Journal of endocrinological investigation *30,* RC26-30.

Billon, N., and Dani, C. (2012). Developmental origins of the adipocyte lineage: new insights from genetics and genomics studies. Stem cell reviews *8,* 55-66.

Boudina, S., and Graham, T. E. (2014). Mitochondrial function/dysfunction in white adipose tissue. Experimental physiology *99,* 1168-1178.

Choi, O.M., Cho, Y.H., Choi, S., Lee, S. H., Seo, S. H., Kim, H. Y., Han, G., Min, D. S., Park, T., and Choi, K. Y. (2013). The small molecule indirubin-3'-oxime activates Wnt/β-catenin signaling and inhibits adipocyte differentiation and obesity. International journal of obesity (2005) *38,* 1044-1052.

Crossno, J.T., Majka, S. M., Grazia, T., Gill, R. G., and Klemm, D. J. (2006). Rosiglitazone promotes development of a novel adipocyte population from bone marrow-derived circulating progenitor cells. The Journal of clinical investigation *116,* 3220–3228.

Cypess, A.M., Lehman, S., Williams, G., Tal, I., Rodman, D., Goldfine, A. B., Kuo, F. C., Palmer, E. L., Tseng, Y. H., Doria, A., Kolodny, G. M., and Kahn, C. R. (2009). Identification and importance of brown adipose tissue in adult humans. The New England journal of medicine *360,* 1509-1517.

De Girolamo, L., Stanco, D., Salvatori, L., Coroniti, G., Arrigoni, E., Silecchia, G., Russo, M. A., Niada, S., Petrangeli, E., and Brini, A. T. (2013). Stemness and osteogenic and adipogenic potential are differently impaired in subcutaneous and visceral adipose derived stem cells (ASCs) isolated from obese donors. International journal of immunopathology and pharmacology *26,* 11-21.

Derecka, M., Gornicka, A., Koralov, S. B., Szczepanek, K., Morgan, M., Raje, V., Sisler, J., Zhang, Q., Otero, D., Cichy, J., Rajewsky, K., Shimoda, K., Poli, V., Strobl, B., Pellegrini, S., Harris, T. E., Seale, P., Russell, A. P., McAinch, A. J., O'Brien, P. E., Keller, S. R., Croniger, C. M., Kordula, T., and Larner, A. C. (2012). Tyk2 and Stat3 regulate brown adipose tissue differentiation and obesity. Cell metabolism *16,* 814-824.

Drehmer, D. L., de Aguiar, A. M., Brandt, A. P., Petiz, L., Cadena, S. M., Rebelatto, C. K., Brofman, P. R., Filipak Neto, F., Dallagiovanna, B., and Abud, A. P. (2016). Metabolic switches during the first steps of adipogenic stem cells differentiation. Stem cell research *17,* 413-421.

Foley, B., Clewell, R. and Deisenroth, C. (2015). Development of a Human Adipose-Derived Stem Cell Model for Characterization of Chemical Modulation of Adipogenesis. Applied in vitro Toxicology *1,* 66-78.

Gustafson, B., Hedjazifar, S., Gogg, S., Hammarstedt, A., and Smith, U. (2015). Insulin resistance and impaired adipogenesis. Trends in endocrinology and metabolism: TEM *26,* 193-200.

Idris, A. I., Sophocleous, A., Landao-Bassonga, E., Canals, M., Milligan, G., Baker, D., van't Hof, R. J., and Ralston, S. H. (2009). Cannabinoid receptor type 1 protects against age-related osteoporosis by regulating osteoblast and adipocyte differentiation in marrow stromal cells. Cell metabolism *10,* 139–147.

Kajno, E., McGraw, T. E., and Gonzalez, E. (2015). Development of a new model system to dissect isoform specific Akt signalling in adipocytes. The Biochemical journal *468,* 425–434.

Kim, G.Y., Jeong, H.H., Yeom, S.J., Lee, C.S., and Roh, C. (2016). Efficient and reliable screening of anti-obesity agents on a micro-cell pattern chip. Journal of chemical technology & biotechnology *91,* 2688-2692.

Lane, J. M., Doyle, J. R., Fortin, J. P., Kopin, A. S., and Ordovas, J. M. (2014). Development of an OP9 derived cell line as a robust model to rapidly study adipocyte differentiation. PloS one *9,* e112123.

Lau, D.C., Douketis, J. D., Morrison, K. M., Hramiak, I. M., Sharma, A. M., and Ur, E. (2007). 2006 Canadian clinical practice guidelines on the management and prevention of obesity in adults and children [summary]. CMAJ: Canadian Medical Association journal = journal de l'Association medicale canadienne *176,* S1-13.

Li, Y., Fromme, T., Schweizer, S., Schottl, T., and Klingenspor, M. (2014). Taking control over intracellular fatty acid levels is essential for the analysis of thermogenic function in cultured primary brown and brite/beige adipocytes. EMBO reports *15,* 1069-1076.

Lu, W., Wang, W., Wang, S., Feng, Y., and Liu, K. (2016). Rosiglitazone Promotes Bone Marrow Adipogenesis to Impair Myelopoiesis under Stress. PloS one *11,* e0149543.

Merlin, J., Sato, M., Nowell, C., Pakzad, M., Fahey, R., Gao, J., Dehvari, N., Summers, R. J., Bengtsson, T., Evans, B. A., & Hutchinson, D. S. (2017). The PPARγ agonist rosiglitazone promotes the induction of brite adipocytes, increasing β-adrenoceptor-mediated mitochondrial function and glucose uptake. Cellular signalling *42,* 54-66.

Mikkelsen, T. S., Xu, Z., Zhang, X., Wang, L., Gimble, J. M., Lander, E. S., and Rosen, E. D. (2010). Comparative epigenomic analysis of murine and human adipogenesis. Cell *143,* 156-169.

Moisan, A., Lee, Y. K., Zhang, J. D., Hudak, C. S., Meyer, C. A., Prummer, M., Zoffmann, S., Truong, H. H., Ebeling, M., Kiialainen, A., Gerard, R., Xia, F., Schinzel, R. T., Amrein, K. E., and Cowan, C. A. (2015). White-to-brown metabolic conversion of human adipocytes by JAK inhibition. Nature cell biology *17,* 57-67.

Nie, T., Hui, X., Mao, L., Nie, B., Li, K., Sun, W., Gao, X., Tang, X., Xu, Y., Jiang, B., Tu, Z., Li, P., Ding, K., Han, W., Zhang, S., Xu, A., Ding, S., Liu, P., Patterson, A., Cooper, G., and Wu, D. (2016). Harmine Induces Adipocyte Thermogenesis through RAC1-MEK-ERK-CHD4 Axis. Scientific reports *6,* 36382.

Okada-Iwabu, M., Yamauchi, T., Iwabu, M., Honma, T., Hamagami, K., Matsuda, K., Yamaguchi, M., Tanabe, H., Kimura-Someya, T., Shirouzu, M., Ogata, H., Tokuyama, K., Ueki, K., Nagano, T., Tanaka, A., Yokoyama, S., and Kadowaki, T. (2013). A small-molecule AdipoR agonist for type 2 diabetes and short life in obesity. Nature *503,* 493–499.

Perez, L. M., Bernal, A., San Martin, N., Lorenzo, M., Fernandez-Veledo, S., and Galvez, B. G. (2013). Metabolic rescue of obese adipose-derived stem cells by Lin28/Let7 pathway. Diabetes *62,* 2368-2379.

Qin, J., Li, W. Q., Zhang, L., Chen, F., Liang, W. H., Mao, F. F., Zhang, X. M., Lahn, B. T., Yu, W. H., and Xiang, A. P. (2010). A stem cell-based tool for small molecule screening in adipogenesis. PloS one *5,* e13014.

Rosen, E. D., and MacDougald, O. A. (2006). Adipocyte differentiation from the inside out. Nature reviews. Molecular cell biology *7,* 885-896.

Schnabl, K., Westermeier, J., Li, Y., and Klingenspor, M. (2019). Opposing Actions of Adrenocorticotropic Hormone and Glucocorticoids on UCP1-Mediated Respiration in Brown Adipocytes. Frontiers in physiology *9,* 1931.

Shen, W., Hao, J., Feng, Z., Tian, C., Chen, W., Packer, L., Shi, X., Zang, W., and Liu, J. (2011). Lipoamide or lipoic acid stimulates mitochondrial biogenesis in 3T3-L1 adipocytes via the endothelial NO synthase-cGMP-protein kinase G signalling pathway. British journal of pharmacology *162,* 1213–1224.

Sohle, J., Machuy, N., Smailbegovic, E., Holtzmann, U., Gronniger, E., Wenck, H., Stab, F., and Winnefeld, M. (2012). Identification of new genes involved in human adipogenesis and fat storage. PloS one *7,* e31193.

Sottile, V., and Seuwen, K. (2001). A high-capacity screen for adipogenic differentiation. Analytical biochemistry *293,* 124-128.

Tomiyama, K., Nakata, H., Sasa, H., Arimura, S., Nishio, E., and Watanabe, Y. (1995). Wortmannin, a specific phosphatidylinositol 3-kinase inhibitor, inhibits adipocytic differentiation of 3T3-L1 cells. Biochemical and biophysical research communications *212,* 263–269.

Tomiyama, K., Nishio, E., and Watanabe, Y. (1999). Both wortmannin and simvastatin inhibit the adipogenesis in 3T3-L1 cells during the late phase of differentiation. Japanese journal of pharmacology *80,* 375–378.

Virtanen, K. A., Lidell, M. E., Orava, J., Heglind, M., Westergren, R., Niemi, T., Taittonen, M., Laine, J., Savisto, N. J., Enerback, S., and Nuutila, P. (2009). Functional brown adipose tissue in healthy adults. The New England journal of medicine *360,* 1518-1525.

Waki, H., Park, K. W., Mitro, N., Pei, L., Damoiseaux, R., Wilpitz, D. C., Reue, K., Saez, E., and Tontonoz, P. (2007). The small molecule harmine is an antidiabetic cell-type-specific regulator of PPARgamma expression. Cell metabolism *5,* 357-370.

Wilson-Fritch, L., Burkart, A., Bell, G., Mendelson, K., Leszyk, J., Nicoloro, S., Czech, M., and Corvera, S. (2003). Mitochondrial biogenesis and remodeling during adipogenesis and in response to the insulin sensitizer rosiglitazone. Molecular and cellular biology *23,* 1085-1094.

Wu, J., Bostrom, P., Sparks, L. M., Ye, L., Choi, J. H., Giang, A. H., Khandekar, M., Virtanen, K. A., Nuutila, P., Schaart, G., Huang, K., Tu, H., van Marken Lichtenbelt, W. D., Hoeks, J., Enerback, S., Schrauwen, P., and Spiegelman, B. M. (2012). Beige adipocytes are a distinct type of thermogenic fat cell in mouse and human. Cell *150,* 366-376.

Yanovski, S. Z., and Yanovski, J. A. (2002). Obesity. The New England journal of medicine *346,* 591-602.

Zhang, Y., Marsboom, G., Toth, P. T., and Rehman, J. (2013). Mitochondrial respiration regulates adipogenic differentiation of human mesenchymal stem cells. PloS one *8,* e77077.

Zingaretti, M. C., Crosta, F., Vitali, A., Guerrieri, M., Frontini, A., Cannon, B., Nedergaard, J., and Cinti, S. (2009). The presence of UCP1 demonstrates that metabolically active adipose tissue in the neck of adult humans truly represents brown adipose tissue. FASEB journal: official publication of the Federation of American Societies for Experimental Biology *23,* 3113-3120.

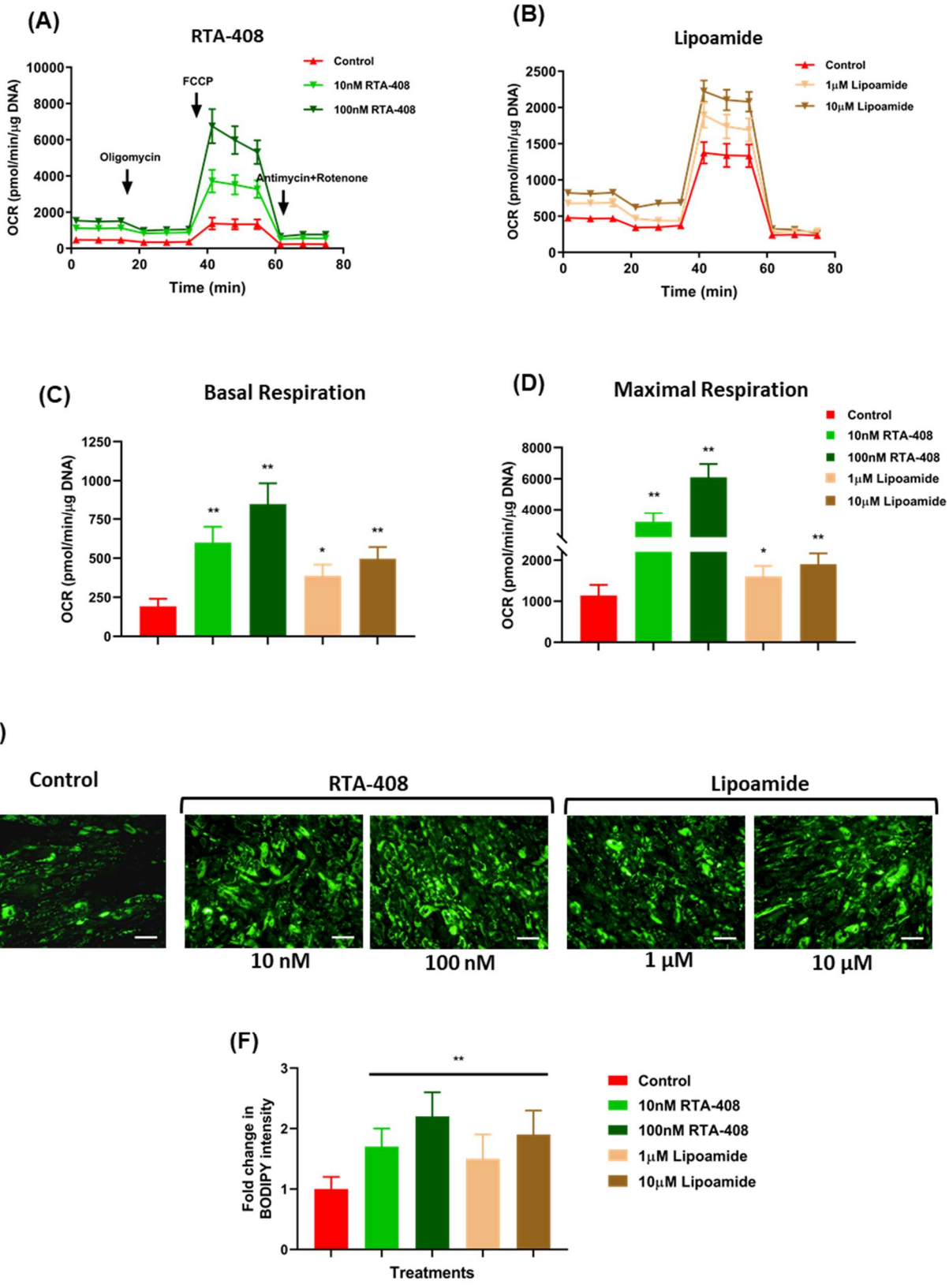
(A)
RTA-408
Control
10nM RTA-408
100nM RTA-408
FCCP
Oligomycin
Antimycin+Rotenone
OCR (pmol/min/µg DNA)
Time (min)
(B)
Lipoamide
Control
1µM Lipoamide
10µM Lipoamide
OCR (pmol/min/µg DNA)
Time (min)
(C)
Basal Respiration
OCR (pmol/min/µg DNA)
(D)
Maximal Respiration
Control
10nM RTA-408
100nM RTA-408
1µM Lipoamide
10µM Lipoamide
OCR (pmol/min/µg DNA)
(E)
Control
RTA-408
Lipoamide
10 nM
100 nM
1 µM
10 µM
(F)
Fold change in BODIPY intensity
Treatments
Control
10nM RTA-408
100nM RTA-408
1µM Lipoamide
10µM Lipoamide

Fig. 1: Mitochondrial biogenesis/function inducers improve mitochondrial function and adipogenesis in obese ADSCs. (A) Representative mitochondrial respiration traces for day 14 vehicle (control) and RTA-408- (10 nM and 100 nM) treated and differentiated obese ADSCs. **(B)** Representative mitochondrial respiration traces for day 14 vehicle (control) and lipoamide- (1 μM and 10 μM) treated and differentiated obese ADSCs. Mitochondrial function parameters: basal **(C)** and maximal **(D)** respiration calculated from OCR measurements at day 14 of differentiation in control and compound-treated obese cells (n=4 experiments). **(E)** Representative BODIPY stain images at day 14 of adipogenic differentiation for control and compound-treated obese cells. **(F)** Fold change in BODPIY intensity normalized to cell numbers (DAPI). 15 images were quantified for each treatment. Scale bar represents 100 μm. Statistical significance was determined by using multiple unpaired student's two-tailed t-tests. * $p<0.05$, ** $p<0.01$.

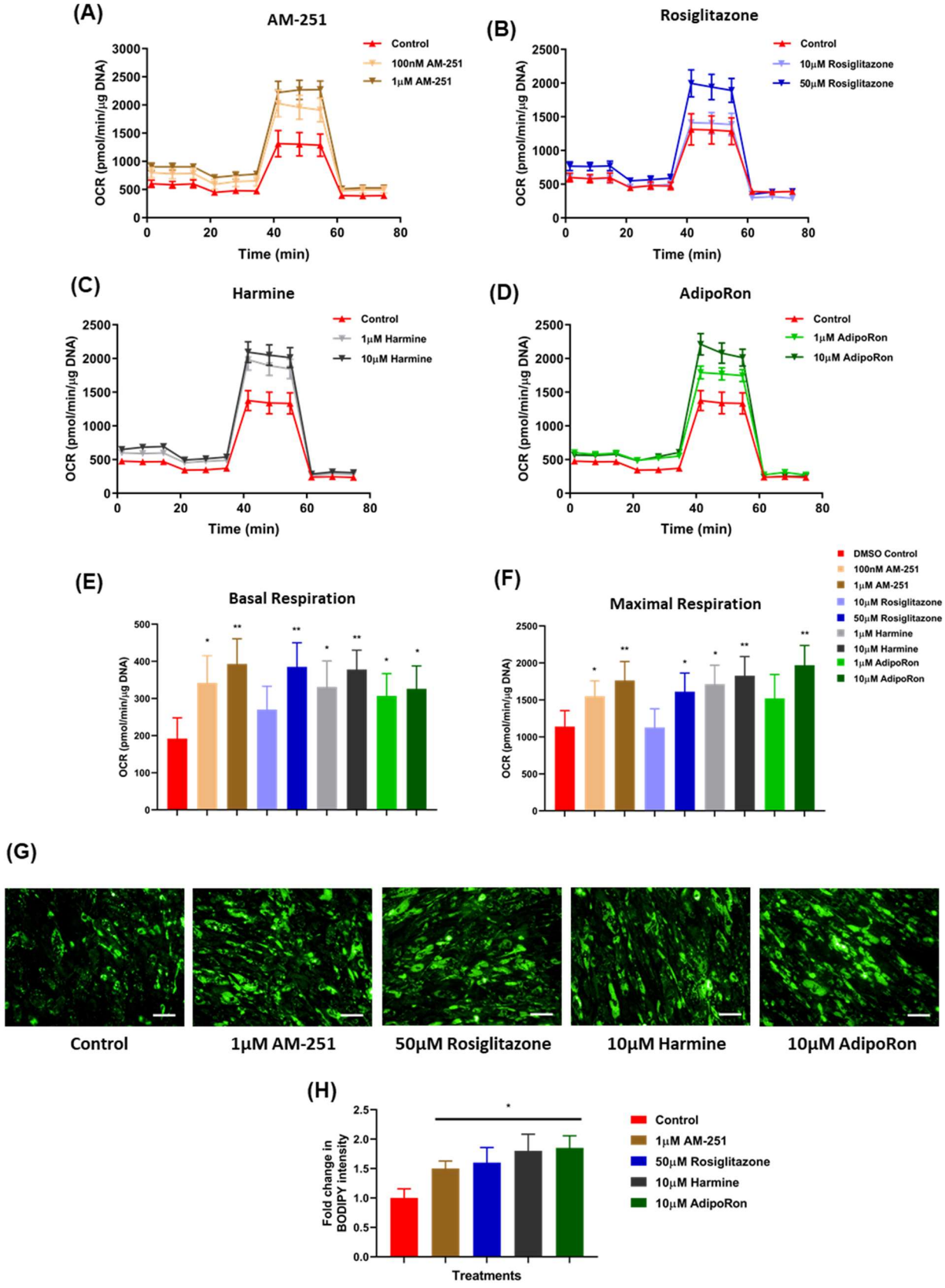
(A)
AM-251
Control
100nM AM-251
1μM AM-251
OCR (pmol/min/μg DNA)
Time (min)
(B)
Rosiglitazone
Control
10μM Rosiglitazone
50μM Rosiglitazone
(C)
Harmine
Control
1μM Harmine
10μM Harmine
(D)
AdipoRon
Control
1μM AdipoRon
10μM AdipoRon
(E)
Basal Respiration
(F)
Maximal Respiration
DMSO Control
100nM AM-251
1μM AM-251
10μM Rosiglitazone
50μM Rosiglitazone
1μM Harmine
10μM Harmine
1μM AdipoRon
10μM AdipoRon
(G)
Control
1μM AM-251
50μM Rosiglitazone
10μM Harmine
10μM AdipoRon
(H)
Fold change in BODIPY intensity
Treatments
Control
1μM AM-251
50μM Rosiglitazone
10μM Harmine
10μM AdipoRon

Fig. 2: Adipogenesis inducers and insulin sensitizers stimulate mitochondrial respiration and promote adipogenesis in obese ADSCs. Representative mitochondrial respiration traces for day 14 differentiated obese ADSCs differentiated in the presence of DMSO vehicle (control) and **(A)** AM-251 (100 nM and 1 μM), **(B)** Rosiglitazone (10 μM and 50 μM), **(C)** Harmine (1 μM and 10 μM), and **(D)** AdipoRon (1 μM and 10 μM). Mitochondrial function parameters: basal **(E)** and maximal **(F)** respiration calculated from OCR measurements at day 14 of differentiation in control and compound-treated obese cells (n=4 experiments). **(G)** Representative BODIPY stained images at day 14 of adipogenic differentiation for control and compound-treated obese cells. **(H)** Fold change in BODPIY intensity normalized to cell numbers (DAPI). 15 images were quantified for each treatment. Scale bar represents 100 μm. Statistical significance was determined by using multiple unpaired student's two-tailed t-tests. * $p<0.05$, ** $p<0.01$.

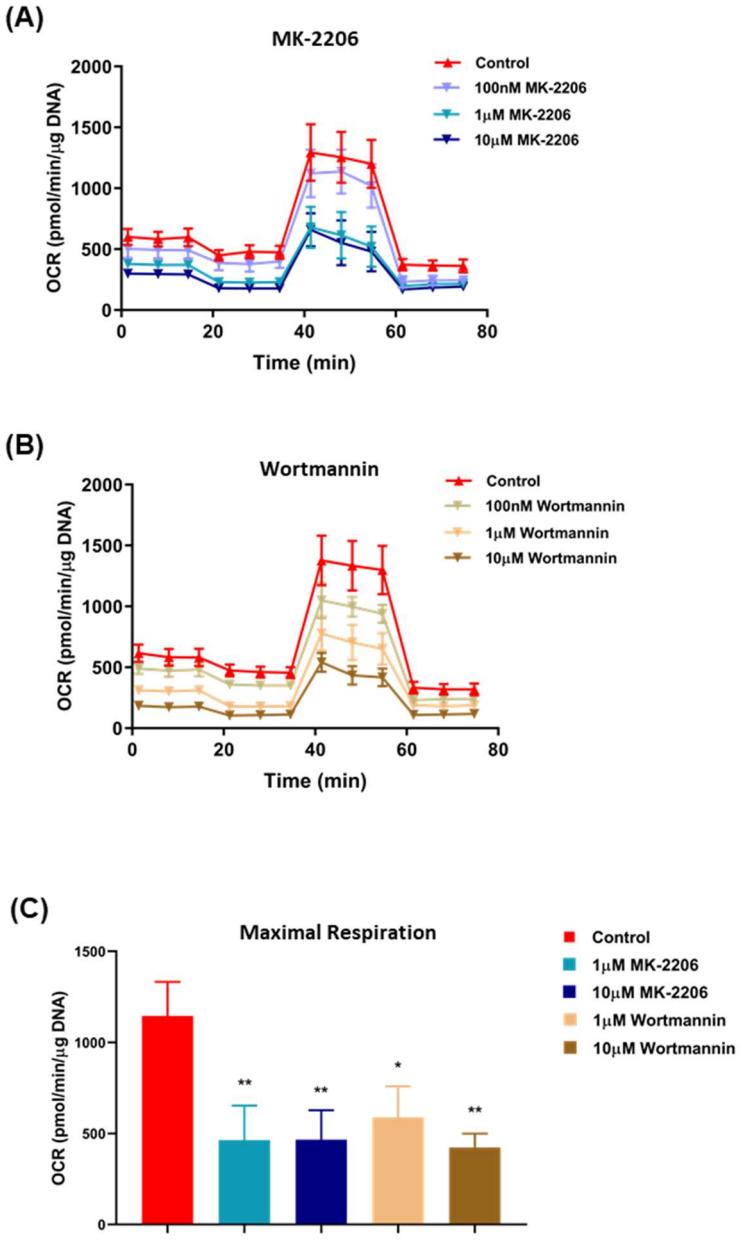
(A)
MK-2206
Control
100nM MK-2206
1μM MK-2206
10μM MK-2206
OCR (pmol/min/μg DNA)
Time (min)
(B)
Wortmannin
Control
100nM Wortmannin
1μM Wortmannin
10μM Wortmannin
OCR (pmol/min/μg DNA)
Time (min)
(C)
Maximal Respiration
Control
1μM MK-2206
10μM MK-2206
1μM Wortmannin
10μM Wortmannin
OCR (pmol/min/μg DNA)

Fig. 3: Adipogenesis inhibitors decrease mitochondrial respiration during adipogenesis in obese ADSCs. Representative mitochondrial respiration traces for day 14 obese ADSC-derived adipocytes in the presence of DMSO vehicle (control) and **(A)** MK-2206 (100 nM, 1 μM and 10 μM) and **(B)** Wortmannin (100 nM, 1 μM and 10μM). **(C)** Graph representing maximal mitochondrial respiration at day 14 of differentiation in control and compound-treated obese cells (n=3 experiments). Statistical significance was determined using multiple unpaired student's two-tailed t-tests. * $p<0.05$, ** $p<0.01$.

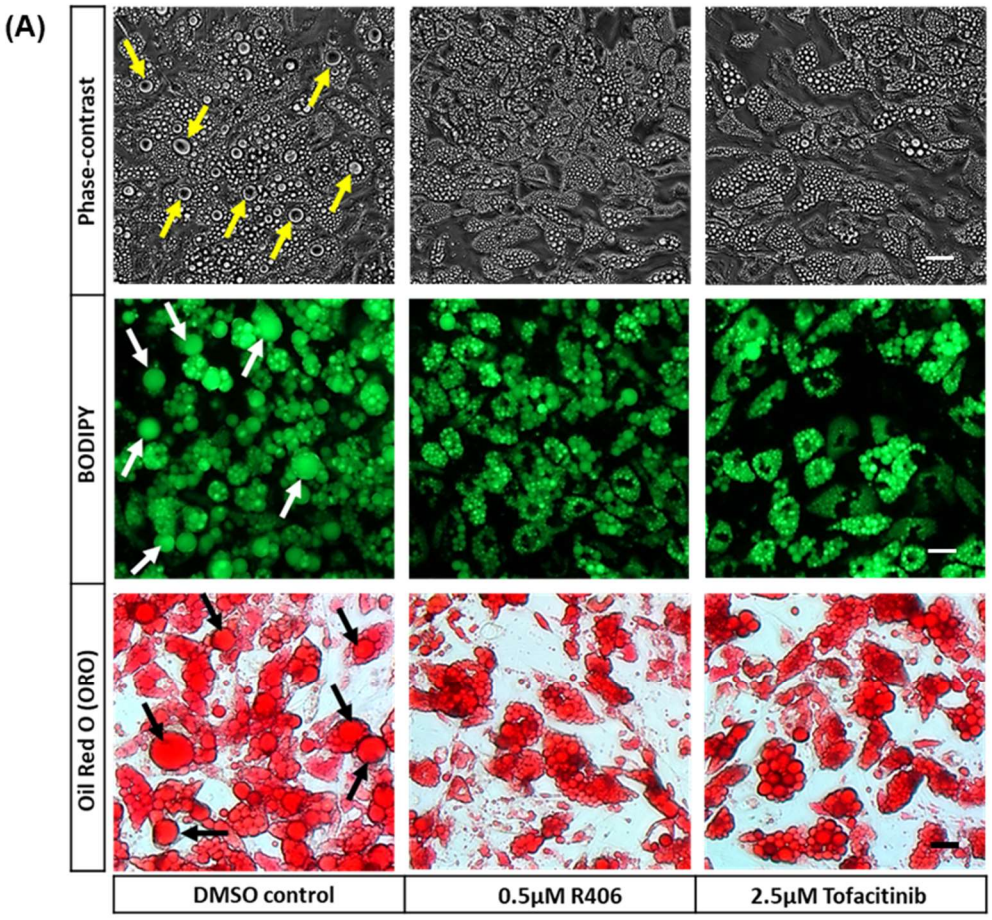
(A)
Phase-contrast
BODIPY
Oil Red O (ORO)
DMSO control
0.5μM R406
2.5μM Tofacitinib

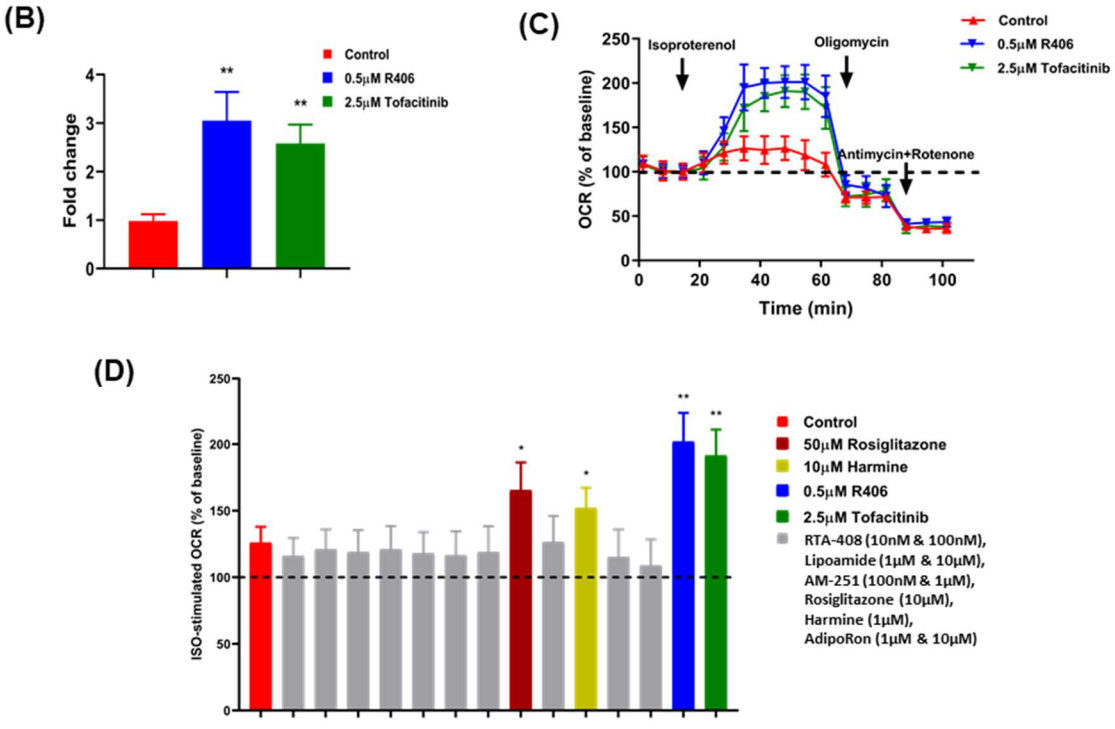
(B)
Fold change
Control
0.5μM R406
2.5μM Tofacitinib
(C)
Isoproterenol
Oligomycin
Antimycin+Rotenone
OCR (% of baseline)
Time (min)
(D)
ISO-stimulated OCR (% of baseline)
Control
50μM Rosiglitazone
10μM Harmine
0.5μM R406
2.5μM Tofacitinib
RTA-408 (10nM & 100nM),
Lipoamide (1μM & 10μM),
AM-251 (100nM & 1μM),
Rosiglitazone (10μM),
Harmine (1μM),
AdipoRon (1μM & 10μM)

Fig. 4: R406 and Tofacitinib induce browning of adipocytes during healthy ADSC differentiation. (A) Representative phase-contrast, BODIPY and ORO images of healthy ADSCs differentiated in the presence of 0.5 μM R406 and 2.5 μM tofacitinib and control differentiated cells at day 14 of differentiation. Arrows in the images point to the unilocular lipid-bearing cells observed in control differentiated cells. Scale bar represents 100 μm. **(B)** Fold change in UCP1 gene expression in healthy ADSCs treated and differentiated with R406 and tofacitinib compared to control cells (n=3 experiments). **(C)** Changes in OCR pattern for R406- and tofacitinib-treated and control healthy differentiated cells measured upon sequential exposure to isoproterenol, oligomycin and antimycin+rotenone. OCR is expressed as percent relative to baseline OCR measurements. **(D)** ISO (isoproterenol)-stimulated OCR expressed as percent of baseline OCR measured on day 14 of adipogenic differentiation of healthy ADSCs differentiated in the presence of indicated compounds (n=5 experiments). Statistical significance was determined using multiple unpaired student's two-tailed t-tests. * $p<0.05$, ** $p<0.01$.

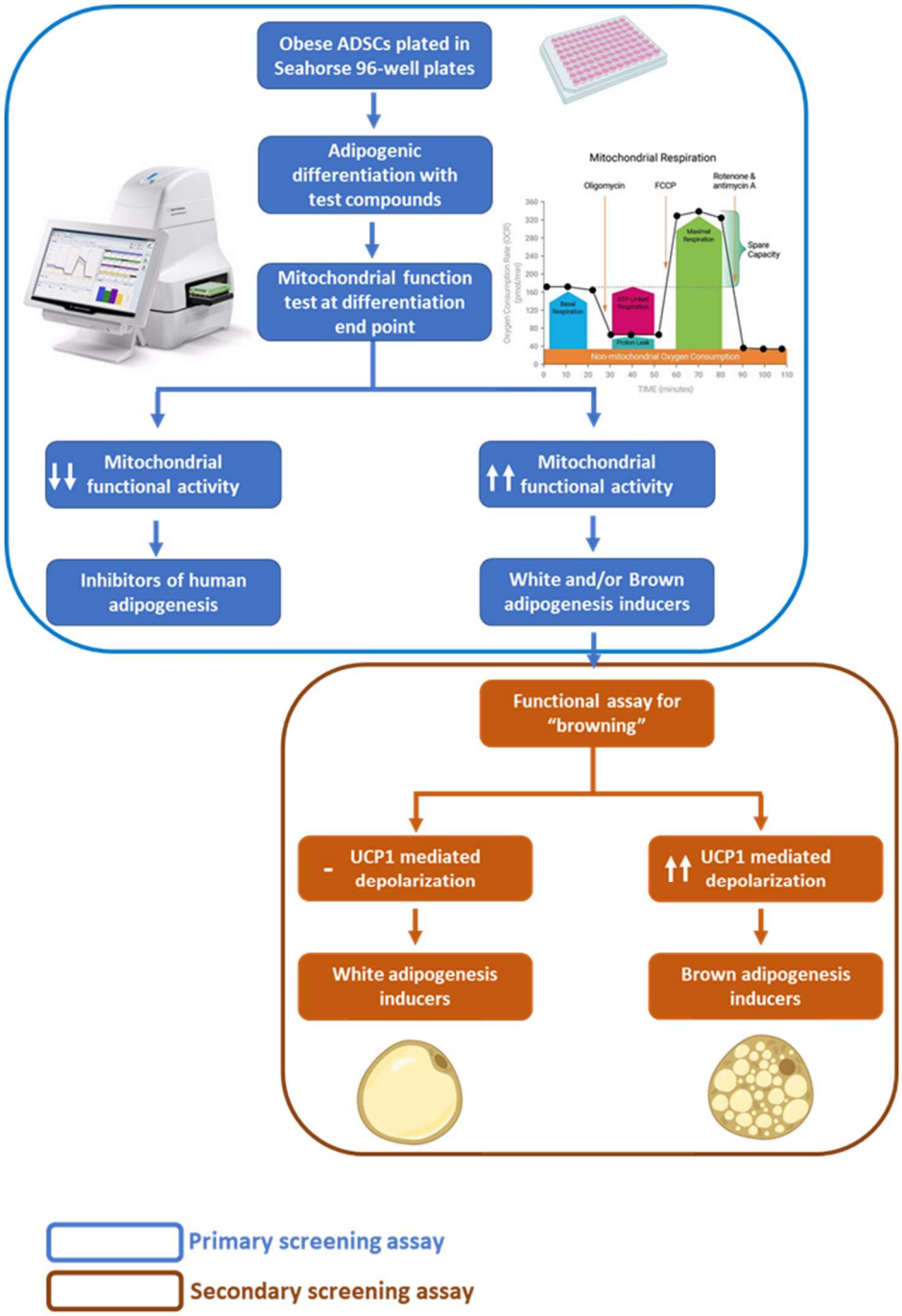

Fig 5: Flowchart showing the scheme of a novel functional screening strategy developed in this study.

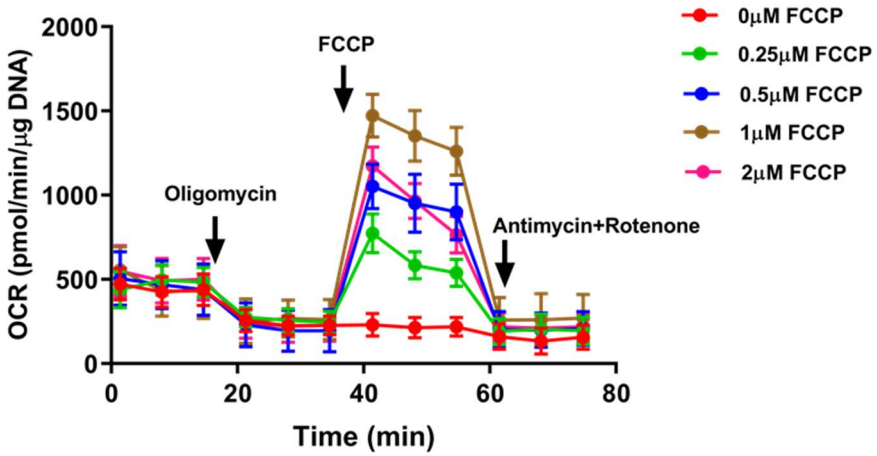

Fig. S1: FCCP optimization in a mito stress test (MST). Mitochondrial respiration traces for day 14 obese adipocytes showing changes in OCR upon stimulation with indicated concentrations of FCCP along with oligomycin (2 μM) and antimycin+rotenone (0.5 μM each).

CHAPTER 5: DISCUSSION

This thesis set out to investigate the molecular and metabolic mechanisms that control aberrant adipogenesis in a healthy versus obese setting. I hypothesized that resident stem cells isolated from obese individuals would provide an ideal *in vitro* model for studying the pathways that uniquely regulate aberrant adipogenesis in obesity, which can be targeted for improving metabolic health in an obese setting. Through my studies I was able to identify inherent obesity-associated molecular and metabolic aberrations in obese ADSCs leading to reduced adipogenic differentiation in these cells. Here, I discuss the significance, limitations, and future directions of my findings.

5.1 Comprehensive molecular and functional metabolic mapping of the human adipogenesis timeline

The process of *in vitro* adipogenesis is divided into two stages: commitment and terminal differentiation. Multipotent stem cells commit to become unipotent preadipocytes in the commitment phase, and committed preadipocytes differentiate into mature adipocytes in the terminal differentiation phase (Siersbaek and Mandrup, 2011). This thesis describes comprehensive metabolic profiling using transcriptomic, proteomic, and functional cellular metabolic analyses at different timepoints during the course of adipogenic differentiation, capturing both early (days 0-3) and late (days 7 and 14) cellular transition events in adipocyte development.

Changes in transcriptional networks (Siersbaek et al., 2012; Rangwala and Lazar, 2000) and epigenetic status (Musri and Parrizas, 2012; Andersen et al., 2019) that happen during the early and late phases of adipogenic differentiation have been studied in detail. However, the metabolic profiling has largely been limited to baseline analyses in undifferentiated cells (stem cells or preadipocytes) and endpoint (mature adipocytes) analyses (Wilson-Fritch et al., 2003; von Heimburg et al., 2005). Also, some previous studies have focused on early changes in mitochondrial metabolism only (Ducluzeau et al., 2011; Zhang et al., 2013; Drehmer et al., 2016) and do not illustrate a complete dynamic metabolic profile that accompanies the cellular changes across the adipogenesis process. Moreover, many prior studies were performed in murine models. Hence, translatability of these findings to a human system remains largely unclear given the interspecies differences in adipocyte development and metabolism.

Through my studies, using healthy ADSCs as a model system for human adipogenesis, I observed dynamic metabolic triggers that happen as early as day 1 of differentiation, as indicated by upregulation of metabolic pathway gene expression. This was followed by upregulation of functional cellular bioenergetics during early stages of differentiation, with further enrichment taking place at both functional and molecular levels as differentiation proceeded towards mature adipocytes (day 14 of differentiation timeline, Chapter 2).

The currently accepted metabolic perspective of stem cell differentiation suggests that as stem cells differentiate into mature cell types metabolism switches from a predominantly glycolytic phenotype to aerobic respiration/oxidative phosphorylation to meet most of the energy demands of the differentiating cell (Hu et al., 2016). Accordingly, increasing evidence suggests that cellular differentiation is an energy demanding process, which is driven by a shift from

glycolysis to oxidative phosphorylation, as this pathway generates significantly more net ATP than glycolysis (36 mol of ATP produced per mol of glucose consumed in oxidative phosphorylation vs 2 mol of ATP produced per mol of glucose consumed in glycolysis). For example, stem cell differentiation into neural precursors and mature neurons (Calvo-Garrido et al., 2019; Zheng et al., 2016), osteocytes (Chen et al., 2008), hepatocytes (Wanet et al., 2014; Hopkinson et al., 2017) and cardiomyocytes (Hu et al., 2018), as well as hematopoietic stem cell differentiation (Klimmeck et al., 2012; Suda et al., 2011; Takubo et al., 2013) have been shown to be accompanied by a metabolic switch from glycolysis to mitochondrial respiration. In addition to the changes in ATP demands, differentiating cells require a continuous supply of precursor molecules for biosynthesis of amino acids, lipids, and nucleotides for the cellular transitions that take place during differentiation. These anabolic molecules are primarily biosynthesized *de novo* from TCA cycle intermediates (Costello and Franklin, 2013).

However, contrary to current views of stem cell metabolism changes during differentiation, my results (Chapter 2) showed that adipogenesis is accompanied by a several fold increase in both cellular energy producing pathways, glycolysis and mitochondrial respiration. The upregulation in gene expression of these pathways starts to occur as early as day 3 of differentiation and shows continued enrichment until day 14. This suggests that adipogenesis is a highly energy demanding process requiring a constant supply of biosynthetic precursors and NADPH-reducing equivalents for the synthesis of lipids and other biomolecules, and those energy and biosynthetic precursor requirements are met by an upregulation of both glycolysis and oxidative phosphorylation. Further, since the enrichment in the molecular gene signatures for metabolic pathways and the changes in functional cellular bioenergetics starts very early-on during adipogenic differentiation, this

indicates that the upregulation of cellular energy metabolism drives, and is required for, efficient adipogenesis, rather than being a passive consequence of this process.

Moreover, my analyses indicated that an increase in mitochondrial respiration starts as early as day 3 of adipocyte differentiation with an accompanying increase in reactive oxygen species (ROS) production. I mapped the dynamic changes in cellular ROS levels across the adipogenesis timeline, which indicated a gradual increase during adipogenesis, peaking at day 7, followed by a decrease by day 14 of differentiation to levels similar to day 0 of differentiation (Fig. 1B), suggesting that ROS is required for adipogenesis but only during the initial steps of differentiation (Chapter 2). These data also demonstrate that evaluation of ROS levels in the undifferentiated state and mature adipocytes alone would be misleading, as the dynamic changes that are observed during the differentiation timeline would be completely missed. A few other studies have also suggested that ROS may be required at early stages of adipogenesis without showing how the levels are impacted in mature adipocytes upon completion of adipogenesis (Drehmer et al., 2016; Tormos et al., 2011; Zhang et al., 2013).

Hence, my study is the first report showing a complete functional cellular energy metabolic landscape that is supported by transcriptomic and proteomic analyses capturing all the stages of *in vitro* human adipogenesis (Fig. 1). These datasets provide the obesity and adipogenesis fields not only a resource to mine for metabolic and molecular signaling aberrations during adipogenesis, but also for novel stage-specific markers of adipocyte development. In addition, my study provides a more systematic understanding of human adipogenesis at both molecular and metabolic levels.

5.2 Development of a robust cellular model for studying obesity *in vitro*

"Well begun is half done" holds true for cellular disease modeling as well. One of the primary aims of this study was to elucidate the molecular mechanisms underlying the altered adipogenesis observed in human obesity by using *in vitro* cellular models that are able to mimic the *in vivo* disease environment as closely as possible. This made the choice of our cellular model of obesity critical for the success of this project. Most of the available *in vitro* models of obesity and insulin resistance rely on the use of non-physiological concentrations of FFAs and inflammatory mediators to induce an obese environment in an *in vitro* setting and hence, are capable of capturing isolated events only. These models do not provide a complete overview of the deranged metabolic profile associated with obesity and thus, generate fairly inconsistent conclusions (Wu et al., 2013; Stephens et al., 1997; Lo et al., 2013). Moreover, with regard to ADSCs; age, gender, and the location of adipose tissue source material have been shown to affect their proliferation and differentiation characteristics (Aksu et al., 2008; Alt et al., 2012; Choudhery et al., 2014; de Girolamo et al., 2009; van Harmelen et al., 2004; Padoin et al., 2008; Wong et al., 2018; van Harmelen et al., 2004; Faustini et al., 2010; Jurgens et al., 2008; Di Taranto et al., 2015).

Thus, in an effort to develop the best possible *in vitro* model that most closely mimics the human *in vivo* obese microenvironment, I isolated and characterized ADSCs from abdominal subcutaneous adipose tissue samples obtained from age-, and gender-matched patients with varying BMI levels: ranging between normal weight, overweight and obese (including different classes of obesity). Interestingly, there were no significant differences in the morphology or MSC surface marker expression observed between ADSCs isolated from the different classes of obese, overweight and healthy patients. However, I observed a spectrum of differences in their adipogenic

differentiation potential, with healthy ADSCs at the top, with highest adipogenic capacity, and morbidly obese (class III) ADSCs at the bottom, demonstrating severely impaired adipogenic differentiation *in vitro*. Further comparative experiments revealed significant differences in insulin sensitivity and mitochondrial function between healthy- and morbidly obese-ADSC-derived adipocytes, suggesting that they provided a robust model for studying obesity *in vitro*.

In addition, our results from Chapter 2 illustrate that obese ADSCs retain obesity-associated differences even after culturing *in vitro*. Accordingly, the cellular metabolism and insulin sensitivity profiles of these *in vitro* cultures during the course of adipogenesis reflect patient specific-aberrations. This holds particular significance for the application of ADSCs in the field of regenerative medicine and provides grounds for caution in their use in a clinical setting, with strong indications that development of clear guidelines for their use is absolutely critical.

Nevertheless, ADSCs derived from obese patients provide an improved platform for disease modeling *in vitro*. If properly quality controlled, ADSCs are an excellent cellular source for tissue engineering and reconstructive surgery applications, primarily because of the following ADSC properties: (1) they are able to differentiate into multiple lineages; (2) they secrete cytokines such as TGFβ, vascular endothelial growth factor (VEGF), granulocyte/macrophage colony-stimulating factor (GM-CSF), hepatocyte growth factor (HGF) and stromal derived factor 1 (SDF-1); (3) they are readily available and relatively straightforward to harvest and purify; and (4) they exhibit limited donor-site morbidity (Naderi et al., 2017). As such, ADSCs have been used in wound healing (Hong et al., 2013); angiogenesis and regeneration of several tissue types including: skin (Lu et al., 2012), muscle (Rodriguez et al., 2006), neural (Ghoreishian et al., 2013), adipose

(Ito et al., 2014), tendon Uysal., 2012) and cartilage (Oliveira et al., 2010); and in cosmetic reconstructive procedures.

My results have shown significant inherent differences in cellular metabolism (Chapter 2) and Wnt signaling cascades (Chapter 3), which were strongly associated with reduced differentiation potential of ADSCs from morbidly obese donors, suggesting that ADSCs used for regenerative and reconstructive purposes should be more stringently quality controlled and also indicating that obese ADSCs should not be utilized for regenerative medicine purposes.

Currently, MSCs are defined based on minimal criteria proposed by the Mesenchymal and Tissue Stem Cell Committee of the International Society for Cellular Therapy (ISCT) that includes: (1) adherence to normal cell-culture plasticware; (2) ≥ 95% surface expression for MSC markers, CD73, CD90 and CD105; and (3) ability to differentiate *in vitro* into adipogenic, chondrogenic and osteogenic lineages (Dominici et al., 2006; Bourin et al., 2013). Our results show, based on these ISCT criteria, that it was not possible to differentiate between age- and sex-matched healthy and obese ADSCs that we have profiled in this study. Similarly, others have found significant differences in the proliferation capacity in age- and sex-matched donor-derived MSCs, which were otherwise indistinguishable based on ISCT minimal criteria (Samsonraj et al., 2015). Together, this suggests that additional assessments including, quantification of differentiation potential, cellular metabolism, and proliferation, needs to be combined with existing ISCT minimum criteria, which will allow for a better determination of MSC effectiveness and quality prior to their use for therapeutic applications.

5.3 Identification of metabolic and transcriptional switches that can act as early markers for adipogenesis using a cellular model of morbid obesity

Studying changes in cellular metabolism throughout the time course of adipogenesis, by using healthy and obese cellular models, allowed me to identify metabolic triggers that do not initiate in obese cells during early stages of adipogenesis (days 1 - 3) in response to adipogenic stimuli. Hence, obese cells fail to follow the differentiation trajectory of healthy cells (Chapter 2). The obese cells retain a more primitive phenotype, with minimal insulin responsiveness and significantly reduced differentiation capacity, which may be, in part, responsible for promotion of an insulin resistant phenotype in an obese setting.

My analyses showed that initiation of mitochondrial gene networks and mitochondrial function is minimally activated in obese ADSCs during the early stages of adipogenesis (day 0-3). This indicates that oxidative phosphorylation-specific pathways, which have been suggested to be critical for specification of stem cells and for normal differentiation, are not triggered and are delayed in obese ADSCs, resulting in reduced activation of adipocyte regulatory networks and functional lipid metabolism. Collectively, the observed defects are indicative of an adipogenic differentiation blockade in obesity (Fig. 2). Overcoming this blockade and allowing obese cells to respond to metabolic stimuli would provide an alternative strategy for the treatment of obesity.

The transcriptomic and proteomic analyses not only showed that metabolic pathways, specifically mitochondrial metabolism, are not appropriately triggered in obese cells, but it also showed enrichment for canonical Wnt pathway genes in these cells (Fig. 2). Canonical Wnt signaling has been shown to negatively regulate the differentiation of MSCs towards adipocytes, while favoring differentiation towards osteogenic and myogenic lineages (Shang et al., 2007a;

Shang et al., 2007b; Bennett et al., 2002; Kang et al., 2007). I modulated Wnt/β-catenin signaling in healthy and obese cells during the course of adipogenesis by using both endogenous and small molecule ligands and antagonists and showed the negative consequences of dysregulated Wnt signaling on adipogenic differentiation potential and mitochondrial function (Chapter 3). The determination that prolonged Wnt signaling hinders adipogenesis and metabolic function of obese adipocytes offers the opportunity for the development of Wnt-targeted therapeutic approaches for obesity.

More studies on these metabolic and transcriptional signaling switches are critical, as they will provide a better understanding of how adipocyte development is affected by obesity. As such, the omics data we obtained for healthy and obese human adipogenesis provide the basis for further studies focusing on the requirement of stage-specific signaling pathways, such as the TGFβ, interleukin, and integrin signaling pathways, that are dysregulated in obese adipogenesis. Adipose tissue secretes a variety of adipokines, which play an important role in the manifestation of obesity-associated comorbidities. Secretion of adipokines with pro-inflammatory properties are overproduced with increasing adiposity, whereas secretion of some adipokines with anti-inflammatory or insulin sensitizing properties, like adiponectin, are decreased. These pro- and anti-inflammatory adipokines, which are differentially secreted depending on the degree of obesity, are being viewed as potential biomarkers indicative of pathophysiological obesity and its complications (Katsareli and Dedoussis, 2014).

My studies suggest that the transcriptome and proteome of developing adipocytes also offer the opportunity to identify potential molecular and metabolic markers of morbid obesity. Moreover, through my studies, I analyzed obese patient samples across overweight and different

groups of obesity, and it became evident that some overweight and obese group I and II patient derived ADSCs also exhibited hallmarks of mitochondrial dysfunction and reduced adipogenic capacity, while others within these groups did not exhibit these signs (Fig. 3B). This suggests that there may be a subset of overweight and obese class I and II patients that is more prone to becoming morbidly obese and insulin resistant. Hence, molecular and metabolic biomarkers could provide an alternative means to treat obesity and could provide a window towards implementation of preventative strategies for these patients.

5.4 Altered cellular metabolism governs impaired adipogenesis and insulin resistance in cellular models of obesity

In this thesis, by using ADSCs derived from subcutaneous adipose tissue of different individuals within a spectrum of BMI scores, I have shown a positive association between mitochondrial dysfunction and BMI at a cellular level. Morbidly obese individuals, with highest BMI scores, showed the greatest alterations in their mitochondrial function. Other reports have also shown a similar positive correlation between alterations in mitochondrial bioenergetics and BMI, however, by using primary adipocytes (Fischer et al., 2015) rather than isolated stem cell populations. Our results have shown a positive association between BMI and metabolic defects (Fig. 3) in adipose tissue-resident stem cells (ADSCs). We believe our model captures the inherent defects in the cellular energetics in these cells, as these defects are retained through *in vitro* culturing and passaging and only emerge upon induction of adipogenic differentiation.

Many studies, in humans and in animal models, have shown that subcutaneous adipose tissue in obesity is characterized by hypertrophic expansion of adipocytes, which leads to dysfunctional adipose tissue exhibiting increased tissue fibrosis, infiltration and activation of

inflammatory cells, aberrant adipokine secretion, and local and systemic insulin resistance (Hoffstedt et al., 2010; Andersson et al., 2014; Larson-Meyer et al., 2006; Cinti et al., 2005; Strissel et al., 2007).

Through my studies, I observed that obese cells exhibited hallmarks of insulin resistance. They failed to show a switch from IGF1R to INSR expression, which happens during early stages of adipogenic differentiation and is required for initiation of INSR-mediated insulin signaling and normal adipogenesis that we observed in our healthy ADSCs and which has also been reported for murine 3T3-L1 adipogenic differentiation (Smith et al., 1988). This suggests that obesity-associated insulin insensitivity defects are retained in obese ADSCs and contribute to their reduced adipogenic differentiation, which is an insulin signaling-dependent process.

There is fairly inconsistent evidence linking mitochondrial dysfunction to the development of insulin resistance and metabolic disorders. Some studies have shown a positive association between reduced expression of markers of mitochondrial function and insulin resistance (Heilbronn et al., 2007; Morino et al., 2005; Ritov et al., 2005), whereas others have reported no association between these processes (Holloway et al., 2007; Samocha-Bonet et al., 2012). However, the evidence is relatively more consistent at the cellular level in white adipose tissue, where mitochondrial number and function have been shown to be reduced in mouse models of obesity and diabetes, suggesting a positive correlation between mitochondrial dysfunction and insulin resistance in white adipose tissue (Wilson-Fritch et al., 2004; Choo et al., 2006; Gao et al., 2010). Similarly, our *in vitro* obesity model also exhibited indicators of an association between reduced mitochondrial biogenesis and function with insulin insensitivity during adipogenesis, which were not observed during healthy cell adipogenesis.

Another consequence of altered mitochondrial metabolism is excessive ROS generation and accumulation in cells. Although low physiological levels of ROS are required for adipogenic differentiation (Tormos et al., 2011; Drehmer et al., 2016), chronic ROS production has been shown to be an important contributor to the pathogenesis of obesity-associated insulin resistance (Wang et al., 2013; Houstis et al., 2006; Han, 2016). I observed that obese cells exhibited continuously elevated levels of ROS throughout the adipogenic time course compared to healthy cells, revealing another level of metabolic insult that potentially contributes to the differentiation and insulin sensitivity defects observed in obese cells (Fig. 2).

Some recent high impact studies have suggested the existence of distinct subpopulations of adipose stem and precursor cells within the stromal vascular fraction (SVF) obtained from subcutaneous and visceral adipose tissues, with significant differences in their adipogenic potential. Using single-cell transcriptomics, a unique population of LY6C+ PDGFRβ+ cells that display fibrogenic and functional pro-inflammatory phenotypes, and lack inherent adipogenic capacity, 'fibro-inflammatory progenitors' (FIPs), has been identified in the visceral adipose tissue of adult mice. LY6C- CD9- PDGFRβ+ cells that represent a distinct pool of highly adipogenic adipocyte precursor cells (APCs) has also been identified in the same model (Hepler et al., 2018). Similarly, functionally distinct subpopulations of stromal cells have also been identified in subcutaneous adipose tissue. Adipogenesis-regulatory cells (Aregs), characterized by high surface expression of CD142 are refractory to adipogenesis and have been shown to suppress adipocyte formation *in vivo* and *in vitro* in a paracrine manner. Interestingly, SVF obtained from obese mice showed significantly more Aregs than lean mice, in both the subcutaneous and the visceral adipose depots, and it was shown that Aregs control the formation of mature adipocytes *in vivo* (Schwalie

et al., 2018). This suggests that increased numbers of Aregs in obese adipose tissue potentially contribute to the reduced adipogenesis observed in the context of obesity.

Approaches aimed at increasing adipogenesis over adipocyte hypertrophy are now being considered as a means to treat obesity-associated metabolic complications. Studies on mouse models have suggested that healthy expansion of fat mass (adipogenesis) is associated with improved metabolic health. Transgenic expression of Tenomodulin, a protective adipose tissue factor, has been shown to promote preadipocyte proliferation, adipogenesis, adipose tissue health and insulin responsiveness *in vivo* in HFD-induced obese mice models (Senol-Cosar et al., 2016). Using gain-of-function and loss-of-function models for mitoNEET, a dimeric mitochondrial outer membrane protein, massive adipose tissue expansion through adipogenesis, coupled with upregulation of adiponectin production and release from adipocytes, has been reported in obese mice models wherein, despite of the resulting massive obesity, insulin sensitivity was shown to be preserved (Kusminski et al., 2012). Similarly, loss-of-function mice models of the protein phosphatase and tensin homologue (PTEN) were shown to gain more weight on both chow- and high-fat diet exposure. However, despite the increase in weight, they retained enhanced insulin sensitivity, and showed improvements in oral glucose tolerance tests, together with reduced adipose tissue inflammation and elevated adiponectin levels (Morley et al., 2015). Furthermore, a class of insulin-sensitizing drugs for the treatment of type 2 diabetes, called thiazolidinediones (TZDs) promote adipogenesis and hence stimulate healthy expansion of adipose tissue. TZDs exhibit potent insulin-sensitizing and antidiabetic effects through a ‘lipid steal’ mechanism, which is defined as a partitioning of circulating lipids into adipose tissue thereby providing a ‘safe haven’ to neutralize and store excess free fatty acids away from other more sensitive organs such as muscle

and liver (Ye at al., 2004; Semple et al., 2006). Taken together these studies suggest that increased adipogenesis during weight gain can offset the negative metabolic consequences of high fat exposure.

I was able to rescue the BMI-associated defects in adipogenesis I observed in obese cells by improving mitochondrial biogenesis and metabolism with a small molecule approach. I decided to use a small molecule approach, as it offered an advantage over knockdown/overexpression approaches in providing a proof-of-concept for pharmacological targeting and development of drug screening tools in our cellular model. Selectively targeting mitochondrial metabolism by using pharmacological compounds with known mode of action showed improvement of adipogenic defects, suggesting that cellular metabolism governs impaired adipogenesis and, potentially, insulin resistance in obese stem cells. Moreover, there are other pathways, such as the Wnt pathway that were also found to be dysregulated in the obese patient samples, which might provide an alternative target for treatments. It is clear from my studies that obesity is a complex disease with many factors and pathways affected. As such, treatment strategies may have to be tailored to a patient's specific metabolic and molecular profile. That is, obesity may require a personalized medicine approach for effective treatment.

5.5 Novel cellular bioenergetics-based drug screening strategies for improving adipogenesis and insulin resistance in obesity

My observations of a positive association between altered energy metabolism and reduced adipogenesis in obese ADSCs, together with the proof-of-concept data obtained by using small molecule mitochondrial function inducers that supported the idea that pharmacological

interventions could improve overall metabolic state and adipogenesis in obese cells (Chapter 2), established the foundation for a novel screening platform (Fig. 4).

I developed a mitochondrial function-based high throughput drug screening platform to identify compounds that promote adipogenesis and potentially improve insulin sensitivity in obese cells. The screen is based on measuring changes in the oxygen consumption rate (OCR), one of the most informative parameters for the assessment of mitochondrial status, in tandem with quantification of lipid accumulation. As both white and brown adipogenic processes are accompanied by increased mitochondrial function and activity, to distinguish whether "hits" identified in the screening assay promoted mitochondrial function accompanied with white and/or brown adipogenesis, I established a secondary screen for the "hits" to examine their "browning" potential in a brown adipocyte-specific functional assay (Chapter 4).

The screening method I developed provides a functional readout of improved metabolism and adipogenesis in obese cells and offers clear advantages over current screening methods based solely on image-based quantification of lipid droplets in murine 3T3-L1 preadipocytes or human MSCs (Lane et al., 2014; Foley et al., 2015). My approach uses obese ADSCs, which we have shown to possess inherent obesity-associated metabolic complications and, hence, serve as a disease model, which most closely mimics a bona fide obese environment when compared to the available *in vitro* models of obesity. My strategy also provides label-free and functional readouts of adipogenesis in contrast to fluorescent BODIPY- or ORO-stained image quantification methods that require lengthy staining and image analysis steps that yield reproducibility issues (Lane et al., 2014; Foley et al., 2015). My platform is also capable of identifying the "browning" potential of compounds, in addition to white adipogenesis, by evaluating functional metabolic parameters,

which is an improvement over current image lipid droplet imaging-based or UCP1 mRNA quantification-based browning assays that are tedious to perform in a high throughput manner and require high content image analyses (Moisan et al., 2015). Finally, my new drug-screening platform provides an economic advantage as it uses one third of the media, reagents, human growth factors, and cell numbers required by current 96-well cell-based screening methods, hence significantly reducing the cost associated with running a high throughput screen.

To my knowledge, this is the first drug-screening platform that provides functional activity readouts of adipogenesis in disease-specific (obese) cells in the primary screening assay. This approach is likely to reduce drug attrition rates in subsequent orthogonal and validation assays for lead compounds. Moreover, since this screening assay is based on measuring mitochondrial function in obese cells after their continuous exposure to test compounds throughout the adipogenic differentiation timeline of 14 days, "hits" coming from the primary screening assay are automatically screened for their mitochondrial liabilities as well, which is crucial for avoiding late-stage attrition during drug development of new chemical entities (Dykens et al., 2007).

5.6 Concluding Remarks

In vitro adipogenesis was first reported using murine 3T3-L1 preadipocytes almost forty years ago (Green and Meuth, 1974), and subsequent studies have reported development of several additional murine and human *in vitro* models for studying adipogenesis. Most attention has been focused on elucidation of transcriptional networks and signaling events controlling early and late stages of adipogenesis. Very few studies have attempted to study the role of cellular metabolism in this critical process, primarily because of the unavailability of sensitive methods to study cellular bioenergetics until recently. To address this deficiency, I have reported a comprehensive functional

metabolic profile of human adipogenesis, together with transcriptomic and proteomic datasets capturing early and late stages of differentiation, which indicate that cellular bioenergetics can drive adipogenic differentiation of healthy ADSCs.

I developed a robust cellular model for studying obesity *in vitro*, and using this model, I identified differences in metabolic and signaling cascades at very early stages of adipogenic differentiation that contribute to defects in adipogenesis observed in obesity. My results show that obese ADSCs retain obesity-associated metabolic derangements, which emerge as the cells differentiate and result in impaired adipogenesis. I also conducted experiments that support the possibility of rescuing adipogenic defects in obese cells through small molecule-mediated improvements in cellular metabolic health. Taken together, my results demonstrate that cellular metabolic defects drive alterations in stem cell function, particularly in their adipogenic differentiation potential in an obese setting.

Lastly, I used metabolically impaired obese ADSCs to develop a novel high-throughput drug screening platform to identify small molecule compounds that can improve obese ADSC energy metabolism and, hence, adipogenesis. I also established an additional functional high-throughput secondary assay to identify browning adipogenesis inducing activity for potential 'hits'. Taken together, the results reported in this thesis provide novel insights into the druggable unique pathways that govern adipogenesis in the context of obesity.

5.7 Future Directions

While my studies have provided novel insight into cellular metabolism dynamics and their potential as therapeutic targets for human obesity, there are some avenues available for this work to be improved upon and continued. My studies show that not all obese ADSCs have the potential

to give rise to adipocytes, This suggests the existence of heterogeneous populations within harvested obese cells, where there is the possibility that one or more sub-populations lack adipogenic differentiation potential altogether, while others may be completely free of any defects in their adipogenic potential. Identification and segregation of these adipogenic and non-adipogenic sub-populations from obese ADSCs would permit further confirmation of the association between cellular metabolism and adipogenesis defects by allowing direct comparisons between sub-populations obtained from the same tissue source. More importantly, studying the functional activity of the adipocytes obtained from adipogenic obese sub-populations would allow for an improved understanding of the similarities between obese and healthy adipocytes in an *in vitro* setting.

Further, identification and molecular analysis of different sub-populations within isolated ADSCs would more provide a more definitive answer to another important question in the MSC field, whether all cells have the same multilineage differentiation potential towards all three lineages, namely, adipocytes, chondrocytes and osteocytes.

Moreover, I have developed and validated a primary drug screening strategy using obese ADSCs along with a secondary assay for the identified "hits," and the platform is ready for running an actual high throughput drug screen using either FDA approved structurally diverse drug libraries like PRESTWICK™, DiscoveryProbe™, ChemBridge™ or LOPAC™; or structure–activity relationship (SAR)-based novel compound synthesis approaches.

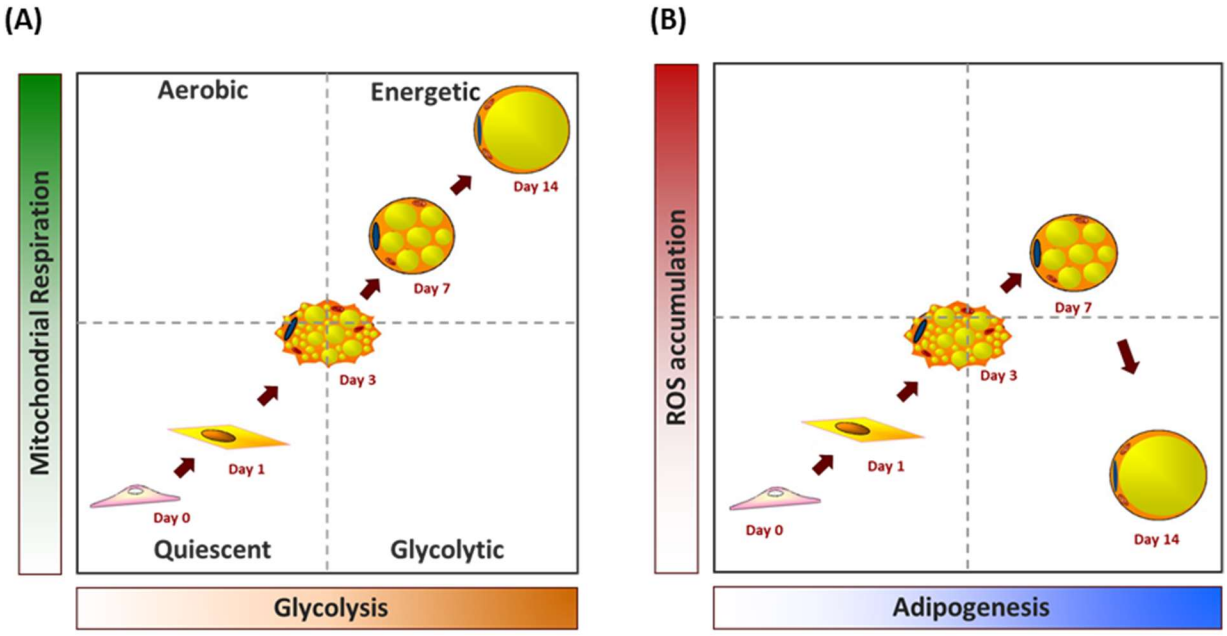

Fig. 1: Energy map of healthy human adipogenesis. (A) Healthy ADSCs show gradual upregulation in glycolysis and mitochondrial respiration along the course of adipogenic differentiation resulting in highly energetic mature adipocytes. **(B)** ROS have been shown to be required for adipogenesis. The healthy differentiation exhibits dynamic changes in the ROS levels where there is gradual increase in ROS generation and accumulation until day 7 followed by a decline in ROS levels. This suggests that ROS are required for normal adipogenesis during early stages and is not required for maturation of adipocytes.

Fig. 2: Healthy and obese cells show distinct signaling and metabolic cascades during the course of adipogenesis.

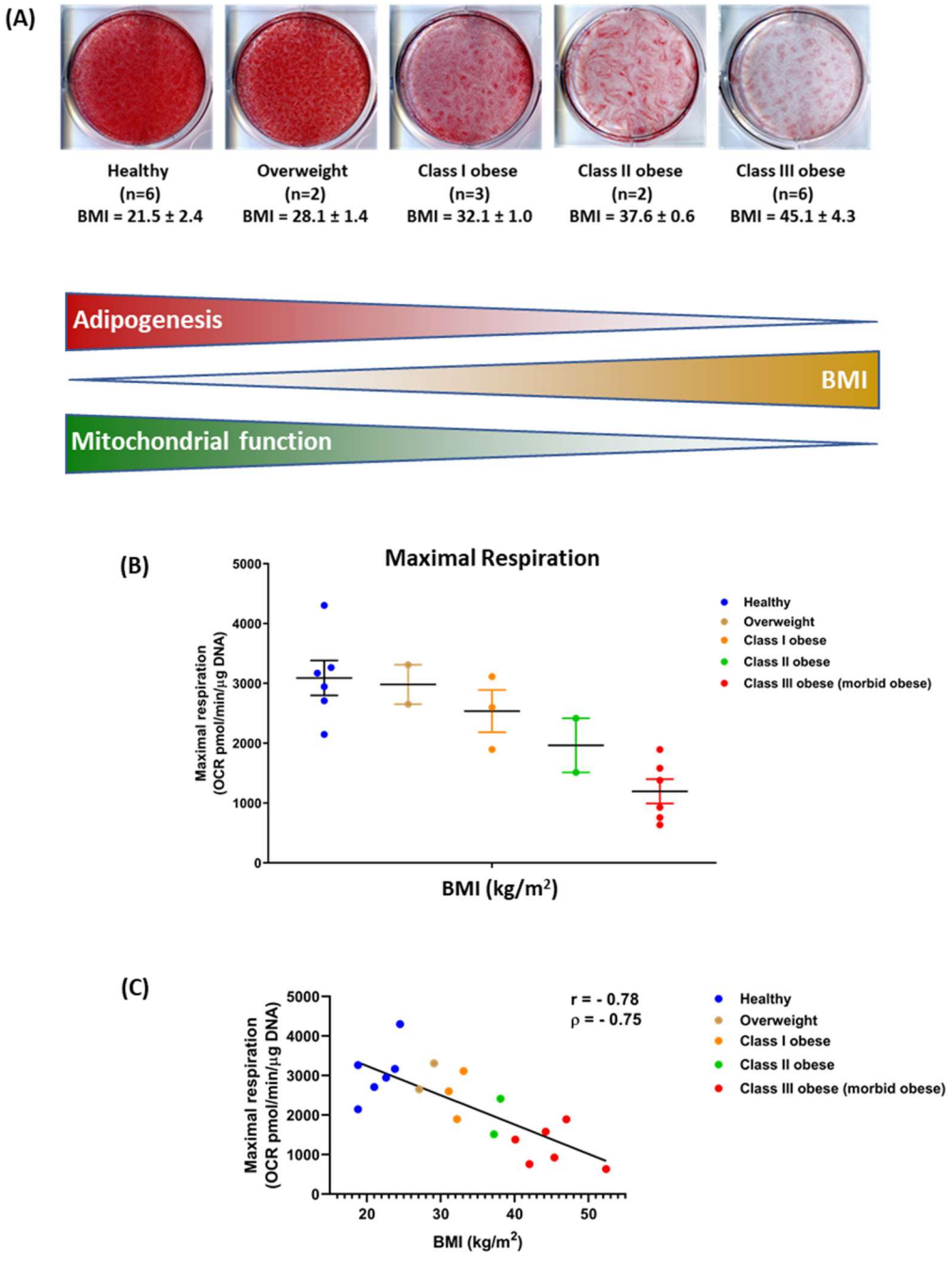

Fig. 3: BMI negatively correlates with mitochondrial activity and the adipogenic potential in ADSCs.

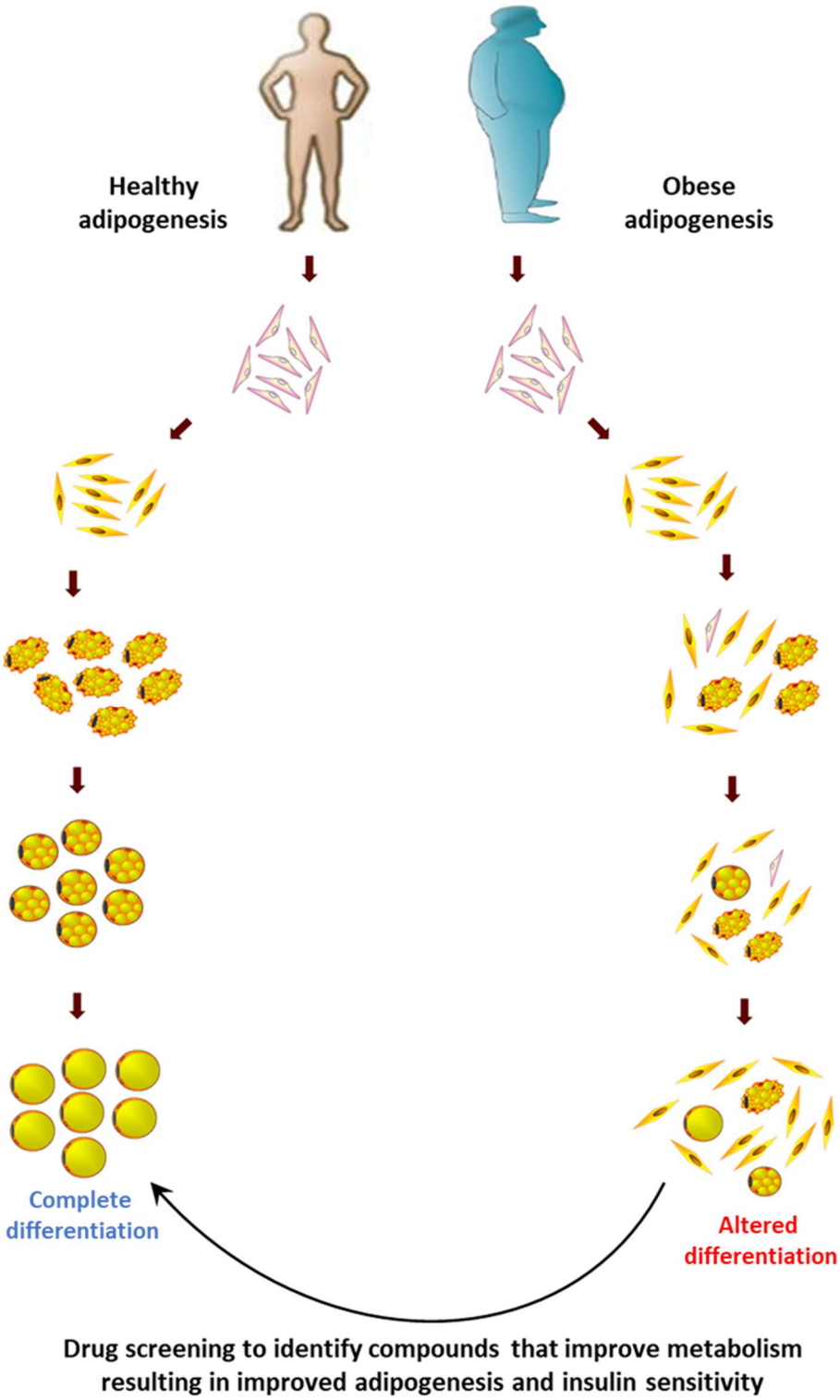
Healthy adipogenesis
Obese adipogenesis
Complete differentiation
Altered differentiation
Drug screening to identify compounds that improve metabolism resulting in improved adipogenesis and insulin sensitivity

Fig. 4: Principle for developing drug screening platforms using obese ADSCs. Adipogenesis is significantly reduced in obesity and the ADSCs isolated from morbid obese patients inherently retain these alterations and hence provide an ideal model system for developing drug screening platforms aimed at identifying compounds that could promote metabolic health and adipogenesis in the context of obesity.

BIBLIOGRAPHY

Accili, D., and Taylor, S. I. (1991). Targeted inactivation of the insulin receptor gene in mouse 3T3-L1 fibroblasts via homologous recombination. Proceedings of the National Academy of Sciences of the United States of America *88,* 4708-4712.

Aksu, A. E., Rubin, J. P., Dudas, J. R., and Marra, K. G. (2008). Role of gender and anatomical region on induction of osteogenic differentiation of human adipose-derived stem cells. Annals of plastic surgery *60,* 306-322.

Ailhaud, G., Amri, E., Cermolacce, C., Djian, P., Forest, C., Gaillard, D., Grimaldi, P., Khoo, J., Negrel, R., and Serrero-Dave, G. (). Hormonal requirements for growth and differentiation of ob17 preadipocyte cells in vitro. Diabete & metabolisme *9,* 125–133.

Alkhouri, N., Gornicka, A., Berk, M. P., Thapaliya, S., Dixon, L. J., Kashyap, S., Schauer, P. R., and Feldstein, A. E. (2009). Adipocyte apoptosis, a link between obesity, insulin resistance, and hepatic steatosis. The Journal of biological chemistry *285,* 3428-3438.

Alt, E. U., Senst, C., Murthy, S. N., Slakey, D. P., Dupin, C. L., Chaffin, A. E., Kadowitz, P. J., and Izadpanah, R. (2011). Aging alters tissue resident mesenchymal stem cell properties. Stem cell research *8,* 215-225.

Andersen, E., Ingerslev, L. R., Fabre, O., Donkin, I., Altintas, A., Versteyhe, S., Bisgaard, T., Kristiansen, V. B., Simar, D., and Barres, R. (2018). Preadipocytes from obese humans with type 2 diabetes are epigenetically reprogrammed at genes controlling adipose tissue function. International journal of obesity *43,* 306-318.

Andersson, D. P., Eriksson Hogling, D., Thorell, A., Toft, E., Qvisth, V., Naslund, E., Thorne, A., Wiren, M., Lofgren, P., Hoffstedt, J., Dahlman, I., Mejhert, N., Ryden, M., Arner, E., and Arner, P. (2014). Changes in subcutaneous fat cell volume and insulin sensitivity after weight loss. Diabetes care *37,* 1831-1836.

Anis, A. H., Zhang, W., Bansback, N., Guh, D. P., Amarsi, Z., and Birmingham, C. L. (2009). Obesity and overweight in Canada: an updated cost-of-illness study. Obesity reviews: an official journal of the International Association for the Study of Obesity *11,* 31-40.

Apovian, C. M., Aronne, L. J., Bessesen, D. H., McDonnell, M. E., Murad, M. H., Pagotto, U., Ryan, D. H., Still, C. D., and, . (2015). Pharmacological management of obesity: an endocrine Society clinical practice guideline. The Journal of clinical endocrinology and metabolism *100,* 342-362.

Arner, P. (1997). Regional adipocity in man. The Journal of endocrinology *155,*191-192.

Asin-Cayuela, J., and Gustafsson, C. M. (2007). Mitochondrial transcription and its regulation in mammalian cells. Trends in biochemical sciences *32,* 111-117.

Bach, D., Pich, S., Soriano, F. X., Vega, N., Baumgartner, B., Oriola, J., Daugaard, J. R., Lloberas, J., Camps, M., Zierath, J. R., Rabasa-Lhoret, R., Wallberg-Henriksson, H., Laville, M., Palacin, M., Vidal, H., Rivera, F., Brand, M., and Zorzano, A. (2003). Mitofusin-2 determines mitochondrial network architecture and mitochondrial metabolism. A novel regulatory mechanism altered in obesity. The Journal of biological chemistry *278,* 17190-17197.

Banerjee, S. S., Feinberg, M. W., Watanabe, M., Gray, S., Haspel, R. L., Denkinger, D. J., Kawahara, R., Hauner, H., and Jain, M. K. (2002). The Kruppel-like factor KLF2 inhibits peroxisome proliferator-activated receptor-gamma expression and adipogenesis. The Journal of biological chemistry *278,* 2581-2584.

Bartelt, A., and Heeren, J. (2013). Adipose tissue browning and metabolic health. Nature reviews. Endocrinology *10,* 24-36.

Beegle, J., Lakatos, K., Kalomoiris, S., Stewart, H., Isseroff, R. R., Nolta, J. A., and Fierro, F. A. (2015). Hypoxic preconditioning of mesenchymal stromal cells induces metabolic changes, enhances survival, and promotes cell retention in vivo. Stem cells (Dayton, Ohio) *33,* 1818-1828.

Bennett, C. N., Longo, K. A., Wright, W. S., Suva, L. J., Lane, T. F., Hankenson, K. D., and MacDougald, O. A. (2005). Regulation of osteoblastogenesis and bone mass by Wnt10b. Proceedings of the National Academy of Sciences of the United States of America *102,* 3324-3329.

Bennett, C. N., Ross, S. E., Longo, K. A., Bajnok, L., Hemati, N., Johnson, K. W., Harrison, S. D., and MacDougald, O. A. (2002). Regulation of Wnt signaling during adipogenesis. The Journal of biological chemistry *277,* 30998-31004.

Bhaskaran, K., Douglas, I., Forbes, H., dos-Santos-Silva, I., Leon, D. A., and Smeeth, L. (2014). Body-mass index and risk of 22 specific cancers: a population-based cohort study of 5·24 million UK adults. Lancet (London, England) *384,* 755-765.

Birsoy, K., Chen, Z., and Friedman, J. (2008). Transcriptional regulation of adipogenesis by KLF4. Cell metabolism *7,* 339-347.

Bjorndal, B., Burri, L., Staalesen, V., Skorve, J., and Berge, R. K. (2011). Different adipose depots: their role in the development of metabolic syndrome and mitochondrial response to hypolipidemic agents. Journal of obesity *2011, 490650*.

Bluher, M. (2013). Adipose tissue dysfunction contributes to obesity related metabolic diseases. Best practice & research. Clinical endocrinology & metabolism *27,* 163-177.

Bohan, A. E., Purvis, K. N., Bartosh, J. L., and Brandebourg, T. D. (2014). The proliferation and differentiation of primary pig preadipocytes is suppressed when cultures are incubated at 37°Celsius compared to euthermic conditions in pigs. Adipocyte *3,* 322-332.

Boucher, J., Softic, S., El Ouaamari, A., Krumpoch, M. T., Kleinridders, A., Kulkarni, R. N., O'Neill, B. T., and Kahn, C. R. (2016). Differential Roles of Insulin and IGF-1 Receptors in Adipose Tissue Development and Function. Diabetes *65,* 2201-2213.

Boudina, S., and Graham, T. E. (2014). Mitochondrial function/dysfunction in white adipose tissue. Experimental physiology *99,* 1168-1178.

Bourin, P., Bunnell, B. A., Casteilla, L., Dominici, M., Katz, A. J., March, K. L., Redl, H., Rubin, J. P., Yoshimura, K., and Gimble, J. M. (2013). Stromal cells from the adipose tissue-derived stromal vascular fraction and culture expanded adipose tissue-derived stromal/stem cells: a joint statement of the International Federation for Adipose Therapeutics and Science (IFATS) and the International Society for Cellular Therapy (ISCT). Cytotherapy *15,* 641-648.

Bowers, R. R., and Lane, M. D. (2007). A role for bone morphogenetic protein-4 in adipocyte development. Cell cycle (Georgetown, Tex.) *6,* 385-389.

Brashier, D. B., Sharma, A. K., Dahiya, N., Singh, S. K., and Khadka, A. (2014). Lorcaserin: A novel antiobesity drug. Journal of pharmacology & pharmacotherapeutics *5,* 175178.

Brunet, A., Sweeney, L. B., Sturgill, J. F., Chua, K. F., Greer, P. L., Lin, Y., Tran, H., Ross, S. E., Mostoslavsky, R., Cohen, H. Y., Hu, L. S., Cheng, H. L., Jedrychowski, M. P., Gygi, S. P., Sinclair, D. A., Alt, F. W., and Greenberg, M. E. (2004). Stress-dependent regulation of FOXO transcription factors by the SIRT1 deacetylase. Science (New York, N.Y.) *303,* 2011-2015.

Buechling, T., and Boutros, M. (2011). Wnt signaling signaling at and above the receptor level. Current topics in developmental biology *97,* 21-53.

Bunnell, B. A., Flaat, M., Gagliardi, C., Patel, B., and Ripoll, C. (2008). Adipose-derived stem cells: isolation, expansion and differentiation. Methods (San Diego, Calif.) *45,* 115-120.

Calvo-Garrido, J., Maffezzini, C., Schober, F. A., Clemente, P., Uhlin, E., Kele, M., Stranneheim, H., Lesko, N., Bruhn, H., Svenningsson, P., Falk, A., Wedell, A., Freyer, C., and Wredenberg, A. (2019). SQSTM1/p62-Directed Metabolic Reprogramming Is Essential for Normal Neurodifferentiation. Stem cell reports *12,* 696-711.

Calzadilla, P., Sapochnik, D., Cosentino, S., Diz, V., Dicelio, L., Calvo, J. C., and Guerra, L. N. (2011). N-acetylcysteine reduces markers of differentiation in 3T3-L1 adipocytes. International journal of molecular sciences *12,* 6936-6951.

Canadian Obesity Network-Réseau canadien en obésité. (2017). Report Card on Access to Obesity Treatment for Adults in Canada 2017. Edmonton, AB: Canadian Obesity Network Inc.; 2017, April.

Cao, Y. (2013). Angiogenesis and vascular functions in modulation of obesity, adipose metabolism, and insulin sensitivity. Cell metabolism *18,* 478-489.

Cao, Z., Umek, R. M., and McKnight, S. L. (1991). Regulated expression of three C/EBP isoforms during adipose conversion of 3T3-L1 cells. Genes & development *5,* 1538-1552.

Capurso, C., and Capurso, A. (2012). From excess adiposity to insulin resistance: the role of free fatty acids. Vascular pharmacology *57,* 91–97.

Carriere, A., Carmona, M. C., Fernandez, Y., Rigoulet, M., Wenger, R. H., Penicaud, L., and Casteilla, L. (2004). Mitochondrial reactive oxygen species control the transcription factor CHOP-10/GADD153 and adipocyte differentiation: a mechanism for hypoxia-dependent effect. The Journal of biological chemistry *279,* 40462-40469.

Carriere, A., Fernandez, Y., Rigoulet, M., Penicaud, L., and Casteilla, L. (2003). Inhibition of preadipocyte proliferation by mitochondrial reactive oxygen species. FEBS letters *550,* 163-167.

Castro, J. P., Grune, T., and Speckmann, B. (2016). The two faces of reactive oxygen species (ROS) in adipocyte function and dysfunction. Biological chemistry *397,* 709-724.

Cawthorn, W. P., Scheller, E. L., and MacDougald, O. A. (2011). Adipose tissue stem cells meet preadipocyte commitment: going back to the future. Journal of lipid research *53,* 227-246.

Chan, D. C. (2006). Mitochondrial fusion and fission in mammals. Annual review of cell and developmental biology *22,* 79-99.

Chattopadhyay, M., Guhathakurta, I., Behera, P., Ranjan, K. R., Khanna, M., Mukhopadhyay, S., and Chakrabarti, S. (2011). Mitochondrial bioenergetics is not impaired in nonobese subjects with type 2 diabetes mellitus. Metabolism: clinical and experimental *60,* 1702-1710.

Chen, C. T., Shih, Y. R., Kuo, T. K., Lee, O. K., and Wei, Y. H. (2008). Coordinated changes of mitochondrial biogenesis and antioxidant enzymes during osteogenic differentiation of human mesenchymal stem cells. Stem cells (Dayton, Ohio) *26,* 960-968.

Cho, Y. M., Kwon, S., Pak, Y. K., Seol, H. W., Choi, Y. M., Park, D. J., Park, K. S., and Lee, H. K. (2006). Dynamic changes in mitochondrial biogenesis and antioxidant enzymes during the spontaneous differentiation of human embryonic stem cells. Biochemical and biophysical research communications *348,* 1472-1478.

Choban, P. S., Jackson, B., Poplawski, S., and Bistolarides, P. (2002). Bariatric surgery for morbid obesity: why, who, when, how, where, and then what? Cleveland Clinic journal of medicine *69,* 897-903.

Choo, H. J., Kim, J. H., Kwon, O. B., Lee, C. S., Mun, J. Y., Han, S. S., Yoon, Y. S., Yoon, G., Choi, K. M., and Ko, Y. G. (2006). Mitochondria are impaired in the adipocytes of type 2 diabetic mice. Diabetologia *49,* 784-791.

Choudhery, M. S., Badowski, M., Muise, A., Pierce, J., and Harris, D. T. (2014). Donor age negatively impacts adipose tissue-derived mesenchymal stem cell expansion and differentiation. Journal of translational medicine *12,* 8.

Choy, L., Skillington, J., and Derynck, R. (2000). Roles of autocrine TGF-beta receptor and Smad signaling in adipocyte differentiation. The Journal of cell biology *149,* 667-682.

Christodoulides, C., Laudes, M., Cawthorn, W. P., Schinner, S., Soos, M., O'Rahilly, S., Sethi, J. K., and Vidal-Puig, A. (2006). The Wnt antagonist Dickkopf-1 and its receptors are coordinately regulated during early human adipogenesis. Journal of cell science *119,* 2613-2620.

Chung, S., Dzeja, P. P., Faustino, R. S., Perez-Terzic, C., Behfar, A., and Terzic, A. (2007). Mitochondrial oxidative metabolism is required for the cardiac differentiation of stem cells. Nature clinical practice. Cardiovascular medicine *4,* S60-S67.

Church, C., Brown, M., and Rodeheffer, M. S. (2015). Conditional immortalization of primary adipocyte precursor cells. Adipocyte *4,* 203-211.

Cinti, S., Mitchell, G., Barbatelli, G., Murano, I., Ceresi, E., Faloia, E., Wang, S., Fortier, M., Greenberg, A. S., and Obin, M. S. (2005). Adipocyte death defines macrophage localization and function in adipose tissue of obese mice and humans. Journal of lipid research *46,* 2347-2355.

Cipolat, S., Martins de Brito, O., Dal Zilio, B., and Scorrano, L. (2004). OPA1 requires mitofusin 1 to promote mitochondrial fusion. Proceedings of the National Academy of Sciences of the United States of America *101,* 15927-15932.

Cornelius, P., MacDougald, O. A., and Lane, M. D. (1994). Regulation of adipocyte development. *Annual review of nutrition 14,* 99-129.

Costello, L. C., and Franklin, R. B. (2013). A review of the important central role of altered citrate metabolism during the process of stem cell differentiation. Journal of regenerative medicine & tissue engineering *2,* 1.

Cummins, T. D., Holden, C. R., Sansbury, B. E., Gibb, A. A., Shah, J., Zafar, N., Tang, Y., Hellmann, J., Rai, S. N., Spite, M., Bhatnagar, A., and Hill, B. G. (2014). Metabolic remodeling of white adipose tissue in obesity. American journal of physiology. Endocrinology and metabolism *307,* E262-77.

Dahlman, I., Forsgren, M., Sjogren, A., Nordstrom, E. A., Kaaman, M., Naslund, E., Attersand, A., and Arner, P. (2006). Downregulation of electron transport chain genes in visceral adipose tissue in type 2 diabetes independent of obesity and possibly involving tumor necrosis factor-alpha. Diabetes *55,* 1792-1799.

Darimont, C., and Mace, K. (2003). Immortalization of human preadipocytes. Biochimie *85,* 1231-1233.

de Girolamo, L., Lopa, S., Arrigoni, E., Sartori, M. F., Baruffaldi Preis, F. W., and Brini, A. T. (2009). Human adipose-derived stem cells isolated from young and elderly women: their differentiation potential and scaffold interaction during in vitro osteoblastic differentiation. Cytotherapy *11,* 793-803.

De Pauw, A., Tejerina, S., Raes, M., Keijer, J., and Arnould, T. (2009). Mitochondrial (dys)function in adipocyte (de)differentiation and systemic metabolic alterations. The American journal of pathology *175,* 927-939.

Di Taranto, G., Cicione, C., Visconti, G., Isgro, M. A., Barba, M., Di Stasio, E., Stigliano, E., Bernardini, C., Michetti, F., Salgarello, M., and Lattanzi, W. (2015). Qualitative and quantitative differences of adipose-derived stromal cells from superficial and deep subcutaneous lipoaspirates: a matter of fat. Cytotherapy *17,* 1076-1089.

Ding, W. X., and Yin, X. M. (2012). Mitophagy: mechanisms, pathophysiological roles, and analysis. Biological chemistry *393,* 547-564.

Distel, R. J., Ro, H. S., Rosen, B. S., Groves, D. L., and Spiegelman, B. M. (1987). Nucleoprotein complexes that regulate gene expression in adipocyte differentiation: direct participation of c-fos. Cell *49,* 835-844.

Doan-Xuan, Q. M., Sarvari, A. K., Fischer-Posovszky, P., Wabitsch, M., Balajthy, Z., Fesus, L., and Bacso, Z. (2013). High content analysis of differentiation and cell death in human adipocytes. Cytometry. Part A: the journal of the International Society for Analytical Cytology *83,* 933–943.

Dominici, M., Le Blanc, K., Mueller, I., Slaper-Cortenbach, I., Marini, F., Krause, D., Deans, R., Keating, A., Prockop, D. j., and Horwitz, E. (2006). Minimal criteria for defining multipotent mesenchymal stromal cells. The International Society for Cellular Therapy position statement. Cytotherapy *8,*315-317.

Dos Santos, F., Andrade, P. Z., Boura, J. S., Abecasis, M. M., da Silva, C. L., and Cabral, J. M. (2010). Ex vivo expansion of human mesenchymal stem cells: a more effective cell proliferation kinetics and metabolism under hypoxia. Journal of cellular physiology *223,* 27-35.

Dowell, P., Otto, T. C., Adi, S., and Lane, M. D. (2003). Convergence of peroxisome proliferator-activated receptor gamma and Foxo1 signaling pathways. The Journal of biological chemistry *278,* 45485-45491.

Drehmer, D. L., de Aguiar, A. M., Brandt, A. P., Petiz, L., Cadena, S. M., Rebelatto, C. K., Brofman, P. R., Filipak Neto, F., Dallagiovanna, B., and Abud, A. P. (2016). Metabolic switches during the first steps of adipogenic stem cells differentiation. Stem cell research *17,* 413-421.

Ducluzeau, P. H., Priou, M., Weitheimer, M., Flamment, M., Duluc, L., Iacobazi, F., Soleti, R., Simard, G., Durand, A., Rieusset, J., Andriantsitohaina, R., and Malthiery, Y. (2011). Dynamic regulation of mitochondrial network and oxidative functions during 3T3-L1 fat cell differentiation. Journal of physiology and biochemistry *67,* 285-296.

Dykens, J. A., Marroquin, L. D., and Will, Y. (2007). Strategies to reduce late-stage drug attrition due to mitochondrial toxicity. Expert review of molecular diagnostics *7,* 161-175.

Ernster, L., and Schatz, G. (1981). Mitochondria: a historical review. The Journal of cell biology *91,* 227s-255s.

Fajas, L., Auboeuf, D., Raspe, E., Schoonjans, K., Lefebvre, A. M., Saladin, R., Najib, J., Laville, M., Fruchart, J. C., Deeb, S., Vidal-Puig, A., Flier, J., Briggs, M. R., Staels, B., Vidal, H., and Auwerx, J. (1997). The organization, promoter analysis, and expression of the human PPARgamma gene. The Journal of biological chemistry *272,* 18779-18789.

Falkenberg, M., Larsson, N. G., and Gustafsson, C. M. (2007). DNA replication and transcription in mammalian mitochondria. Annual review of biochemistry *76,* 679-699.

Faustini, M., Bucco, M., Chlapanidas, T., Lucconi, G., Marazzi, M., Tosca, M. C., Gaetani, P., Klinger, M., Villani, S., Ferretti, V. V., Vigo, D., and Torre, M. L. (2010). Nonexpanded mesenchymal stem cells for regenerative medicine: yield in stromal vascular fraction from adipose tissues. Tissue engineering. Part C, Methods *16,* 1515-1521.

Fei, Z., Bera, T. K., Liu, X., Xiang, L., and Pastan, I. (2011). Ankrd26 gene disruption enhances adipogenesis of mouse embryonic fibroblasts. The Journal of biological chemistry *286,* 27761-27768.

Fischer, B., Schottl, T., Schempp, C., Fromme, T., Hauner, H., Klingenspor, M., and Skurk, T. (2015). Inverse relationship between body mass index and mitochondrial oxidative phosphorylation capacity in human subcutaneous adipocytes. American journal of physiology. Endocrinology and metabolism *309,* E380-7.

Fischer-Posovszky, P., Newell, F. S., Wabitsch, M., & Tornqvist, H. E. (2008). Human SGBS cells - a unique tool for studies of human fat cell biology. Obesity facts *1,* 184-189.

Flachs, P., Horakova, O., Brauner, P., Rossmeisl, M., Pecina, P., Franssen-van Hal, N., Ruzickova, J., Sponarova, J., Drahota, Z., Vlcek, C., Keijer, J., Houstek, J., and Kopecky, J. (2005). Polyunsaturated fatty acids of marine origin upregulate mitochondrial biogenesis and induce beta-oxidation in white fat. Diabetologia *48,* 2365-2375.

Floyd, Z. E., and Stephens, J. M. (2003). STAT5A promotes adipogenesis in nonprecursor cells and associates with the glucocorticoid receptor during adipocyte differentiation. Diabetes *52,* 308-314.

Foley, B., Clewell, R. and Deisenroth, C. (2015). Development of a Human Adipose-Derived Stem Cell Model for Characterization of Chemical Modulation of Adipogenesis. Applied in vitro Toxicology *1,* 66-78.

Fontana, L., Eagon, J. C., Trujillo, M. E., Scherer, P. E., and Klein, S. (2007). Visceral fat adipokine secretion is associated with systemic inflammation in obese humans. Diabetes *56,* 1010-1013.

Freytag, S. O., Paielli, D. L., and Gilbert, J. D. (1994). Ectopic expression of the CCAAT/enhancer-binding protein alpha promotes the adipogenic program in a variety of mouse fibroblastic cells. Genes & development *8,* 1654-1663.

Fruhbeck, G. (2008). Overview of adipose tissue and its role in obesity and metabolic disorders. Methods in molecular biology (Clifton, N.J.) *456,* 1-22.

Gagnon, A., Chen, C. S., and Sorisky, A. (1999). Activation of protein kinase B and induction of adipogenesis by insulin in 3T3-L1 preadipocytes: contribution of phosphoinositide-3,4,5-trisphosphate versus phosphoinositide-3,4-bisphosphate. Diabetes *48,* 691-698.

Gao, C. L., Zhu, C., Zhao, Y. P., Chen, X. H., Ji, C. B., Zhang, C. M., Zhu, J. G., Xia, Z. K., Tong, M. L., and Guo, X. R. (2010). Mitochondrial dysfunction is induced by high levels of glucose and free fatty acids in 3T3-L1 adipocytes. Molecular and cellular endocrinology *320,* 25-33.

Garfield, A. S. (2010). Derivation of primary mouse embryonic fibroblast (PMEF) cultures. Methods in molecular biology (Clifton, N.J.) *633,* 19-27.

Ghaben, A. L., and Scherer, P. E. (2019). Adipogenesis and metabolic health. Nature reviews. Molecular cell biology *20,* 242-258.

Ghoreishian, M., Rezaei, M., Beni, B. H., Javanmard, S. H., Attar, B. M., and Zalzali, H. (2012). Facial nerve repair with Gore-Tex tube and adipose-derived stem cells: an animal study in dogs. Journal of oral and maxillofacial surgery: official journal of the American Association of Oral and Maxillofacial Surgeons *71,* 577-587.

Giralt, M., and Villarroya, F. (2013). White, brown, beige/brite: different adipose cells for different functions? Endocrinology *154,* 2992-3000.

Global Burden of Disease study GBD Obes. Collab., Afshin, A., Forouzanfar, M. H., Reitsma, M. B., Sur, P., Estep, K., Lee, A., Marczak, L., Mokdad, A. H., Moradi-Lakeh, M., Naghavi, M., Salama, J. S., Vos, T., Abate, K. H., Abbafati, C., Ahmed, M. B., Al-Aly, Z., Alkerwi, A., Al-Raddadi, R., Amare, A. T., Amberbir, A., Amegah, A. K., Amini, E., Amrock, S. M., Anjana, R. M., Arnlov, J., Asayesh, H., Banerjee, A., Barac, A., Baye, E., Bennett, D. A., Beyene, A. S., Biadgilign, S., Biryukov, S., Bjertness, E., Boneya, D. J., Campos-Nonato, I., Carrero, J. J., Cecilio, P., Cercy, K., Ciobanu, L. G., Cornaby, L., Damtew, S. A., Dandona, L., Dandona, R., Dharmaratne, S. D., Duncan, B. B., Eshrati, B., Esteghamati, A., Feigin, V. L., Fernandes, J. C., FÃ¼rst, T., Gebrehiwot, T. T., Gold, A., Gona, P. N., Goto, A., Habtewold, T. D., Hadush, K. T., Hafezi-Nejad, N., Hay, S. I., Horino, M., Islami, F., Kamal, R., Kasaeian, A., Katikireddi, S. V., Kengne, A. P., Kesavachandran, C. N., Khader, Y. S., Khang, Y. H., Khubchandani, J., Kim, D., Kim, Y. J., Kinfu, Y., Kosen, S., Ku, T., Defo, B. K., Kumar, G. A., Larson, H. J., Leinsalu, M., Liang, X., Lim, S. S., Liu, P., Lopez, A. D., Lozano, R., Majeed, A., Malekzadeh, R., Malta, D. C., Mazidi, M., McAlinden, C., McGarvey, S. T., Mengistu, D. T., Mensah, G. A., Mensink, G. B. M., Mezgebe, H. B., Mirrakhimov, E. M., Mueller, U. O., Noubiap, J. J., Obermeyer, C. M., Ogbo, F. A., Owolabi, M. O., Patton, G. C., Pourmalek, F., Qorbani, M., Rafay, A., Rai, R. K., Ranabhat, C. L., Reinig, N., Safiri, S., Salomon, J. A., Sanabria, J. R., Santos, I. S., Sartorius, B., Sawhney, M., Schmidhuber, J., Schutte, A. E., Schmidt, M. I., Sepanlou, S. G., Shamsizadeh, M., Sheikhbahaei, S., Shin, M. J., Shiri, R., Shiue, I., Roba, H. S., Silva, D. A. S., Silverberg, J. I., Singh, J. A., Stranges, S., Swaminathan, S., Tabares-Seisdedos, R., Tadese, F., Tedla, B. A.,

Tegegne, B. S., Terkawi, A. S., Thakur, J. S., Tonelli, M., Topor-Madry, R., Tyrovolas, S., Ukwaja, K. N., Uthman, O. A., Vaezghasemi, M., Vasankari, T., Vlassov, V. V., Vollset, S. E., Weiderpass, E., Werdecker, A., Wesana, J., Westerman, R., Yano, Y., Yonemoto, N., Yonga, G., Zaidi, Z., Zenebe, Z. M., Zipkin, B., and Murray, C. J. L. (2017). Health Effects of Overweight and Obesity in 195 Countries over 25 Years. The New England journal of medicine *377,* 13-27.

Goldenthal, M. J., and Marin-Garcia, J. (2004). Mitochondrial signaling pathways: a receiver/integrator organelle. Molecular and cellular biochemistry *262,* 1-16.

Gomes, L. C., Di Benedetto, G., and Scorrano, L. (2011). During autophagy mitochondria elongate, are spared from degradation and sustain cell viability. Nature cell biology *13,* 589–598.

Gornicka, A., Fettig, J., Eguchi, A., Berk, M. P., Thapaliya, S., Dixon, L. J., and Feldstein, A. E. (2012). Adipocyte hypertrophy is associated with lysosomal permeability both in vivo and in vitro: role in adipose tissue inflammation. American journal of physiology. Endocrinology and metabolism *303,* E597-606.

Green, D. R., and Van Houten, B. (2011). SnapShot: Mitochondrial quality control. Cell *147,* 950, 950.e1.

Green, H., and Kehinde, O. (1975). An established preadipose cell line and its differentiation in culture. II. Factors affecting the adipose conversion. Cell *5,* 19-27.

Green, H., and Meuth, M. (1974). An established pre-adipose cell line and its differentiation in culture. Cell *3,* 127-133.

Greenberg, A. S., and Obin, M. S. (2006). Obesity and the role of adipose tissue in inflammation and metabolism. The American journal of clinical nutrition *83,* 461S-465S.

Guo, W., Flanagan, J., Jasuja, R., Kirkland, J., Jiang, L., and Bhasin, S. (2008). The effects of myostatin on adipogenic differentiation of human bone marrow-derived mesenchymal stem cells are mediated through cross-communication between Smad3 and Wnt/beta-catenin signaling pathways. The Journal of biological chemistry *283,* 9136-9145.

Gustafson, B., and Smith, U. (2012). The WNT inhibitor Dickkopf 1 and bone morphogenetic protein 4 rescue adipogenesis in hypertrophic obesity in humans. Diabetes *61,* 1217-1224.

Gustafson, B., Hammarstedt, A., Hedjazifar, S., and Smith, U. (2013). Restricted adipogenesis in hypertrophic obesity: the role of WISP2, WNT, and BMP4. Diabetes *62,* 2997-3004.

Gustafson, B., Hammarstedt, A., Hedjazifar, S., Hoffmann, J. M., Svensson, P. A., Grimsby, J., Rondinone, C., and Smith, U. (2015). BMP4 and BMP Antagonists Regulate Human White and Beige Adipogenesis. Diabetes *64,* 1670-1681.

Gustafson, B., Hedjazifar, S., Gogg, S., Hammarstedt, A., and Smith, U. (2015). Insulin resistance and impaired adipogenesis. Trends in endocrinology and metabolism: TEM *26,* 193-200.

Haczeyni, F., Bell-Anderson, K. S., and Farrell, G. C. (2017). Causes and mechanisms of adipocyte enlargement and adipose expansion. Obesity reviews: an official journal of the International Association for the Study of Obesity *19,* 406-420.

Haeusler, R. A., McGraw, T. E., and Accili, D. (2017). Biochemical and cellular properties of insulin receptor signalling. Nature reviews. Molecular cell biology *19,* 31-44.

Han, C. Y. (2016). Roles of Reactive Oxygen Species on Insulin Resistance in Adipose Tissue. Diabetes and metabolism journal *40,* 272-279.

Harp, J. B., Franklin, D., Vanderpuije, A. A., and Gimble, J. M. (2001). Differential expression of signal transducers and activators of transcription during human adipogenesis. Biochemical and biophysical research communications *281,* 907-912.

Hashimoto, Y., Niikura, T., Tajima, H., Yasukawa, T., Sudo, H., Ito, Y., Kita, Y., Kawasumi, M., Kouyama, K., Doyu, M., Sobue, G., Koide, T., Tsuji, S., Lang, J., Kurokawa, K., and Nishimoto, I. (2001). A rescue factor abolishing neuronal cell death by a wide spectrum of familial Alzheimer's disease genes and Abeta. Proceedings of the National Academy of Sciences of the United States of America *98,* 6336-6341.

Hauner, H. (1990). Complete adipose differentiation of 3T3 L1 cells in a chemically defined medium: comparison to serum-containing culture conditions. Endocrinology *127,* 865-872.

Hausman, D. B., DiGirolamo, M., Bartness, T. J., Hausman, G. J., and Martin, R. J. (2001). The biology of white adipocyte proliferation. Obesity reviews: an official journal of the International Association for the Study of Obesity *2,* 239-254.

He, W., Barak, Y., Hevener, A., Olson, P., Liao, D., Le, J., Nelson, M., Ong, E., Olefsky, J. M., and Evans, R. M. (2003). Adipose-specific peroxisome proliferator-activated receptor gamma knockout causes insulin resistance in fat and liver but not in muscle. Proceedings of the National Academy of Sciences of the United States of America *100,* 15712-15717.

Heilbronn, L. K., Gan, S. K., Turner, N., Campbell, L. V., and Chisholm, D. J. (2007). Markers of mitochondrial biogenesis and metabolism are lower in overweight and obese insulin-resistant subjects. The Journal of clinical endocrinology and metabolism *92,* 1467-1473.

Henness, S., and Perry, C. M. (2006). Orlistat: a review of its use in the management of obesity. Drugs *66,* 1625-1656.

Henry, S. L., Bensley, J. G., Wood-Bradley, R. J., Cullen-McEwen, L. A., Bertram, J. F., and Armitage, J. A. (2012). White adipocytes: more than just fat depots. The international journal of biochemistry & cell biology *44,* 435-440.

Hepler, C., Shan, B., Zhang, Q., Henry, G. H., Shao, M., Vishvanath, L., Ghaben, A. L., Mobley, A. B., Strand, D., Hon, G. C., and Gupta, R. K. (2018). Identification of functionally distinct fibro-inflammatory and adipogenic stromal subpopulations in visceral adipose tissue of adult mice. eLife *7,* e39636.

Herpin, A., Lelong, C., and Favrel, P. (2004). Transforming growth factor-beta-related proteins: an ancestral and widespread superfamily of cytokines in metazoans. Developmental and comparative immunology *28,* 461-485.

Heymsfield, S. B., and Wadden, T. A. (2017). Mechanisms, Pathophysiology, and Management of Obesity. The New England journal of medicine *376,* 254-266.

Hirai, S., Yamanaka, M., Kawachi, H., Matsui, T., and Yano, H. (2005). Activin A inhibits differentiation of 3T3-L1 preadipocyte. Molecular and cellular endocrinology *232,* 21-26.

Hoffstedt, J., Arner, E., Wahrenberg, H., Andersson, D. P., Qvisth, V., Lofgren, P., Ryden, M., Thorne, A., Wiren, M., Palmer, M., Thorell, A., Toft, E., and Arner, P. (2010). Regional impact of adipose tissue morphology on the metabolic profile in morbid obesity. Diabetologia *53,* 2496-2503.

Holloway, G. P., Thrush, A. B., Heigenhauser, G. J., Tandon, N. N., Dyck, D. J., Bonen, A., and Spriet, L. L. (2007). Skeletal muscle mitochondrial FAT/CD36 content and palmitate oxidation are not decreased in obese women. American journal of physiology. Endocrinology and metabolism *292,* E1782-9.

Hong, S. J., Jia, S. X., Xie, P., Xu, W., Leung, K. P., Mustoe, T. A., and Galiano, R. D. (2013). Topically delivered adipose derived stem cells show an activated-fibroblast phenotype and enhance granulation tissue formation in skin wounds. PloS one *8,* e55640.

Hopkinson, B. M., Desler, C., Kalisz, M., Vestentoft, P. S., Juel Rasmussen, L., and Bisgaard, H. C. (2017). Bioenergetic Changes during Differentiation of Human Embryonic Stem Cells along the Hepatic Lineage. Oxidative medicine and cellular longevity *2017,* 5080128.

Hoppins, S., Lackner, L., and Nunnari, J. (2007). The machines that divide and fuse mitochondria. Annual review of biochemistry *76,* 751-780.

Hossain, P., Kawar, B., and El Nahas, M. (2007). Obesity and diabetes in the developing world--a growing challenge. The New England journal of medicine *356,* 213-215.

Houstis, N., Rosen, E. D., and Lander, E. S. (2006). Reactive oxygen species have a causal role in multiple forms of insulin resistance. Nature *440,* 944-948.

Houtkooper, R. H., Canto, C., Wanders, R. J., and Auwerx, J. (2009). The secret life of NAD+: an old metabolite controlling new metabolic signaling pathways. Endocrine reviews *31,* 194-223.

Hu, C., Fan, L., Cen, P., Chen, E., Jiang, Z., and Li, L. (2016). Energy Metabolism Plays a Critical Role in Stem Cell Maintenance and Differentiation. International journal of molecular sciences *17,* 253.

Hu, D., Linders, A., Yamak, A., Correia, C., Kijlstra, J. D., Garakani, A., Xiao, L., Milan, D. J., van der Meer, P., Serra, M., Alves, P. M., and Domian, I. J. (2018). Metabolic Maturation of Human Pluripotent Stem Cell-Derived Cardiomyocytes by Inhibition of HIF1α and LDHA. Circulation research *123,* 1066-1079.

Hua, X., Wu, J., Goldstein, J. L., Brown, M. S., and Hobbs, H. H. (1995). Structure of the human gene encoding sterol regulatory element binding protein-1 (SREBF1) and localization of SREBF1 and SREBF2 to chromosomes 17p11.2 and 22q13. Genomics *25,* 667-673.

Ijichi, N., Ikeda, K., Horie-Inoue, K., Yagi, K., Okazaki, Y., and Inoue, S. (2007). Estrogen-related receptor alpha modulates the expression of adipogenesis-related genes during adipocyte differentiation. Biochemical and biophysical research communications *358,* 813-818.

Isakson, P., Hammarstedt, A., Gustafson, B., and Smith, U. (2009). Impaired preadipocyte differentiation in human abdominal obesity: role of Wnt, tumor necrosis factor-alpha, and inflammation. Diabetes *58,* 1550-1557.

Ito, R., Morimoto, N., Liem, P. H., Nakamura, Y., Kawai, K., Taira, T., Tsuji, W., Toi, M., and Suzuki, S. (2012). Adipogenesis using human adipose tissue-derived stromal cells combined with a collagen/gelatin sponge sustaining release of basic fibroblast growth factor. Journal of tissue engineering and regenerative medicine *8,* 1000-1008.

Jernas, M., Palming, J., Sjoholm, K., Jennische, E., Svensson, P. A., Gabrielsson, B. G., Levin, M., Sjogren, A., Rudemo, M., Lystig, T. C., Carlsson, B., Carlsson, L. M., and Lonn, M. (2006). Separation of human adipocytes by size: hypertrophic fat cells display distinct gene expression. FASEB journal: official publication of the Federation of American Societies for Experimental Biology *20,* 1540-1542.

Jones, S. E., and Jomary, C. (2002). Secreted Frizzled-related proteins: searching for relationships and patterns. BioEssays: news and reviews in molecular, cellular and developmental biology *24,* 811-820.

Jornayvaz, F. R., and Shulman, G. I. (2010). Regulation of mitochondrial biogenesis. Essays in biochemistry *47,* 69-84.

Jurgens, W. J., Oedayrajsingh-Varma, M. J., Helder, M. N., Zandiehdoulabi, B., Schouten, T. E., Kuik, D. J., Ritt, M. J., and van Milligen, F. J. (2008). Effect of tissue-harvesting site on yield of stem cells derived from adipose tissue: implications for cell-based therapies. Cell and tissue research *332,* 415-426.

Kajimura, S., and Saito, M. (2013). A new era in brown adipose tissue biology: molecular control of brown fat development and energy homeostasis. Annual review of physiology *76,* 225-249.

Kanazawa, A., Tsukada, S., Kamiyama, M., Yanagimoto, T., Nakajima, M., and Maeda, S. (2005). Wnt5b partially inhibits canonical Wnt/beta-catenin signaling pathway and promotes adipogenesis in 3T3-L1 preadipocytes. Biochemical and biophysical research communications *330,* 505-510.

Kang, S., Bennett, C. N., Gerin, I., Rapp, L. A., Hankenson, K. D., and Macdougald, O. A. (2007). Wnt signaling stimulates osteoblastogenesis of mesenchymal precursors by suppressing CCAAT/enhancer-binding protein alpha and peroxisome proliferator-activated receptor gamma. The Journal of biological chemistry *282,* 14515-14524.

Katsareli, E. A., and Dedoussis, G. V. (2014). Biomarkers in the field of obesity and its related comorbidities. Expert opinion on therapeutic targets *18,* 385-401.

Kawai, M., Namba, N., Mushiake, S., Etani, Y., Nishimura, R., Makishima, M., and Ozono, K. (2007). Growth hormone stimulates adipogenesis of 3T3-L1 cells through activation of the Stat5A/5B-PPARgamma pathway. Journal of molecular endocrinology *38,* 19-34.

Kawamura, Y., Tanaka, Y., Kawamori, R., and Maeda, S. (2005). Overexpression of Kruppel-like factor 7 regulates adipocytokine gene expressions in human adipocytes and inhibits glucose-induced insulin secretion in pancreatic beta-cell line. Molecular endocrinology (Baltimore, Md.) *20,* 844-856.

Kawano, Y., and Kypta, R. (2003). Secreted antagonists of the Wnt signalling pathway. Journal of cell science *116,* 2627-2634.

Kim, G.Y., Jeong, H.H., Yeom, S.J., Lee, C.S., and Roh, C. (2016). Efficient and reliable screening of anti-obesity agents on a micro-cell pattern chip. Journal of chemical technology & biotechnology *91,* 2688-2692.

Kim, J.B., Wright, H. M., Wright, M., and Spiegelman, B. M. (1998). ADD1/SREBP1 activates PPARgamma through the production of endogenous ligand. Proceedings of the National Academy of Sciences of the United States of America *95,* 4333-4337.

Kim, J.I., Huh, J. Y., Sohn, J. H., Choe, S. S., Lee, Y. S., Lim, C. Y., Jo, A., Park, S. B., Han, W., and Kim, J. B. (2015). Lipid-overloaded enlarged adipocytes provoke insulin resistance independent of inflammation. Molecular and cellular biology *35,* 1686-1699.

Klemm, D.J., Leitner, J.W., Watson, P., Nesterova, A., Reusch, J.E., Goalstone, M.L., and Draznin, B. (2001). Insulin-induced adipocyte differentiation. Activation of CREB rescues adipogenesis from the arrest caused by inhibition of prenylation. The Journal of biological chemistry *276,* 28430-28435.

Klimmeck, D., Hansson, J., Raffel, S., Vakhrushev, S. Y., Trumpp, A., and Krijgsveld, J. (2012). Proteomic cornerstones of hematopoietic stem cell differentiation: distinct signatures of multipotent progenitors and myeloid committed cells. Molecular & cellular proteomics: MCP *11,* 286-302.

Kloting, N., Fasshauer, M., Dietrich, A., Kovacs, P., Schon, M. R., Kern, M., Stumvoll, M., and Bluher, M. (2010). Insulin-sensitive obesity. American journal of physiology. Endocrinology and metabolism *299,* E506-15.

Kopecky, J., Rossmeisl, M., Flachs, P., Bardova, K., and Brauner, P. (2001). Mitochondrial uncoupling and lipid metabolism in adipocytes. Biochemical Society transactions *29,* 791-797.

Kuhlbrandt, W. (2015). Structure and function of mitochondrial membrane protein complexes. BMC biology *13,* 89.

Kusminski, C.M., and Scherer, P. E. (2012). Mitochondrial dysfunction in white adipose tissue. Trends in endocrinology and metabolism: TEM *23,* 435-443.

Kusminski, C. M., Bickel, P. E., and Scherer, P. E. (2016). Targeting adipose tissue in the treatment of obesity-associated diabetes. Nature reviews. Drug discovery *15,* 639-660.

Kusminski, C. M., Holland, W. L., Sun, K., Park, J., Spurgin, S. B., Lin, Y., Askew, G. R., Simcox, J. A., McClain, D. A., Li, C., and Scherer, P. E. (2012). MitoNEET-driven alterations in adipocyte mitochondrial activity reveal a crucial adaptive process that preserves insulin sensitivity in obesity. Nature medicine *18,* 1539-1549.

Kwok, K. H., Lam, K. S., and Xu, A. (2016). Heterogeneity of white adipose tissue: molecular basis and clinical implications. Experimental & molecular medicine *48,* e215.

Laforest, S., Labrecque, J., Michaud, A., Cianflone, K., and Tchernof, A. (2015). Adipocyte size as a determinant of metabolic disease and adipose tissue dysfunction. Critical reviews in clinical laboratory sciences *52,* 301-313.

Lane, J. M., Doyle, J. R., Fortin, J. P., Kopin, A. S., and Ordovas, J. M. (2014). Development of an OP9 derived cell line as a robust model to rapidly study adipocyte differentiation. PloS one *9,* e112123.

Lee, M. J. (2017). Hormonal Regulation of Adipogenesis. Comprehensive Physiology *7,* 1151–1195.

Lee, M. J., and Fried, S. K. (2014). Optimal protocol for the differentiation and metabolic analysis of human adipose stromal cells. Methods in enzymology *538,* 49-65.

Lee, S. Y., Lee, J. H., Kim, J. Y., Bae, Y. C., Suh, K. T., and Jung, J. S. (2014). BMP2 increases adipogenic differentiation in the presence of dexamethasone, which is inhibited by the treatment of TNF-α in human adipose tissue-derived stromal cells. Cellular physiology and biochemistry: international journal of experimental cellular physiology, biochemistry, and pharmacology *34,* 1339-1350.

Lefterova, M. I., Zhang, Y., Steger, D. J., Schupp, M., Schug, J., Cristancho, A., Feng, D., Zhuo, D., Stoeckert, C. J., Liu, X. S., and Lazar, M. A. (2008). PPARgamma and C/EBP factors orchestrate adipocyte biology via adjacent binding on a genome-wide scale. Genes & development *22,* 2941-2952.

Lindroos, J., Husa, J., Mitterer, G., Haschemi, A., Rauscher, S., Haas, R., Groger, M., Loewe, R., Kohrgruber, N., Schrogendorfer, K. F., Prager, G., Beck, H., Pospisilik, J. A., Zeyda, M., Stulnig, T. M., Patsch, W., Wagner, O., Esterbauer, H., and Bilban, M. (2013). Human but not mouse adipogenesis is critically dependent on LMO3. Cell metabolism *18,* 62-74.

Lo, K. A., and Sun, L. (2013). Turning WAT into BAT: a review on regulators controlling the browning of white adipocytes. Bioscience reports *33,* e00065.

Lo, K.A., Labadorf, A., Kennedy, N. J., Han, M. S., Yap, Y. S., Matthews, B., Xin, X., Sun, L., Davis, R. J., Lodish, H. F., and Fraenkel, E. (2013). Analysis of in vitro insulin-resistance models and their physiological relevance to in vivo diet-induced adipose insulin resistance. Cell reports *5,* 259-270.

Logan, C. Y., and Nusse, R. (2004). The Wnt signaling pathway in development and disease. Annual review of cell and developmental biology *20,* 781-810.

Lolmede, K., Duffaut, C., Zakaroff-Girard, A., and Bouloumie, A. (2011). Immune cells in adipose tissue: key players in metabolic disorders. Diabetes & metabolism *37,* 283-290.

Longo, K. A., Wright, W. S., Kang, S., Gerin, I., Chiang, S. H., Lucas, P. C., Opp, M. R., and MacDougald, O. A. (2004). Wnt10b inhibits development of white and brown adipose tissues. The Journal of biological chemistry *279,* 35503-35509.

Lonn, M., Mehlig, K., Bengtsson, C., and Lissner, L. (2009). Adipocyte size predicts incidence of type 2 diabetes in women. FASEB journal: official publication of the Federation of American Societies for Experimental Biology *24,*326-331.

Lowe, C. E., O'Rahilly, S., and Rochford, J. J. (2011). Adipogenesis at a glance. Journal of cell science *124,* 2681-2686.

Lu, Q., Li, M., Zou, Y., and Cao, T. (2014). Induction of adipocyte hyperplasia in subcutaneous fat depot alleviated type 2 diabetes symptoms in obese mice. Obesity (Silver Spring, Md.) *22,* 1623-1631.

Lu, W., Yu, J., Zhang, Y., Ji, K., Zhou, Y., Li, Y., Deng, Z., and Jin, Y. (2011). Mixture of fibroblasts and adipose tissue-derived stem cells can improve epidermal morphogenesis of tissue-engineered skin. Cells, tissues, organs *195,*197-206.

Ma, S., Xie, N., Li, W., Yuan, B., Shi, Y., and Wang, Y. (2013). Immunobiology of mesenchymal stem cells. Cell death and differentiation *21,* 216-225.

Mandal, S., Lindgren, A. G., Srivastava, A. S., Clark, A. T., and Banerjee, U. (2011). Mitochondrial function controls proliferation and early differentiation potential of embryonic stem cells. Stem cells (Dayton, Ohio) *29,* 486-495.

Mandrup, S., Loftus, T. M., MacDougald, O. A., Kuhajda, F. P., and Lane, M. D. (1997). Obese gene expression at in vivo levels by fat pads derived from s.c. implanted 3T3-F442A preadipocytes. Proceedings of the National Academy of Sciences of the United States of America *94,* 4300-4305.

Manolopoulos, K. N., Karpe, F., and Frayn, K. N. (2010). Gluteofemoral body fat as a determinant of metabolic health. International journal of obesity (2005) *34,* 949-959.

Marin, P., Andersson, B., Ottosson, M., Olbe, L., Chowdhury, B., Kvist, H., Holm, G., Sjostrom, L., and Bjorntorp, P. (1992). The morphology and metabolism of intraabdominal adipose tissue in men. Metabolism: clinical and experimental *41,* 1242-1248.

Maryanovich, M., and Gross, A. (2013). A ROS rheostat for cell fate regulation. Trends in cell biology *23,* 129-134.

McKenzie, M., Lazarou, M., and Ryan, M. T. (2009). Chapter 18 Analysis of respiratory chain complex assembly with radiolabeled nuclear- and mitochondrial-encoded subunits. Methods in enzymology *456,* 321-339.

Miki, H., Yamauchi, T., Suzuki, R., Komeda, K., Tsuchida, A., Kubota, N., Terauchi, Y., Kamon, J., Kaburagi, Y., Matsui, J., Akanuma, Y., Nagai, R., Kimura, S., Tobe, K., and Kadowaki, T. (2001). Essential role of insulin receptor substrate 1 (IRS-1) and IRS-2 in adipocyte differentiation. Molecular and cellular biology *21,* 2521-2532.

Mikkelsen, T. S., Xu, Z., Zhang, X., Wang, L., Gimble, J. M., Lander, E. S., and Rosen, E. D. (2010). Comparative epigenomic analysis of murine and human adipogenesis. Cell *143,* 156-169.

Mitchell, N. S., Catenacci, V. A., Wyatt, H. R., and Hill, J. O. (2011). Obesity: overview of an epidemic. The Psychiatric clinics of North America *34,* 717-732.

Moisan, A., Lee, Y. K., Zhang, J. D., Hudak, C. S., Meyer, C. A., Prummer, M., Zoffmann, S., Truong, H. H., Ebeling, M., Kiialainen, A., Gerard, R., Xia, F., Schinzel, R. T., Amrein, K. E., and Cowan, C. A. (2014). White-to-brown metabolic conversion of human adipocytes by JAK inhibition. Nature cell biology *17,* 57-67.

Moitra, J., Mason, M. M., Olive, M., Krylov, D., Gavrilova, O., Marcus-Samuels, B., Feigenbaum, L., Lee, E., Aoyama, T., Eckhaus, M., Reitman, M. L., and Vinson, C. (1998). Life without white fat: a transgenic mouse. Genes & development *12,* 3168-3181.

Mootha, V. K., Handschin, C., Arlow, D., Xie, X., St Pierre, J., Sihag, S., Yang, W., Altshuler, D., Puigserver, P., Patterson, N., Willy, P. J., Schulman, I. G., Heyman, R. A., Lander, E. S., and Spiegelman, B. M. (2004). Erralpha and Gabpa/b specify PGC-1alpha-dependent oxidative phosphorylation gene expression that is altered in diabetic muscle. Proceedings of the National Academy of Sciences of the United States of America *101,* 6570-6575.

Morin, C. L., Gayles, E. C., Podolin, D. A., Wei, Y., Xu, M., and Pagliassotti, M. J. (1998). Adipose tissue-derived tumor necrosis factor activity correlates with fat cell size but not insulin action in aging rats. Endocrinology *139,* 4998-5005.

Morino, K., Petersen, K. F., Dufour, S., Befroy, D., Frattini, J., Shatzkes, N., Neschen, S., White, M. F., Bilz, S., Sono, S., Pypaert, M., and Shulman, G. I. (2005). Reduced mitochondrial density and increased IRS-1 serine phosphorylation in muscle of insulin-resistant offspring of type 2 diabetic parents. The Journal of clinical investigation *115,* 3587-3593.

Morley, T. S., Xia, J. Y., and Scherer, P. E. (2015). Selective enhancement of insulin sensitivity in the mature adipocyte is sufficient for systemic metabolic improvements. Nature communications *6,* 7906.

Morrison, S. F., Madden, C. J., and Tupone, D. (2014). Central neural regulation of brown adipose tissue thermogenesis and energy expenditure. Cell metabolism *19,* 741-756.

Musri, M. M., and Parrizas, M. (2012). Epigenetic regulation of adipogenesis. Current opinion in clinical nutrition and metabolic care *15,* 342-349.

Nadeau, C., Asakawa, K., Flanagan, W., Wall, R., Bancej, C., and Morrison, H. (2013). Projection of body mass index (BMI), chronic conditions and healthcare costs in Canada: an application of microsimulation. Canadian journal of Diabetes *37,* S243-S244.

Naderi, N., Combellack, E. J., Griffin, M., Sedaghati, T., Javed, M., Findlay, M. W., Wallace, C. G., Mosahebi, A., Butler, P. E., Seifalian, A. M., and Whitaker, I. S. (2016). The regenerative role of adipose-derived stem cells (ADSC) in plastic and reconstructive surgery. International wound journal *14,* 112-124.

Nakae, J., Kitamura, T., Kitamura, Y., Biggs, W. H., Arden, K. C., and Accili, D. (2003). The forkhead transcription factor Foxo1 regulates adipocyte differentiation. Developmental cell *4,* 119-129.

Nanbu-Wakao, R., Morikawa, Y., Matsumura, I., Masuho, Y., Muramatsu, M. A., Senba, E., and Wakao, H. (2002). Stimulation of 3T3-L1 adipogenesis by signal transducer and activator of transcription 5. Molecular endocrinology (Baltimore, Md.) *16,* 1565-1576.

NCD Risk Factor Collab. 2016. (2016). Trends in adult body-mass index in 200 countries from 1975 to 2014: a pooled analysis of 1698 population-based measurement studies with 19·2 million participants. Lancet (London, England) *387,* 1377-1396.

Negrel, R., Grimaldi, P., and Ailhaud, G. (1978). Establishment of preadipocyte clonal line from epididymal fat pad of ob/ob mouse that responds to insulin and to lipolytic hormones. Proceedings of the National Academy of Sciences of the United States of America *75,* 6054-6058.

Nishizuka, M., Koyanagi, A., Osada, S., and Imagawa, M. (2008). Wnt4 and Wnt5a promote adipocyte differentiation. FEBS letters *582,* 3201-3205.

Noureddin, M., and Rinella, M. E. (2015). Nonalcoholic Fatty liver disease, diabetes, obesity, and hepatocellular carcinoma. Clinics in liver disease *19,* 361-379.

O'Connell, J., Lynch, L., Cawood, T. J., Kwasnik, A., Nolan, N., Geoghegan, J., McCormick, A., O'Farrelly, C., and O'Shea, D. (2010). The relationship of omental and subcutaneous adipocyte size to metabolic disease in severe obesity. PloS one *5,* e9997.

Oishi, Y., Manabe, I., Tobe, K., Tsushima, K., Shindo, T., Fujiu, K., Nishimura, G., Maemura, K., Yamauchi, T., Kubota, N., Suzuki, R., Kitamura, T., Akira, S., Kadowaki, T., and Nagai, R. (2005).

Kruppel-like transcription factor KLF5 is a key regulator of adipocyte differentiation. Cell metabolism *1,* 27-39.

Oliveira, J. T., Gardel, L. S., Rada, T., Martins, L., Gomes, M. E., and Reis, R. L. (2010). Injectable gellan gum hydrogels with autologous cells for the treatment of rabbit articular cartilage defects. Journal of orthopaedic research: official publication of the Orthopaedic Research Society *28,* 1193-1199.

Ouchi, N., Higuchi, A., Ohashi, K., Oshima, Y., Gokce, N., Shibata, R., Akasaki, Y., Shimono, A., and Walsh, K. (2010). Sfrp5 is an anti-inflammatory adipokine that modulates metabolic dysfunction in obesity. Science (New York, N.Y.*) 329,* 454-457.

Padoin, A. V., Braga-Silva, J., Martins, P., Rezende, K., Rezende, A. R., Grechi, B., Gehlen, D., and Machado, D. C. (2008). Sources of processed lipoaspirate cells: influence of donor site on cell concentration. Plastic and reconstructive surgery *122,* 614-618.

Pei, Z., Yang, Y., Kiess, W., Sun, C., and Luo, F. (2014). Dynamic profile and adipogenic role of growth differentiation factor 5 (GDF5) in the differentiation of 3T3-L1 preadipocytes. Archives of biochemistry and biophysics *560,* 27-35.

Pereira, S. L., Rodrigues, A. S., Sousa, M. I., Correia, M., Perestrelo, T., and Ramalho-Santos, J. (2014). From gametogenesis and stem cells to cancer: common metabolic themes. Human reproduction update *20,* 924-943.

Perez, L. M., Bernal, A., de Lucas, B., San Martin, N., Mastrangelo, A., Garcia, A., Barbas, C., and Galvez, B. G. (2015). Altered metabolic and stemness capacity of adipose tissue-derived stem cells from obese mouse and human. PloS one *10,* e0123397.

Pfeifer, A., and Hoffmann, L. S. (2014). Brown, beige, and white: the new color code of fat and its pharmacological implications. Annual review of pharmacology and toxicology *55,* 207-227.

Pietilainen, K. H., Naukkarinen, J., Rissanen, A., Saharinen, J., Ellonen, P., Keranen, H., Suomalainen, A., Gotz, A., Suortti, T., Yki-Jarvinen, H., Oresic, M., Kaprio, J., and Peltonen, L. (2008). Global transcript profiles of fat in monozygotic twins discordant for BMI: pathways behind acquired obesity. PLoS medicine *5,* e51.

Pietilainen, K. H., Rog, T., Seppanen-Laakso, T., Virtue, S., Gopalacharyulu, P., Tang, J., Rodriguez-Cuenca, S., Maciejewski, A., Naukkarinen, J., Ruskeepaa, A. L., Niemela, P. S., Yetukuri, L., Tan, C. Y., Velagapudi, V., Castillo, S., Nygren, H., Hyotylainen, T., Rissanen, A., Kaprio, J., Yki-Jarvinen, H., Vattulainen, I., Vidal-Puig, A., and Oresic, M. (2011). Association of lipidome remodeling in the adipocyte membrane with acquired obesity in humans. PLoS biology *9,* e1000623.

Pi-Sunyer, X., Astrup, A., Fujioka, K., Greenway, F., Halpern, A., Krempf, M., Lau, D. C., le Roux, C. W., Violante Ortiz, R., Jensen, C. B., Wilding, J. P., and , . (2015). A Randomized,

Controlled Trial of 3.0 mg of Liraglutide in Weight Management. The New England journal of medicine *373,* 11-22.

Porras, D. P., Abbaszadeh, M., Bhattacharya, D., D'Souza, N. C., Edjiu, N. R., Perry, C. G. R., and Scimé, A. (2017). p107 determines a metabolic checkpoint required for adipocyte lineage fates. Stem cells (Dayton, Ohio) *35,* 1378-1391.

Poulos, S. P., Hausman, D. B., and Hausman, G. J. (2009). The development and endocrine functions of adipose tissue. Molecular and cellular endocrinology *323,* 20–34.

Prigione, A., Fauler, B., Lurz, R., Lehrach, H., and Adjaye, J. (2010). The senescence-related mitochondrial/oxidative stress pathway is repressed in human induced pluripotent stem cells. Stem cells (Dayton, Ohio) *28,* 721-733.

Purnell, J.Q. (2018). Definitions, Classification, and Epidemiology of Obesity. In: Feingold, K.R., Anawalt, B., Boyce, A., Chrousos, G., Dungan, K., Grossman, A., Hershman, J.M., Kaltsas, G., Koch, C., Kopp, P., Korbonits, M., McLachlan, R., Morley, J.E., New, M., Perreault, L., Purnell, J., Rebar, R., Singer, F., Trence, D.L., Vinik, A., Wilson, D.P., editors. Source Endotext [Internet]. South Dartmouth (MA): MDText.com, Inc.; 2000-.

Qin, J., Li, W. Q., Zhang, L., Chen, F., Liang, W. H., Mao, F. F., Zhang, X. M., Lahn, B. T., Yu, W. H., and Xiang, A. P. (2010). A stem cell-based tool for small molecule screening in adipogenesis. PloS one 5, e13014.

Rangwala, S. M., and Lazar, M. A. (2000). Transcriptional control of adipogenesis. Annual review of nutrition *20,* 535-559.

Rehman, J. (2010). Empowering self-renewal and differentiation: the role of mitochondria in stem cells. Journal of molecular medicine (Berlin, Germany) *88,* 981-986.

Ren, D., Collingwood, T. N., Rebar, E. J., Wolffe, A. P., and Camp, H. S. (2002). PPARgamma knockdown by engineered transcription factors: exogenous PPARgamma2 but not PPARgamma1 reactivates adipogenesis. Genes & development *16,* 27-32.

Reznikoff, C. A., Brankow, D. W., and Heidelberger, C. (1973). Establishment and characterization of a cloned line of C3H mouse embryo cells sensitive to post confluence inhibition of division. Cancer research *33,* 3231-3238.

Riedel, J., Badewien-Rentzsch, B., Kohn, B., Hoeke, L., and Einspanier, R. (2015). Characterization of key genes of the renin-angiotensin system in mature feline adipocytes and during in vitro adipogenesis. Journal of animal physiology and animal nutrition *100,* 1139-1148.

Ritov, V. B., Menshikova, E. V., He, J., Ferrell, R. E., Goodpaster, B. H., and Kelley, D. E. (2005). Deficiency of subsarcolemmal mitochondria in obesity and type 2 diabetes. Diabetes *54,* 8-14.

Rodriguez, A. M., Elabd, C., Amri, E. Z., Ailhaud, G., and Dani, C. (2005). The human adipose tissue is a source of multipotent stem cells. Biochimie *87,* 125-128.

Rodriguez, L. V., Alfonso, Z., Zhang, R., Leung, J., Wu, B., and Ignarro, L. J. (2006). Clonogenic multipotent stem cells in human adipose tissue differentiate into functional smooth muscle cells. Proceedings of the National Academy of Sciences of the United States of America *103,* 12167-12172.

Rong, J. X., Qiu, Y., Hansen, M. K., Zhu, L., Zhang, V., Xie, M., Okamoto, Y., Mattie, M. D., Higashiyama, H., Asano, S., Strum, J. C., and Ryan, T. E. (2007). Adipose mitochondrial biogenesis is suppressed in db/db and high-fat diet-fed mice and improved by rosiglitazone. Diabetes *56,* 1751-1760.

Rosen, E. D., and MacDougald, O. A. (2006). Adipocyte differentiation from the inside out. Nature reviews. Molecular cell biology *7,* 885-896.

Rosen, E. D., and Spiegelman, B. M. (2001). PPARgamma: a nuclear regulator of metabolism, differentiation, and cell growth. The Journal of biological chemistry *276,* 37731-37734.

Rosen, E. D., Sarraf, P., Troy, A. E., Bradwin, G., Moore, K., Milstone, D. S., Spiegelman, B. M., and Mortensen, R. M. (1999). PPAR gamma is required for the differentiation of adipose tissue in vivo and in vitro. Molecular cell *4,* 611-617.

Ross, R., Shaw, K. D., Rissanen, J., Martel, Y., de Guise, J., and Avruch, L. (1994). Sex differences in lean and adipose tissue distribution by magnetic resonance imaging: anthropometric relationships. The American journal of clinical nutrition *59,* 1277-1285.

Ruiz-Ojeda, F. J., Ruperez, A. I., Gomez-Llorente, C., Gil, A., and Aguilera, C. M. (2016). Cell Models and Their Application for Studying Adipogenic Differentiation in Relation to Obesity: A Review. International journal of molecular sciences *17,* E1040.

Samocha-Bonet, D., Campbell, L. V., Mori, T. A., Croft, K. D., Greenfield, J. R., Turner, N., and Heilbronn, L. K. (2012). Overfeeding reduces insulin sensitivity and increases oxidative stress, without altering markers of mitochondrial content and function in humans. PloS one *7,* e36320.

Samsonraj, R. M., Rai, B., Sathiyanathan, P., Puan, K. J., Rotzschke, O., Hui, J. H., Raghunath, M., Stanton, L. W., Nurcombe, V., and Cool, S. M. (2015). Establishing criteria for human mesenchymal stem cell potency. Stem cells (Dayton, Ohio) 33, 1878-1891.

Sarjeant, K., and Stephens, J. M. (2012). Adipogenesis. Cold Spring Harbor perspectives in biology *4,* a008417.

Sethi, J.K., and Vidal-Puig, A. (2010). Wnt signalling and the control of cellular metabolism. The Biochemical journal *427,* 1-17.

Scarpulla, R. C. (2008). Transcriptional paradigms in mammalian mitochondrial biogenesis and function. Physiological reviews *88,* 611-638.

Scarpulla, R. C. (2010). Metabolic control of mitochondrial biogenesis through the PGC-1 family regulatory network. Biochimica et biophysica acta *1813,* 1269-1278.

Schreiber, S. N., Emter, R., Hock, M. B., Knutti, D., Cardenas, J., Podvinec, M., Oakeley, E. J., and Kralli, A. (2004). The estrogen-related receptor alpha (ERRalpha) functions in PPARgamma coactivator 1alpha (PGC-1alpha)-induced mitochondrial biogenesis. Proceedings of the National Academy of Sciences of the United States of America *101,* 6472-6477.

Schwalie, P. C., Dong, H., Zachara, M., Russeil, J., Alpern, D., Akchiche, N., Caprara, C., Sun, W., Schlaudraff, K. U., Soldati, G., Wolfrum, C., and Deplancke, B. (2018). A stromal cell population that inhibits adipogenesis in mammalian fat depots. Nature *559,* 103-108.

Scimé, A., Grenier, G., Huh, M. S., Gillespie, M. A., Bevilacqua, L., Harper, M. E., and Rudnicki, M. A. (2005). Rb and p107 regulate preadipocyte differentiation into white versus brown fat through repression of PGC-1alpha. Cell metabolism *2,* 283-295.

Semple, R. K., Chatterjee, V. K., and O'Rahilly, S. (2006). PPAR gamma and human metabolic disease. The Journal of clinical investigation *116,* 581-589.

Senol-Cosar, O., Flach, R. J., DiStefano, M., Chawla, A., Nicoloro, S., Straubhaar, J., Hardy, O. T., Noh, H. L., Kim, J. K., Wabitsch, M., Scherer, P. E., and Czech, M. P. (2016). Tenomodulin promotes human adipocyte differentiation and beneficial visceral adipose tissue expansion. Nature communications *7,* 10686.

Shang, Y. C., Wang, S. H., Xiong, F., Zhao, C. P., Peng, F. N., Feng, S. W., Li, M. S., Li, Y., and Zhang, C. (2007a). Wnt3a signaling promotes proliferation, myogenic differentiation, and migration of rat bone marrow mesenchymal stem cells. Acta pharmacologica Sinica *28,* 1761-1774.

Shang, Y., Zhang, C., Wang, S., Xiong, F., Zhao, C., Peng, F., Feng, S., Yu, M., Li, M., and Zhang, Y. (2007b). Activated beta-catenin induces myogenesis and inhibits adipogenesis in BM-derived mesenchymal stromal cells. Cytotherapy *9,* 667-681.

Shi, X., Burkart, A., Nicoloro, S. M., Czech, M. P., Straubhaar, J., and Corvera, S. (2008). Paradoxical effect of mitochondrial respiratory chain impairment on insulin signaling and glucose transport in adipose cells. The Journal of biological chemistry *283,* 30658-30667.

Siersbaek, R., and Mandrup, S. (2011). Transcriptional networks controlling adipocyte differentiation. Cold Spring Harbor symposia on quantitative biology *76,* 247-255.

Siersbaek, R., Nielsen, R., and Mandrup, S. (2011). Transcriptional networks and chromatin remodeling controlling adipogenesis. Trends in endocrinology and metabolism: TEM *23,* 56-64.

Skurk, T., Alberti-Huber, C., Herder, C., and Hauner, H. (2006). Relationship between adipocyte size and adipokine expression and secretion. The Journal of clinical endocrinology and metabolism *92,* 1023-1033.

Smirnova, E., Griparic, L., Shurland, D. L., and van der Bliek, A. M. (2001). Dynamin-related protein Drp1 is required for mitochondrial division in mammalian cells. Molecular biology of the cell *12,* 2245-2256.

Smith, P. J., Wise, L. S., Berkowitz, R., Wan, C., and Rubin, C. S. (1988). Insulin-like growth factor-I is an essential regulator of the differentiation of 3T3-L1 adipocytes. The Journal of biological chemistry *263,* 9402-9408.

Sohle, J., Machuy, N., Smailbegovic, E., Holtzmann, U., Gronniger, E., Wenck, H., Stab, F., and Winnefeld, M. (2012). Identification of new genes involved in human adipogenesis and fat storage. PloS one *7,* e31193.

Spalding, K. L., Arner, E., Westermark, P. O., Bernard, S., Buchholz, B. A., Bergmann, O., Blomqvist, L., Hoffstedt, J., Naslund, E., Britton, T., Concha, H., Hassan, M., Ryden, M., Frisen, J., and Arner, P. (2008). Dynamics of fat cell turnover in humans. Nature *453,* 783-787.

Spiegelman, B. M., Puigserver, P., and Wu, Z. (2000). Regulation of adipogenesis and energy balance by PPARgamma and PGC-1. International journal of obesity and related metabolic disorders: journal of the International Association for the Study of Obesity *24,* S8-10.

Srivastava, G., and Apovian, C. M. (2017). Current pharmacotherapy for obesity. Nature reviews. Endocrinology *14,* 12-24.

St John, J. C., Ramalho-Santos, J., Gray, H. L., Petrosko, P., Rawe, V. Y., Navara, C. S., Simerly, C. R., and Schatten, G. P. (2005). The expression of mitochondrial DNA transcription factors during early cardiomyocyte in vitro differentiation from human embryonic stem cells. Cloning and stem cells *7,* 141-153.

Stacey, D. H., Hanson, S. E., Lahvis, G., Gutowski, K. A., and Masters, K. S. (2009). In vitro adipogenic differentiation of preadipocytes varies with differentiation stimulus, culture dimensionality, and scaffold composition. Tissue engineering. Part A *15,* 3389-3399.

Stephens, J. M., Lee, J., and Pilch, P. F. (1997). Tumor necrosis factor-alpha-induced insulin resistance in 3T3-L1 adipocytes is accompanied by a loss of insulin receptor substrate-1 and GLUT4 expression without a loss of insulin receptor-mediated signal transduction. The Journal of biological chemistry *272,* 971-976.

Stephens, J. M., Morrison, R. F., and Pilch, P. F. (1996). The expression and regulation of STATs during 3T3-L1 adipocyte differentiation. The Journal of biological chemistry *271,* 10441-10444.

Storck, K., Ell, J., Regn, S., Rittler-Ungetum, B., Mayer, H., Schantz, T., Muller, D., and Buchberger, M. (2015). Optimization of in vitro cultivation strategies for human adipocyte derived stem cells. Adipocyte *4,* 181-187.

Strissel, K. J., Stancheva, Z., Miyoshi, H., Perfield, J. W., DeFuria, J., Jick, Z., Greenberg, A. S., and Obin, M. S. (2007). Adipocyte death, adipose tissue remodeling, and obesity complications. Diabetes *56,* 2910-2918.

Suda, T., Takubo, K., and Semenza, G. L. (2011). Metabolic regulation of hematopoietic stem cells in the hypoxic niche. Cell stem cell *9,* 298-310.

Suganami, T., Tanimoto-Koyama, K., Nishida, J., Itoh, M., Yuan, X., Mizuarai, S., Kotani, H., Yamaoka, S., Miyake, K., Aoe, S., Kamei, Y., and Ogawa, Y. (2006). Role of the Toll-like receptor 4/NF-kappaB pathway in saturated fatty acid-induced inflammatory changes in the interaction between adipocytes and macrophages. Arteriosclerosis, thrombosis, and vascular biology *27,* 84-91.

Sun, K., Kusminski, C. M., and Scherer, P. E. (2011). Adipose tissue remodeling and obesity. The Journal of clinical investigation *121,* 2094-2101.

Sutherland, L. N., Capozzi, L. C., Turchinsky, N. J., Bell, R. C., and Wright, D. C. (2008). Time course of high-fat diet-induced reductions in adipose tissue mitochondrial proteins: potential mechanisms and the relationship to glucose intolerance. American journal of physiology. Endocrinology and metabolism *295,* E1076-83.

Takubo, K., Nagamatsu, G., Kobayashi, C. I., Nakamura-Ishizu, A., Kobayashi, H., Ikeda, E., Goda, N., Rahimi, Y., Johnson, R. S., Soga, T., Hirao, A., Suematsu, M., and Suda, T. (2013). Regulation of glycolysis by Pdk functions as a metabolic checkpoint for cell cycle quiescence in hematopoietic stem cells. Cell stem cell *12,* 49-61.

Tanaka, T., Yoshida, N., Kishimoto, T., and Akira, S. (1997). Defective adipocyte differentiation in mice lacking the C/EBPbeta and/or C/EBPdelta gene. The EMBO journal *16,* 7432-7443.

Tang, Q. Q., and Lane, M. D. (2012). Adipogenesis: from stem cell to adipocyte. Annual review of biochemistry *81,* 715-736.

Tang, Q. Q., Otto, T. C., and Lane, M. D. (2003). CCAAT/enhancer-binding protein beta is required for mitotic clonal expansion during adipogenesis. Proceedings of the National Academy of Sciences of the United States of America *100,* 850-855.

Tang, Q., Chen, C., Zhang, Y., Dai, M., Jiang, Y., Wang, H., Yu, M., Jing, W., and Tian, W. (2017). Wnt5a regulates the cell proliferation and adipogenesis via MAPK-independent pathway in early stage of obesity. Cell biology international *42,* 63-74.

Tek, C. (2016). Naltrexone HCl/bupropion HCl for chronic weight management in obese adults: patient selection and perspectives. Patient preference and adherence *10,* 751-759.

Tontonoz, P., Hu, E., and Spiegelman, B. M. (1994). Stimulation of adipogenesis in fibroblasts by PPAR gamma 2, a lipid-activated transcription factor. Cell *79,* 1147-1156.

Tormos, K. V., Anso, E., Hamanaka, R. B., Eisenbart, J., Joseph, J., Kalyanaraman, B., and Chandel, N. S. (2011). Mitochondrial complex III ROS regulate adipocyte differentiation. Cell metabolism *14,* 537-544.

Tsatsoulis, A., Mantzaris, M. D., Bellou, S., and Andrikoula, M. (2012). Insulin resistance: an adaptive mechanism becomes maladaptive in the current environment - an evolutionary perspective. Metabolism: clinical and experimental *62,* 622-633.

Tseng, Y. H., Cypess, A. M., and Kahn, C. R. (2010). Cellular bioenergetics as a target for obesity therapy. Nature reviews. Drug discovery *9,* 465-482.

Unamuno, X., Gomez-Ambrosi, J., Rodriguez, A., Becerril, S., Fruhbeck, G., and Catalan, V. (2018). Adipokine dysregulation and adipose tissue inflammation in human obesity. European journal of clinical investigation *48,* e12997.

Uysal, C. A., Tobita, M., Hyakusoku, H., and Mizuno, H. (2012). Adipose-derived stem cells enhance primary tendon repair: biomechanical and immunohistochemical evaluation. Journal of plastic, reconstructive & aesthetic surgery: JPRAS *65,* 1712-1719.

Valerio, A., Cardile, A., Cozzi, V., Bracale, R., Tedesco, L., Pisconti, A., Palomba, L., Cantoni, O., Clementi, E., Moncada, S., Carruba, M. O., and Nisoli, E. (2006). TNF-alpha downregulates eNOS expression and mitochondrial biogenesis in fat and muscle of obese rodents. The Journal of clinical investigation *116,* 2791-2798.

Valorani, M. G., Montelatici, E., Germani, A., Biddle, A., D'Alessandro, D., Strollo, R., Patrizi, M. P., Lazzari, L., Nye, E., Otto, W. R., Pozzilli, P., and Alison, M. R. (2012). Pre-culturing human adipose tissue mesenchymal stem cells under hypoxia increases their adipogenic and osteogenic differentiation potentials. Cell proliferation *45,* 225-238.

van Harmelen, V., Rohrig, K., and Hauner, H. (2004). Comparison of proliferation and differentiation capacity of human adipocyte precursor cells from the omental and subcutaneous adipose tissue depot of obese subjects. Metabolism: clinical and experimental *53,* 632-637.

van Harmelen, V., Skurk, T., Rohrig, K., Lee, Y. M., Halbleib, M., Aprath-Husmann, I., and Hauner, H. (2003). Effect of BMI and age on adipose tissue cellularity and differentiation capacity in women. International journal of obesity and related metabolic disorders: journal of the International Association for the Study of Obesity *27,* 889-895.

Vance, J. E. (1990). Phospholipid synthesis in a membrane fraction associated with mitochondria. The Journal of biological chemistry *265,* 7248-7256.

Virbasius, J. V., and Scarpulla, R. C. (1994). Activation of the human mitochondrial transcription factor A gene by nuclear respiratory factors: a potential regulatory link between nuclear and mitochondrial gene expression in organelle biogenesis. Proceedings of the National Academy of Sciences of the United States of America *91,* 1309-1313.

Visweswaran, M., Schiefer, L., Arfuso, F., Dilley, R. J., Newsholme, P., and Dharmarajan, A. (2015). Wnt antagonist secreted frizzled-related protein 4 upregulates adipogenic differentiation in human adipose tissue-derived mesenchymal stem cells. PloS one *10,* e0118005.

von Heimburg, D., Hemmrich, K., Zachariah, S., Staiger, H., and Pallua, N. (2005). Oxygen consumption in undifferentiated versus differentiated adipogenic mesenchymal precursor cells. Respiratory physiology & neurobiology *146,* 107-116.

Wabitsch, M., Brenner, R. E., Melzner, I., Braun, M., MÃķller, P., Heinze, E., Debatin, K. M., and Hauner, H. (2001). Characterization of a human preadipocyte cell strain with high capacity for adipose differentiation. International journal of obesity and related metabolic disorders : journal of the International Association for the Study of Obesity *25,* 8-15.

Wadden, T. A., Webb, V. L., Moran, C. H., and Bailer, B. A. (2012). Lifestyle modification for obesity: new developments in diet, physical activity, and behavior therapy. Circulation 125, 1157-1170.

Wajchenberg, B. L. (2000). Subcutaneous and visceral adipose tissue: their relation to the metabolic syndrome. Endocrine reviews *21,* 697-738.

Waki, H., Park, K. W., Mitro, N., Pei, L., Damoiseaux, R., Wilpitz, D. C., Reue, K., Saez, E., and Tontonoz, P. (2007). The small molecule harmine is an antidiabetic cell-type-specific regulator of PPARgamma expression. Cell metabolism *5,* 357-370.

Waki, H., Park, K. W., Mitro, N., Pei, L., Damoiseaux, R., Wilpitz, D. C., Reue, K., Saez, E., and Tontonoz, P. (2007). The small molecule harmine is an antidiabetic cell-type-specific regulator of PPARgamma expression. Cell metabolism *5,* 357-370.

Wanet, A., Arnould, T., Najimi, M., and Renard, P. (2015). Connecting Mitochondria, Metabolism, and Stem Cell Fate. Stem cells and development *24,* 1957-1971.

Wanet, A., Remacle, N., Najar, M., Sokal, E., Arnould, T., Najimi, M., and Renard, P. (2014). Mitochondrial remodeling in hepatic differentiation and dedifferentiation. The international journal of biochemistry & cell biology *54,* 174-185.

Wang, C. H., Wang, C. C., Huang, H. C., and Wei, Y. H. (2013a). Mitochondrial dysfunction leads to impairment of insulin sensitivity and adiponectin secretion in adipocytes. The FEBS journal *280,* 1039-1050.

Wang, P. W., Kuo, H. M., Huang, H. T., Chang, A. Y., Weng, S. W., Tai, M. H., Chuang, J. H., Chen, I. Y., Huang, S. C., Lin, T. K., and Liou, C. W. (2014). Biphasic response of mitochondrial biogenesis to oxidative stress in visceral fat of diet-induced obesity mice. Antioxidants & redox signaling *20,* 2572-2588.

Wang, Q. A., Tao, C., Gupta, R. K., and Scherer, P. E. (2013b). Tracking adipogenesis during white adipose tissue development, expansion and regeneration. Nature medicine *19,* 1338-1344.

Wang, Q. A., Tao, C., Jiang, L., Shao, M., Ye, R., Zhu, Y., Gordillo, R., Ali, A., Lian, Y., Holland, W. L., Gupta, R. K., and Scherer, P. E. (2015). Distinct regulatory mechanisms governing embryonic versus adult adipocyte maturation. Nature cell biology *17,* 1099-1111.

Weisberg, S. P., McCann, D., Desai, M., Rosenbaum, M., Leibel, R. L., and Ferrante, A. W. (2003). Obesity is associated with macrophage accumulation in adipose tissue. The Journal of clinical investigation *112,* 1796-1808.

Weyer, C., Foley, J. E., Bogardus, C., Tataranni, P. A., and Pratley, R. E. (2000). Enlarged subcutaneous abdominal adipocyte size, but not obesity itself, predicts type II diabetes independent of insulin resistance. Diabetologia *43,* 1498-1506.

White, U. A., and Stephens, J. M. (2009). Transcriptional factors that promote formation of white adipose tissue. Molecular and cellular endocrinology *318,* 10–14.

Wilson-Fritch, L., Burkart, A., Bell, G., Mendelson, K., Leszyk, J., Nicoloro, S., Czech, M., and Corvera, S. (2003). Mitochondrial biogenesis and remodeling during adipogenesis and in response to the insulin sensitizer rosiglitazone. Molecular and cellular biology *23,* 1085-1094.

Wilson-Fritch, L., Nicoloro, S., Chouinard, M., Lazar, M. A., Chui, P. C., Leszyk, J., Straubhaar, J., Czech, M. P., and Corvera, S. (2004). Mitochondrial remodeling in adipose tissue associated with obesity and treatment with rosiglitazone. The Journal of clinical investigation *114,* 1281-1289.

Wolins, N. E., DeHaan, K. N., Cifarelli, V., and Stoeckman, A. K. (2018). Normalized neutral lipid quantitation by flow cytometry. Journal of lipid research *59,* 1294-1300.

Wolins, N. E., Quaynor, B. K., Skinner, J. R., Tzekov, A., Park, C., Choi, K., and Bickel, P. E. (2005). OP9 mouse stromal cells rapidly differentiate into adipocytes: characterization of a useful new model of adipogenesis. Journal of lipid research *47,* 450-460.

Wong, J. S. C., Chu, W. K., Li, B. F., Pang, C. P., and Chong, K. K. (2018). Depot-specific characteristics of adipose tissue-derived stromal cells in thyroid-associated orbitopathy. The British journal of ophthalmology *102,* 1173-1178.

Wu, C. L., Diekman, B. O., Jain, D., and Guilak, F. (2012). Diet-induced obesity alters the differentiation potential of stem cells isolated from bone marrow, adipose tissue and infrapatellar fat pad: the effects of free fatty acids. International journal of obesity (2005) *37,* 1079-1087.

Wu, Z., Puigserver, P., Andersson, U., Zhang, C., Adelmant, G., Mootha, V., Troy, A., Cinti, S., Lowell, B., Scarpulla, R. C., and Spiegelman, B. M. (1999). Mechanisms controlling mitochondrial biogenesis and respiration through the thermogenic coactivator PGC-1. Cell *98,* 115-124.

Wu, Z., Rosen, E. D., Brun, R., Hauser, S., Adelmant, G., Troy, A. E., McKeon, C., Darlington, G. J., and Spiegelman, B. M. (1999). Cross-regulation of C/EBP alpha and PPAR gamma controls the transcriptional pathway of adipogenesis and insulin sensitivity. Molecular cell *3,* 151-158.

Wu, Z., Xie, Y., Morrison, R. F., Bucher, N. L., and Farmer, S. R. (1998). PPARgamma induces the insulin-dependent glucose transporter GLUT4 in the absence of C/EBPalpha during the conversion of 3T3 fibroblasts into adipocytes. The Journal of clinical investigation *101,* 22-32.

Xue, R., Wan, Y., Zhang, S., Zhang, Q., Ye, H., and Li, Y. (2013). Role of bone morphogenetic protein 4 in the differentiation of brown fat-like adipocytes. American journal of physiology. Endocrinology and metabolism *306,* E363-72.

Ye, J. M., Dzamko, N., Cleasby, M. E., Hegarty, B. D., Furler, S. M., Cooney, G. J., and Kraegen, E. W. (2004). Direct demonstration of lipid sequestration as a mechanism by which rosiglitazone prevents fatty-acid-induced insulin resistance in the rat: comparison with metformin. Diabetologia *47,* 1306-1313.

Yeh, W. C., Cao, Z., Classon, M., and McKnight, S. L. (1995). Cascade regulation of terminal adipocyte differentiation by three members of the C/EBP family of leucine zipper proteins. Genes & development *9,* 168-181.

Yehuda-Shnaidman, E., Buehrer, B., Pi, J., Kumar, N., and Collins, S. (2010). Acute stimulation of white adipocyte respiration by PKA-induced lipolysis. Diabetes *59,* 2474-2483.

Yuan, C., Chakraborty, S., Chitta, K. K., Subramanian, S., Lim, T. E., Han, W., Bhanu Prakash, K. N., and Sugii, S. (2019). Fast Adipogenesis Tracking System (FATS)-a robust, high-throughput, automation-ready adipogenesis quantification technique. Stem cell research & therapy *10,* 38.

Zaragosi, L. E., Wdziekonski, B., Villageois, P., Keophiphath, M., Maumus, M., Tchkonia, T., Bourlier, V., Mohsen-Kanson, T., Ladoux, A., Elabd, C., Scheideler, M., Trajanoski, Z., Takashima, Y., Amri, E. Z., Lacasa, D., Sengenes, C., Ailhaud, G., Clement, K., Bouloumie, A., Kirkland, J. L., and Dani, C. (2010). Activin a plays a critical role in proliferation and differentiation of human adipose progenitors. Diabetes *59,* 2513-2521.

Zhang, H. H., Huang, J., Duvel, K., Boback, B., Wu, S., Squillace, R. M., Wu, C. L., and Manning, B. D. (2009). Insulin stimulates adipogenesis through the Akt-TSC2-mTORC1 pathway. PloS one *4,* e6189.

Zhang, J. W., Klemm, D. J., Vinson, C., and Lane, M. D. (2003). Role of CREB in transcriptional regulation of CCAAT/enhancer-binding protein beta gene during adipogenesis. The Journal of biological chemistry *279,* 4471-4478.

Zhang, Y., Marsboom, G., Toth, P. T., and Rehman, J. (2013). Mitochondrial respiration regulates adipogenic differentiation of human mesenchymal stem cells. PloS one *8,* e77077.

Zheng, X., Boyer, L., Jin, M., Mertens, J., Kim, Y., Ma, L., Ma, L., Hamm, M., Gage, F. H., and Hunter, T. (2016). Metabolic reprogramming during neuronal differentiation from aerobic glycolysis to neuronal oxidative phosphorylation. eLife *5,* e13374.

Zhou, S., Eid, K., and Glowacki, J. (2003). Cooperation between TGF-beta and Wnt pathways during chondrocyte and adipocyte differentiation of human marrow stromal cells. Journal of bone and mineral research: the official journal of the American Society for Bone and Mineral Research *19,* 463-470.

APPENDICES

Preface

Besides working on the "Aberrant metabolic and signaling checkpoints underlie impaired stem cell function in human obesity" project described in this thesis, I also led a collaborative project that our lab had with an industry partner, Agilent Technologies Inc.

The collaborative project involved studying ***metabolic check points as cells undergo differentiation from human iPSCs to sensory neurons***.

Our lab developed a novel multistage differentiation protocol for induced pluripotent stem cells (iPSCs) that produced a pure sensory neuron population, which exhibited the expression of peripheral sensory neuron markers and was functionally active. Using this protocol, I performed continuous cellular metabolic analyses during the neuronal differentiation timeline and observed dynamic metabolic changes over the differentiation time course. The metabolic shifts were validated by performing orthogonal assays such as qPCR and immunofluorescent stainings. Our results indicated that dynamic cellular metabolic changes could serve as potential checkpoints for tracing sensory neuronal differentiation and could provide indications of a successful differentiation protocol at very early timepoints. We also observed that a simple substitution of carbon source significantly improved the differentiation efficiency of NPCs from iPSCs, revealing the impact that media components have in deciding stem cell fates.

The results were divided into two application notes by Agilent Technologies:

Application Note 1: ***Metabolic Phenotyping to Identify Cellular Transitions During Early Neuronal Differentiation from Neural Precursor Cells Using Seahorse XF Technology.***

Application Note 2: ***Glycolytic Suppression – The Impact of Metabolic Modulation on Neural Stem Cell Fate.***

Both the application notes have been published by Agilent Technologies and are presented in their original format.

For both of the application notes, I performed all experiments, which included: maintaining and differentiating iPSCs into neural progenitor cells (NPCs) and subsequently, into peripheral sensory neurons; performing cellular metabolic analyses (glycolysis and mitochondrial respiration) along the course of differentiation; and validating observed metabolic changes by performing orthogonal assays such as quantitative PCR and immunofluorescent staining for stage-specific markers. Data analysis for all metabolism assays was performed by the Agilent scientist, Dr. Yoonseok Kam. I wrote the application notes together with Dr. Yoonseok Kam and Ned Jastromb. All reagents for the metabolism assays were provided by Agilent Technologies Inc. I have also presented these results at a Nano symposium at the annual Society for Neuroscience meeting (2018).

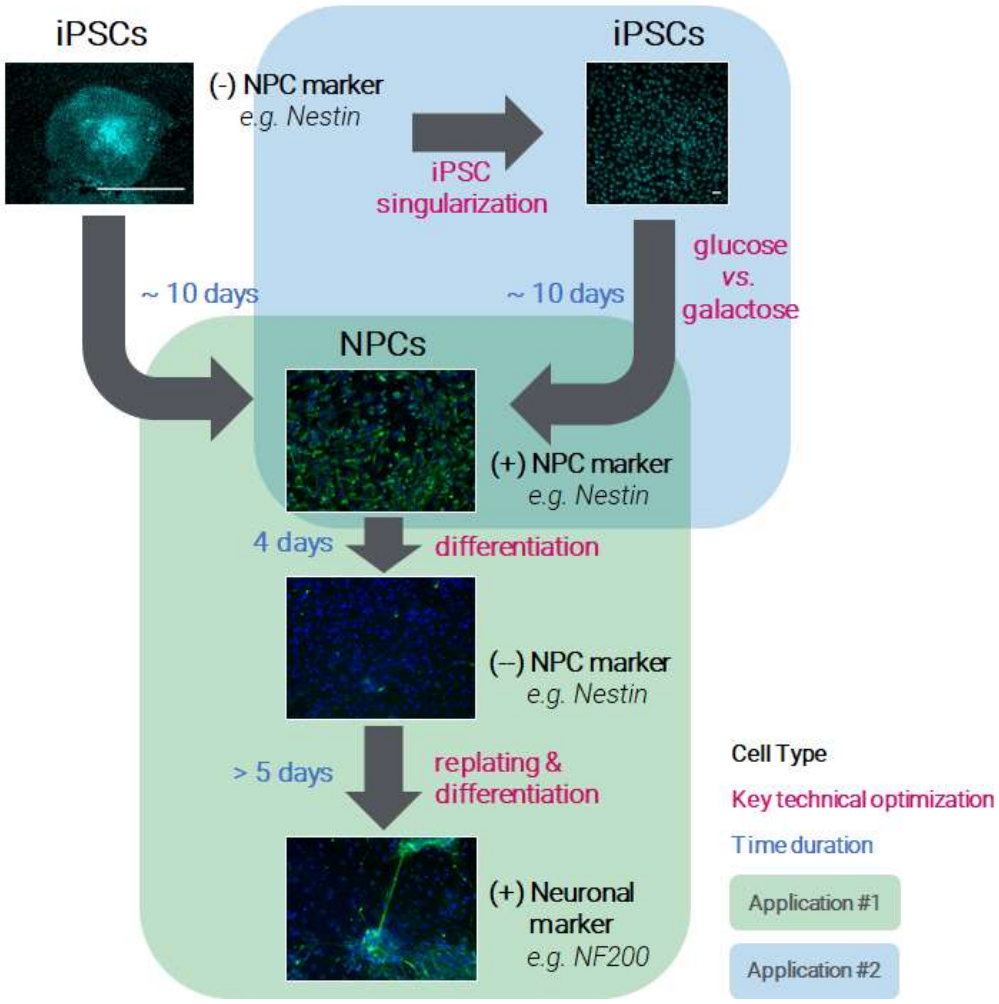

Fig. 1: Summary of the collaborative project for studying metabolic checkpoints during differentiation of iPSCs to sensory neurons.

APPENDIX I

Metabolic phenotyping to identify cellular transitions during early neuronal differentiation from neural precursor cells using Seahorse XF technology

This application note uncovers the metabolic trajectory prompting neuronal differentiation and details a metabolic analysis during the early differentiation of nociceptor sensory neurons from committed neural precursor/stem cells (NPCs) to premature neurons. It includes cell preparation protocols for XF analysis, Ara-C-mediated negative selection of highly proliferative cell types, and data normalization by genomic DNA.

Application Note
Stem Cell Biology

Agilent
Trusted Answers

Metabolic Phenotyping to Identify Cellular Transitions During Early Neuronal Differentiation from Neural Precursor Cells Using Seahorse XF Technology

Authors

Kanwaldeep Singh
and Eva Szabo
Stem Cell and Cancer Research Institute, McMaster University, Hamilton, Ontario, CA

Yoonseok Kam
Agilent Technologies, Inc

Abstract

In vitro stem cell differentiation systems enable the examination of the essential factors regulating cell differentiation and the generation of fully functional cells. Generation of functional cells from pluripotent cells such as induced pluripotent stem cells (iPSCs) involves dynamic changes in cellular metabolism. These metabolic changes occur continuously from the initial steps of cell commitment to differentiation and maturation, and thus time-dependent live cell analysis of cellular metabolism through the process is desired. Agilent Seahorse XF technology can provide a continuous and quantitative analysis platform to monitor the phenotypic changes of cell metabolism. This Application Note details a metabolic analysis during the early differentiation of nociceptor sensory neurons from committed neural precursor/stem cells (NPCs) to premature NPCs. It includes cell preparation protocols for XF analysis, Ara-C-mediated negative selection of highly proliferative cell types, and data normalization by genomic DNA. The data produced revealed a persistent downregulation of glycolysis in NPCs following the commitment stage in contrast to mitochondrial respiration, which showed more dynamic changes. This application model can be expanded for analysis over a prolonged differentiation period, through maturation and to the terminally differentiated neurons. It can also be adapted to studies on time-dependent metabolic changes of other stem cells, and more particularly in assessing cellular dynamics like metabolic oscillation.

Introduction

The development of reprogramming technologies that convert somatic cells into iPSCs has led to the creation of patient specific cell types and in vitro cell-based disease models. However, a major challenge is the lack of directed differentiation protocols for the generation of a pure population of the cell type of interest from PSCs[1]. As such, the differentiated cells that are produced are highly heterogeneous. This heterogeneity makes it difficult to evaluate the exact contribution of a specific cell type to disease development or to qualitatively analyze the molecular and metabolic trajectory of the differentiated cell types. Previous studies have identified a functional link between metabolism and stem cell development[2-3]. For example, a few recent studies have shown that NPCs have different metabolic profiles than their mature central nervous system (CNS) counterparts. This difference suggests that metabolic pathways have a regulatory role in stem cell fate decisions[4-5].

Numerous studies have used iPSCs to derive CNS neurons[6] and the subtypes of these neurons that are central for modeling neurodegenerative diseases, including Parkinson's disease and amyotrophic lateral sclerosis[7-10]. However, only a few recent studies report methods to differentiate PSCs into neurons of the peripheral nervous system (PNS)[11-12]. Therefore, there are limited protocols describing the derivation of pure populations of specific sensory neurons of the PNS and their application for modeling neurodegenerative diseases. Understanding the metabolic requirements during normal peripheral neural development and the metabolic defects that could drive aberrant neurogenesis would provide new metabolic checkpoints during NPC differentiation and peripheral nerve maturation. This understanding would also lead to the development of targeted treatment strategies for neuropathy.

Cellular metabolic changes in live NPCs and differentiated neurons can be studied using Seahorse XF technology. Mitochondrial function of those cells can be measured by using the XF Cell Mito Stress Test in which mitochondrial respiration activity is analyzed by monitoring real-time oxygen consumption rate (OCR) with serial administrations of mitochondrial complex inhibitors. Glycolytic activity of the cells can be assessed by using the XF Glycolytic Rate Assay, which measures extracellular acidification rate (ECAR) and calculates proton efflux rate (PER) out of it. More particularly, by applying HEPES buffered assay conditions, PER solely dependent on glycolysis can be assessed as glycolytic PER (glycoPER).

Results

Measurements of mitochondrial respiration and glycolysis in early differentiating NPCs

Initially, human iPSCs were differentiated towards an NPC phenotype, which were then banked and expanded as needed. The NPCs were then exposed to conditions that induce peripheral neural differentiation, through treatment with inhibitors and small molecules, such as CHIR, SU5402, and DAPT for the first four days. The differentiating cells were then dissociated and replated in the presence or absence of Ara-C and growth factors NGF and GDNF (Figure 1A; see methods for specific details). Ara-C treatment was performed to remove the proliferating cells, which tend to overtake the differentiating neural cultures, thus promoting a more homogeneous neural culture. Homogeneity in the differentiating cultures is required for accurate and representative measurement of molecular and functional parameters.

As shown in Figure 1, the metabolism of NPCs from day 0 to day 9 was compared after normalization. As differentiation of the NPCs progressed, cells became less energetic with the glycolytic rate, glycoPER decreasing more significantly than mitochondrial respiration rate, OCR. This decrease suggests that as stem/progenitor cells start differentiating they undergo a metabolic switch where glycolysis is downregulated.

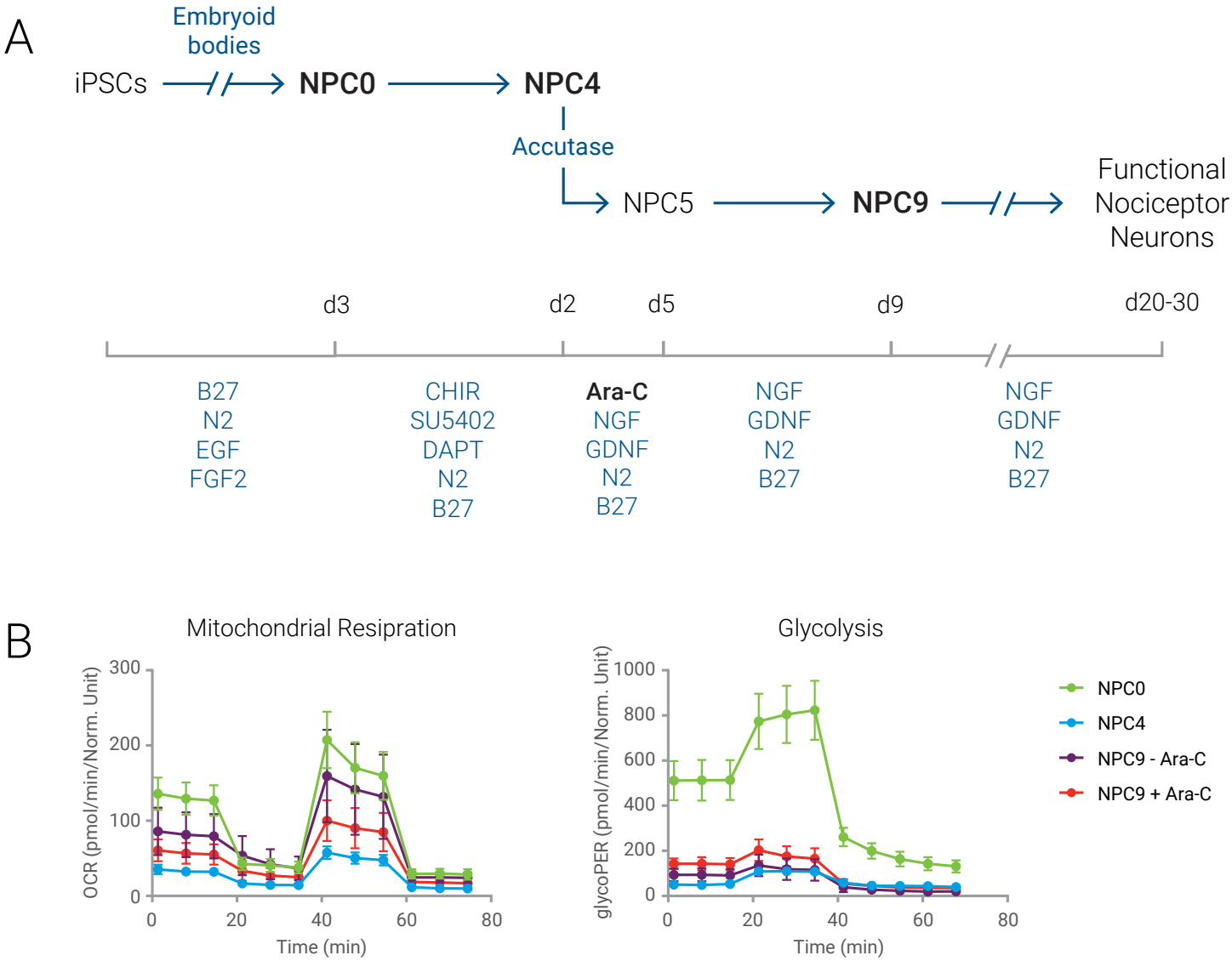

Figure 1. Sensory neuron differentiation timeline and cellular metabolism profile during early NPC differentiation. (**A**) Schematic showing the differentiation protocol from iPSCs to functional sensory neurons: Differentiation of iPSCs to NPCs was performed using the embryoid body procedure as mentioned in the materials and methods section. NPCs undergoing differentiation were dissociated at day 4 and replated on Matrigel coated cell culture dishes with and without Ara-C. (**B**) Metabolic changes during early NPC differentiation: mitochondrial respiration and glycolysis were measured by the XF Cell Mito Stress Test and the XF Glycolytic Rate Assay Kits respectively at specific time points during early NPC differentiation. Error bars reported as mean ± standard deviation (n=26).

Metabolic transition during the early differentiation stages from NPCs

As differentiation progressed from day 0 to day 9, a significant drop in basal and compensatory glycolysis was observed. This drop suggests that the cells dependence on glycolysis is downregulated within the first four days of differentiation (Figure 2A). In addition, during these first four days of NPC differentiation basal oxygen consumption rates and spare respiratory capacity also decreased. However, by day 9 of differentiation oxygen consumption levels and spare respiratory capacity recovered to similar levels to those levels observed for undifferentiated NPCs (Figure 2B). This recovery may be indicative of metabolic oscillations during the early differentiation. It is important to note that in the presence of Ara-C, which removes proliferating cells, the recovery of mitochondrial respiration was slower. This slower recovery was likely due to an effect of the Ara-C treatment on the cells resulting in slower recovery.

To demonstrate that NPCs followed the expected differentiation trajectory, gene expression of NPC markers (Nestin, Lin28B, Hes1, and NCAM2), mature general neuronal markers (Notch1, NeuN, NeuroD1), and peripheral neuronal markers (NF200) were examined (Figure 2C and D). As differentiation progressed over the nine-day timeline, the expression of NPC markers significantly decreased (Figure 2C) and neuronal marker expression gradually increased (Figure 2D).

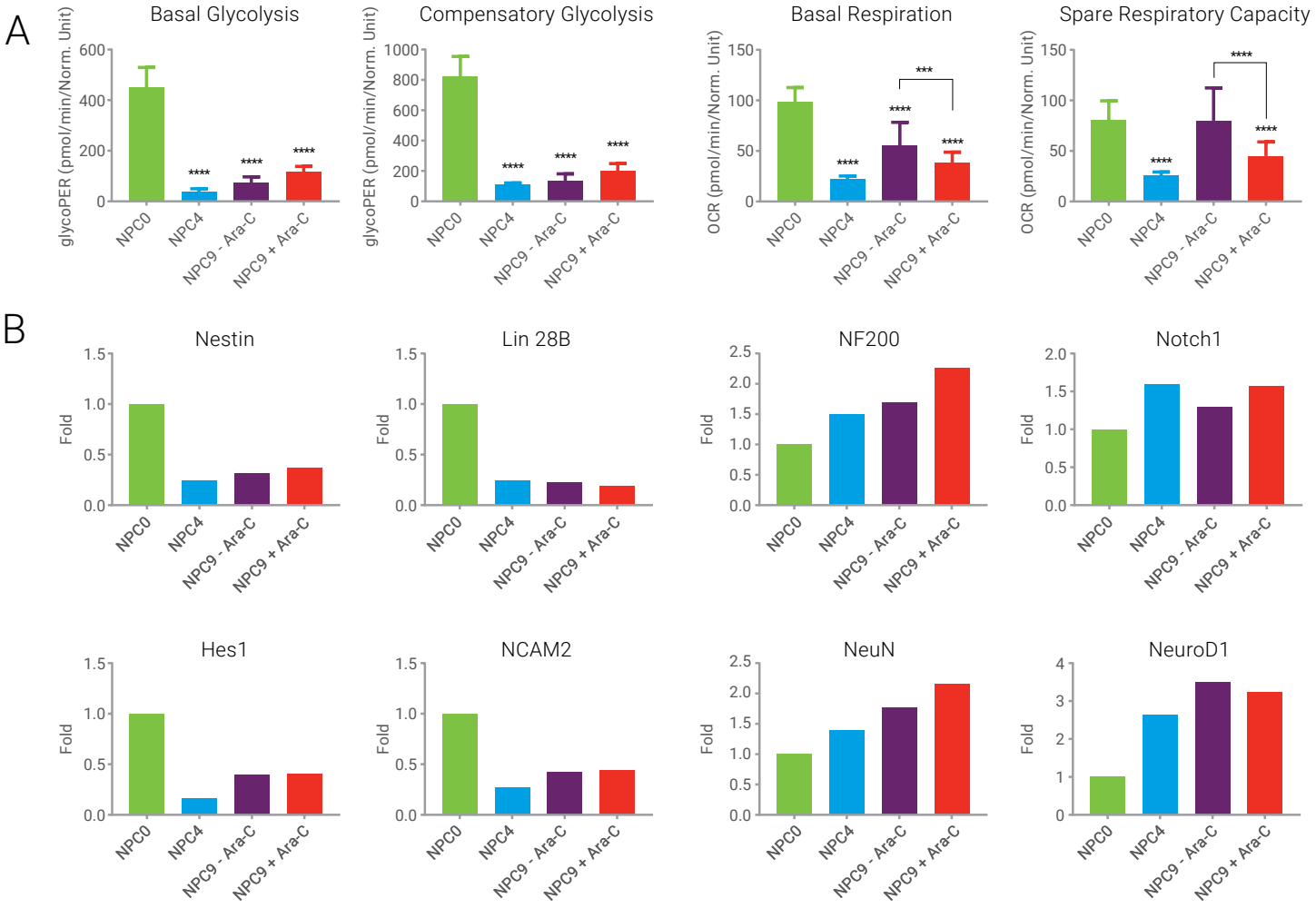

Figure 2. Cellular metabolism parameters correspond with neuronal gene expression during early NPC differentiation. (**A**) Glycolysis was measured at specific time points using the XF Glycolytic Rate Assay Kit. Basal and compensatory glycolysis was calculated using the report generator (Agilent) and the data was normalized to total cellular DNA content. (**B**) Mitochondrial respiration parameters, basal OCR, and spare respiratory capacity were calculated using the XF Cell Mito Stress Test Kit at and the report generator (Agilent). (**C**) Gene expression for NPC markers: Nestin, Lin28B, Hes1, and NCAM2 were measured at different time points during the NPC differentiation by qRT-PCR and fold change w.r.t. day 0 NPCs was calculated. (**D**) Gene expression data for neuronal markers: NF200, Notch1, NeuN, and NeuroD1. (****p<0.00001)

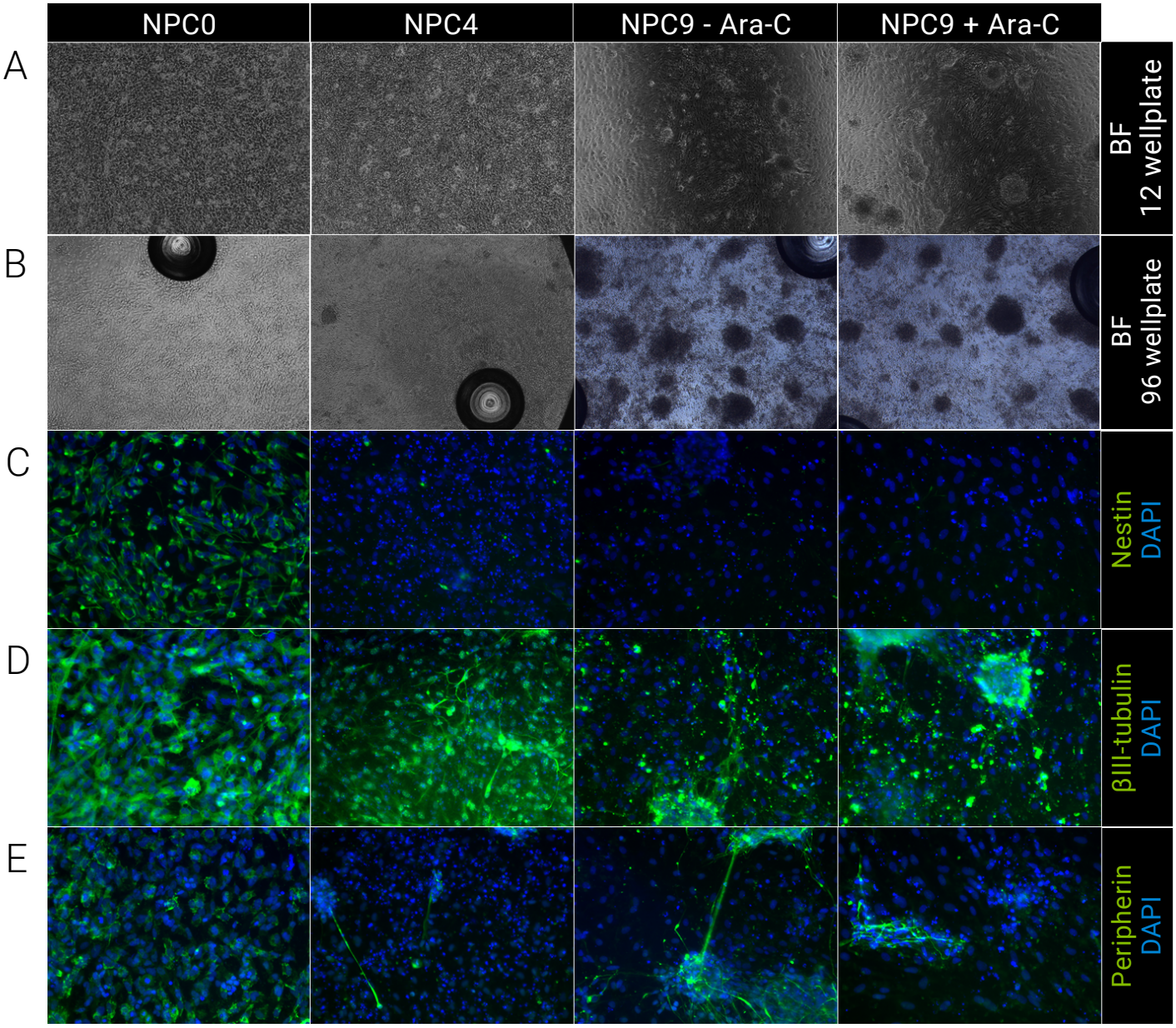

Figure 3. Phenotypic changes during early NPC differentiation. Representative 4X phase contrast images of the cells at specified time points during early NPC differentiation in 12-well plates (**A**) and in XF96 Seahorse plates (**B**). Cells were also stained with an NPC marker, Nestin (**C**), and the neuronal markers βIII-tubulin (**D**) and Peripherin (**E**). DAPI was used to stain the nuclei. (n=3)

The differentiation from NPCs to day 9 maturing neurons was evaluated by immunofluorescence analysis to demonstrate the presence of the neuronal markers at the protein level (Figure 3). As differentiation progresses the NPCs change morphology, beginning to form cell clumps by day 4 and axonal projections by day 9 (Figure 3A and B). As NPCs differentiate they lose expression of the NPC marker, Nestin (Figure 3C), show localization of the neuronal marker, beta-III tubulin (Figure 3D), and gain expression of the peripheral neuronal marker, Peripherin (Figure 3E).

Overall, comparison of mitochondrial respiration to mitochondrial independent glycolysis demonstrates that as differentiation progresses from day 0 to day 9 there is a clear shift in the metabolic dependence of the cells from glycolysis to mitochondrial respiration (Figure 4).

Discussion

Metabolic analysis and surrogate neuronal marker expression were performed on different days (0, 4, 5, and 9) during the initial peripheral neural differentiation timeline. It is critical that cell number per well is optimized, and a robust normalization method for the data points (i.e. protein or DNA content) is established. There should also be rigorous consideration given to the heterogeneity of the differentiating culture as numerous cell types are emerging alongside the peripheral neurons. At the early stage of neuronal differentiation, heterogeneity of the cultures is evidenced by morphological differences and well-to-well variation of the metabolic measurements. Therefore, it is important to monitor the cellular morphology of NPCs and differentiating cultures as an indicator of cellular health to minimize resources spent on metabolic analysis. If the cells are unhealthy, the metabolic profiles will reflect this by showing minimal OCR and glycoPER with substantial fluctuations between readings.

Another aspect of metabolic profiling that should be considered is the possibility that OCR and glycoPER measurements will oscillate during the differentiation timeline. The OCR showed oscillations between day 0 to day 9, which were similar to those oscillations observed in the numerous differentiation protocols examining gene expression profiles through the differentiation timeline. Thus, there may be multiple metabolic switches as the cells mature into peripheral neurons, which would be missed if metabolic parameters were only analyzed at the initial and final stage of differentiation. Establishing a robust protocol that improves purity of the differentiating neurons is also critical for the reliable and reproducible measurement of metabolic transitions during differentiation. A homogeneous population of neurons would also avoid the presence of other cell types masking any metabolic changes.

Conclusion

Metabolic profiling using the XF Cell Mito Stress Test and the XF Glycolytic Rate Assay to measure mitochondrial respiration and glycolysis in differentiating neurons demonstrated that this technology can be used to identify metabolic transitions that mirror cellular transitions during the neuronal differentiation timeline. These assays therefore provide a robust measurement, which is a step towards predicting the differentiation trajectory of peripheral neurons.

Materials and methods

NPCs culture and differentiation into peripheral sensory neurons

Human iPSC derived NPCs were cultured on Matrigel (Corning, 354234) coated cell culture dishes in DMEM/F12 media (Corning, 10-090-CV) supplemented with 1X N2 (Thermo, 17502048), 1X B27 (Thermo, 17504044), 10 ng/mL bFGF (PeproTech, 100-18B), and 50 ng/mL EGF (PeproTech, AF-100-15). For differentiation, cells were dissociated with Accutase (Corning, 25-058-CI), counted, and plated at a density of 5.6 x 106 cells/cm2 on cell culture plates coated twice with 1:15 Matrigel. The following day, neuronal differentiation was induced on a confluent NPCs monolayer with a Neurobasal media (Thermo, A3582901) containing 1X N2 (Thermo, 17502048), 1X B27 Plus (Thermo, A3582801), 10 µM DAPT (Abcam, Ab120633), 10 µM SU5402 (Cayman Chemicals, 13182), and 3 µM CHIR 99021 (Stem Cell Technologies, 72054). Differentiation was continued for five days with daily complete media changes using fresh differentiation media. At day 5 post induction, cells were dissociated with Accutase and replated on cell culture dishes coated twice with 1:15 Matrigel in Neurobasal media supplemented with 1X N2, 1X B27 Plus (Thermo, A3582801), 25 ng/mL NGF (PeproTech, 450-01), and 10 ng/mL GDNF (PeproTech, 450-10) with and without 10 µM Ara-C (Sigma, C1768) for 24 hours. Media was replaced next day and every second day thereafter.

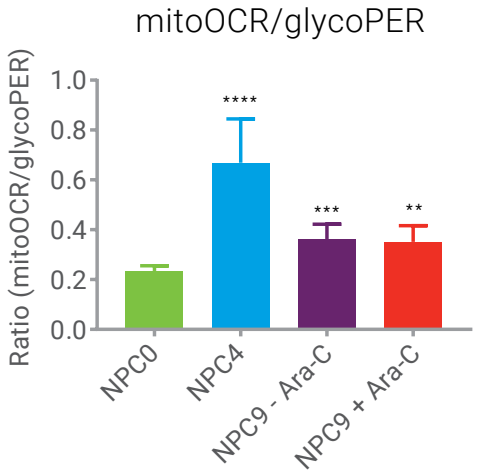

Figure 4. Glycolysis to mitochondrial respiration shift during early NPC differentiation. Ratios of mitochondrial OCR (mitoOCR) to glycolytic PER (glycoPER) were calculated from the XF Glycolytic Rate Assay data at the specific time points using the GRA assay report generator. Error bars reported as mean ± standard deviation (n=26; ****p<0.00001; *** p<0.0001; **p<0.001).

RNA isolation, cDNA synthesis, and quantitative real time PCR

NPCs were plated in 6-well plates and differentiated as described. RNA isolation was performed at specified time points along the differentiation course by Norgen RNA Isolation Plus kit (Norgen Biotek, 48400) following manufacturer's protocol. For each reverse transcription reaction, 1 µg of RNA was used, with the Bioline SensiFast cDNA synthesis kit (Bioline, BIO-65054) as per the kit protocol. 1 µL of cDNA was used as template for each qRT-PCR reaction using gene-specific primers for tracking downregulation of NPC markers and upregulation of neuronal markers along the differentiation timeline.

Cellular metabolic profiling

NPCs were plated and differentiated in XF96 microplates as described earlier. For day 0, XF Cell Mito Stress Test and XF Glycolytic Rate Assay, NPCs were plated at a density of 6 x 10^4 cells/well on Matrigel coated XF96 seahorse plates on day 1. In previous cell number optimization experiments, 6 x 10^4 cells/well was found to be the optimal cell density for the XF Cell Mito Stress Test and the XF Glycolytic Rate Assay. For day 4 measurements, NPCs were plated at 6 x 10^4 cells/well on day 1 and differentiated for four days as mentioned previously. For day 9 measurements, NPCs were plated at 4.8 x 10^6 cells/well on Matrigel coated 6-well plates and differentiated for five days as mentioned previously. On day 5, the cells were dissociated with Accutase and replated on Matrigel-coated XF96 seahorse plates, with and without Ara-C, and maintained until day 9 as mentioned previously. At specific time points, cells were rinsed twice with the complete XF assay media and XF Cell Mito Stress Test and the XF Glycolytic Rate Assay were performed as per the instructions provided with the respective kits. XF assay media for the XF Cell Mito Stress Test was XF DMEM base media without phenol red (Agilent, 103335-100) supplemented with 2.5 mM L-Glutamine, 1 mM sodium pyruvate, and 17.5 mM glucose. For the XF Glycolytic Rate Assay, the same media was further supplemented with 5 mM HEPES, pH 7.4 (Agilent, 103337-100). The pH of all media was adjusted to 7.4 at 37 °C. An optimized FCCP concentration (0.5 µM) was used for the XF Cell Mito Stress Test. OCR and glycoPER readouts were normalized to cellular DNA content after XF assays. Cellular DNA content was measured using CyQuant Cell Proliferation assay kit (Thermo, C7026) following the manufacturer's protocol.

Immunofluorescence staining

NPCs were plated in 12-well plates and differentiated as described. Cells were fixed at specified time points using BD Cytofix/CytoPerm kit (BD Bioscience, 554714). Upon fixation, cells were blocked in 10 % normal donkey serum for 1 hour at room temperature followed by overnight incubation with primary unconjugated antibodies against Nestin (Abcam, Ab22035), NF200 (Abcam, Ab78078), and Peripherin (Abcam, Ab123576) at 4 °C. The next day, cells were washed three times and stained with Alexa Fluor-488 conjugated secondary antibodies (Thermo, A11008, A11001) at room temperature for 1 hour. Cells were washed three times, stained with DAPI (Thermo, D3571), and then imaged.

References

1. Robinton, D.A. and Daley, G.Q. The promise of induced pluripotent stem cells in research and therapy. *Nature* **481**, 295–305 (2012).
2. Ochocki, J.D. and Simon, M.C. Nutrient-sensing pathways and metabolic regulation in stem cells. *The Journal of cell biology* **203**, 23–33 (2013).
3. Shyh-Chang, N., et al. Stem cell metabolism in tissue development and aging. *Development* 140, 2535–2547 (2013).
4. Kim, D.Y., et al. Metabolic circuits in neural stem cells. *Cellular and molecular life sciences : CMLS* **71**, 4221–4241 (2014).
5. Knobloch, M., et al. Metabolic control of adult neural stem cell activity by Fasn-dependent lipogenesis. *Nature* **493**, 226–230 (2013).
6. Engel, M., et al. Common pitfalls of stem cell differentiation: a guide to improving protocols for neurodegenerative disease models and research. *Cellular and molecular life sciences : CMLS* **73**, 3693–3709 (2016).
7. Kriks, S., et al. Dopamine neurons derived from human ES cells efficiently engraft in animal models of Parkinson's disease. *Nature* **480**, 547–551 (2011).
8. Park, S., et al. Generation of dopaminergic neurons in vitro from human embryonic stem cells treated with neurotrophic factors. *Neuroscience letters* **359**, 99–103 (2004).
9. Maroof, A.M., et al. Directed differentiation and functional maturation of cortical interneurons from human embryonic stem cells. *Cell stem cell* **12**, 559–572 (2013).
10. Dimos, J.T., et al. Induced pluripotent stem cells generated from patients with ALS can be differentiated into motor neurons. *Science* **321**, 1218–1221 (2008).
11. Lee, J.H., et al. Single Transcription Factor Conversion of Human Blood Fate to NPCs with CNS and PNS Developmental Capacity. *Cell reports* **11**, 1367–1376 (2015).
12. Chambers, S.M., et al. Combined small-molecule inhibition accelerates developmental timing and converts human pluripotent stem cells into nociceptors. *Nature biotechnology* **30**, 715–720 (2012).

www.agilent.com/chem/stemcells

Printed in the USA, May 31, 2018
5991-9493EN

APPENDIX II

Glycolytic suppression – the impact of metabolic modulation on neural stem cell fate.

This application note illustrates the significance of glycolytic shutdown during early neural differentiation from induced pluripotent stem cells. It also highlights the affect that carbon source modification has on deriving neural cell lineages from stem cells, and particularly describes the effect of switching carbon source in the differentiation media from glucose to galactose on the neural differentiation efficiency and the neural precursor cell yield as the stem cells exit pluripotency.

Application Note
Stem Cell Research

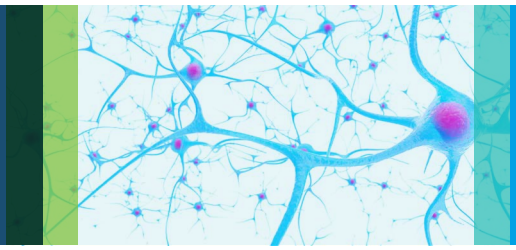

Agilent
Trusted Answers

Glycolytic Suppression - The Impact of Metabolic Modulation on Neural Stem Cell Fate

Authors

Kanwaldeep Singh*,
McMaster University,
Hamilton, Ontario, Canada

Ned Jastromb,
Agilent Technologies, Inc.
Cell Analysis Division,
Lexington, MA USA

Yoonseok Kam,
Agilent Technologies, Inc.
Cell Analysis Division,
Lexington, MA USA

George W. Rogers
Agilent Technologies, Inc.
Cell Analysis Division,
La Jolla, CA USA

Abstract

Cellular metabolism is emerging as a critical factor in stem cell research with recent reports suggesting that both metabolic status and cell culture conditions can significantly alter the differentiation trajectory of stem cells. *In vitro* metabolic profiling provides information to identify key metabolic changes associated with stem cell differentiation. Agilent Seahorse XF technology enables real-time measurement of glycolytic and mitochondrial function along the cell differentiation axis. By changing the metabolic environment in the design of differentiation experiments, metabolic profiling can be incorporated to probe cell function, and more importantly, to guide improved differentiation outcomes. Here, an assay design is introduced for sequential metabolic profiling during induced pluripotent stem cell (iPSC) differentiation toward neural progenitor cells (NPCs) using human skin fibroblast-derived iPSCs, singularized and cultured *in vitro*. Results suggest that metabolic modulation during stem cell differentiation can affect stem cell specification, as well as the final differentiated cell yield and quality. This design can be applied to better understand the interrelationship between metabolic poise and differentiation, thus enabling the development of improved differentiation protocols.

Introduction

Human induced pluripotent stem cells (iPSCs) provide an ideal platform for patient-specific disease modeling and regenerative therapies. These cells offer an unlimited patient-specific stem cell source with the potential for differentiation into unique cell types within the body[1]. Neuronal lineages are extensively explored for both disease modeling and regenerative therapeutics purposes[2-6]. A critical and transitionary step in the process of neuronal lineage formation is derivation of NPCs which have the capacity to proliferate and differentiate into most neuronal cell types within the human body. Current studies have started to decipher the molecular and metabolic checkpoints that occur during iPSC differentiation into neurons[7-10], yet, protocols to induce iPSC differentiation towards an NPC phenotype can be inefficient and yield low numbers of cells[11-15].

*with guidance from Dr. Eva Szabo's Laboratory

Recently, the use of alternative carbon sources to drive specific metabolic pathways that initiate lineage specification has been investigated[16-18]. For example, switching glucose to galactose as an alternative carbon source in the culture media results in the promotion of oxidative phosphorylation and hence, differentiation-specific pathways which ultimately direct cell fate decisions[19]. Here, the metabolic drivers for specification by use of alternative carbon sources are evaluated for the neuronal lineage by measuring both mitochondrial and glycolytic function with the Agilent Seahorse XF Cell Mito Stress Test and the Agilent Seahorse XF Glycolytic Rate Assay, respectively. Results indicate that altering the carbon source from glucose to galactose promotes switching from a glycolytic to an oxidative phosphorylation phenotype that is correlated to improved NPC differentiation from human iPSCs.

Results

Experimental design of metabolic rate measurements using singularized iPSCs *in vitro*

iPSCs derived from human skin fibroblasts were singularized to facilitate tracking of the changes in metabolic phenotype, as well as the expression of molecular markers for iPSCs and NPCs. As briefly summarized in Figure 1 and detailed in the Materials and Methods section, iPSCs were singularized and transferred to Agilent Seahorse XF96 Cell Culture Microplates and differentiated for 10 days towards NPC phenotype by sequential media changes within the XF96 plates and on conventional 12-well plates, for XF analysis and immunostaining,

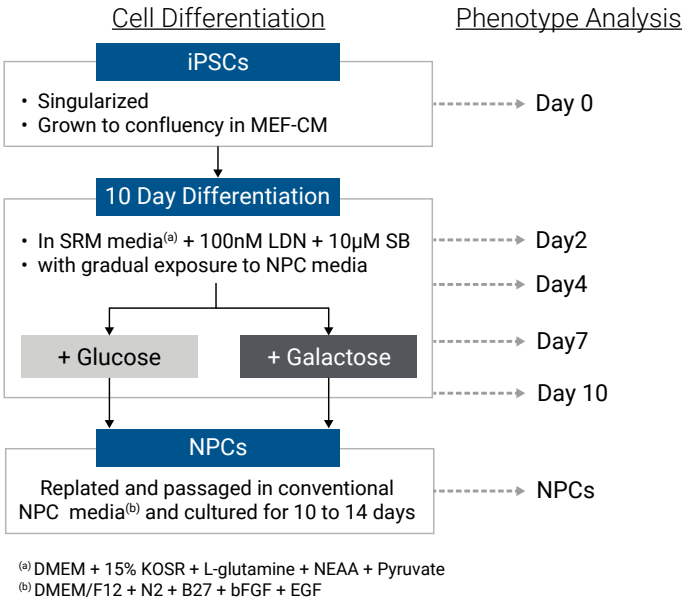

Figure 1. Schematic of the iPSC differentiation to NPC workflow, protocol, and phenotypic measurement time points. The metabolic profile and differentiation status were monitored at the indicated time points using Agilent Seahorse XF analysis and immunofluorescence staining during the differentiation process.

respectively. The singularized and monolayer-cultured iPSCs showed stable expression of the stem cell markers Oct4 and Nanog, similar to the parental colonies (Figure 2).

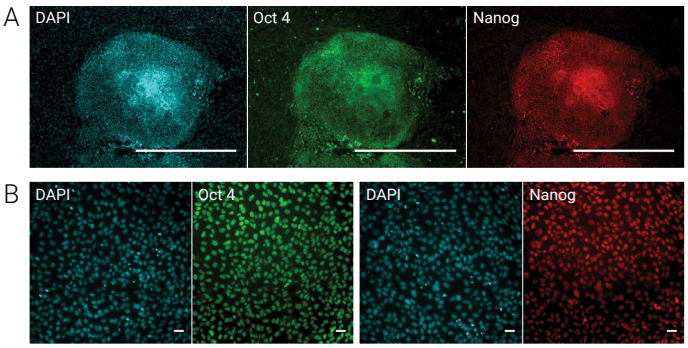

Figure 2. iPSCs in 2D culture express pluripotency markers. Representative images show expression of pluripotency markers, Oct4 and Nanog in parental iPSC colonies (A) and singularized iPSCs (B). Scale bar = 100 μm.

Replacement of glucose with galactose promotes iPSC differentiation to an NPC phenotype

It has been well established that when the major carbon source of glucose is replaced with galactose, glycolytic energy metabolism is suppressed while mitochondrial respiration remains intact[19]. Interestingly, the NPC population obtained after performance of the complete iPCS differentiation to NPC workflow/protocol (Figure 1) showed different metabolic activities depending on the carbon source supplemented during differentiation. As shown in Figures 3A-D, NPCs obtained from galactose differentiation conditions showed overall lower metabolic function when compared to Day 0 iPSCs. Metabolic parameters of basal OCR, spare respiratory capacity (SRC), basal PER and compensatory glycolysis all decreased in the presence of galactose when compared to the NPC cells obtained with glucose, which maintained a metabolic phenotype similar to the original iPSCs. Further, galactose containing media increased the Nestin-positive cells in the NPC population obtained after differentiation, indicating increased efficiency of the differentiation process (Figure 3E). In summary, this suggests that while galactose reduces metabolic activity as measured by OCR and PER, it causes an increased reliance on aerobic metabolism, and promotes faster, more efficient differentiation, as measured by Nestin expression.

Modulation of iPSC culture conditions influences iPSC differentiation quality

The improvement of differentiation quality when substituting the iPSC media with galactose was evident several days after the induction, and could be detected earlier than NPC marker expression. In the presence of galactose, the NPC differentiation appeared to be more homogeneous, with a gradual appearance of Nestin (+) cells (Figure 4A). A significant majority of the iPSCs appeared to be differentiated into Nestin (+) cells by day 10, whereas in the presence of glucose, the differentiation was heterogeneous and less

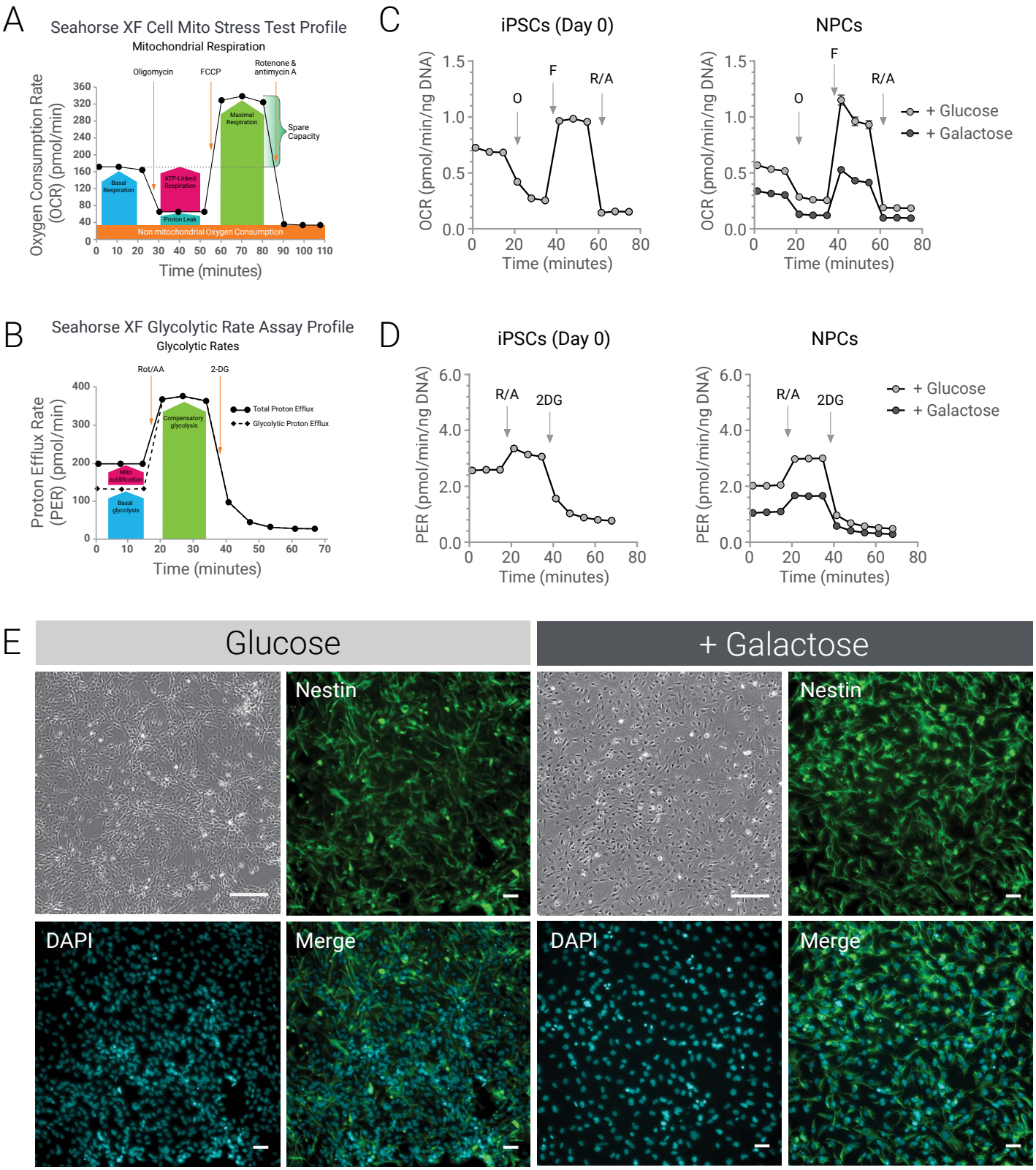

Figure 3. Metabolic function and NPC marker expression are altered by the change in carbon source. Mitochondrial and glycolytic function of iPSCs (Day 0) and resulting NPCs in the presence of glucose or galactose (Figure 1) were compared by using the Seahorse XF Cell Mito Stress Test (A, C) and Glycolytic Rate Assay (B, D). Error bars reported as mean ± S.E.M. (n = 60 for iPSCs and 20 for NPCs). (E) NPC differentiation was confirmed by immunofluorescence staining of the NPC marker, Nestin. Scale bar = 100 µm.

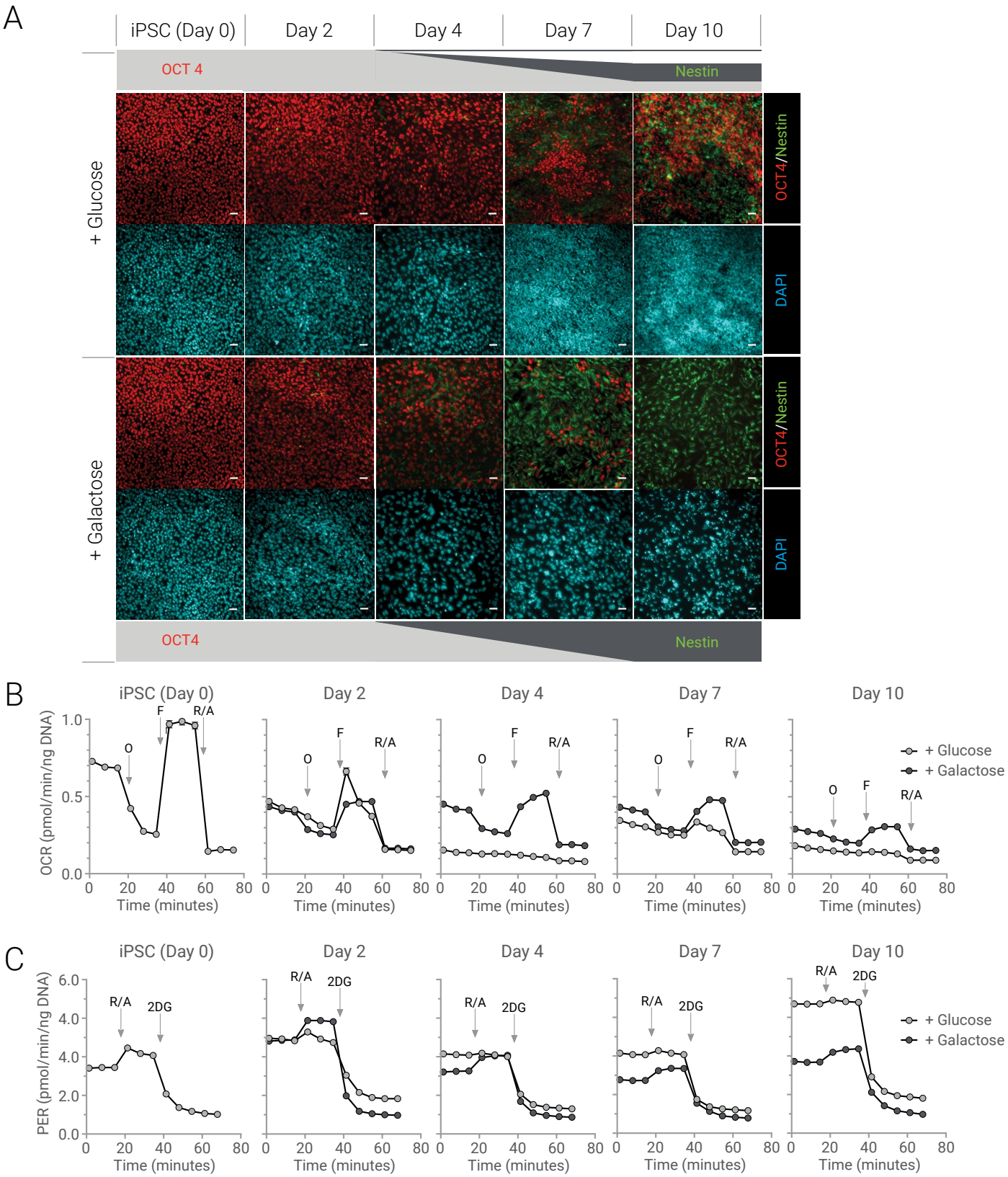

Figure 4. Carbon source change affects metabolic reprograming and the quality of differentiation from iPSCs to NPCs. Representative immunofluorescence images stained for the pluripotency marker, Oct4 and the NPC marker, Nestin at the indicated time points during differentiation in either glucose- or galactose-containing media (A). Scale bar = 100 µm. Mitochondrial respiration (B) and glycolysis (C) were traced from day 0 to day 10 of the iPCS differentiation to NPC workflow as described in Figure 1 and Materials and Methods. Error bars reported as mean ± S.E.M. (n=24 from Day 2 to Day 10 and n=60 for iPSCs).

efficient, as a significant proportion of Oct4(+) and Oct4(-)/Nestin(-) cells were still present at day 10 in the differentiation timeline (Figure 4A). Differences were also identified in metabolic functional changes (Figures 4B-C and Figure 5). In the presence of galactose, cells showed more sustained mitochondrial basal respiration and higher SRC throughout the differentiation process when compared to cells differentiated in the presence of glucose (Figure 4B and 5A-B). In contrast, mitochondrial respiration was significantly decreased in the presence of glucose, especially SRC and further, the cells showed higher basal glycolytic rates, with similar or slightly increased compensatory glycolysis (Figure 4C and 5C-D). These substantially different outcomes of the differentiation process in the presence of glucose or galactose as the main carbon source are summarized in Table 1, illustrating more rapid and efficient differentiation of iPSCs.

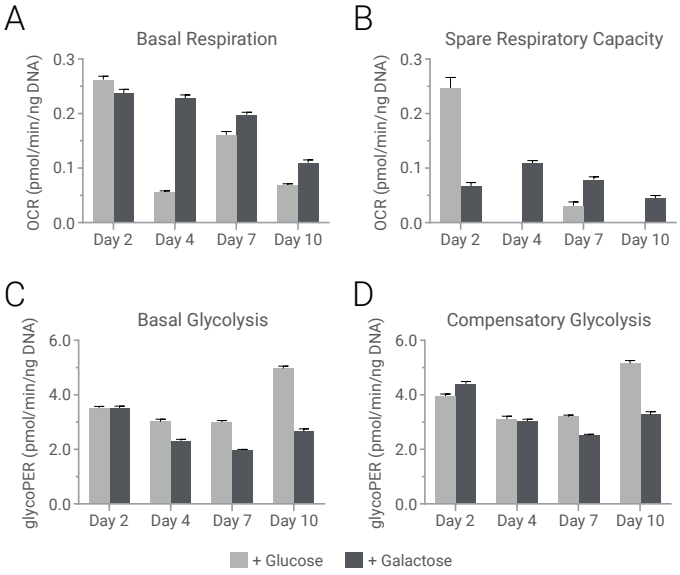

Figure 5. Differentiation-associated early metabolic phenotype transition is altered by a change in carbon source. Mitochondrial functional parameters (A, B) and glycolytic functional parameters (C, D) are compared. Significant differences were detected from day 4-10 between groups differentiated in the presence of glucose or galactose. Error bars reported as mean ± S.E.M. (n > 14).

Carbon Source		Glucose	Galactose
Cell yield on Day 10 of differentiation	Total (x10^6 cells)	8.44 ± 0.21	5.55 ± 0.21
	Viable (x10^6 cells)	2.37 ± 0.29	3.75 ± 0.22
	Viability (%)	28.0 ± 2.8	67.0 ± 3.5
NPC yield at the first passage	Total (x10^6 cells)	3.45 ± 0.14	16.47 ± 1.01
	Viable (x10^6 cells)	3.18 ± 0.18	15.30 ± 1.27 [a]
	Viability (%)	92.0 ± 0.7	92.0 ± 2.1
Time to the 1st NPC passage		18 days	4 days [b]
NPC Differentiation Efficiency		+	++++

(a) 4.8 fold increase in live NPC cell numbers obtained under Galactose condition vs. Glucose
(b) 4.5 fold increase in proliferation capacity of Day 10 populations when replated in NPC media

Table 1. The efficiency of iPSC to NPC differentiation was improved by differentiation media conditions that included galactose as a replacement for glucose as a carbon source.

Discussion

Metabolic analysis, surrogate pluripotency and early neural stem/progenitor cell marker expression were examined during the timeline of human iPSC differentiation towards an NPC. Analysis of glycolytic activity and mitochondrial respiration over the time course of differentiation demonstrated that under glucose conditions, basal respiration rates and spare respiratory capacity are significantly decreased. Further, glycolytic activity is significantly higher than that observed for galactose conditions. Conversely, under galactose conditions, basal respiration and spare respiratory capacity are maintained (albeit at decreasing rates) throughout the differentiation timeline, with a concomitant decrease in glycolytic function. The results in Table 1 illustrate that by replacing glucose with galactose during the early stage of differentiation (i.e. exit from pluripotency) the differentiation timeline was accelerated (4 vs. 18 days to first NPC passage) and the yield of NPCs improved approximately 5 fold, as measured by decreasing Oct4 expression and increasing Nestin expression.

With respect to metabolic function under galactose conditions, the decrease in glycolysis with maintenance of mitochondrial respiration during the differentiation process suggests that these forced metabolic conditions. Therefore, establishing NPC differentiation protocols that drive a metabolic transition from glycolysis to oxidative phosphorylation may enhance the formation of stable and more homogeneous NPC populations. These results underscore the power of real-time functional metabolic analysis, in conjunction with orthogonal data, to enable a better understanding of the role of metabolism during cellular differentiation, with the goal of developing more efficient and robust differentiation methods.

Conclusion

Metabolic profiling using the Seahorse XF Cell Mito Stress Test and Glycolytic Rate Assay to measure mitochondrial respiration and glycolysis can be used to analyze and pinpoint metabolic switches and mechanisms that affect iPSC differentiation with respect to speed and efficiency. Here, decreases in glycolysis and maintenance of mitochondrial respiration appear to be correlated with increased NPC differentiation efficiency from iPSCs. In general, these types of assays provide a robust means towards understanding the metabolic drivers of cell differentiation and thus predicting and programing cell fate specification toward an NPC (or other) terminal phenotype.

Materials and Methods

Cell culture

Human skin fibroblast-derived iPSCs derived were cultured in Mouse Embryonic Fibroblasts-Conditioned Media (MEF-CM) supplemented with 8 ng/mL bFGF (PeproTech, 100-18B) on culture dishes coated with Matrigel (Corning, 354234). NPCs derived from iPSCs were cultured on Matrigel-coated cell culture dishes in 10 mM glucose-supplemented NPC media; glucose-free DMEM (Thermo, 11966025), 1X N2 (Thermo, 17502048), 1X B27 (Thermo, 17504044), 10 ng/mL bFGF, and 50 ng/mL EGF (PeproTech, AF-100-15).

Differentiation of iPSCs into NPCs

For differentiation of iPSCs into NPCs, iPSCs were dissociated with Accutase (Corning, 25-058-CI) and filtered through a 0.45 µm filter to remove any remaining cell clumps. They were then resuspended in MEF-CM, supplemented with 10 µM Y-27632 (Abcam, ab144494) and 8 ng/mL bFGF, and plated on gelatin-coated cell culture dishes at 37 °C for 30 minutes to remove fibroblasts. Nonadherent cells were collected, counted, and plated at a density of 5.0×10^4 cells/cm^2 in MEF-CM supplemented with 10 µM Y-27632 and 8 ng/mL bFGF on Matrigel-coated cell culture plates with daily media changes until the cells reached confluency. Upon confluency, the neural differentiation was induced (day 0) in either 10 mM glucose (Sigma, G7021) or 10mM galactose (Sigma, G5388) supplemented differentiation media. This differentiation media composition is glucose-free DMEM with 15% KOSR (Knock-Out Serum Replacement; Thermo, 10828028), 1X NEAA (Non-essential amino acids; Thermo, 11140050), 1 mM sodium pyruvate (Thermo, 11360070), 100 nM LDN-193189 (Cayman Chemicals, 11802), and 10 µM SB-431542 (Cayman Chemicals, 13031). The media was refreshed daily until day 2. On day 4, media was replaced with the respective differentiation media mix with glucose- or galactose-containing NPC media at 3:1 ratio. The media mix rate was changed to 1:1 on day 6 and to 1:3 on day 8. On day 10, the cells were dissociated with Accutase and replated on Matrigel-coated cell culture dishes in 10 mM glucose-containing NPC media until cells reached confluency with media changes every other day.

Cellular metabolic profiling

Singularized iPSCs were plated and differentiated in Seahorse XF96 V3 PS Cell Culture Microplates (Agilent, 101085-004) plates as described previously. The metabolic data were measured on the days indicated in Figure 1 using both the Seahorse XF Cell Mito Stress Test Kit and the Seahorse XF Glycolytic Rate Assay. Both assays were performed in Seahorse XF DMEM without phenol red, pH 7.4 (Agilent 103575-100) supplemented with 2.5 mM L-Glutamine (Agilent, 103579-100), 1 mM sodium pyruvate (Agilent, 103578-100), and 10 mM glucose (Agilent, 103577-100). The optimal FCCP concentration (0.5 µM) was used for the XF Cell Mito Stress Test kit. Once iPSCs reached confluency, the mitochondrial and glycolytic metabolic profiles were measured before the induction of differentiation (day 0) data, this was followed by a series of assays on days after the onset of differentiation on the Seahorse XF96 plates as indicated in Figure 1 to track the metabolic changes during differentiation. To obtain the metabolic profiles of NPCs, cells were cultured for an additional 10-14 days in NPC culturing conditions after seeding at a density of 6×10^4 cells/well on Matrigel-coated Seahorse XF96 plates. XF Cell Mito Stress Test and XF Glycolytic Rate Assay measurements were performed on these cell using the Agilent Seahorse XFe96 Analyzer, and were normalized to cellular DNA content using the CyQuant Cell Proliferation assay kit (Thermo, C7026). All functional parameters were calculated using the XF Cell Mito Stress Test and XF Glycolytic Rate Assay report generators.

Immunofluorescence staining

iPSCs were plated in 12-well plates and differentiated as described previously. After 10 days of differentiation, cells were replated on Matrigel-coated 12-well plates in NPC media and grown until 70–80% confluency. iPSC colonies, NPCs, and the differentiating cells at specified time points during NPC differentiation were fixed using BD Cytofix/CytoPerm kit (BD Bioscience, 554714). Upon fixation, cells were blocked in 10% normal donkey serum (Millipore Sigma, S30-100ML) for 1 hour at room temperature. This was then followed by overnight incubation with primary unconjugated antibodies against Oct4 (Cell Signaling Technology, 2890S) and Nestin (Abcam, Ab22035) at 4 °C. The next day, cells were washed three times and stained with Alexa Fluor-488 (Thermo, A11029) and Alexa Fluor-647 (Thermo, A21245) conjugated secondary antibodies at room temperature for 1 hour. Cells were washed three times, stained with DAPI (Thermo, D3571), and then imaged.

References

1. Robinton, D. A.; Daley, G. Q., The promise of induced pluripotent stem cells in research and therapy. *Nature* **2012**, 481 (7381), 295–305.
2. Bordoni, M.; Rey, F.; Fantini, V.; Pansarasa, O.; Di Giulio, A. M.; Carelli, S.; Cereda, C., From Neuronal Differentiation of iPSCs to 3D Neuro-Organoids: Modelling and Therapy of Neurodegenerative Diseases. *International journal of molecular sciences* **2018**, 19 (12).
3. Brennand, K. J.; Simone, A.; Jou, J.; Gelboin-Burkhart, C.; Tran, N.; Sangar, S.; Li, Y.; Mu, Y.; Chen, G.; Yu, D.; McCarthy, S.; Sebat, J.; Gage, F. H., Modelling schizophrenia using human induced pluripotent stem cells. *Nature* **2011**, 473 (7346), 221-5.
4. Kaye, J. A.; Finkbeiner, S., Modeling Huntington's disease with induced pluripotent stem cells. *Molecular and cellular neurosciences* **2013**, 56, 50–64.
5. Lai, W. S.; el-Fakahany, E. E., Interaction of 4-aminopyridine with [3H]phencyclidine receptors in rat brain homogenates. *Neuroscience letters* **1986**, 67 (1), 87–91.
6. Li, L.; Chao, J.; Shi, Y., Modeling neurological diseases using iPSC-derived neural cells : iPSC modeling of neurological diseases. *Cell and tissue research* **2018**, 371 (1), 143–151.
7. Christie, K. J.; Emery, B.; Denham, M.; Bujalka, H.; Cate, H. S.; Turnley, A. M., Transcriptional regulation and specification of neural stem cells. *Advances in experimental medicine and biology* **2013**, 786, 129-55.
8. Lees, J. G.; Gardner, D. K.; Harvey, A. J., Mitochondrial and glycolytic remodeling during nascent neural differentiation of human pluripotent stem cells. *Development* **2018**, 145 (20).
9. O'Brien, L. C.; Keeney, P. M.; Bennett, J. P., Jr., Differentiation of Human Neural Stem Cells into Motor Neurons Stimulates Mitochondrial Biogenesis and Decreases Glycolytic Flux. *Stem cells and development* **2015**, 24 (17), 1984-94.
10. Zheng, X.; Boyer, L.; Jin, M.; Mertens, J.; Kim, Y.; Ma, L.; Ma, L.; Hamm, M.; Gage, F. H.; Hunter, T., Metabolic reprogramming during neuronal differentiation from aerobic glycolysis to neuronal oxidative phosphorylation. *eLife* **2016**, 5.
11. Cheng, C.; Fass, D. M.; Folz-Donahue, K.; MacDonald, M. E.; Haggarty, S. J., Highly Expandable Human iPS Cell-Derived Neural Progenitor Cells (NPC) and Neurons for Central Nervous System Disease Modeling and High-Throughput Screening. *Current protocols in human genetics* **2017**, 92, 21 8 1–21 8 21.
12. Hook, L.; Vives, J.; Fulton, N.; Leveridge, M.; Lingard, S.; Bootman, M. D.; Falk, A.; Pollard, S. M.; Allsopp, T. E.; Dalma-Weiszhausz, D.; Tsukamoto, A.; Uchida, N.; Gorba, T., Non-immortalized human neural stem (NS) cells as a scalable platform for cellular assays. *Neurochemistry international* **2011**, 59 (3), 432-44.
13. Kim, D. S.; Lee, D. R.; Kim, H. S.; Yoo, J. E.; Jung, S. J.; Lim, B. Y.; Jang, J.; Kang, H. C.; You, S.; Hwang, D. Y.; Leem, J. W.; Nam, T. S.; Cho, S. R.; Kim, D. W., Highly pure and expandable PSA-NCAM-positive neural precursors from human ESC and iPSC-derived neural rosettes. *PloS one* **2012**, 7 (7), e39715.
14. Koch, P.; Opitz, T.; Steinbeck, J. A.; Ladewig, J.; Brustle, O., A rosette-type, self-renewing human ES cell-derived neural stem cell with potential for in vitro instruction and synaptic integration. *Proceedings of the National Academy of Sciences of the United States of America* **2009**, 106 (9), 3225-30.
15. Nemati, S.; Hatami, M.; Kiani, S.; Hemmesi, K.; Gourabi, H.; Masoudi, N.; Alaei, S.; Baharvand, H., Long-term self-renewable feeder-free human induced pluripotent stem cell-derived neural progenitors. *Stem cells and development* **2011**, 20 (3), 503-14.
16. Correia, C.; Koshkin, A.; Duarte, P.; Hu, D.; Teixeira, A.; Domian, I.; Serra, M.; Alves, P. M., Distinct carbon sources affect structural and functional maturation of cardiomyocytes derived from human pluripotent stem cells. *Scientific reports* **2017**, 7 (1), 8590.
17. Marsboom, G.; Zhang, G. F.; Pohl-Avila, N.; Zhang, Y.; Yuan, Y.; Kang, H.; Hao, B.; Brunengraber, H.; Malik, A. B.; Rehman, J., Glutamine Metabolism Regulates the Pluripotency Transcription Factor OCT4. *Cell reports* **2016**, 16 (2), 323–332.
18. Tohyama, S.; Fujita, J.; Hishiki, T.; Matsuura, T.; Hattori, F.; Ohno, R.; Kanazawa, H.; Seki, T.; Nakajima, K.; Kishino, Y.; Okada, M.; Hirano, A.; Kuroda, T.; Yasuda, S.; Sato, Y.; Yuasa, S.; Sano, M.; Suematsu, M.; Fukuda, K., Glutamine Oxidation Is Indispensable for Survival of Human Pluripotent Stem Cells. *Cell metabolism* **2016**, 23 (4), 663-74.
19. Kase, E. T.; Nikolic, N.; Bakke, S. S.; Bogen, K. K.; Aas, V.; Thoresen, G. H.; Rustan, A. C., Remodeling of oxidative energy metabolism by galactose improves glucose handling and metabolic switching in human skeletal muscle cells. *PloS one* **2013**, 8 (4), e59972.

www.agilent.com/chem/discoverxf

Printed in the USA, June 13, 2019
5994-1057EN

Agilent
Trusted Answers